Higgs and beyond in the LHC era

Candidate:
David Marzocca

Supervisor:
Andrea Romanino
Co-Supervisor:
Marco Serone

Thesis submitted in partial fulfillment of the requirements
for the degree of Doctor Philosophiae
Academic Year 2013/2014

Abstract

The last few years witnessed some major breakthroughs in the field of fundamental particle physics, which had a big impact in our understanding of Nature at a microscopic level.

On March 30th, 2010, the first proton-proton collisions took place at the Large Hadron Collider (LHC), marking the beginning of a new era in particle physics. The excellent performance of the machine and the detectors, due to the fantastic work of all the researchers involved in the experiments, lead, in only two years, to the announcement of the discovery of the Higgs boson on July 4th, 2012. This event could be considered as the peak of success for the Standard Model (SM) of elementary particles, which predicted the existence of this particle – as well as all its properties – since more than forty years before. In the following two years the ATLAS and CMS experiments at the LHC measured the properties of the Higgs particle with a good accuracy, showing no significant deviation from the SM. In the meanwhile, also the numerous direct searches for other new particles turned out to give only negative results, against all expectations from the theory community, pushing the scale of new physics to higher and higher values. Also, while the cosmological evidence for Dark Matter (DM) is now stronger than ever, so far all direct and indirect searches provided negative results (albeit with some isolated exceptions which, however, are still much debated in the literature and seem to be incompatible with other negative results) and the bounds on weakly interacting massive particle DM are extremely strong.

In neutrino physics an important event took place in June 2011, when the Tokay-to-Kamioka (T2K) collaboration reported an evidence for a non-zero, and sizable, value of the reactor neutrino mixing angle, θ_{13}. This was confirmed in March 2012 by the Daya Bay collaboration, which measured this mixing angle with a very high precision, confirming that its value lies on the high-end of previous upper bounds. Since many popular and well motivated models of neutrino mixing predicted a zero, or very small, value of the reactor angle, this result was very important and offered a new insight in the quest for understanding the origin of flavor in the lepton sector. Also, since CP violation in the lepton sector effects vanish in the $\theta_{13} \to 0$ limit, the fact that this angle is sizable opens up many interesting possibilities for measuring CP violation in the neutrino sector.

The work presented in this thesis was largely stimulated by these two major breakthroughs in particle physics.

On the one hand the Higgs discovery and the measurement of its properties, in particular its mass, lead us to study the consequences of these measurements for a specific class of models beyond the SM: composite Higgs models [1, 2] (and also in supersymmetric versions of these models [3]). In particular, we found that a very definite (and testable) prediction for the spectrum of new physics can be obtained [1]: fermionic top partners are expected to be near the $\sim 1\,\mathrm{TeV}$

scale. Also, the measurements of the Higgs couplings and the fact that the bounds for the new physics scale are often much higher than the electroweak scale, open up the possibility of studying possible deformations from the SM in an effective field theory framework. In this context we studied the possibility of linking the properties of the Higgs with other electroweak observables, very well constrained by LEP, via renormalization group effects, finding that they already allow to derive constraining, and independent, bounds on some Higgs properties [4]. In the future, when some deviation from the SM will be – hopefully – observed, these effects could provide a new window on the new physics sector. Some results regarding expectations from possible future colliders have been presented in ref. [5].

On the other hand, we studied how the measured value of θ_{13} can be accommodated in some motivated models of neutrino mixing by exploiting corrections due to the mixing among the charged leptons [6, 7]. Such corrections are expected, for example, in Grand Unified Theories, which allow to link the charged lepton sector with the quark sector, and therefore the neutrino mixing matrix with the quark mixing one. This analysis allowed us to obtain a precise prediction for the value of the Dirac CP violating phase in neutrino mixing, testable by future neutrino experiments.

Contents

CHAPTER 1

The Standard Model

Of course our model has too many
arbitrary features for these predictions
to be taken very seriously

Steven Weinberg [8]

The discovery of the Higgs boson at the Large Hadron Collider (LHC) in Geneva, by the AT-LAS and CMS experiments on July 4th, 2012, [9, 10], was a milestone in the progress of the understanding of fundamental particle physics. This particle, predicted fifty years ago [11–13] as a consequence of a mechanism able to provide a mass to spin-1 gauge bosons, and included as the cornerstone of the electroweak (EW) sector of the Standard Model (SM) [8, 14, 15], was the last missing piece of this extraordinary theory. The incredible success of the SM to correctly describe, and predict, a great variety of physical phenomena, ranging several orders of magnitude in energy scale, sometimes with a very high precision, is unattained in any other field of human knowledge. Furthermore, since G. t'Hooft [16] proved that the SM is a renormalizable theory, it can also be seen as a theoretically consistent theory up to extremely high energies. There are, however, both experimental observations – such as the presence of gravity, neutrino oscillations, dark matter and the baryonic asymmetry in the Universe – and theoretical issues – as the naturalness problems for the cosmological constant, the Higgs mass and the QCD θ angle – which make us expect that this should not be the case, i.e. that the SM should be extended in order to provide an explanation to these issues. In particular, the naturalness problem for the Higgs mass points to a scale of new physics (NP) near the TeV, that is in the range of energies currently probed at the LHC. In this chapter we review some basic concepts regarding the SM and present some of the experimental and theoretical problems of the SM mentioned above.

1.1   The SM action

The SM [8,14,15] is a renormalizable quantum field theory based on the local non-abelian gauge group

$$\mathcal{G}_{\text{SM}} = \text{SU}(3)_c \times \text{SU}(2)_L \times \text{U}(1)_Y \ , \tag{1.1}$$

where the first factor is the quantum chromodynamics (QCD) gauge symmetry while the other two represent the electroweak symmetry group $\mathcal{G}_{\text{EW}}$. It can be described by the Lagrangian

$$\mathcal{L}^{\text{SM}} = \mathcal{L}^{gauge} + \mathcal{L}^{mat} + \mathcal{L}^{Higgs} + \mathcal{L}^{Yuk} \ , \tag{1.2}$$

where the addends on the r.h.s. are, respectively, the gauge-invariant kinetic terms of the gauge bosons and of the fermion matter fields, the gauge-invariant kinetic and potential terms of the Higgs scalar and finally the Yukawa interaction between the Higgs and the SM fermions. Let us now briefly discuss each term separately.

Gauge Term

The Yang-Mills Lagrangian for the SM gauge fields G_μ^A, W_μ^a and B_μ, with $A = 1, \ldots, 8$ and $a = 1, 2, 3$, is

$$\mathcal{L}^{gauge} = -\frac{1}{4} G_{\mu\nu}^A G^{A\,\mu\nu} - \frac{1}{4} W_{\mu\nu}^a W^{a\,\mu\nu} - \frac{1}{4} B_{\mu\nu} B^{\mu\nu} \ , \tag{1.3}$$

where the field strength are defined as $V_{\mu\nu}^i = \partial_\mu V_\nu^i - \partial_\nu V_\mu^i + i g_V f^{ijk} V_\mu^j V_\nu^k$, and f^{ijk} represent the structure constants of the non-abelian gauge groups.[1] In order to quantize the theory, to eq. (1.3) one should add also the gauge fixing terms for the three SM gauge factors and the Lagrangian for the ghost fields. For simplicity we omit these terms here, the relevant ones will be specified in the text whenever necessary.

The field content of the SM is such that the QCD coupling constant g_s has a negative β-function, meaning that its value decreases when increasing the energy of the process, a behavior called *asymptotic freedom.* This also implies that upon reducing the energy of a process g_s increases, eventually becoming non-perturbative at a scale

$$\Lambda_{\text{QCD}} \sim \Lambda \exp\left(\frac{1}{2\beta_0 g_s^2(\Lambda)}\right) \sim 1\text{GeV} \ , \tag{1.4}$$

where Λ is either the UV cutoff of the theory or any other matching scale from which the running starts. The dynamical generation of an energy scale from the renormalization group flow of an adimensional coupling is called *dimensional transmutation* [17]. Below this QCD scale, all degrees of freedom charged under the QCD gauge group condense and become confined in color-neutral

---

[1]Here and in the following, otherwise explicitly stated, repeated indices imply a sum.

composite states, the hadrons. In general, at the renormalizable level, another operator could be added to the QCD Lagrangian:

$$\Delta\mathcal{L}^\theta = -i\theta_{QCD}\frac{g^2}{32\pi^2}G^A_{\mu\nu}\widetilde{G}^{A\mu\nu} , \tag{1.5}$$

where $\widetilde{G}^A_{\mu\nu} = \frac{1}{2}\epsilon_{\mu\nu\rho\sigma}G^{A\rho\sigma}$. Even though this term can be written as a total derivative, using the Bardeen identity, the non-trivial topology at infinity of the $SU(3)_c$ gauge group makes it physical. This CP-odd operator, in fact, reflects non-perturbative topological properties of the QCD gauge group and in general one would expect $\theta_{QCD} \sim \mathcal{O}(1)$. Assuming non-vanishing quark masses, a non-zero value of θ_{QCD} would generate, for example, an electric dipole moment for the neutron $d_N \sim |\theta_{QCD}|\, e\, m_\pi^2/m_N^3 \sim 10^{-16}\,|\theta|\, e\, \text{cm}$.[2] The experimental upper bound $d_N \lesssim 10^{-25}e\,\text{cm}$ implies $|\theta_{QCD}| \lesssim 10^{-9}$. This big hierarchy between the expected value and the measured upper bound, and the fine-tuning this implies, is known as the *strong CP problem*.

The EW gauge group is spontaneously broken to the electromagnetic subgroup $U(1)_{em}$ via the Higgs mechanism, described in the following, providing a mass for three linear combinations of the four gauge bosons of $\mathcal{G}_{EW}$: the $W^\pm$ and Z bosons. The remaining combination is massless and is identified with the photon.

Matter

The matter content of the SM consists of three copies (generations) of a set of chiral fermions transforming under fundamental representations of $\mathcal{G}_{SM}$ as

	q_L^j	u_R^j	d_R^j	ℓ_L^j	e_R^j
$SU(3)_c$	**3**	**3**	**3**	**1**	**1**
$SU(2)_L$	**2**	**1**	**1**	**2**	**1**
Y	1/6	2/3	-1/3	-1/2	-1

,

where Y is the hypercharge of $U(1)_Y$, the components of the doublets are $q_L^j = (u_L^j, d_L^j)$, $\ell_L^j = (\nu_L^j, e_L^j)$ and $j = 1,2,3$ is the generation index. The second term in eq. (1.2) contains the gauge-invariant kinetic terms for all the SM fermions, schematically

$$\mathcal{L}^{mat} = \sum_{f=q,\ell;j} \bar{f}_L^j i\gamma^\mu D_\mu f_L^j + \sum_{f=u,d,e;j} \bar{f}_R^j i\gamma^\mu D_\mu f_R^j , \tag{1.6}$$

where $D_\mu = \partial_\mu - ig_s G^A_\mu t_f^A - igW^a_\mu T_f^a - ig'B_\mu Y$ and t_f^A, T_f^a are the generators of the $SU(3)_c$ and $SU(2)_L$ groups in the representation of the fermion f (for doublets of $SU(2)_L$ the T^a are given by the Pauli matrices, $\sigma^a/2$, and for triplets of QCD the t^A are given by the Gell-Mann matrices $\lambda^A/2$).

---

[2]This expression holds in a particular phase convention for the quarks. In general physical observables depend on an phase parametrization-invariant combination of the QCD θ angle and the quark phases.

Higgs Lagrangian

The SM Higgs boson is a complex scalar, singlet under the color group, doublet of $\mathrm{SU}(2)_L$ and with hypercharge $Y = 1/2$: $H = (\mathbf{1}, \mathbf{2}, 1/2)$. It is the only elementary scalar of the SM. Its Lagrangian is

$$\mathcal{L}^{Higgs} = |D_\mu H|^2 - V(H), \tag{1.7}$$

where $D_\mu H = \partial_\mu H - ig W_\mu^a \frac{\sigma^a}{2} H - ig' \frac{1}{2} B_\mu H$ and the potential $V(H)$ can be parametrized as

$$V(H) = -\frac{1}{2} m_H^2 |H|^2 + \lambda |H|^4 , \tag{1.8}$$

with $\lambda, m_H^2 > 0$. This potential has an obvious minimum away from the origin, therefore the Higgs takes a vacuum expectation value (VEV) at $\langle |H|^2 \rangle = v^2/2 = m_H^2/(4\lambda)$, where we introduced the VEV parameter $v = (\sqrt{2} G_F)^{-1/2} \simeq 246\text{GeV}$. In this class of minima the EW symmetry is spontaneously broken to a $U(1)$ subgroup, which we identify with the electromagnetic gauge group. As a consequence of this spontaneous symmetry breaking, three Nambu-Goldstone bosons (NGB) are present in the theory. An efficient way to parametrize the physics around one of these vacua is to define

$$H(x) = \Sigma(x) \frac{1}{\sqrt{2}} \begin{pmatrix} 0 \\ v + h(x) \end{pmatrix}, \tag{1.9}$$

where $h(x)$ is the physical Higgs boson and $\Sigma(x)$ is a matrix containing the three NGBs $\chi^a(x)$:

$$\Sigma(x) = \exp\left(i \frac{\sigma^a \chi^a(x)}{v} \right) , \tag{1.10}$$

which satisfies $\Sigma \Sigma^\dagger = \mathbf{1}_2$, where $\mathbf{1}_2$ is the 2×2 identity matrix. In this parametrization the kinetic term of the Higgs can be written as

$$\mathcal{L}_{kin}^{Higgs} = \frac{1}{2} (\partial_\mu h)^2 + \frac{v^2}{4} \mathrm{Tr}\left[(D_\mu \Sigma)^\dagger D^\mu \Sigma \right] \left(1 + \frac{h}{v} \right)^2 , \tag{1.11}$$

where $D_\mu \Sigma = \partial_\mu \Sigma - i\frac{g}{2} W_\mu^a \sigma^a \Sigma + i\frac{g'}{2} \Sigma \sigma^3$. The gauge choice in which $\Sigma = \mathbf{1}$ is called *unitary gauge* and makes explicit the fact that the fields $W_\mu^\pm = (W_\mu^1 \mp i W_\mu^2)/\sqrt{2}$ and $Z_\mu = \cos\theta_W W_\mu^3 - \sin\theta_W B_\mu$ become massive with

$$m_W = \frac{gv}{2} \simeq 80.4\text{GeV} , \qquad m_Z = \frac{m_W}{\cos\theta_W} \simeq 91.2\text{GeV} , \tag{1.12}$$

where the Weinberg angle is given by $\tan\theta_W = g'/g$. In this gauge, the three NGB modes have become the longitudinal polarization of the massive W and Z bosons. The orthogonal combination to Z_μ, $A_\mu = \cos\theta_W B_\mu + \sin\theta_W W_\mu^3$, remains massless and is the photon. The electric charge is defined as $Q = Y + T_f^{3L}$ and the fine structure constant is given by $\alpha = e^2/4\pi$, where electric coupling is $e = g \sin\theta_W$.

In this parametrization it is also manifest that the potential depends only on the physical field h. Expanding in powers of this field one gets the physical tree-level Higgs mass [18, 19]

$$M_H^2 = m_H^2 = 2\lambda v^2 \simeq (125 \text{ GeV})^2 \ .$$ (1.13)

Given the knowledge of v from muon decay, in the SM the measurement of the Higgs mass at the LHC corresponds to an indirect measurement of the self coupling $\lambda \simeq 0.13$.

Yukawa Lagrangian

The EW gauge symmetry forbids a mass term between the left-handed and the right-handed fermions. Yukawa interactions with the Higgs, therefore, are needed in order to provide masses to SM fermions. The last term in eq. (1.2) is:

$$\mathcal{L}^{Yuk} = -y_u^{ij} \bar{q}_L^i H^c u_R^j - y_d^{ij} \bar{q}_L^i H d_R^j - y_e^{ij} \bar{\ell}_L^i H e_R^j + h.c. \ ,$$ (1.14)

where $H^c = i\sigma^2 H^*$ and y_u, y_d, y_e are $3{\times}3$ complex matrices. In the unitary gauge this Lagrangian provides mass terms for the SM quarks and charged leptons, $m_{u,d,e} = y_{u,d,e} v/\sqrt{2}$, as well as interactions with the Higgs. These mass matrices can be diagonalized by biunitary transformations acting on the three generations of fermions

$$m_{u,d,e} = U_{u_L,d_L,e_L} m_{u,d,e}^{\text{diag}} (U_{u_R,d_R,e_R})^\dagger \ .$$ (1.15)

Since u_L and d_L are part of the same $\text{SU}(2)_L$ doublet, in general it is not possible to diagonalize both the up and down quark matrices while at the same time respecting the gauge invariance. For example, one can choose to diagonalize the down-quark mass matrix, obtaining from eq. (1.14), in the unitary gauge,

$$\mathcal{L}^{Yuk} = -\left(m_{u_j} \bar{u}_L^i (V_{\text{CKM}})_{ij} u_R^j + m_{d_i} \bar{d}_L^i d_R^i + m_{e_i} \bar{e}_L^i e_R^i + h.c. \right) \left(1 + \frac{h}{v} \right) \ ,$$ (1.16)

where m_{u_j,d_j,e_j} are (real and positive) the singular values of the three mass matrices and $V_{\text{CKM}} = (U_{d_L})^\dagger U_{u_L}$ is the Cabibbo-Kobayashi-Maskawa (CKM) matrix which contains the 3 physical quark mixing angles and the only physical CP violating phase. Note that the three neutrinos ν_L^i remain massless at this level. A Dirac neutrino mass term is forbidden since the SM does not contain their right-handed counterpart. Also, even though in principle a Majorana mass term could be allowed, since neutrinos are neutral, gauge invariance forbids this at the renormalizable level. As we explain in more detail in section 5.1, this offers a simple and elegant explanation to why neutrinos are much lighter than all the other fermions.

1.1.1 Global symmetries of the SM

The SM Lagrangian presented above, eq. (1.2), enjoys many accidental, exact or approximate, global symmetries. These symmetries have an important role in shaping the phenomenology of the theory. Let us introduce here the most relevant ones.

Custodial symmetry

Let us rewrite the Higgs doublet in 2×2 matrix notation as $\Phi(x) = h_i(x)\sigma^i + h_4(x)\mathbf{1}_2$, and the Lagrangian in eq. (1.7) as

$$\mathcal{L}^{Higgs} = \frac{1}{4}\mathrm{Tr}\left[D_\mu\Phi^\dagger D^\mu\Phi\right] - \lambda\left(\frac{1}{4}\mathrm{Tr}\left[\Phi^\dagger\Phi\right] - \frac{v^2}{2}\right)^2 , \tag{1.17}$$

where $D_\mu\Phi = \partial_\mu\Phi - i\frac{g}{2}W_\mu^a\sigma^a\Phi + i\frac{g'}{2}B_\mu\Phi\sigma^3$. In the limit in which $g' = 0$, this Lagrangian enjoys a global $\mathrm{SU}(2)_L \times \mathrm{SU}(2)_R$ symmetry, acting on the Higgs field as $\Phi \to U_L\Phi U_R^\dagger$. This symmetry is broken, other than the hypercharge (which, in this formalism, corresponds to the gauging of only the third generator of $\mathrm{SU}(2)_R$), also by the difference of the Yukawa couplings between the up-type and down-type quarks. The Higgs VEV breaks spontaneously this $\mathrm{SU}(2)_L \times \mathrm{SU}(2)_R \sim \mathrm{SO}(4)$ symmetry to the diagonal subgroup $\mathrm{SU}(2)_C \sim \mathrm{SO}(3)_C$, called *custodial symmetry group*. The three NGBs arising from this symmetry breaking pattern are exactly the NGBs of the electroweak symmetry breaking, eaten by the massive W and Z bosons.

In the SM, the gauge bosons masses and couplings satisfy the tree level relation [20]

$$\rho \equiv \frac{m_W^2}{m_Z^2\cos^2\theta_W} = 1 . \tag{1.18}$$

This tree-level relation is a consequence of the custodial symmetry, which also protects the ρ parameter from receiving big quantum corrections [21, 22]. In fact, in the SM these corrections vanish in the limit of zero hypercharge and equal up and down quark masses.

In general, new physics model, as well as higher dimension effective operators, violate this symmetry at tree-level and predict sizable corrections to ρ. Experimentally, LEP [23] put very strong bounds on the deviations from the SM prediction, which put very strong constraints on the NP sector.

Flavor symmetries

Let us now discuss the global symmetries of the matter sector of the SM. The kinetic Lagrangian of the SM fermions, eq. (1.6), is symmetric under the global flavor group

$$\mathrm{U}(3)_q \times \mathrm{U}(3)_u \times \mathrm{U}(3)_d \times \mathrm{U}(3)_\ell \times \mathrm{U}(3)_e , \tag{1.19}$$

under which the generation-index of each type of fermion transforms in the fundamental representation. This big symmetry group is explicitly broken by the Yukawa Lagrangian, eq. (1.14). The bigger the Yukawa coupling, the stronger the breaking.

The only exact global symmetries left are the *baryon number* and the *lepton numbers*.

- The baryon number is the conserved charge of the $U(1)_B$ global symmetry under which all quarks change phase: $q \to e^{i\alpha}q$. Since baryons carry a non-zero net baryon number, the proton – which is the lightest baryon – is predicted to be stable. Higher dimension effective operators, in general, violate this symmetry and therefore can mediate proton decay. Experimental constraints on the proton lifetime pushed the scale of baryon number violation to $\sim 10^{15}\text{GeV}$.

- The electron, muon and tau lepton numbers are conserved charges corresponding to three independent $U(1)$ phase redefinitions of each lepton generation. These independent quantum numbers are slightly violated by non-vanishing neutrino masses, the most important effect being neutrino oscillation. If neutrinos are Dirac particles then a global $U(1)_L$ is left, like the baryon number, where $L = L_e + L_\mu + L_\tau$; if instead the neutrinos are Majorana particles, then also this symmetry is violated. The nature of neutrinos is currently tested for, experimentally, by searching for neutrino-less double-β decays.

- At the quantum level, due to the matter content of the SM, the L and B global symmetries are anomalous and are broken, in particular, by instanton effects. Only the linear combination $B - L$ remains unbroken, unless neutrinos have a non-vanishing Majorana mass.

1.2 Naturalness problem

Big and small numbers found in Nature have always puzzled physicists trying to unveil the laws of the Universe.[3] Dirac's "Large Number Hypothesis" [25, 26] was an attempt to explain the smallness of the proton mass with respect to the Planck mass, or why the gravitational interaction in an atom is so much weaker than the electromagnetic one:

$$\frac{e^2}{G_N m_e m_p} = 2.85 \times 10^{40}. \tag{1.20}$$

Now we know that the generation of the QCD scale is due to the quantum nature of the theory and, in particular, to dimensional transmutation which suppresses exponentially the QCD scale with respect to the Planck scale, see eq. (1.4).

---

[3]For a review on naturalness problems in physics see ref. [24].
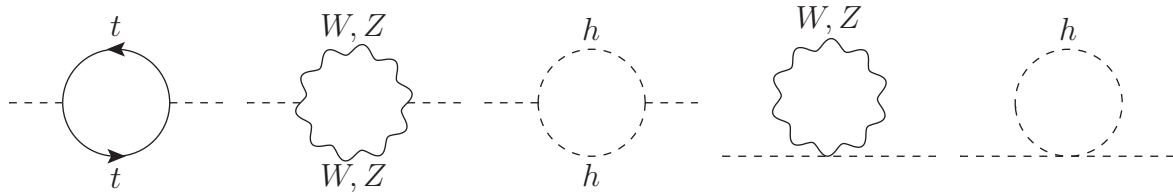
Figure 1.1: Diagrams contributing at one-loop to the Higgs mass in the SM.

Other examples of a very small (or big) numbers in the SM are the value of the QCD CP-violating angle $\theta_{QCD} \lesssim 10^{-9}$ (see eq. (1.5)) and the ratio of the strength of the weak and gravitational forces,

$$\frac{G_F \hbar^2}{G_N c^2} = 1.738\,59(15) \times 10^{33} \ . \tag{1.21}$$

In terms of energy scales, this translates in the question of why the electroweak scale v is much smaller than the Planck mass M_{Pl}. The rest of this section is devoted to discuss the problems associated with this hierarchy and to show that this is not only an aesthetical and philosophical issue, but a deep problem related to fundamental properties of quantum field theories.

1.2.1   Understanding the problem

Since the electroweak scale can be traded for the Higgs mass parameter m_H which enters in the potential in our parametrization, let us discuss the problem associated to the value of the Higgs mass.

To appreciate the problem it is necessary to consider the quantum nature of the theory. Interactions of the Higgs with virtual particles in the quantum vacuum produce corrections to the Higgs mass of the order of the largest energy scale available to these virtual particles, i.e. the maximum energy up to which the theory is valid. At the technical level this reflects in quadratic divergencies in the computation of quantum corrections to m_H^2 as in fig. 1.1 which, barring cancellations, can be estimated to be

$$\delta m_H^2 \sim g^2 \frac{\Lambda^2}{16\pi^2} \ , \tag{1.22}$$

where Λ is the cutoff of the computation. If the SM was valid up to the Planck mass M_{Pl}, this would mean that the ratio of eq. (1.21) would be expected to be of order 1 (or only slightly bigger due to the loop factor).

An important assumption we took in the previous argument was the introduction of a physical energy scale much bigger than the Higgs mass. This is crucial, in fact the SM is a renormalizable theory, which means that all divergencies can be reabsorbed by unphysical counter-terms, in this

case the bare Higgs mass itself. After this process the only remnant of the divergence is the renormalization group (RG) flow of the Higgs mass parameter:

$$\beta_{m_H^2} = \frac{dm_H^2}{d\log\mu} \simeq \left(3y_t^2 - \frac{3}{4}(3g^2 + g'^2) + 6\lambda\right)\frac{m_H^2}{8\pi^2} \ , \tag{1.23}$$

where we neglected higher order corrections and contributions from fermions lighter than the top (see e.g. ref. [27] for the complete RG equations in the SM up to three loops). We see that, as expected, any dependence on the cutoff has disappeared, in fact if we would have used dimensional regularization for the computation, we would not have found any quadratic divergence to begin with. Eq. (1.23) also shows that the RG of the Higgs mass is proportional to the mass itself. This means that if the SM would be the complete theory of Nature and no other energy threshold would be present at high scales, then any value of the electroweak scale would be equally natural at the technical level.

The problem hinted by eq. (1.22) arises if the SM has to be completed by some other dynamics at a scale $\Lambda^2 \gg m_H^2$. The motivations for such a new dynamics are manifold, here we will only list some of them briefly: the quantization of gravity most probably involves some new effects at (or before) the Planck scale; reproducing the dark matter abundance of the Universe requires some degree of freedom beyond the SM, even though the scale is almost arbitrary; Majorana neutrino masses (assuming $\mathcal{O}(1)$ Yukawa couplings) and unification of the gauge couplings both point to some new dynamics at the 10^{14-16}GeV scale; many models explaining baryogenesis and inflation also hint to some new physics at a very high energy scale. Moreover, even neglecting altogether gravity or these other new physics phenomena, the SM itself presents a new scale at energies of $\sim 10^{41}$GeV, where the hypercharge (and the Higgs quartic coupling) become non-perturbative.

As a simple example to understand what could such a heavy new dynamics lead to, let us consider a new complex scalar field ϕ with mass $M \gg M_H$, coupled to the Higgs via a portal interaction $V \supset \lambda_\phi |H|^2 |\phi|^2$. Above the scale M, where the scalar is present in the theory, this interaction generates an *additive* contribution to the Higgs mass β function given by

$$\delta\beta_{m_H^2} = \delta\frac{dm_H^2}{d\log\mu} = -\frac{\lambda_\phi}{16\pi^2}M^2 \ . \tag{1.24}$$

This RG effect from a scale $M_* > M$ down to M (below which the scalar has to be integrated out and one recovers the SM), gives a contribution to the Higgs mass much bigger (in absolute value) than the physical Higgs mass:

$$\delta m_H^2 = -\frac{\lambda_\phi}{16\pi^2}M^2 \log\frac{M_*}{M} \ . \tag{1.25}$$

As can be seen from the blue line in fig. 1.2, immediately above M the (running) Higgs mass saturates near the value of eq. (1.25). This means that a big tuning between the boundary condition at the UV scale M_* and this RG contribution is therefore needed in order to keep the
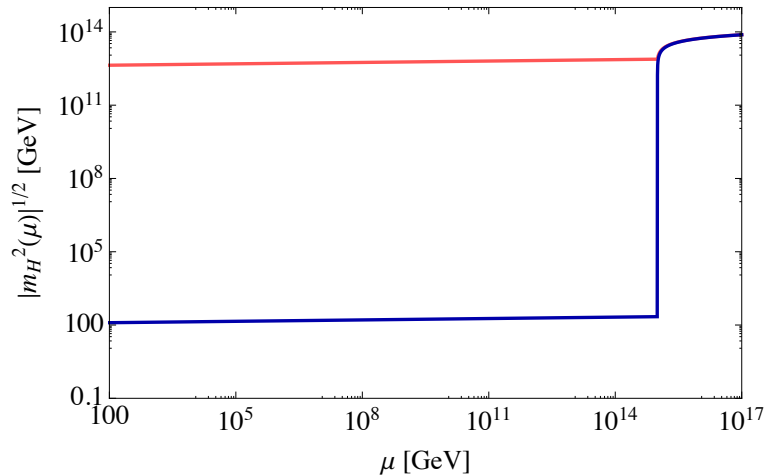
Figure 1.2: Running of the Higgs mass parameter in the SM plus a heavy complex scalar at $M = 10^{15}$GeV, where we fixed the portal coupling $\lambda_\phi = 0.2$. The blue line is obtained by fixing the boundary condition $m_H^2(M_H) \equiv M_H^2 \simeq (125\text{GeV})^2$, this provides a (tuned) UV value at $M_* = 10^{17}$GeV for $m_H^2(M_*)$. By changing this UV condition by 1% and running back down we get the red line, and a value of the Higgs mass $\tilde{m}_H^2(M_H) \simeq -(4 \times 10^{12}\text{GeV})^2$, showing that a small change in the UV condition destabilizes the physical Higgs mass.

physical Higgs light. To see this, for the red line of fig. 1.2 we changed the UV boundary condition at M_* by 1% and then followed the RG back into the IR to obtain the physical Higgs mass, obtaining a much bigger value $\tilde{M}_H^2 \simeq -(4 \times 10^{12}\text{GeV})^2$. We see that the mass scale M destabilizes the Higgs mass and brings its value close to that scale. The same phenomenon would appear for any kind of new heavy dynamics coupled to the Higgs boson. For example, in supersymmetric models with large stop masses, the one-loop correction to m_H^2 grows quadratically with the stop mass $\tilde{m}_t^2$. This quadratic sensitivity of the Higgs mass to any heavy mass scale was first pointed out in 1976 by Gildener [28] and then by Weinberg [29] and Susskind [30] in the context of grand unified theories (GUT).

By the end of the 70s it became clear that the naturalness problem is indeed fundamentally connected with two of the most important concepts in physics: effective field theories (EFT) and symmetries. If the NP scale is higher than the EW one, at low energy the physics can be described by an EFT approach. This consists in adding to the SM action non-renormalizable operators with dimension bigger than 4. In general an effective Lagrangian has a form

$$\mathcal{L}^{\text{EFT}} = \sum_{d \geq 0} \sum_i c_i \Lambda^{4-d} \mathcal{O}_i^{(d)}, \qquad (1.26)$$

where d indicates the classical scaling-dimension of the operators, $i = 1, 2, \ldots$ counts the operators with same dimension and the c_i are adimensional Wilson coefficients expected to be of $\mathcal{O}(1)$, unless they are protected by some symmetry. A physical, and intuitive, explanation for the

naturalness problem, due to Wilson, is based on the observation that operators with scaling dimension equal to 2 have a coefficient which is naturally of the order Λ^2, unless it breaks some symmetry [31]. The Higgs mass term in the potential, eq. (1.8), is the only such operator in the SM. Therefore, one would expect its natural value to be $m_H^2 \sim \Lambda^2$: either Λ is not far from the EW scale or the theory has a certain amount of tuning needed to keep the Higgs mass much smaller than its natural value.

Finally, the naturalness criterion proposed by 't Hooft [32] states that a parameter of the theory is allowed to be much smaller than unity[4] only if the theory acquires a new symmetry when such a parameter is set to zero. In fact, when a parameter breaks some symmetry all quantum its corrections are necessarily proportional to the breaking of the symmetry, therefore to the parameter itself, which ensures that a small breaking parameter remains small also after quantum corrections. Following this criterion, small fermion masses – or small Yukawa interactions – are naturale since the theory gains a chiral symmetry when putting them to zero. Analogously, light spin-1 particles are always natural because when their mass is set to zero the theory gains gauge invariance. An example of an unnaturally small parameter is the QCD angle θ_{QCD}. This parameter breaks the CP symmetry, however the same symmetry is also broken by the CP violating phase in the CKM matrix, δ, so no new symmetry is obtained when $\theta_{QCD} = 0$. Even if no quadratic divergence is present in its quantum corrections, these will tend to bring it near the value of δ, which implies that one would expect $\theta_{QCD} \sim \mathcal{O}(1)$, making the observed value $\theta_{QCD} \lesssim 10^{-9}$ very unnatural.

In the same category falls also the Higgs mass. In fact, setting m_H^2 to zero does not enhance the symmetries of the SM, therefore quantum corrections tend to push this parameter to the highest mass scale available in the theory. This property is typical of any scalar particle, unless its mass is protected by some symmetry. The difference of this behavior between scalars and spin-1 or spin-1/2 particles can also be understood in terms of degrees of freedom (d.o.f.). Massless fermions and vectors have 2 physical d.o.f. while massive ones have four and three, respectively: there is a discrete difference between the massless and massive case, which reflects the change in the symmetries of the theory. A massive scalar particle, on the other hand, has the same number of d.o.f. as a massless one.

In order to obtain a light Higgs, a delicate fine tuning between the values of the high scale parameters entering in the quantum correction to the Higgs mass is necessary. If the only UV scale is the Planck one, the amount of tuning is approximately given by eq. (1.21), which means that the value UV boundary condition and the RG contribution to the Higgs mass squared should cancel almost exactly, with a precision in the 33rd decimal place. An efficient analogy by Giudice [24] can help us get a feeling of the amount of this tuning: balancing a pen with length

---

[4]Mass parameters should be measured in units of the cutoff of the theory Λ

R and a tip with a surface of radius r is a challenge of tuning the position of the center of mass to be exactly over the surface of the tip. The amount of tuning needed is of order of one part in R^2/r^2. The tuning needed to keep the electroweak scale so small compared to the Planck scale is the same as the necessary one to balance a pen as long as the solar system on a millimeter wide tip. Does Nature present such a behavior just by accident or is there a mechanism which can explain this?

1.2.2 Many solutions but no experimental evidence

From the previous discussion it is clear that there are, at least, two ways to solve the naturalness problem associated with light elementary scalars: either its mass breaks some symmetry, and therefore is protected from big additive quantum corrections, or such a particle does not exist.

Supersymmetry [33] (SUSY), as a way to solve the naturalness problem [34, 35], introduces a new symmetry which connects bosons with fermions. In this setup, the Higgs mass arises only when supersymmetry is broken. Quantum corrections to m_H^2, therefore, are proportional to the SUSY breaking soft terms $\widetilde{m}^2$. If this scale is small enough, SUSY provides an elegant solution to the problem[5].

A solution of the second kind (of the two listed above) was proposed in 1979 by Susskind [30] and is known as Technicolor. In this setup there is no Higgs particle and EW symmetry breaking (EWSB) is due to the condensate of a new strongly coupled sector, at a scale of a few TeV, in a similar way as the QCD condensate breaks the chiral symmetry $\mathrm{SU}(2)_L \times \mathrm{SU}(2)_R \to \mathrm{SU}(2)_D$ (as well as the EW symmetry, albeit at the low scale $f_\pi \sim 10^2$ MeV). In Technicolor, the hierarchy between the Planck mass and the EW scale is explained by dimensional transmutation, as in QCD, where this big mass hierarchy is completely natural. By now this proposal has been excluded experimentally by the discovery of a scalar particle which shows characteristics (production and decay rates) very similar to those of the SM Higgs boson. However, even before LHC, already LEP put these models in strong tension due to the very precise measurements performed at the Z pole which showed none of the deviations from the SM predictions expected in Technicolor models.

Finally, many solutions which interpolate between these two concepts, and include the Higgs in the spectrum, have been proposed. The naturalness problem is solved by either assuming that the Higgs is a composite state of a new strong dynamics [37, 38], in which case the hierarchy between the weak and Planck scale is explained by dimensional transmutation, or assuming the existence of some compactified warped extra dimension [39], in which case the suppression of the EW scale is due to the exponential warping factor of the Anti-de-Sitter (AdS) metric in the fifth

---

[5]In this setup, the soft terms scale is assumed to arise dynamically [36], and many models which realize this mechanism have been proposed,

dimension. The AdS/CFT correspondence [40], suggests that these two approaches could be related to each other and can describe the same low-energy physics [41,42]. The most successful holographic composite Higgs models predict that the Higgs is a pseudo-Nambu-Goldstone boson (pNGB) of some spontaneously broken approximate global symmetry at a scale $f \sim 1\text{TeV}$ [43], which explain naturally how the Higgs can be lighter than the strongly coupled scale, in the same way as pions are lighter than the QCD scale.

In the last two decades, all these frameworks started to be in more and more tension with the experimental results coming from LEP and, now, from the LHC. The most natural versions of the minimal supersymmetric SM (MSSM) predicted a spectrum of SUSY partners near the $\sim 100\text{GeV}$ scale, as well as a light value of the Higgs mass which, at tree level, is expected to be lighter than the Z boson. Already LEP showed that this was not the case and that the SM is a valid description of Nature at the electroweak scale. The LEP bound on the Higgs mass, $m_H \gtrsim 114\,\text{GeV}$, suggested that the scale of the superpartners could be higher than expected and, therefore, some amount of tuning in the Higgs mass was necessary. Analogously, also composite Higgs models were being pushed by LEP to regions with some $\sim 10\%$ tuning. In other words, the scale of NP was pushed by LEP to $\sim \text{TeV}$, introducing what has been called *small hierarchy problem*. The measured value of the Higgs mass at the LHC [18,19] at $m_H \simeq 125\text{GeV}$ pushed the MSSM to even more uncomfortable regions, where the necessary size of the one-loop correction to m_H^2 has to be of the same order as the tree-level contribution. Moreover, the bounds on superpartners from direct searches pushed most of the MSSM parameter space to percent tuned regions, or worse. The strongest bounds on Composite Higgs models, on the other hand, are still coming from LEP, even though LHC constraints on the Higgs couplings and resonances masses are reaching the same level, and will be the dominant ones in the near future. While the Higgs mass is lower than what could be expected for this class of models, it has been noted recently that it offers a quite clear prediction for the spectrum of resonances, which can be tested by LHC [1,44–47].

On the one hand, as we showed, the naturalness problem is definitely a deep issue in our understanding of fundamental particle physics. However, even though theorists have produced a huge variety of results and models able to solve it (often times these models are able to solve, at the same time, also other open problems in particle physics and cosmology in a unified setup), so far all hopes of finding new physics crushed against the reality of experimental data, which do not show any deviation from the SM. On the other hand, the naturalness approach seems to have failed at least in one instance: the cosmological constant Λ_{cosm}. The measurement of the accelerated expansion of the Universe [48,49] is explained, in the cosmological standard model, by a small value of the cosmological constant, $\Lambda_{cosm} \sim 10^{-47}\,\text{GeV}^4$. This parameter, in QFT, receives contributions proportional to the cutoff to the fourth power. Assuming the cutoff of the

theory to be the Planck scale, this would imply that a tuning of one part in $\sim 10^{122}$ would be necessary to keep Λ_{cosm} to the observed value. In 1987, before Λ_{cosm} was measured, Weinberg [50] suggested an upper bound for the cosmological constant based on the anthropic principle, which turned out to be very close to the observed value. Very briefly, his observation was based on the fact that a too big value of Λ_{cosm} would imply a too fast expansion of the Universe, which would not allow structures to form and, therefore, life to develop. Since this is obviously not the case, the cosmological constant can not be too big in our Universe. A similar argument can be done also for the EW scale since a much bigger value would not allow the complex chemistry, needed for complex organisms – and life – to develop [51]. This anthropic reasoning, however, needs a mechanism in which all the possible values for the relevant parameter are populated in some region of the Universe, so that we happen to live in the one which allows the development of life. Such a mechanism could be provided by the string landscape and eternal inflation. For the moment, however, it is not clear if it could ever be tested experimentally.

What is the maximal amount of tuning one can accept? At which point will we be forced to abandon the naturalness guideline and start focusing on alternatives? Today the conscience of many particle physicists is struggled by these philosophical questions, to which of course there is no objective answer until experimental results will push us towards one side or the other.

Our approach for the rest of this thesis is a pragmatic one: the naturalness problem offers a deep guideline to our understanding of electroweak symmetry breaking. Let us follow this line to its consequences and study what predictions it allows us to make. From the bottom up, the naturalness argument predicts some NP at the TeV scale. If this is the case, oservables at lower energies can be successfully described by an effective field theory (EFT) framework. Some work in this setup is described in chapter 2. Another approach is to assume one of the explicit frameworks described above, study what predictions can be obtained and confront them with experimental data. This is described for composite Higgs models in chapter 3, while in chapter 4 we study a composite Higgs model which offers also a dark matter candidate and confront this with experimental constraints from both astrophysical and collider data.

CHAPTER 2

SM as an Effective Theory and RG-induced Bounds

The idea that the dynamics of a complex system with some typical scale L can be studied without the necessity of describing each of the microscopic constituents at smaller scales $\ell \ll L$ is at the foundation of the scientific progress. In the context of quantum field theories, this idea has been rigorously formulated by Wilson [52] in the early 70s and is now one of the pillars of our understanding of Nature at the quantum level. Wilson's idea is that, after mediating over the dynamics of the modes shorter than some cutoff scale Λ^{-1}, the resulting non-local effective action can be expanded in a series of local operators with increasing scaling dimension, suppressed by powers of Λ, with a procedure known as *operator product expansion.* In general, the number of effective operators one obtains is infinite. However, when studying processes at energies much smaller than the cutoff and given a certain precision desired for the computation, only operators with dimension lower than a certain value will matter, allowing to reduce the parameters to a finite number. While before this approach had been established the requirement of renormalizability of a quantum field theory was a necessary condition for having a consistent picture, almost all modern particle physics models are regarded as some *effective field theories* (EFTs) of some more fundamental theory and the non-renormalizable operators play a major role.

In particle phenomenology, studying effective operators can often offer important insights into the nature of the UV theory above the cutoff Λ. For example, the study of weak decays and neutrino scattering in terms of effective Fermi operators allowed to understand the nature of the electroweak theory and develop the SM much earlier than the direct discovery of the Z and W bosons.

Since, as we discussed in the previous chapter, the naturalness problem is a serious hint for some new physics lying not too far from the EW scale, and since so far all evidence suggest that

this dynamics should be somewhat heavy, i.e. near the TeV scale, studying the effective theory of the SM could be a powerful tool in the understanding of the NP sector in a model-independent way.

While these higher dimensional operators are generated at the new physics scale Λ, their effects are measured at the lower scale of the experiments. In order to compare the predictions for the coefficients of some NP model with the experimental results it is necessary to follow the renormalization group (RG) flow of the effective theory between the two scales. Due to this scaling, the Wilson coefficients run and mix as we go down from Λ to the experimental scale $\sim m_W$. The coefficients at the two scales are related to each other via the so-called anomalous dimension matrix. This operator mixing opens also the possibility of linking different kinds of deformations of the SM which are otherwise unrelated. Assuming that the different RG contributions to low-energy observables are not tuned against each other (i.e. that no correlations from the UV theory are present), and exploiting the wide range of experimental precision in the determination of some EW and Higgs observables, we are able to cast RG-induced bounds on some of these observables which are already stronger, or of the same order, than the direct experimental constraints.

In section 2.1 we introduce the dimension-6 operators in the SM and define the operator basis which is used in the rest of the chapter. In particular, here we concentrate on a subset of 13 operators made of gauge bosons and Higgs which give the most important contributions to the EW and Higgs observables we consider. In section 2.2 we present our computation of the anomalous dimension matrix of this subset of operators while the EW and Higgs observables we study are presented in section 2.3. The RG-induced bounds, as well as the tuning assumptions, are described in section 2.4. Finally, in section 2.5 we study prospects for these RG effects for high luminosity LHC and at future possible lepton colliders. This chapter is mainly based on the work done in refs. [4,5] and in previous literature on the subject.

2.1   Dimension-6 operators in the SM

Let us assume that the new physics sector at the scale Λ, which should cure the SM naturalness problem, does not contain any light (i.e. near the EW scale) degree of freedom. We also assume that the observed scalar at 125 GeV is indeed the SM Higgs boson, i.e. part of the same $SU(2)_L$ doublet as the Nambu-Goldstone bosons of EWSB. This is strongly suggested by the fact that the observed couplings of this particle with SM fermions and gauge bosons are in good agreement with the SM prediction, in particular they are proportional to the mass as can be seen from the
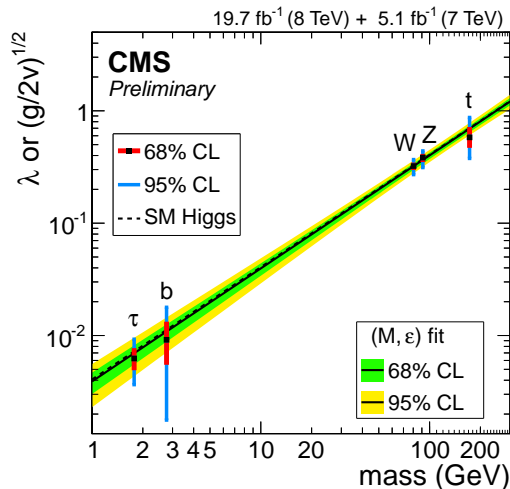
Figure 2.1: CMS summary of the fits for the Higgs couplings expressed as a function of the particle mass. No extra contributions to the couplings with $\gamma\gamma$ and gg are introduced in the fit.

plot in fig. 2.1.[1] In this case small deformations from the SM in experiments performed at the EW scale can be described by an effective Lagrangian containing non-renormalizable operators, invariant under the SM gauge group of eq. (1.1), written in an expansion in powers of $1/\Lambda$ [55]:

$$\mathcal{L}^{\mathrm{EFT}} = \sum_d \sum_i \frac{c_i^d}{\Lambda^{d-4}} \mathcal{O}_i^{(d)} = \mathcal{L}_0 + \frac{1}{\Lambda}\mathcal{L}_5 + \frac{1}{\Lambda^2}\mathcal{L}_6 + \dots \; . \tag{2.1}$$

The operators in $\mathcal{L}_0$, with dimension $d \leq 4$ define the SM action as described in the first chapter: the SM is the most general renormalizable theory compatible with the given gauge symmetries and field content. In this framework, all other global symmetries of the SM discussed in section 1.1.1, like baryon and lepton number conservation, are just accidental and not imposed by hand. The fact that the baryon number B and each lepton number L_i are good quantum numbers implies that the non-renormalizable operators which violate these symmetries should be suppressed by a very high scale Λ_{B,L_i}. Here we will assume that these scales are much higher than Λ, which suppresses the operators which violate B and L_i and allows as to discard those operators when studying processes at the EW scale.

The only gauge-invariant operator at dimension 5 present in $\mathcal{L}_5$ is the Weinberg operator for Majorana neutrino masses [56], discussed in section 5.1. However, since this operator violates Lepton number its scale is constrained to be very high, therefore we will neglect it in the following.

Let us then focus on the dimension 6 operators in $\mathcal{L}_6$. Since here we will not discuss flavor

---

[1]An alternative analysis can be performed in a more generic framework, in which the EW symmetry is non-linearly realized and the observed scalar is introduced as a generic singlet under the custodial symmetry. In this case $\mathcal{O}(1)$ deviations can be expected, which are however constrained by experimental data, albeit not for all observables, see e.g. refs. [53,54]. We do not discuss further this approach in this thesis.

observables and constraints, we will assume flavor universality in $\mathcal{L}_6$, which amounts to reducing the study of the operators for only one generation of the SM fermions. The classification of all SM dim-6 operators was first attempted in ref. [55], while the complete basis of independent operators was obtained in ref. [57], where the authors found that, for one generation of fermions, it contains 59 independent operators. In order to find the complete set, relations among operators can be found by using Fierz identities, integration by part and, most importantly, by performing small field redefinitions, which corresponds to applying the equations of motion (EoM) obtained from the renormalizable Lagrangian $\mathcal{L}_0$. Let us briefly prove this point. Consider an EFT

$$\mathcal{L}_{\text{EFT}} = \mathcal{L}_0(\phi, \partial_\mu \phi) + \frac{1}{\Lambda^2}\mathcal{L}_6(\phi, \partial_\mu \phi) + \mathcal{O}(\Lambda^{-4}) \ , \tag{2.2}$$

where ϕ is some generic field with given quantum numbers, and consider the field redefinition

$$\phi' = \phi + \frac{\alpha}{\Lambda^2}\delta\phi \ , \tag{2.3}$$

where α is an order 1 coefficient and $\delta\phi$ is some generic *current* of dimension $[\delta\phi] = 2 + [\phi]$ and with the same quantum numbers as ϕ [2]. Under eq. (2.3) the Lagrangian becomes

$$\begin{aligned}\mathcal{L}_{\text{EFT}}(\phi', \partial_\mu \phi') &= \mathcal{L}_0(\phi, \partial_\mu \phi) + \frac{1}{\Lambda^2}\left(\mathcal{L}_6(\phi, \partial_\mu \phi) + \frac{\delta\mathcal{L}_0}{\delta\phi}\delta\phi + \frac{\delta\mathcal{L}_0}{\delta\partial_\mu\phi}\delta\partial_\mu\phi\right) + \mathcal{O}(\Lambda^{-4}) = \\ &= \mathcal{L}_{\text{EFT}}(\phi, \partial_\mu \phi) - \frac{1}{\Lambda^2}\left(\partial_\mu \frac{\delta\mathcal{L}_0}{\delta\partial_\mu\phi} - \frac{\delta\mathcal{L}_0}{\delta\phi}\right)\delta\phi + \mathcal{O}(\Lambda^{-4}) \ , \end{aligned} \tag{2.4}$$

where we neglected contributions suppressed by more powers of Λ. The last term in the second line is an operator of dimension 6 which vanishes upon the EoM. Since physics has to be independent of any such field redefinition, they, or equivalently EoM, can be used to obtain relations between different dim-6 operators. Something to be noticed is that operators generated by such field redefinitions are necessarily constructed as a product of two separate currents, each with spin ≤ 1 (since we do not consider fields with spin greater than 1). We call this class as *(current) $\times$ (current)* (CC) operators. It is useful to notice here that field redefinitions always take CC operators into operators in this same class. More details on the field redefinitions and their effects on SM dim-6 operators are reported in appendix A.2.

2.1.1   Our choice of basis

While in principle any basis is equally viable for the study of the phenomenology of dim-6 operators, some basis are better suited than others for studying some particular processes, or as low-energy description of given UV theories. From the UV point of view one could require

---

[2]Here by current we do not mean only some spin-1 operator, but any operator with the same quantum numbers as ϕ. In particular, if ϕ is a spin-1 field then the current will be a vector, if ϕ is a scalar then $\delta\phi$ is a scalar and, analogously, $\delta\phi$ is a fermionic current if ϕ is a spin-1/2 field.

that the operators have a clear connection with the UV dynamics. For example, it could be convenient to work in a basis in which operators generated when integrating out at tree-level the heavy degrees of freedom in a large class of theories (minimally coupled, renormalizable, weakly-interacting) are kept distinct from operators generated only at loop level, which are expected to have suppressed Wilson coefficients. An example of such basis is the one used in ref. [58], where the authors focus on the low-energy description of a wide class of strongly interacting light Higgs (SILH) models (containing also *composite Higgs models*), while the one used in ref. [57] does not classify operators into tree-level and loop ones.

From the phenomenological point of view, a good feature of the basis is to be able to describe as much clearly and univocally as possible some particular set of observables, for example dividing operators which are strongly constrained from weakly constrained ones, or at least by reducing as much as possible the strong correlations among coefficients. Since it is impossible to find a single basis which satisfies all these properties for any UV theory and any observable, a choice has to be made depending on the problem at hand.

Our choice of basis is motivated by the observables we are interested in, and the subset of operators we consider is defined by those which (in our basis) give a tree-level contribution to our set of observables. In this work, we shall be interested in EW observables, Higgs couplings to gauge bosons and QCD observables involving gluons only and the relations among each other as imposed from the running between the scale of new physics to the weak scale. These include the four electroweak oblique pseudo-observables $\hat{S}$, $\hat{T}$, W and Y [59,60], the three triple gauge coupling observables g_1^Z, κ_γ and λ_γ, the Higgs couplings to vector bosons, a shift on the Higgs width, the gluon oblique parameter Z [60] and the anomalous triple gluon coupling parameter $\hat{c}_{3G}$. We describe these observables in more detail in section 2.3. For ealier systematic studies of the effects of higher-dimensional operators on these observables, see refs. [61, 62]. We have not included the Higgs decays to fermions in our list of observables. The only dim-6 operators contributing to these observables are $\mathcal{O}_{y_u}, \mathcal{O}_{y_d}$ and $\mathcal{O}_{y_e}$ (see definition in table 2.3)[3] and their RG effects have already been studied in ref. [65]. These are weakly constrained operators and new RG-induced constraints can be derived only if they contribute to the running of more strongly constrained operators. In ref. [65] it has been shown that there is no such contribution and therefore we do not include these operators in our analysis.

Our basis is also well suited to study universal new physics scenarios, that is models (e.g. composite Higgs models) in which the most important effects induce universal couplings of the

---

[3]The flat direction [63] between the operators $\mathcal{O}_{y_u}, \mathcal{O}_{BB}$ and $\mathcal{O}_{GG}$ from the measurements of Higgs couplings to photons and gluons is lifted by considering the (still loose) upper limit on the cross section production of a Higgs boson in association with a pair of top-antitop quarks [64]. Stronger bounds on the Wilson coefficients of $\mathcal{O}_{BB}$ and $\mathcal{O}_{GG}$ can be obtained by imposing some theoretical priors on the value of the Wilson coefficient of $\mathcal{O}_{y_u}$ but we did not consider these stronger bounds here and we can safely ignore the operator $\mathcal{O}_{y_u}$ in our analysis.

fermions to the SM gauge fields, like in the SILH case [58]. A first phenomenological study of some EW observables in the context of dim-6 operators, assuming universal new physics, was performed in refs. [66, 67].

In this context, NP effects can be described by the subset of 14 operators made of SM bosons listed in table 2.1, which we will denote in the following as *bosonic operators*. These operators can also efficiently parametrize dim-6 contributions to the observables specified above and therefore we include them in the basis. The basis therefore contains a total of 14 CP-even bosonic operators, notice however that $\mathcal{O}_6$ does not contribute to any of the observables we are interested in, neither at tree-level nor by RG running [65]; it contributes instead to the Higgs self-coupling which however is still not directly measured. For this reason we did not include this observable in our list and did not compute its RG scaling. The operators in table 2.1 have been grouped in two different categories, corresponding to operators of the CC form (left box) and operators which are not products of SM currents (right box). As discussed above, the CC operators can be related to each other and to other fermionic CC operators using the SM EoM or, equivalently, by performing field redefinitions. This means that one has to be careful in choosing the other operators in the basis to ensure that there are no redundancies. These relationships provide an important consistency check on the anomalous dimension matrix, which is discussed in ref. [4].

To this set of operators we add the 6 CP-odd counterparts of the bosonic operators, as listed in table 2.2. The rest of the basis is a small variation of the one adopted in ref. [65] where, from the ones in table 2 therein, using field redefinitions we trade the four-fermions operators of the first family $\{\mathcal{O}_{RR}^{(8)u_1d_1}, \mathcal{O}_{LL}^{(3)\,l_1}, \mathcal{O}_{RR}^{e_1}\}$ for $\{\mathcal{O}_{2G}, \mathcal{O}_{2W}, \mathcal{O}_{2B}\}$ and the Higgs-lepton operators of the first family $\{\mathcal{O}_L^{(3)\,l_1}, \mathcal{O}_R^{e_1}\}$ in favor of the ones in table 2.1. The remaining operators of our basis are listed in table 2.3. The conventions in tables 2.1, 2.2, 2.3 and in the rest of the text are as follows: $D_\rho W_{\mu\nu}^a = \partial_\rho W_{\mu\nu}^a + g\epsilon^{abc}W_\rho^b W_{\mu\nu}^c$ and $H^\dagger \overset{\leftrightarrow}{D}_\mu H \equiv H^\dagger D_\mu H - (D_\mu H)^\dagger H$, where $D_\mu H$ is defined below eq. (1.7).

Let us comment on other bases of common use in the literature. The set of operators

$$\{\mathcal{O}_W, \mathcal{O}_B, \mathcal{O}_{WW}, \mathcal{O}_{WB}, \mathcal{O}_{BB}\} \tag{2.5}$$

is in one-to-one correspondence with the operators used in ref. [67]

$$\{\mathcal{O}_{HW}, \mathcal{O}_{HB}, \mathcal{O}_{WW}, \mathcal{O}_{WB}, \mathcal{O}_{BB}\}\,, \tag{2.6}$$

where $\mathcal{O}_{HW} \equiv ig(D^\mu H)^\dagger \sigma^a (D^\nu H)W_{\mu\nu}^a$, $\mathcal{O}_{HB} \equiv ig'(D^\mu H)^\dagger(D^\nu H)B_{\mu\nu}$, and with the ones used in ref. [58]

$$\{\mathcal{O}_W, \mathcal{O}_B, \mathcal{O}_{HW}, \mathcal{O}_{HB}, \mathcal{O}_{BB}\}\,. \tag{2.7}$$

$$\mathcal{O}_H = \tfrac{1}{2}(\partial^\mu |H|^2)^2$$

$$\mathcal{O}_T = \tfrac{1}{2}\left(H^\dagger \overset{\leftrightarrow}{D}_\mu H\right)^2$$

$$\mathcal{O}_6 = \lambda |H|^6$$

$$\mathcal{O}_W = ig/2\left(H^\dagger \sigma^a \overset{\leftrightarrow}{D}^\mu H\right) D^\nu W_{\mu\nu}^a$$

$$\mathcal{O}_B = ig' Y_H \left(H^\dagger \overset{\leftrightarrow}{D}^\mu H\right) \partial^\nu B_{\mu\nu}$$

$$\mathcal{O}_{2W} = -\tfrac{1}{2}(D^\mu W_{\mu\nu}^a)^2$$

$$\mathcal{O}_{2B} = -\tfrac{1}{2}(\partial^\mu B_{\mu\nu})^2$$

$$\mathcal{O}_{2G} = -\tfrac{1}{2}(D^\mu G_{\mu\nu}^A)^2$$

$$\mathcal{O}_{BB} = g'^2 |H|^2 B_{\mu\nu} B^{\mu\nu}$$

$$\mathcal{O}_{WB} = gg' H^\dagger \sigma^a H W_{\mu\nu}^a B^{\mu\nu}$$

$$\mathcal{O}_{WW} = g^2 |H|^2 W_{\mu\nu}^a W^{a\mu\nu}$$

$$\mathcal{O}_{GG} = g_s^2 |H|^2 G_{\mu\nu}^A G^{A\mu\nu}$$

$$\mathcal{O}_{3W} = \tfrac{1}{3!} g\epsilon_{abc} W_\mu^{a\,\nu} W_{\nu\rho}^b W^{c\,\rho\mu}$$

$$\mathcal{O}_{3G} = \tfrac{1}{3!} g_s f_{ABC} G_\mu^{A\,\nu} G_{\nu\rho}^B G^{C\,\rho\mu}$$

Table 2.1: The 14 CP-even operators made of SM bosons. The operators have been grouped in two different categories corresponding to (current) $\times$ (current) ones (left box) and operators which are not products of SM currents (right box).

$$\mathcal{O}_{B\widetilde{B}} = g'^2 |H|^2 B_{\mu\nu} \widetilde{B}^{\mu\nu}$$

$$\mathcal{O}_{W\widetilde{B}} = gg' H^\dagger \sigma^a H W_{\mu\nu}^a \widetilde{B}^{\mu\nu}$$

$$\mathcal{O}_{W\widetilde{W}} = g^2 |H|^2 W_{\mu\nu}^a \widetilde{W}^{a\mu\nu}$$

$$\mathcal{O}_{G\widetilde{G}} = g_s^2 |H|^2 G_{\mu\nu}^A \widetilde{G}^{A\mu\nu}$$

$$\mathcal{O}_{3\widetilde{W}} = \tfrac{1}{3!} g\epsilon_{abc} \widetilde{W}_\mu^{a\,\nu} W_{\nu\rho}^b W^{c\,\rho\mu}$$

$$\mathcal{O}_{3\widetilde{G}} = \tfrac{1}{3!} g_s f_{ABC} \widetilde{G}_\mu^{A\,\nu} G_{\nu\rho}^B G^{C\,\rho\mu}$$

Table 2.2: The 6 CP-odd operators made of SM bosons.

The relations between these operators are simply obtained from integration by parts and read

$$\mathcal{O}_W = \mathcal{O}_{HW} + \frac{1}{4}(\mathcal{O}_{WW} + \mathcal{O}_{WB}) ,$$

$$\mathcal{O}_B = \mathcal{O}_{HB} + \frac{1}{4}(\mathcal{O}_{WB} + \mathcal{O}_{BB}) .$$

$$(2.8)$$

From this relation it is clear that the two particular linear combinations of not-CC operators in the r.h.s. reconstruct two CC operators, even if no operator of this kind is present in the subset, as in the case of eq. (2.6) [67]. Since in a wide class of NP models CC operators can arise at tree-level while the not-CC ones can only be generated at loop level, it might be desirable to work in a basis which keeps this separation explicit, as in our basis, eq. (2.5), or the SILH one, eq.(2.7). Our basis has a further advantage that the anomalous dimension matrix of the sector $\{\mathcal{O}_B, \mathcal{O}_W\} \times \{\mathcal{O}_{BB}, \mathcal{O}_{WB}, \mathcal{O}_{WW}\}$ is block diagonal [68]. As the SILH basis [58], our basis also separates the operators generated at tree-level from the ones obtained at the radiative level only, when the new physics degrees of freedom, assumed to be weakly coupled, are integrated out [68]. When the Higgs emerges as pseudo Nambu–Goldstone boson, the SILH basis further

$$\mathcal{O}_{y_u} = y_u |H|^2 \bar{Q}_L \widetilde{H} u_R \qquad\qquad \mathcal{O}_{y_d} = y_d |H|^2 \bar{Q}_L H d_R$$

$$\mathcal{O}_{y_e} = y_e |H|^2 \bar{L}_L H e_R$$

$$\mathcal{O}_L^q = (iH^\dagger \overleftrightarrow{D}_\mu H)(\bar{Q}_L \gamma^\mu Q_L) \qquad\qquad \mathcal{O}_R^u = (iH^\dagger \overleftrightarrow{D}_\mu H)(\bar{u}_R \gamma^\mu u_R)$$

$$\mathcal{O}_L^{(3)\,q} = (iH^\dagger \sigma^a \overleftrightarrow{D}_\mu H)(\bar{Q}_L \gamma^\mu \sigma^a Q_L) \qquad\qquad \mathcal{O}_R^d = (iH^\dagger \overleftrightarrow{D}_\mu H)(\bar{d}_R \gamma^\mu d_R)$$

$$\mathcal{O}_L^l = (iH^\dagger \overleftrightarrow{D}_\mu H)(\bar{L}_L \gamma^\mu L_L)$$

$$\mathcal{O}_R^{ud} = y_u^\dagger y_d (i\widetilde{H}^\dagger \overleftrightarrow{D}_\mu H)(\bar{u}_R \gamma^\mu d_R)$$

$$\mathcal{O}_{LR}^u = (\bar{Q}_L \gamma^\mu Q_L)(\bar{u}_R \gamma_\mu u_R) \qquad\qquad \mathcal{O}_{LR}^d = (\bar{Q}_L \gamma^\mu Q_L)(\bar{d}_R \gamma_\mu d_R)$$

$$\mathcal{O}_{LR}^{(8)\,u} = (\bar{Q}_L \gamma^\mu T^A Q_L)(\bar{u}_R \gamma_\mu T^A u_R) \qquad\qquad \mathcal{O}_{LR}^{(8)\,d} = (\bar{Q}_L \gamma^\mu T^A Q_L)(\bar{d}_R \gamma_\mu T^A d_R)$$

$$\mathcal{O}_{RR}^u = (\bar{u}_R \gamma^\mu u_R)(\bar{u}_R \gamma_\mu u_R) \qquad\qquad \mathcal{O}_{RR}^d = (\bar{d}_R \gamma^\mu d_R)(\bar{d}_R \gamma_\mu d_R)$$

$$\mathcal{O}_{LL}^q = (\bar{Q}_L \gamma^\mu Q_L)(\bar{Q}_L \gamma_\mu Q_L) \qquad\qquad \mathcal{O}_{LR}^e = (\bar{L}_L \gamma^\mu L_L)(\bar{e}_R \gamma_\mu e_R)$$

$$\mathcal{O}_{LL}^{(8)\,q} = (\bar{Q}_L \gamma^\mu T^A Q_L)(\bar{Q}_L \gamma_\mu T^A Q_L)$$

$$\mathcal{O}_{LL}^{ql} = (\bar{Q}_L \gamma^\mu Q_L)(\bar{L}_L \gamma_\mu L_L) \qquad\qquad \mathcal{O}_{RR}^{ud} = (\bar{u}_R \gamma^\mu u_R)(\bar{d}_R \gamma_\mu d_R)$$

$$\mathcal{O}_{LL}^{(3)\,ql} = (\bar{Q}_L \gamma^\mu \sigma^a Q_L)(\bar{L}_L \gamma_\mu \sigma^a L_L) \qquad\qquad \mathcal{O}_{RR}^{ue} = (\bar{u}_R \gamma^\mu u_R)(\bar{e}_R \gamma_\mu e_R)$$

$$\mathcal{O}_{LR}^{qe} = (\bar{Q}_L \gamma^\mu Q_L)(\bar{e}_R \gamma_\mu e_R) \qquad\qquad \mathcal{O}_{RR}^{de} = (\bar{d}_R \gamma^\mu d_R)(\bar{e}_R \gamma_\mu e_R)$$

$$\mathcal{O}_{LR}^{lu} = (\bar{L}_L \gamma^\mu L_L)(\bar{u}_R \gamma_\mu u_R) \qquad\qquad \mathcal{O}_{LR}^{ld} = (\bar{L}_L \gamma^\mu L_L)(\bar{d}_R \gamma_\mu d_R)$$

$$\mathcal{O}_{y_u y_d} = y_u y_d (\bar{Q}_L^r u_R)\epsilon_{rs}(\bar{Q}_L^s d_R) \qquad\qquad \mathcal{O}_{y_u y_d}^{(8)} = y_u y_d (\bar{Q}_L^r T^A u_R)\epsilon_{rs}(\bar{Q}_L^s T^A d_R)$$

$$\mathcal{O}_{y_u y_e} = y_u y_e (\bar{Q}_L^r u_R)\epsilon_{rs}(\bar{L}_L^s e_R) \qquad\qquad \mathcal{O}'_{y_u y_e} = y_u y_e (\bar{Q}_L^{r\,\alpha} e_R)\epsilon_{rs}(\bar{L}_L^s u_R^\alpha)$$

$$\mathcal{O}_{y_e y_d} = y_e y_d^\dagger (\bar{L}_L e_R)(\bar{d}_R Q_L)$$

$$\mathcal{O}_{DB}^u = y_u \bar{Q}_L \sigma^{\mu\nu} u_R \, \widetilde{H} g' B_{\mu\nu} \qquad\qquad \mathcal{O}_{DW}^u = y_u \bar{Q}_L \sigma^{\mu\nu} u_R \, \sigma^a \widetilde{H} g W^a_{\mu\nu}$$

$$\mathcal{O}_{DB}^d = y_d \bar{Q}_L \sigma^{\mu\nu} d_R \, H g' B_{\mu\nu} \qquad\qquad \mathcal{O}_{DW}^d = y_d \bar{Q}_L \sigma^{\mu\nu} d_R \, \sigma^a H g W^a_{\mu\nu}$$

$$\mathcal{O}_{DB}^e = y_e \bar{L}_L \sigma^{\mu\nu} e_R \, H g' B_{\mu\nu} \qquad\qquad \mathcal{O}_{DW}^e = y_e \bar{L}_L \sigma^{\mu\nu} e_R \, \sigma^a H g W^a_{\mu\nu}$$

$$\mathcal{O}_{DG}^u = y_u \bar{Q}_L \sigma^{\mu\nu} T^A u_R \, \widetilde{H} g_s G^A_{\mu\nu} \qquad\qquad \mathcal{O}_{DG}^d = y_d \bar{Q}_L \sigma^{\mu\nu} T^A d_R \, H g_s G^A_{\mu\nu}$$

Table 2.3: 39 operators made of one-family of SM fermions. The upper box contains operators in the CC class while the lower one does not. Dashed lines separate operators of different structure.

makes the distinction between a loop involving new-physics interactions and a loop involving SM interactions only.

In this study we limit ourselves to the set, $\mathcal{B}_1$, of 13 operators appearing in table 2.1 (omitting $\mathcal{O}_6$ that does not contribute directly to the 13 physical observables we are studying). We compute the running of $\mathcal{B}_1$ into $\mathcal{B}_1$. If the remaining set of independent operators, needed to complete the basis specified above, is denoted by $\mathcal{B}_2$, there could also be *i)* a running of $\mathcal{B}_2$ into $\mathcal{B}_1$, *ii)* a running of $\mathcal{B}_1$ into $\mathcal{B}_2$ and of course *iii)* a running of $\mathcal{B}_2$ into itself. The first effect would reflect itself in new RG contributions to our list of low-energy observables; under our hypothesis of no-tuning (or no correlations) among the different RG contributions these effects do not change our RG-induced bounds on the operators in $\mathcal{B}_1$. In principle new RG-induced bounds on some operators in $\mathcal{B}_2$ could be obtained, however we already commented on the fact that this is not the case for $\mathcal{O}_6$ and $\mathcal{O}_{y_{u,d,e}}$. The second effect could, in principle, allow us to obtain new RG-induced bound on the operators in $\mathcal{B}_1$ via the mixing to some tightly constrained operators in $\mathcal{B}_2$, for example via the mixing to $\mathcal{O}_L$ and $\mathcal{O}_{LL}^{12}$, as we mentioned above. The study of these effects would be an interesting generalization of our ideas but would require the computation of the full anomalous dimension matrix and a complete phenomenological analysis of all the observables relevant to the dimension-6 operators, which is beyond the purpose of this work.

2.2   Scaling of the Wilson coefficients

In general, quantum effects mix all the operators among themselves when going from the scale of new physics down to the scale at which the experimental measurements are performed. However, the 3 operators with gluons, $\mathcal{O}_{GG}, \mathcal{O}_{2G}$ and $\mathcal{O}_{3G}$, constitute a separate sector that does not mix with the other 11 bosonic operators at one-loop.[4] So, even if $\mathcal{O}_{GG}$ affects Higgs physics by controlling the dominant production mode of the Higgs boson at the LHC, it can be treated separately from the 3 other Higgs observables we are interested in here. Furthermore, since the Higgs self-interactions have not been measured yet, and since $\mathcal{O}_6$ does not enter into the anomalous dimensions of any dim-6 operator other than itself, it can also be omitted from our analysis. For the Higgs and EW sector RG study, we can thus restrict to the following set of 10 dim-6 operators and compute the corresponding anomalous dimension matrix

$$\{\mathcal{O}_H, \mathcal{O}_T, \mathcal{O}_B, \mathcal{O}_W, \mathcal{O}_{2B}, \mathcal{O}_{2W}, \mathcal{O}_{BB}, \mathcal{O}_{WW}, \mathcal{O}_{WB}, \mathcal{O}_{3W}\} \ . \tag{2.9}$$

We include all the one-loop contributions proportional to c_i and depending on

$$\{g', g, g_s, \lambda, y_t\} \ , \tag{2.10}$$

---

[4]The only exception is a contribution from $\mathcal{O}_{2B}$ to the RG of $\mathcal{O}_{2G}$, see table 2.7. This mixing, however, is phenomenologically not very relevant since the Wilson coefficient of $\mathcal{O}_{2B}$ is strongly constrained, as we show in section 2.4.1.

where y_t is the Yukawa coupling of the top quark, i.e. we neglect the contributions proportional to the Yukawas of the light fermions ($y_b/y_t \sim 0.02$, y_b is the bottom quark Yukawa) and the other SM couplings are normalised as in chapter 1 (eqs. (1.3,1.6,1.7,1.8,1.14)).

We regularized the loop integrals using dimensional regularisation and used $\overline{\text{MS}}$ subtraction scheme. We performed the computation in the unbroken phase of the SM and in the background field gauge, with the gauge fixing term

$$\mathcal{L}^{g.f.} = -\frac{1}{2\xi_A}(D_\mu^{(A)}\delta A^{a\mu})^2\,, \tag{2.11}$$

where $\delta A = \{\delta B, \delta W, \delta G\}$ is the quantum field with respect to which the dim ≥ 4 SM action is path-integrated and $D_\mu^{(A)}$ is the covariant derivative with respect to the corresponding background field $A = \{B, W, G\}$.

In table 2.4, we give the one-loop anomalous dimensions of the operators of eq. (2.9), in the basis defined in section 2.1.1.[5] We have defined

$$\gamma_{c_i} = 16\pi^2 \frac{dc_i}{d\log\mu}\,. \tag{2.12}$$

A common effect encountered while computing the RG scaling of the above operators is the appearance of counter-terms which correspond to dim-6 operators that are not in our basis [65]. These radiatively-generated redundant operators need to be redefined into operators present in our basis. Upon redefinition, these redundant operators contribute to the anomalous dimensions of the operators in our basis at the same order as other direct contributions coming from one-particle-irreducible graphs. For details on the radiatively generated operators and how we deal with the redundant ones see appendix A.2. Notice that the matrices of table 2.4 already contain these indirect effects. This ensures that the result is gauge invariant and indeed we checked that the result is independent of the gauge fixing parameters ξ_A of eq. (2.11).

Some parts of the anomalous dimension matrix presented here have been calculated in previous literature [65–76]. In some cases these previous computations use methods different from ours, but we find complete agreement in the final results. A detailed comparison with previous literature, including a discussion about the difference in the methods is presented in ref. [4].

2.3 Electroweak, Higgs and gluon observables

Let us now apply the general formulas of the previous section to the electroweak, Higgs and gluon observables we want to constrain. In section 2.1.1 we have considered 10 EW and Higgs operators

$$\mathcal{O}_H,\ \mathcal{O}_T,\ \mathcal{O}_W,\ \mathcal{O}_B,\ \mathcal{O}_{2W},\ \mathcal{O}_{2B},\ \mathcal{O}_{WW},\ \mathcal{O}_{WB},\ \mathcal{O}_{BB},\ \mathcal{O}_{3W}, \tag{2.13}$$

---

[5]The self-renormalization of c_{3W} has been extracted from the computation of refs. [69,70], where the authors calculated the one of c_{3G}.

	c_H	c_T
γ_{c_H}	$-\frac{9}{2}g^2 - 3g'^2 + 24\lambda + 12y_t^2$	$-9g^2 + \frac{9}{2}g'^2 + 12\lambda$
γ_{c_T}	$\frac{3}{2}g'^2$	$\frac{9}{2}g^2 + 12\lambda + 12y_t^2$
γ_{c_B}	$-\frac{1}{3}$	$-\frac{5}{3}$
γ_{c_W}	$-\frac{1}{3}$	$-\frac{1}{3}$
other γ_{c_i}'s	0 or $\mathcal{O}(y_l)$	0 or $\mathcal{O}(y_l)$

	c_B	c_W	c_{2B}	c_{2W}
γ_{c_H}	$-\frac{9}{4}g'^2(g'^2 - 2g^2) - 6\lambda g'^2$	$\frac{9}{4}g^2(2g'^2 - g^2) - 36\lambda g^2$	$-\frac{141}{16}g'^4 + 3g'^2\lambda$	$\frac{63}{8}g^4 + \frac{51}{16}g^2 g'^2 + 18\lambda g^2$
γ_{c_T}	$-\frac{9}{4}g'^2 g^2 - 6\lambda g'^2$	$-\frac{9}{4}g'^2 g^2$	$3g'^4 + \frac{9}{8}g'^2 g^2 + 3\lambda g'^2$	$\frac{9}{8}g'^2 g^2$
γ_{c_B}	$\frac{g'^2}{6} + 6y_t^2$	$\frac{g^2}{2}$	$\frac{59}{4}g'^2$	$-\frac{g^2}{4}$
γ_{c_W}	$\frac{g'^2}{6}$	$\frac{17}{2}g^2 + 6y_t^2$	$\left(\frac{29}{8} - \frac{53g'^2}{4g^2}\right)g'^2$	$\frac{79}{8}g^2 + \frac{29}{4}g'^2$
$\gamma_{c_{2B}}$	$-\frac{2}{3}g'^2$	0	$\frac{94}{3}g'^2$	0
$\gamma_{c_{2W}}$	0	$-\frac{2}{3}g^2$	$\left(\frac{53}{12} - \frac{53g'^2}{4g^2}\right)g'^2$	$\frac{331}{12}g^2 + \frac{29}{4}g'^2$
$\gamma_{c_{BB}}$	0	0	0	0
$\gamma_{c_{WW}}$	0	0	0	0
$\gamma_{c_{WB}}$	0	0	0	0
$\gamma_{c_{3W}}$	0	0	0	0

	c_{BB}	c_{WW}	c_{WB}	c_{3W}
γ_{c_H}	0	0	0	0
γ_{c_T}	0	0	0	0
γ_{c_B}	0	0	0	0
γ_{c_W}	0	0	0	0
$\gamma_{c_{2B}}$	0	0	0	0
$\gamma_{c_{2W}}$	0	0	0	0
$\gamma_{c_{BB}}$	$\frac{g'^2}{2} - \frac{9g^2}{2} + 6y_t^2 + 12\lambda$	0	$3g^2$	0
$\gamma_{c_{WW}}$	0	$-\frac{3g'^2}{2} - \frac{5g^2}{2} + 6y_t^2 + 12\lambda$	g'^2	$\frac{5}{2}g^2$
$\gamma_{c_{WB}}$	$2g'^2$	$2g^2$	$-\frac{g'^2}{2} + \frac{9g^2}{2} + 6y_t^2 + 4\lambda$	$-\frac{g^2}{2}$
$\gamma_{c_{3W}}$	0	0	0	$\frac{53}{3}g^2$

Table 2.4: Anomalous dimension matrix for the Wilson coefficients of the dim-6 bosonic operators, in the basis defined in section 2.1.

and three more operators involving gluons, $\mathcal{O}_{2G}$, $\mathcal{O}_{3G}$, $\mathcal{O}_{GG}$, to parametrize BSM corrections to the SM Lagrangian. The set of pseudo-observables, briefly mentioned in section 2.1.1, that constrain all these operators include the four electroweak oblique parameters $\hat{S}$, $\hat{T}$, Y and W [59, 60], constrained by LEP 1 and LEP 2, the four anomalous triple gauge coupling (TGC) g_1^Z, κ_γ, λ_γ and $\hat{c}_{3G}$, the oblique gluon Z parameter [60] and four observables related to Higgs physics: the gluon-gluon production rate, the decays to $\gamma\gamma$ and γZ and a universal rescaling of all the branching ratios [58].

In general, these observables receive contributions from a particular linear combination of the dim-6 operator's Wilson coefficients, suitably multiplied by the SM couplings:

$$(\text{obs})_i = \kappa_i + \omega_{ij}c_j \equiv \kappa_i + \hat{c}_i \quad \to \quad \delta(\text{obs})_i = \hat{c}_i \ , \tag{2.14}$$

where κ_i is the SM contribution, the c_k's are the Wilson coefficients and ω_{ij} is a matrix containing the SM couplings and ratios of scales ($\omega \sim \mathcal{O}(m_W^2/\Lambda^2)$). We defined $\hat{c}_i$ as the linear combinations of the Wilson coefficients which contribute directly to each observable $(\text{obs})_i$ and we shall refer to them in the following as *observable couplings*, with a slight abuse of language. If the new combinations $\hat{c}_i$ are independent, this corresponds to a change of basis such that to each operator corresponds an observable; we shall call this the *observable basis*. To derive the RG-induced constraints on these observables we therefore first need to relate them to the operators in eq. (2.13), that is define the transformation matrix, ω_{ij}, from the basis in eq. (2.13) to the observable basis. Another possible basis strictly related to the observables which provide the strongest constraints on dim-6 operators has recently been introduced in ref. [77].

As an example, consider the process $h \to \gamma Z$ which receives a contribution from the SM (in this case at one loop) as well as a direct contribution from a linear combination of the dim-6 operators. We parametrize this contribution with the *observable coupling* $\hat{c}_{\gamma Z}$, to be defined in eq. (2.27), which is related to the Wilson coefficients of our basis as (c_{θ_W} and s_{θ_W} are respectively the sinus and cosinus of the weak mixing angle θ_W)

$$\hat{c}_{\gamma Z} = \frac{m_W^2}{\Lambda^2} \left(2c_{\theta_W}^2 c_{WW} - 2s_{\theta_W}^2 c_{BB} - (c_{\theta_W}^2 - s_{\theta_W}^2)c_{WB} \right) \ . \tag{2.15}$$
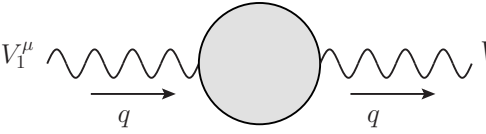
The above relation defines the coefficients $\omega_{\gamma Z,j}$ for this particular observable. Let us now describe in detail all the observables mentioned above, and the relations with the Wilson coefficients of the dim-6 operators.

2.3.1 EW oblique parameters

We begin with the electroweak precision observables constrained by measurements at LEP1, LEP2 and Tevatron. The first step of the analysis is to fix the SM parameters g, g' and v by the three most precise measurements: the Fermi constant G_F from muon decay, the fine-structure constant α_{em} and the Z-boson mass m_Z. With the input parameters fixed, the SM gives

predictions for observables such as Z-pole measurements at LEP 1, the Tevatron measurement of the W-mass and LEP 2 measurements of the $e^+e^- \to f^+f^-$ cross-sections. New physics can affect this analysis by either changing the relationship between the input parameters g, g' and v to the measurement of G_F, α_{em} and m_Z or by directly contributing to the other measurements (see e.g. ref. [64]).

In universal theories some of the most important deviations from the SM reside in the vacuum polarization amplitudes $\Pi_{V_1V_2}(q^2)$ of the SM gauge bosons ($V_1V_2 = \{W^+W^-, W^3W^3, W^3B, BB\}$),

$$V_1^\mu \sim\!\!\sim\!\!\sim \bigcirc \sim\!\!\sim\!\!\sim V_2^\nu \quad = i\Pi_{V_1V_2}(q^2)\eta^{\mu\nu} + (q^\mu q^\nu \text{ terms}) , \qquad (2.16)$$

which can also be read from the effective Lagrangian in momentum space

$$\mathcal{L}_{eff} = \frac{\eta^{\mu\nu}}{2}\left(2\Pi_{W^+W^-}W_\mu^+W_\nu^- + \Pi_{W^3W^3}W_\mu^3W_\nu^3 + 2\Pi_{W^3B}W_\mu^3B_\nu + \Pi_{BB}B_\mu B_\nu\right) + (q^\mu q^\nu \text{ terms}) , \tag{2.17}$$

Assuming a heavy new-physics scale we can expand these amplitudes for small momentum $q^2 \ll \Lambda_{NP}^2$, obtaining

$$\Pi_{V_1V_2}(q^2) = \Pi_{V_1V_2}(0) + q^2\Pi'_{V_1V_2}(0) + \frac{q^4}{2}\Pi''_{V_1V_2}(0) + \dots , \tag{2.18}$$

where $\Pi'_{V_1V_2}(0) = d\Pi_{V_1V_2}(q^2)/dq^2|_{q^2=0}$ and so forth. At these order in the expansion in q^2 there are 12 coefficients. Of these, three enter in the definition of the EW gauge couplings and the Higgs VEV ,

$$1 = -\Pi'_{W^+W^-}(0) , \qquad 1 = -\Pi'_{BB}(0) , \qquad \frac{v^2g^2}{4} = \Pi_{W^+W^-}(0) , \tag{2.19}$$

and two more relations come from the QED Ward identity:

$$\Pi_{W^3B}(0) = \Pi_{BB}(0) = 0 . \tag{2.20}$$

This leaves 7 free parameters $\hat{S}, \hat{T}, \hat{U}, V, X, Y, W$ [60], defined as [6]

$$\hat{T} = -\frac{1}{m_W^2}\left(\Pi_{W^3W^3}(0) - \Pi_{W^+W^-}(0)\right) \qquad \hat{S} = -\frac{g}{g'}\Pi'_{W^3B}(0)$$

$$Y = -\frac{m_W^2}{2}\Pi''_{BB}(0) \qquad W = -\frac{m_W^2}{2}\Pi''_{W^3W^3}(0)$$

$$\hat{U} = \left(\Pi'_{W^3W^3}(0) - \Pi'_{W^+W^-}(0)\right) \qquad X = -\frac{m_W^2}{2}\Pi''_{W^3B}(0)$$

$$V = -\frac{m_W^2}{2}\left(\Pi''_{W^3W^3}(0) - \Pi''_{W^+W^-}(0)\right) . \tag{2.22}$$

---

[6]For convenience, we report here the relation between the $\hat{S}, \hat{T}, \hat{U}$ [60] and the Peskin-Takeuchi S, T, U [59] parameters:

$$S = \frac{16\pi}{g^2}\hat{S} , \qquad T = \frac{4\pi}{g^2 s_{\theta_W}^2}\hat{T} \qquad U = -\frac{16\pi}{g^2}\hat{U} . \tag{2.21}$$

$\hat{T}$ is also related to the ρ parameter introduced in eq. (1.18) by $\rho = (1-\hat{T})^{-1} \simeq 1+\hat{T}$. In the EFT approach, only the four $\hat{S}$, $\hat{T}$, W and Y parameters are generated by dim-6 operators, while the remaining ones are generated by dimension-8 (or higher) terms. In terms of a phenomenological effective Lagrangian these four can be described by

$$\Delta\mathcal{L}_{\text{EWPT}} = -\hat{T}\frac{m_Z^2}{2}Z_\mu Z^\mu - \frac{\hat{S}}{4m_W^2}\frac{gg'v^2}{2}(W_{\mu\nu}^3 B^{\mu\nu}) - \frac{W}{2m_W^2}(\partial^\mu W_{\mu\nu}^3)^2 - \frac{Y}{2m_W^2}(\partial^\mu B_{\mu\nu})^2. \quad (2.23)$$

The contribution of the Wilson coefficients of the operator set in eq. (2.13) to the above observables is

$$\hat{T} = \hat{c}_T(m_W) = \frac{v^2}{\Lambda^2}c_T(m_W)\,, \quad \hat{S} = \hat{c}_S(m_W) = \frac{m_W^2}{\Lambda^2}\left[c_W(m_W) + c_B(m_W) + 4c_{WB}(m_W)\right],$$

$$Y = \hat{c}_Y(m_W) = \frac{m_W^2}{\Lambda^2}c_{2B}(m_W)\,, \qquad W = \hat{c}_W(m_W) = \frac{m_W^2}{\Lambda^2}c_{2W}(m_W)\,. \quad (2.24)$$

The above oblique parameters have been measured very precisely and are constrained at the per-mil level. We present the 95 % CL bounds on these parameters in table 2.5.

2.3.2 Anomalous triple gauge couplings

A second set of independent measurements that constrain the operator set in eq. (2.13) are the TGC that were measured in the $e^+e^- \to W^+W^-$ process at LEP2. The standard phenomenological Lagrangian used to describe deviations in the TGC observables, from their SM values, is [78, 79]

$$\begin{aligned}
\Delta\mathcal{L}_{3V} &= ig\, g_1^Z c_{\theta_W} Z^\mu \left(W^{+\nu}\hat{W}_{\mu\nu}^- - W^{-\nu}\hat{W}_{\mu\nu}^+\right) + ig\left(\kappa_z c_{\theta_W}\hat{Z}^{\mu\nu} + \kappa_\gamma s_{\theta_W}\hat{A}^{\mu\nu}\right)W_\mu^+ W_\nu^- \\
&+ \frac{ig}{m_W^2}\left(\lambda_Z c_{\theta_W}\hat{Z}^{\mu\nu} + \lambda_\gamma s_{\theta_W}\hat{A}^{\mu\nu}\right)\hat{W}_\mu^{-\rho}\hat{W}_{\rho\nu}^+, \quad (2.25)
\end{aligned}$$

where $\hat{V}_{\mu\nu} = \partial_\mu V_\nu - \partial_\nu V_\mu$, the photon field $A_\mu = c_{\theta_W}B_\mu + s_{\theta_W}W_\mu^3$ has field-strength $\hat{A}_{\mu\nu}$, while $Z_\mu = c_{\theta_W}W_\mu^3 - s_{\theta_W}B_\mu$ has field-strength $\hat{Z}_{\mu\nu}$ and we use $s_{\theta_W} \equiv \sin\theta_W = g'/\sqrt{g^2 + g'^2}$, $c_{\theta_W} \equiv \cos\theta_W = g/\sqrt{g^2 + g'^2}$ and $e = gs_{\theta_W}$. Note that the above Lagrangian has only three independent parameters at the dim-6 level taken to be g_1^Z, κ_γ and λ_γ here; the other two can be expressed as : $\lambda_Z = \lambda_\gamma$ and $\kappa_Z = g_1^Z - t_{\theta_W}^2\kappa_\gamma$. These relations are a consequence of the accidental custodial symmetry that is preserved by the dim-6 operators entering in the TGC [80]. The SM contribution is given by $(g_1^Z)_{SM} = (\kappa_\gamma)_{SM} = 1$ and $(\lambda_Z)_{SM} = 0$. The corrections induced by the dim-6 operators in our basis are given by:

$$\delta g_1^Z \equiv \hat{c}_{gZ}(m_W) = -\frac{m_W^2}{\Lambda^2}\frac{1}{c_{\theta_W}^2}c_W(m_W)\,, \qquad \delta\kappa_\gamma \equiv \hat{c}_{\kappa\gamma}(m_W) = \frac{m_W^2}{\Lambda^2}4c_{WB}(m_W)\,,$$

$$\lambda_Z \equiv \hat{c}_{\lambda\gamma}(m_W) = -\frac{m_W^2}{\Lambda^2}c_{3W}(m_W)\,, \qquad (2.26)$$

where $\delta g_1^Z = g_1^Z - (g_1^Z)_{SM}$ and $\delta \kappa_\gamma = \kappa_\gamma - (\kappa_\gamma)_{SM}$. The constraints on these TGC observables are at the percent level (see table 2.5) and thus at least an order of magnitude weaker than the constraints on the electroweak parameters in eq. (2.24). Note that, for this reason, in eq. (2.26) we have ignored contributions to the $e^+e^- \to W^+W^-$ process from the couplings in eq. (2.23).

2.3.3 Higgs couplings

Higgs physics provides the three remaining observables for our observable basis. Indeed, operators in which the Higgs enters with the $|H|^2$ combination, like $\mathcal{O}_H$, $\mathcal{O}_{WW}$ and $\mathcal{O}_{BB}$ (also $\mathcal{O}_{GG}$, $\mathcal{O}_6$ and the $\mathcal{O}_{y_f}$ ones) can only give a physical effect, at tree level, in processes involving the Higgs boson, since otherwise they only provide an unphysical redefinition of the SM couplings [64]. We consider the branching ratios $h \to \gamma\gamma/Z\gamma$ and the correction to the Higgs kinetic term,

$$\Delta \mathcal{L}_{Higgs} \supset \frac{\hat{c}_H}{2}(\partial_\mu h)^2 + \frac{\hat{c}_{\gamma\gamma}e^2}{m_W^2}vh\hat{A}_{\mu\nu}\hat{A}^{\mu\nu} + \frac{\hat{c}_{\gamma Z}\, eg}{m_W^2 c_{\theta_W}}vh\hat{A}_{\mu\nu}\hat{Z}^{\mu\nu}. \tag{2.27}$$

The above coefficients, in terms of the dim-6 operator's Wilson coefficients are given by

$$\begin{aligned} \hat{c}_H(m_H) &= \frac{v^2}{\Lambda^2}c_H(m_H), \\ \hat{c}_{\gamma\gamma}(m_H) &= \frac{m_W^2}{\Lambda^2}\left(c_{BB}(m_H) + c_{WW}(m_H) - c_{WB}(m_H)\right), \\ \hat{c}_{\gamma Z}(m_H) &= \frac{m_W^2}{\Lambda^2}\left(2c_{\theta_W}^2 c_{WW}(m_H) - 2s_{\theta_W}^2 c_{BB}(m_H) - (c_{\theta_W}^2 - s_{\theta_W}^2)c_{WB}(m_H)\right). \end{aligned} \tag{2.28}$$

We present the constraints on these three observables in table 2.5. The coupling $\hat{c}_{\gamma\gamma}$ is constrained at the per mille level although the constraint on the SM diphoton width has been measured only with $\mathcal{O}(1)$ precision. This is because the SM width $\Gamma(h \to \gamma\gamma)$ is already one-loop suppressed and thus the current $\mathcal{O}(1)$ precision of the measurement corresponds to $\hat{c}_{\gamma\gamma} \approx 10^{-3}$. On the other hand, the correction to the Higgs kinetic term $\hat{c}_H$ is still poorly constrained. This is because $\hat{c}_H$ causes a universal shift in all the Higgs couplings and thus drops out from the branching ratios. Moreover, if only gluon fusion production channels are considered, the coupling c_{GG} mimics the effect of $\hat{c}_H$. Therefore, to disentangle the effect of c_{GG} and constrain $\hat{c}_H$, Higgs production cross-sections in different channels have to be compared; in particular the weakly sensitive vector-boson fusion (VBF) channels have to be considered.

2.3.4 Gluon observables

Let us now consider the observables sensitive to the bosonic operators that contain gluons, as defined in table 2.1:

$$\{\mathcal{O}_{2G},\ \mathcal{O}_{GG},\ \mathcal{O}_{3G}\}. \tag{2.29}$$

A first observable is the parameter Z, introduced in ref. [60] from the two point function of the gluon (analogous to the EW W and Y oblique parameters) as

$$Z = \frac{m_W^2}{2} \Pi_{GG}''(0) \ , \tag{2.30}$$

where the constant term of the expansion in q^2 for the gluon polarization amplitude is zero by gauge invariance (as for the photon) and the first-derivative term fixes the strong coupling constant. The Wilson coefficient c_{2G} can be put in one-to-one relation with Z,

$$Z = \frac{m_W^2}{\Lambda^2} c_{2G}. \tag{2.31}$$

A strong bound on this parameter has been obtained by an analysis of dijets events at LHC [81]:

$$-9 \times 10^{-4} \lesssim Z \lesssim 3 \times 10^{-4}. \tag{2.32}$$

A bound on c_{GG} can be obtained from the analysis of the Higgs production cross section at LHC. The relevant phenomenological Lagrangian is

$$\mathcal{L}_h \supset \hat{c}_{GG} \frac{hv}{m_W^2} g_s^2 G_{\mu\nu}^A G^{\mu\nu\,A}, \tag{2.33}$$

where we defined

$$\hat{c}_{GG} \equiv \frac{m_W^2}{\Lambda^2} c_{GG}. \tag{2.34}$$

The most recent bound, obtained in ref. [64] after marginalizing over the other deviations from the SM, reads

$$\hat{c}_{GG} \in [-0.8, 0.8] \times 10^{-3}. \tag{2.35}$$

The coefficient c_{3G}, analogous to the $SU(2)_L$ counterpart c_{3W}, contributes to the anomalous triple gluon couplings. This effect can be measured at LEP, Tevatron and LHC, for example via top-quark pair production, see for example ref. [82] where it is estimated that LHC should be able to put a bound $|\hat{c}_{3G}| \equiv |c_{3G}|\, m_W^2/\Lambda^2 \lesssim 0.1$.

2.3.5 Present constraints

Based on their precision of measurement, the Higgs and EW observables (we neglect the gluon-related observables in the following) can be divided into at least two groups. In the first group, containing highly constrained operators, we have the four electroweak parameters and the Higgs diphoton coupling,

$$\{\hat{c}_S,\ \hat{c}_T,\ \hat{c}_W,\ \hat{c}_Y,\ \hat{c}_{\gamma\gamma}\} \ , \tag{2.36}$$

which have been measured at the per mille level. In the second group we have the $h\gamma Z$ coupling, the couplings related to the three TGC observables $\kappa_\gamma, g_Z^1, \lambda_\gamma$ and $\hat{c}_H$,

$$\{\hat{c}_{\gamma Z},\ \hat{c}_{\kappa\gamma},\ \hat{c}_{gz},\ \hat{c}_{\lambda\gamma}, c_H\} \ , \tag{2.37}$$

Coupling	Direct Constraint	RG-induced Constraint
$\hat{c}_S(m_t)$	$[-1, 2] \times 10^{-3}$ [83]	-
$\hat{c}_T(m_t)$	$[-1, 2] \times 10^{-3}$ [83]	-
$\hat{c}_Y(m_t)$	$[-3, 3] \times 10^{-3}$ [60]	-
$\hat{c}_W(m_t)$	$[-2, 2] \times 10^{-3}$ [60]	-
$\hat{c}_{\gamma\gamma}(m_t)$	$[-1, 2] \times 10^{-3}$ [64]	-
$\hat{c}_{\gamma Z}(m_t)$	$[-0.6, 1] \times 10^{-2}$ [64]	$[-2, 6] \times 10^{-2}$
$\hat{c}_{\kappa\gamma}(m_t)$	$[-10, 7] \times 10^{-2}$ [23]	$[-5, 2] \times 10^{-2}$
$\hat{c}_{gZ}(m_t)$	$[-4, 2] \times 10^{-2}$ [23]	$[-3, 1] \times 10^{-2}$
$\hat{c}_{\lambda\gamma}(m_t)$	$[-6, 2] \times 10^{-2}$ [23]	$[-2, 8] \times 10^{-2}$
$\hat{c}_H(m_t)$	$[-6, 5] \times 10^{-1}$ [64]	$[-2, 0.5] \times 10^{-1}$

Table 2.5: In this table we present the 95 % CL direct constraints on the coefficients in the observable basis (second column). The constraints on $\hat{S}$ and $\hat{T}$ presented here are the ones obtained after marginalizing on the other parameters in the fit of ref. [83]. In the analysis we use the $\hat{S}, \hat{T}$-ellipse from ref. [83] with $U = 0$. Simultaneous constraints on all three of the TGC observables do not exist in the literature, so we have provided the individual constraints on the three couplings without taking into account correlations between them [23]. In the third column we show the RG-induced constraint we are able to obtain under the assumption of no fine-tuning in eq. (2.48), for $\Lambda = 2$ TeV.

which are much more weakly constrained. One can, in fact, further split the above set into c_H which is constrained only at the $\mathcal{O}(1)$ level and the other couplings that are constrained at the few percent level. The present experimental constraints are reported in table 2.5.

2.4   RG-induced bounds and tuning

As we saw, the observables we consider have lower and upper bounds from experimental measurements, which constrain possible deviations from the SM:

$$\delta(\text{obs})_i|_{m_H} = \hat{c}_i(m_H) = \omega_{ij}(m_H)c_j(m_H) \in [\epsilon_i^{low}, \epsilon_i^{up}] \,. \tag{2.38}$$

The observable coupling $\hat{c}_i(m_H)$ (constrained at low energy) is related, through the running, to the high-scale value of the Wilson coefficients $c_j(\Lambda)$, which are not directly known since they are determined by the BSM degrees of freedom that have been integrated out. The matrix $\omega_{ij}(m_H)$ also runs with the scale (in the example of eq. (2.15) this would be the running of g, g' and v inside m_W and θ_W), however we are not interested in such a running because ω_{ij} is determined by measurements performed at the EW scale and because, for the purpose of this work, we are

not interested in the UV value of the SM couplings. This is the reason why we have not taken care of the contributions of the dim-6 operators to the SM couplings, parametrized by κ_i in eq. (2.14), which would only be necessary if we wanted to relate $\omega_{ij}(m_H)$ to $\omega_{ij}(\Lambda)$ at the order we are working.

This discussion leads us to define the scale-dependent observable couplings as

$$\hat{c}_i(\mu) \equiv \omega_{ij}(m_H)c_j(\mu) \,, \tag{2.39}$$

obtaining

$$\delta(\text{obs})_i|_{m_H} = \hat{c}_i(m_H) = \hat{c}_i(\Lambda) - \frac{1}{16\pi^2}\hat{\gamma}_{ij}\hat{c}_j(\Lambda) \log\left(\frac{\Lambda}{m_H}\right) \,, \tag{2.40}$$

where

$$\hat{\gamma}_{ij} \equiv \omega_{ik}(m_H)\,\gamma_{kl}\,\omega_{lj}^{-1}(m_H) \tag{2.41}$$

and γ_{kl} is the matrix computed in sec. 2.2. Our interest in eq. (2.40) is twofold: we want to find instances where a less constrained operator can mix with a more constrained one by appearing in its RGE's and secondly (but closely related), to learn about the new degrees of freedom at the matching scale. In the following we shall work at leading-log order, which is fine if the hierarchy between the new physics scale Λ and the EW scale is not too big.

The fundamental assumption we make in order to obtain an indirect constrain on the $\hat{c}_j(m_H)$ through the RG is that we require each term in the sum on the r.h.s. of eq. (2.40), proportional to some coefficient $\hat{c}_j$, to be contained in the experimental bounds associated to the observable $\delta(\text{obs})_i|_{m_H}$:

$$(1 - \delta_i)\hat{c}_i(\Lambda) \in [\epsilon_i^{low}, \epsilon_i^{up}], \tag{2.42}$$

$$-\frac{1}{16\pi^2}\hat{\gamma}_{i\hat{j}}\hat{c}_{\hat{j}}(m_H) \log\left(\frac{\Lambda}{m_H}\right) \in [\epsilon_i^{low}, \epsilon_i^{up}], \tag{2.43}$$

where we defined $\delta_i = \hat{\gamma}_{ii}/(16\pi^2) \log(\Lambda/m_H)$ and in the last line the index $\hat{j}$ is not summed over.[7] We have also used the fact that substituting $\hat{c}_j(\Lambda)$ for $\hat{c}_j(m_H)$ in the $\hat{\gamma}_{ij}\hat{c}_j$ term of eq. (2.40) amounts to corrections $\mathcal{O}\left((4\pi)^{-4}\log^2(\Lambda/m_H)\right)$ that are beyond our precision (the same is true for the evaluation of γ_{ij}). Notice that this assumption is not only a requirement of the absence of fine-tuning but also an hypothesis on the UV physics, since particular relations, due to symmetry or dynamical accidents, between those combinations could be generically found when considering a BSM theory. From our bottom-up approach we parametrize also this absence of correlations as an absence of tuning. From eq. (2.42) we can put bounds on the matching-scale Wilson coefficients $c_j(\Lambda)$:

$$c_j(\Lambda) \in \left[\sum_i (1 - \delta_i)^{-1}\omega_{ji}^{-1}\epsilon_i^{low}, \sum_i (1 - \delta_i)^{-1}\omega_{ji}^{-1}\epsilon_i^{up}\right] \,, \tag{2.44}$$

---

[7]In the rest of this chapter we shall denote with a hat all repeated indices which are not summed over.

notice that, as expected, they grow quadratically weaker with the increase of the UV scale Λ since $\omega^{-1} \sim \Lambda^2/m_W^2$. Using eq. (2.43), instead, we can put an RG-induced bound on the observable $|\delta(\text{obs})_j|_{m_H} < \epsilon_{ji}^{RG}$ using the direct constraints on $\delta(\text{obs})_i|_{m_H}$, eq. (2.38):

$$
\begin{aligned}
\text{if } \hat{\gamma}_{\hat{i}j} > 0 : \quad \delta(\text{obs})_j|_{m_H} &\in \frac{16\pi^2}{\log(\Lambda/m_H)} (\hat{\gamma}_{\hat{i}j})^{-1} [-\epsilon_{\hat{i}}^{up}, -\epsilon_{\hat{i}}^{low}] \, , \\
\text{if } \hat{\gamma}_{\hat{i}j} < 0 : \quad \delta(\text{obs})_j|_{m_H} &\in \frac{16\pi^2}{\log(\Lambda/m_H)} (\hat{\gamma}_{\hat{i}j})^{-1} [\epsilon_{\hat{i}}^{low}, \epsilon_{\hat{i}}^{up}] \, .
\end{aligned}
\tag{2.45}
$$

The indirect bounds in eq. (2.45) grow logarithmically stronger with the increase of the UV scale Λ. However, since the expected effects from new physics decrease quadratically with Λ, assuming order one coefficients c_i, even if the RG-induced bounds on the observables become slightly stronger, their power in investigating the UV degrees of freedom becomes much weaker for higher values of Λ, as is clear from eq. (2.44). It might seem that these bounds are not significant because of the loop factor in the above equation; the ϵ_i's are, however, not of the same order and if $|\epsilon_i^{low,up}| \ll |\epsilon_j^{low,up}|$, the bound in the above equation can be stronger than the direct bound on $\delta(\text{obs})_j|_{m_H}$, in spite of the loop factor. The RG-induced bounds are, thus, significant only when a weakly constrained coupling appears in the RGE of a strongly coupled one.

Once new physics effects will be, hopefully, observed and the constraints of eq. (2.38) will not include the zero value in the allowed interval $(0 < \epsilon_j^{low} < |\delta(\text{obs})_j|_{m_H} < \epsilon_j^{up})$, another interesting information that could be extracted from RG effects is a quantification of how much tuned, among themselves, are the electroweak and Higgs observables. First of all, let us define the fine-tuning in an observable as [84]

$$
\Delta_i \equiv \text{Max}_j \left| \frac{\partial \log \delta(\text{obs})_i|_{m_H}}{\partial \log \hat{c}_j(\Lambda)} \right| \simeq \text{Max} \left\{ \frac{|\hat{c}_i(\Lambda)|}{|\delta(\text{obs})_i|_{m_H}}, \frac{\log(\Lambda/m_H)}{16\pi^2} \frac{\text{Max}_{j\neq i} |\hat{\gamma}_{ij}| \, |\delta(\text{obs})_{\hat{j}}|_{m_H}}{|\delta(\text{obs})_i|_{m_H}} \right\} \, ,
\tag{2.46}
$$

where in the second step we separated the diagonal contribution from the off-diagonal ones and, for the diagonal term, we neglected the loop contribution since $\hat{c}_i(\Lambda)$ enters already at tree level and this would be its leading contribution to the tuning. Looking at the off-diagonal terms, the fine-tuning Δ_i satisfies,

$$
\Delta_i \geq \frac{\log(\Lambda/m_H)}{16\pi^2} \frac{\text{Max}_{j\neq i} |\hat{\gamma}_{ij}| \, |\delta(\text{obs})_{\hat{j}}|_{m_H}}{|\delta(\text{obs})_i|_{m_H}} > \frac{\log(\Lambda/m_H)}{16\pi^2} \frac{\text{Max}_{j\neq i} |\hat{\gamma}_{ij}| \, \epsilon_j^{low}}{\epsilon_i^{up}} = \text{Max}_{j\neq i} \frac{\epsilon_j^{low}}{\epsilon_{ji}^{RG}} \, ,
\tag{2.47}
$$

and one might be able to conclude that a certain degree of fine-tuning among the contributions to the RG flow of some operator is necessary.

	$\hat{c}_S$	$\hat{c}_T$	$\hat{c}_Y$	$\hat{c}_W$	$\hat{c}_{\gamma\gamma}$
$\gamma_{\hat{c}_S}$	$\frac{1}{3}g'^2 + 6y_t^2$	$-\frac{g^2}{2}$	$\frac{1}{8}g'^2\left(147 - 106t_{\theta_W}^2\right)$	$\frac{1}{8}\left(77g^2 + 58g'^2\right)$	$16e^2$
$\gamma_{\hat{c}_T}$	$-9g'^2 - 24t_{\theta_W}^2\,\lambda$	$\frac{9}{2}g^2 + 12y_t^2 + 12\lambda$	$\frac{9}{2}g'^2 + 12t_{\theta_W}^2\left(g'^2 + \lambda\right)$	$\frac{9}{2}g'^2$	0
$\gamma_{\hat{c}_Y}$	$-\frac{2}{3}g'^2$	0	$\frac{94}{3}g'^2$	0	0
$\gamma_{\hat{c}_W}$	0	0	$\frac{53}{12}g'^2\left(1 - 3t_{\theta_W}^2\right)$	$\frac{331}{12}g^2 + \frac{29}{4}g'^2$	0
$\gamma_{\hat{c}_{\gamma\gamma}}$	0	0	0	0	$-\frac{9}{2}g^2 - \frac{3}{2}g'^2 + 6y_t^2 + 12\lambda$
$\gamma_{\hat{c}_H}$	$18g'^2 - t_{\theta_W}^2\left(9g'^2 + 24\lambda\right)$	$-9g^2 + \frac{9}{2}g'^2 + 12\lambda$	$t_{\theta_W}^2\left(-\frac{141}{4}g'^2 + 12\lambda\right)$	$\frac{63}{2}g^2 + \frac{51}{4}g'^2 + 72\lambda$	0
$\gamma_{\hat{c}_{\gamma Z}}$	0	0	0	0	0
$\gamma_{\hat{c}_{\kappa\gamma}}$	0	0	0	0	$16e^2$
$\gamma_{\hat{c}_{gZ}}$	$-\frac{g'^2}{6c_{\theta_W}^2}$	$\frac{g^2}{12c_{\theta_W}^2}$	$\frac{g'^2}{8c_{\theta_W}^2}\left(106t_{\theta_W}^2 - 29\right)$	$-\frac{1}{8c_{\theta_W}}\left(79g^2 + 58g'^2\right)$	0
$\gamma_{\hat{c}_{\lambda\gamma}}$	0	0	0	0	0

	$\hat{c}_H$	$\hat{c}_{\gamma Z}$	$\hat{c}_{\kappa\gamma}$	$\hat{c}_{gZ}$	$\hat{c}_{\lambda\gamma}$
$\gamma_{\hat{c}_S}$	$-\frac{1}{6}g^2$	$4\left(g^2 - g'^2\right)$	$\frac{11}{2}g^2 + \frac{1}{6}g'^2 + 4\lambda$	$-c_{\theta_W}^2\left(9g^2 - \frac{1}{3}g'^2\right)$	$2g^2$
$\gamma_{\hat{c}_T}$	$\frac{3}{2}g^2$	0	$9g'^2 + 24t_{\theta_W}^2\,\lambda$	$-24s_{\theta_W}^2\,\lambda$	0
$\gamma_{\hat{c}_Y}$	0	0	$\frac{2}{3}g'^2$	$-\frac{2}{3}e^2$	0
$\gamma_{\hat{c}_W}$	0	0	0	$\frac{2}{3}c_{\theta_W}^2\,g^2$	0
$\gamma_{\hat{c}_{\gamma\gamma}}$	0	0	$-\frac{3}{2}g^2 + 2\lambda$	0	$-3g^2$
$\gamma_{\hat{c}_H}$	$-\frac{9}{2}g^2 - 3g'^2 + 12y_t^2 + 24\lambda$	0	$-9g'^2\left(2 - t_{\theta_W}^2\right) + 24t_{\theta_W}^2\,\lambda$	$9\left(g^2c_{\theta_W}^2 - g'^2s_{\theta_W}^2\right) + 24\lambda\left(6c_{\theta_W}^2 - s_{\theta_W}^2\right)$	0
$\gamma_{\hat{c}_{\gamma Z}}$	0	$-\frac{7}{2}g^2 - \frac{1}{2}g'^2 + 6y_t^2 + 12\lambda$	$s_{\theta_W}^2\left(g^2 - 2\lambda\right) - c_{\theta_W}^2\left(2g^2 - 2\lambda\right)$	0	$-\frac{g^2}{2}\left(11c_{\theta_W}^2 - s_{\theta_W}^2\right)$
$\gamma_{\hat{c}_{\kappa\gamma}}$	0	$4\left(g^2 - g'^2\right)$	$\frac{11}{2}g^2 + \frac{g'^2}{2} + 6y_t^2 + 4\lambda$	0	$2g^2$
$\gamma_{\hat{c}_{gZ}}$	$\frac{g^2}{12c_{\theta_W}^2}$	0	$\frac{g'^2}{6c_{\theta_W}^2}$	$\frac{17}{2}g^2 - \frac{g'^2}{6} + 6y_t^2$	0
$\gamma_{\hat{c}_{\lambda\gamma}}$	0	0	0	0	$\frac{53}{3}g^2$

Table 2.6: Anomalous dimension matrix in the observables basis. We defined $t_{\theta_W} = \tan\theta_W$.

	c_{2G}	c_{GG}	c_{3G}	c_{2B}	c_{2W}
$\gamma_{c_{2G}}$	$\frac{266}{9}g_s^2$	0	0	$g'^2\left(\frac{17}{6}(Y_u^2+Y_d^2)+12Y_uY_d\right)$	0
$\gamma_{c_{GG}}$	0	$-\frac{3}{2}g'^2-\frac{9}{2}g^2+12\lambda+6y_t^2$	0	0	0
$\gamma_{c_{3G}}$	0	0	$22g_s^2$	0	0

Table 2.7: Anomalous dimension matrix for the Wilson coefficients of the dim-6 bosonic operators with gluons, in the basis defined in section 2.1. The contributions to and from the other coefficients of the operators in eq. (2.9), not reported here, are zero.

2.4.1   RG-induced bounds on our set of observables

Let us now apply the general formulas of the previous section to the electroweak and Higgs observables we want to constrain.

We are interested in finding instances where the couplings from the second group in eq. (2.37) appear in the RGE's of the first group of couplings in eq. (2.36). To check this we rotate the anomalous dimension matrix to the observable basis defined by eq. (2.24), eq. (2.26), and eq. (2.28). We present the anomalous dimension matrix in the observable basis in table 2.6. Using this, and fixing $\Lambda = 2$ TeV, we write numerically eq. (2.40) as

$$(\hat{c}_S, \hat{c}_T, \hat{c}_Y, \hat{c}_W, \hat{c}_{\gamma\gamma}, \hat{c}_{\gamma Z}, \hat{c}_{\kappa\gamma}, \hat{c}_{gz}, \hat{c}_{\lambda\gamma}, \hat{c}_H)^t (m_t) \simeq \tag{2.48}$$

$$\begin{pmatrix} 0.9 & 0.003 & -0.03 & -0.08 & -0.02 & -0.02 & -0.04 & 0.05 & -0.01 & 0.001 \\ 0.03 & 0.8 & -0.02 & -0.009 & 0 & 0 & -0.03 & 0.01 & 0 & -0.003 \\ 0.001 & 0 & 0.9 & 0 & 0 & 0 & -0.001 & 0.001 & 0 & 0 \\ 0 & 0 & -0.001 & 0.8 & 0 & 0 & 0 & -0.003 & 0 & 0 \\ 0 & 0 & 0 & 0 & 0.9 & 0 & 0.006 & 0 & 0.02 & 0 \\ 0 & 0 & 0 & 0 & 0 & 0.9 & 0.007 & 0 & 0.03 & 0 \\ 0 & 0 & 0 & 0 & -0.02 & -0.02 & 0.9 & 0 & -0.01 & 0 \\ 0.0004 & -0.0007 & -0.0004 & 0.1 & 0 & 0 & -0.0004 & 0.9 & 0 & -0.0007 \\ 0 & 0 & 0 & 0 & 0 & 0 & 0 & 0 & 0.9 & 0 \\ -0.02 & 0.03 & 0.01 & -0.4 & 0 & 0 & 0.02 & -0.3 & 0 & 0.8 \end{pmatrix} \begin{pmatrix} \hat{c}_S(\Lambda) \\ \hat{c}_T(\Lambda) \\ \hat{c}_Y(\Lambda) \\ \hat{c}_W(\Lambda) \\ \hat{c}_{\gamma\gamma}(\Lambda) \\ \hat{c}_{\gamma Z}(\Lambda) \\ \hat{c}_{\kappa\gamma}(\Lambda) \\ \hat{c}_{gz}(\Lambda) \\ \hat{c}_{\lambda\gamma}(\Lambda) \\ \hat{c}_H(\Lambda) \end{pmatrix}.$$

We can now derive the RG-induced constraints by using eq. (2.45) assuming no fine-tuning among the different terms in the RGE's.

The strongest RG-induced constraints come from the direct bounds on the $\hat{S}, \hat{T}, W$ and Y parameters, i.e. the first four lines in eq. (2.48). We require that each observable coupling individually satisfies the four RG-induced constraints from these electroweak precision parameters simultaneously. It is very important to take into account the experimental correlations between $\hat{S}, \hat{T}, W$ and Y while imposing these bounds [85–87]. Note that the RG-mixing contributions to
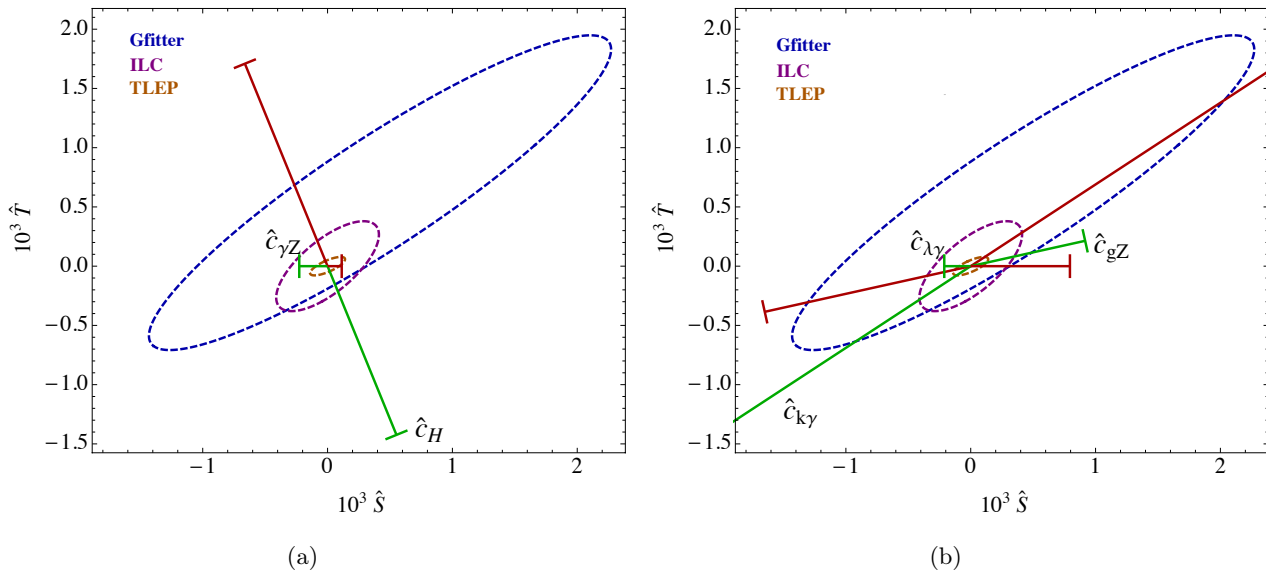
Figure 2.2: The ellipses represent 95% CL bounds on $\hat{S}$ and $\hat{T}$ as obtained in the fit of ref. [83] with $U = 0$ (blue), expected from the ILC (purple) and TLEP (orange). The straight lines represent the RG-induced contribution to the oblique parameters from the weakly constrained observable couplings of eq. (2.37), divided in Higgs couplings (a) and TGC couplings (b), using the first two lines of eq. (2.48), for $\Lambda = 2$ TeV. The length of the lines corresponds to their present 95% CL direct bounds, see table 2.5; the line is green (red) for positive (negative) values of the parameters.

$\hat{c}_W$ and $\hat{c}_Y$, from the couplings in the weakly constrained group in eq. (2.37), is either absent or accidentally much smaller than the ones to $\hat{c}_S$ and $\hat{c}_T$ (see the RG contributions to $\hat{c}_W$ and $\hat{c}_Y$ in the third and fourth row of eq. (2.48)). We, therefore, look at the constraints on the $\hat{S} - \hat{T}$ plane taking $W = Y = 0$. We use the $\hat{S} - \hat{T}$ ellipse in ref. [83], which assumes $W = Y = U = 0$, to derive our constraints. We present these RG-induced bounds and compare them with the direct bounds in table 2.5 and in figure 2.2. We find that for each of the couplings in the second group we can derive a RG-induced constraint stronger than, or of the same order of, the direct tree-level constraint. We also obtain RG-induced bounds from the direct constraint on $\hat{c}_{\gamma\gamma}$ using the fifth line in eq. (2.48) and eq. (2.45),

$$\hat{c}_{\kappa\gamma} \in [-0.2, 0.3] \ ,$$
$$\hat{c}_{\lambda\gamma} \in [-0.05, 0.10] \ ,$$

(2.49)

but at present these bounds are weaker than those from the direct bounds on electroweak parameters.

Let us briefly comment on alternate choices for our observable basis. In general, a change of *observable basis* modifies the anomalous dimension matrix of table 2.6, also for the observables which were maintained in the basis. Thus, the RG-induced constraints we have derived, are applicable only to our particular choice of observables, and for an alternate choice the analysis

must be repeated.[8] For instance, the Higgs decay observables related to $h \rightarrow W^+W^-, ZZ$ decays could have been alternatively chosen as part of our observable basis instead of two of the TGC observables (κ_γ and g_Z) but we have kept the TGC in our basis as they are measured more precisely than these Higgs decay observables. This situation is likely to continue in the future. Although, observables like the relative deviation of $h \rightarrow W^+W^-, ZZ$ with respect to the SM would be strongly constrained at the 5 %(3 %) level at the LHC with $300\,\mathrm{fb}^{-1}$ ($3000\,\mathrm{fb}^{-1}$) data [88], the bounds on TGC are also expected to become stronger by an order of magnitude at the LHC [88] so that the TGC would still be more precisely measured than these Higgs observables. At linear colliders the Higgs $h \rightarrow W^+W^-, ZZ$ is expected to be measured at the level of 0.5 % [88] and the TGC observables at the 10^{-4} level [89]; again the TGC observables would be more constrained.

As can be seen in table 2.7, no mixing to (or from) these gluon operators is present among the operators we considered in table 2.1, the only exception being a contribution from c_{2B} to c_{2G} which, however, is not very interesting since c_{2B} is already very well directly constrained by the oblique Y parameter. For this reason, we are not able to cast any indirect constraint using these gluon operators.

2.5   Future prospects

Let us now discuss the future prospects for the RG-induced bounds, given the expected sensitivities on the observable couplings introduced above for 300 fb^{-1} and 3000 fb^{-1} [90] of luminosity at the LHC and for the ILC [89] and TLEP [91] projects, as collected in table 2.8.

The precision on the oblique parameters could reach the 10^{-4} level at ILC [92] and the 10^{-5} level at a TLEP collider [93]. This would allow to improve sensibly the RG-induced bounds on our set of observable couplings, as can be seen in figure 2.2 and in table 2.9

The measurement of the Higgs couplings, in particular the one to two photons $\hat{c}_{\gamma\gamma}$, will improve substantially in the future: by one order of magnitude at 14TeV LHC with 300 fb^{-1} of integrated luminosity and at the ILC, and almost two orders of magnitude at a high-luminosity LHC phase and at a TLEP collider [88]. The prospects for RG-induced bounds on the observable coefficients which mix to $\hat{c}_{\gamma\gamma}$, that is the TGC $\hat{c}_{k_\gamma}$ and $\hat{c}_{\lambda_\gamma}$, are reported in table 2.10.

If a deviation from the SM will be observed (i.e. one observable coefficient will have a direct bound $0 < \epsilon_j^{low} < |\hat{c}_j(m_W)| < \epsilon_j^{up}$), then by comparing the lower bound ϵ_j^{low} with the RG-induced bound on $\hat{c}_j$ ($|\hat{c}_j| < \epsilon_{ji}^{RG}$) obtained considering its RG mixing to a strongly constrained

---

[8]Note that for our choice of observable basis, $h \rightarrow \gamma\gamma$ does not receive a contribution from the $\hat{S}$ parameter even though there is a dependance on c_{WB} in the anomalous dimension but c_{WB} is actually reconstructing the $\delta\kappa_\gamma$ parameter.

Obs.	Now	LHC (300 fb^{-1})	HL-LHC (3 ab^{-1})	ILC	TLEP
$\hat{c}_S$	$[-1,2] \times 10^{-3}$ [83]	–	–	1.4×10^{-4} [92]	5×10^{-5} [93]
$\hat{c}_T$	$[-1,2] \times 10^{-3}$ [83]	–	–	1.6×10^{-4} [92]	3.1×10^{-5} [93]
$\hat{c}_{gZ}$	$[-4,2] \times 10^{-2}$ [23]	3×10^{-3} [90]	2×10^{-3} [90]	1.8×10^{-4} [89]	n.a.
$\hat{c}_{k\gamma}$	$[-10,7] \times 10^{-2}$ [23]	3×10^{-2} [90]	1×10^{-2} [90]	1.9×10^{-4} [89]	n.a.
$\hat{c}_{\lambda\gamma}$	$[-6,2] \times 10^{-2}$ [23]	9×10^{-4} [90]	4×10^{-4} [90]	2.6×10^{-4} [89]	n.a.
$\hat{c}_{\gamma\gamma}$	$[-1,2] \times 10^{-3}$ [64]	1×10^{-4} [88]	4×10^{-5} [88]	7.6×10^{-5} [88]	2.9×10^{-5} [88,91]
$\hat{c}_{\gamma Z}$	$[-6,10] \times 10^{-3}$ [64]	9×10^{-4} [88]	2×10^{-4} [88]	n.a.	n.a.
$\hat{c}_H$	$[-6,5] \times 10^{-1}$ [64]	1×10^{-1} [88]	5×10^{-2} [88]	5×10^{-2} [88]	1×10^{-2} [88,91]

Table 2.8: Future prospects in the direct determination of the observable couplings discussed here from the LHC, a high-luminosity LHC, the ILC at 800GeV and from TLEP after a first phase at 240GeV and a second one at 350GeV. The precision in $\hat{S}, \hat{T}$ will not improve sensibly at the LHC or HL-LHC and the other missing elements have not yet been studied in the literature.

mix. to $(\hat{S}, \hat{T})$	Now	ILC	TLEP
$\hat{c}_{\gamma Z}$	$[-2,6] \times 10^{-2}$	2×10^{-2}	5×10^{-3}
$\hat{c}_H$	$[-2,0.5] \times 10^{-1}$	7×10^{-2}	2×10^{-2}
$\hat{c}_{gZ}$	$[-3,1] \times 10^{-2}$	8×10^{-3}	3×10^{-3}
$\hat{c}_{k\gamma}$	$[-5,2] \times 10^{-2}$	9×10^{-3}	3×10^{-3}
$\hat{c}_{\lambda\gamma}$	$[-2,8] \times 10^{-2}$	2×10^{-2}	7×10^{-3}

Table 2.9: Present status and future prospects for the RG-induced bounds, for $\Lambda = 2$ TeV, from the mixing to $(\hat{S}, \hat{T})$, given the predicted sensitivity in this observables at ILC and TLEP, as shown in table 2.8.

observable $\hat{c}_i$ (like $\hat{S}$ and $\hat{T}$) we can determine the necessary amount of tuning in eq.(2.40). By taking the logarithmic derivative of eq.(2.40) with respect to the UV coefficient $\hat{c}_j(\Lambda)$ one gets that the tuning is [4] $\Delta_{ij} > \epsilon_j^{low}/\epsilon_{ji}^{RG}$. Therefore, if $\epsilon_j^{low} \gg \epsilon_{ji}^{RG}$ a definite amount of tuning (or of correlation) in the UV dynamics would be necessary. This could provide a new window on the UV physics.

For example, if $\hat{c}_H$ should be measured to be ~ 0.2 (0.1) while no deviation in $(\hat{S}, \hat{T})$ should be observed after TLEP, the RG-induced bound $|\hat{c}_H^{RG,\text{TLEP}}| < 2 \times 10^{-2}$ would imply a tuning $\Delta_{H,(S,T)} > 10$ (5). Similarly, should one measure $\hat{c}_{k\gamma} \sim 5 \times 10^{-2}$, the RG-induced bound from $(\hat{S}, \hat{T})$ at TLEP, $|\hat{c}_{k\gamma}^{RG,\text{TLEP}}| < 3 \times 10^{-3}$, would imply a tuning $\Delta_{k\gamma,(S,T)} > 17$.

mix. to $\hat{c}_{\gamma\gamma}$	Now	LHC	HL-LHC	ILC	TLEP
$\hat{c}_{k\gamma}$	$[-0.2, 0.3]$	2×10^{-2}	7×10^{-3}	1×10^{-2}	5×10^{-3}
$\hat{c}_{\lambda\gamma}$	$[-0.05, 0.10]$	5×10^{-3}	2×10^{-3}	4×10^{-3}	1×10^{-3}

Table 2.10: Present status and future prospects for the RG-induced bounds, for $\Lambda = 2$ TeV, on two anomalous TGC from the mixing to $\hat{c}_{\gamma\gamma}$, given the predicted sensitivity in this observable as shown in table 2.8.

2.6 Summary

We computed the scaling and mixing of 13 dim-6 deformations of the SM affecting EW precision observables (4), anomalous EW triple gauge boson couplings (3), QCD observables (2) and Higgs production and decays (4). This computation has important phenomenological implications. Particularly interesting is the RG-mixing induced among 10 of these observables (the 2 two QCD observables and one Higgs observable, namely $\Gamma(h \to gg)$, constitute a separate sector that does not mix in a relevant way with the severely constrained EW observables.).

These 10 different observables are constrained at very different levels of precision. For example, whereas the electroweak precision observables and the operator coefficient related to the $h \to \gamma\gamma$ partial width are constrained at the per mille level, the TGC and the 2 other Higgs observables are constrained at the percent level at most. As we run down from the new physics scale to the lower scale of experiments, quantum effects mix the observables and the most severely constrained ones receive a contribution from the ones allowed to deviate the most from the SM predictions. These RG-contributions could in principle be of the same size or even larger than the direct experimental bounds, in other words, the difference in the experimental sensitivities can compensate for the RG-loop factor. Requiring that these RG-contributions do obey individually the direct bounds, i.e. dismissing any possible tuning/correlation among the various RG-terms, we can derive some indirect RG-induced bounds on the weakly constrained observables from the direct measurement of the severely constrained ones. This analysis is particularly relevant for the TGC and the universal shift of the Higgs couplings, as reported in figure 2.2 and table 2.5.

We also looked at the future prospects of these RG-induced effects. If a deviation from the SM is observed in some of the observables we considered, in the absence of tuning one would expect a deviation, due to these RG effects, to appear also in other seemingly unrelated observables. If, instead, these RG-induced deviations are not observed, it would mean that some tuning is needed, or it would indicate some correlation among the higher dimensional operators pointing towards a particular structure of the new physics that has been integrated out. We have presented the projected future experimental sensitivity to these RG effects in tables 2.8,2.9,2.10.

CHAPTER 3

Composite Higgs Models

A way to obtain a large hierarchy between two scales in a natural way is by means of dimensional transmutations. In nature this mechanism is realized in the SM itself, where the QCD scale Λ_{QCD} is naturally much smaller than the UV cutoff because of an exponential suppression due to the RG flow of the QCD strong coupling from the UV down to the scale Λ_{QCD} at which it becomes non-perturbative, eq. (1.4). It is therefore possible that an analogous mechanism is at work in explaining the large hierarchy between the EW and the Planck scales, in which case we expect the presence of a strongly coupled sector at a scale $\Lambda \sim$ TeV. The earliest setup realizing this mechanism is Technicolor models, which – in the simplest realizations – resemble just scaled-up versions of QCD and therefore do not predict any light Higgs boson in the spectrum. Obviously, such models have been now definitely excluded by the LHC. However, even after LEP they suffered from severe bounds from EW precision measurements and flavor physics, which disfavored this class of models. A more realistic possibility is that the Higgs boson itself is a composite state of the strongly coupled sector, in which case the UV sensitivity to its mass would be cutoff above the scale Λ by its finite dimension. If, furthermore, the Higgs arises as a pseudo-Nambu-Goldstone boson (pNGB) of the strongly coupled sector (such as pions in QCD), then its mass would be naturally smaller than the typical scale of the other composite resonances, helping to evade the tight phenomenological constraints on these states. The pNGB nature of the Higgs, moreover, allows to construct low-energy effective chiral Lagrangians which are able to capture the low-energy phenomenology of these composite Higgs (CH) models in terms of a few parameters without the need of specifying the fundamental description of the strongly coupled theory, in the same way as the pion dynamics is well described by the effective QCD chiral Lagrangian.

In this chapter we review the most important features of these class of models, focusing on the minimal realistic scenarios, and we explore the phenomenological predictions these models offer.[1]

---

[1]For excellent reviews on composite Higgs models we refer to ref. [94] and to the more recent ref. [95].

3.1   Strong dynamics behind the EWSB

The idea that the electroweak scale could arise as a condensate of some strong dynamics with the typical scale at the TeV, thereby solving the naturalness problem by dimensional transmutation – as in QCD – has its origin in Technicolor models [30]. In this class of models there is no physical Higgs scalar but the EW symmetry is spontaneously broken by the condensate of some composite operator. In many explicit models the constituents of the strong sector are fermions called techniquarks which interact strongly via a Technicolor gauge group and form a condensate at the EW scale v. From the expression of the SM Higgs Lagrangian in the chiral formalism, eq. (1.11), it is evident that the SM is just the simplest linear-σ model for the custodial symmetry breaking pattern $SU(2)_L \times SU(2)_R \to SU(2)_V$ able to provide a UV completion for the EWSB dynamics. In Technicolor models the Higgs is not present and therefore, of the terms in eq. (1.11), only the kinetic term for the NGB in Σ survives. It can then be seen as the leading term of an effective chiral Lagrangian, valid for energies lower than the strong dynamics scale Λ_{TC}, in an expansion of derivatives over the cutoff Λ_{TC}:

$$\mathcal{L}^{chiral} = \frac{v^2}{4}\text{Tr}\left[(D_\mu \Sigma)^\dagger D^\mu \Sigma\right] + \mathcal{O}(D^4/\Lambda_{TC}^2) \ . \tag{3.1}$$

A mass for the SM fermions can be described by the effective Lagrangian

$$\mathcal{L}^{Yuk} = -\frac{v}{\sqrt{2}}\sum_{ij} \bar{Q}_L^i \Sigma \begin{pmatrix} y_{ij}^u u_R^j \\ y_{ij}^d d_R^j \end{pmatrix} + h.c. \ , \tag{3.2}$$

In QCD, the low energy dynamics of the pions, NGBs of the spontaneous breaking of the chiral symmetry $SU(2)_L \times SU(2)_R \to SU(2)_I$, can be described by an analogous chiral Lagrangian (3.1) with the substitution $v \to f_\pi$. Therefore QCD itself breaks the electroweak symmetry to the electromagnetic subgroup, providing a mass to the W boson $m_W^{QCD} = g f_\pi/2 \simeq 29\text{MeV}$. The simplest Technicolor models can thus be seen as scaled-up versions of QCD in which case the physical W mass is given by $m_W^2 = g^2(v_0^2 + f_\pi^2)/4 \equiv g^2 v^2/4$, where v_0 is the Technicolor condensate, given by $v_0^2 = v^2 - f_\pi^2 \simeq v^2$. In the following we will neglect the small effect due to f_π and identify v_0 with v.

One consequence of the absence of a physical Higgs scalar is that the scattering of W and Z bosons loses perturbative unitarity at an energy $E \sim 4\pi v \simeq 3\text{TeV} \simeq \Lambda_{TC}$, which suggests that before this energy scale the strong dynamics should intervene and restore unitarity, possibly in the form of some composite resonances as in QCD. The Equivalence Theorem (ET) [96–98] states that for high energies $E \gg m_W, m_Z$, the scattering amplitudes involving longitudinally polarized massive gauge bosons in the external states can be studied by substituting those states with the corresponding NGBs (see ref. [99] for a more recent take on the ET). Expanding eq. (3.1) in the
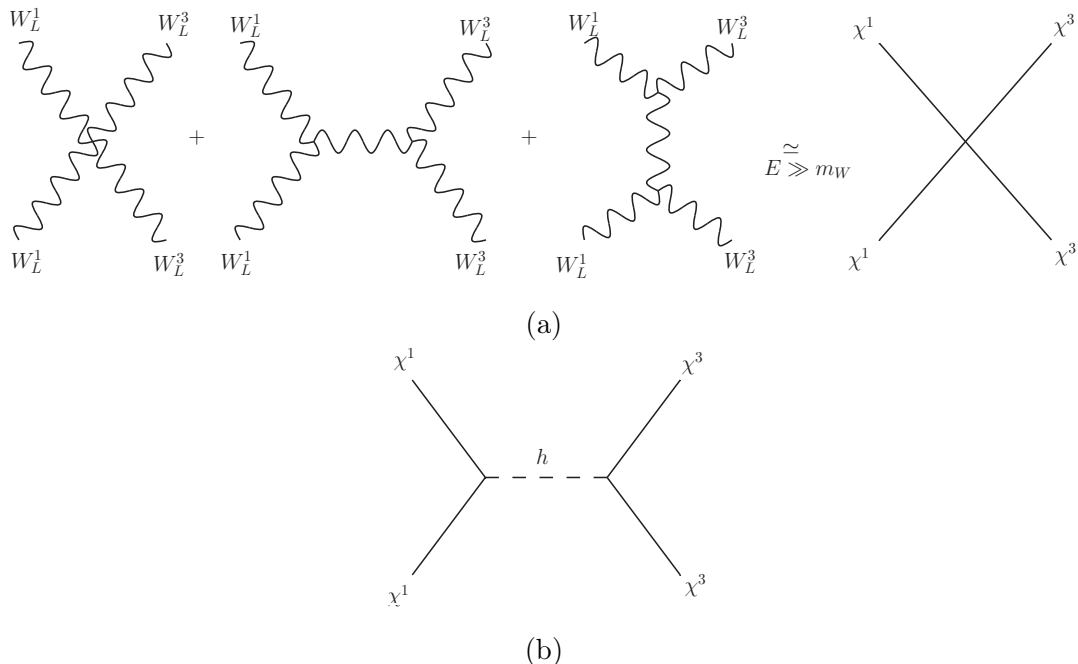
(a)

(b)

Figure 3.1: Diagrams contributing to elastic scattering of longitudinally polarized W bosons. In the first line (a) only the gauge contribution and the simplification due to the equivalence theorem are shown, in the second line (b) we show the contribution from a Higgs scalar.

fields χ^a and computing, for example, the scattering amplitude $\chi^1\chi^1 \to \chi^3\chi^3$, one finds (see diagrams in fig. 3.1(a))

$$\mathcal{A}(\chi^1\chi^1 \to \chi^3\chi^3) \simeq \frac{s}{v^2} \; . \tag{3.3}$$

This tree-level elastic amplitude grows quadratically with the energy. In order to satisfy the unitarity bound, the imaginary contribution to the same amplitude due to loop corrections has to increase. At energies $\sqrt{s} \sim \Lambda_{TC} \sim 4\pi v$ the tree-level and the loop contribution become of the same order, which implies that the theory is no more in a perturbative regime. This problem of perturbative unitarity requires some new dynamics before that scale. In the SM this new dynamics is the physical Higgs, which contributes to the same scattering amplitude exactly cancelling this quadratic growth with the energy when $s \gg m_H^2$, as can be easily obtained by computing the diagram in fig. 3.1(b) using the Lagrangian in eq. (1.11):

$$\mathcal{A}(\chi^1\chi^1 \to \chi^3\chi^3)_{SM} \simeq \frac{s}{v^2}\left(1 - \frac{s}{s - m_H^2}\right) \; . \tag{3.4}$$

In Technicolor, instead, no Higgs is present and the NGB scattering is cured by the strong dynamics, possibly in form of exchange of some composite resonances, as in QCD the pion scattering is unitarized by the exchange of resonances like the spin-1 ρ meson.

From an early age, these Technicolor models suffered from severe experimental constraints, both from electroweak and flavor physics. On the EW side, Naïve Dimensional Analysis (NDA)

estimates show that generically these models predict sizable corrections to EW gauge bosons two point functions, which reflects – for example – in too big values for the EW oblique parameter S. The main reason for this is that the scale of the strong dynamics Λ_{TC} – for example the masses of the first composite resonances – is fixed to be not far from EW scale and therefore its effect are not suppressed enough. On the flavor side, as we explain in more detail in sec. 3.2, constraints on flavor changing neutral currents (FCNC) and CP violation put very strong limits on the sector responsible for generating SM fermion masses via SM fermion bilinears coupled to some operator of the strong dynamics.

Models where the Higgs arises as a composite pNGB of a strong dynamics and in which the elementary SM fermions mix linearly with fermonic operators of the strong sector (*partial compositeness*) offer a solution to both problems. The idea of a composite Higgs as a way to be able to interpolate continuously between the SM and Technicolor models was proposed in a series of seminal papers by Georgi, Kaplan and other collaborators in the early 80s [37, 38], see also refs. [100, 101]. In this class of models the strong sector enjoys a bigger global symmetry group, spontaneously broken at some scale $f > v$. The NGBs of this breaking pattern include the complete Higgs doublet. Contrary to Technicolor, the condensate of the strong sector responsible for this symmetry breaking is aligned – at tree-level – with the EW gauge group and thus preserves it. A potential for the Higgs is then generated at the quantum level by interactions which break explicitly the global symmetry of the strong sector. Different contributions to the potential have to be tuned so that the mass term for the Higgs doublet becomes negative and of the order of the EW scale, thus inducing a non-zero VEV for the Higgs and a misalignment of the vacuum with respect to the EW symmetry preserving direction, thereby breaking the EW symmetry and generating a mass for the W and Z gauge bosons. It was soon realized [102, 103] that a strong constraint on the global symmetry breaking pattern was given by the EW ρ parameter, see eq. (1.18). In order to avoid big tree-level corrections to the SM value, the unbroken global symmetry group should contain the custodial symmetry as a subgroup.

In these models the Higgs Lagrangian after EWSB can be parametrized as [104]

$$\mathcal{L}^{Higgs} = \frac{1}{2}(\partial_\mu h)^2 + \frac{v^2}{4}\text{Tr}\left[(D_\mu \Sigma)^\dagger D^\mu \Sigma\right]\left(1 + 2a\frac{h}{v} + b\frac{h^2}{v^2} + \dots\right) - V(h) , \qquad (3.5)$$

where a and b are generic coefficients and the dots represent interactions with higher powers of the Higgs. $V(h)$ represents the potential for the physical Higgs particle. The effective Yukawa Lagrangian, for example for the quarks, is

$$\mathcal{L}^{Yuk} = -\frac{v}{\sqrt{2}}\sum_{ij}\bar{Q}_L^i \Sigma \begin{pmatrix} y_{ij}^u u_R^j \\ y_{ij}^d d_R^j \end{pmatrix}\left(1 + c\frac{h}{v} + \dots\right) + h.c. \qquad (3.6)$$

In this parametrization, the SM is a particular point in which $a = b = c = 1$ and all higher order terms vanish. In composite Higgs models, instead, these parameters deviate from the SM

value by $\mathcal{O}(v^2/f^2)$. As we will shortly see, in the minimal composite Higgs model (MCHM) these parameters are given by $a = \sqrt{1-\xi}$, $b = 1 - 2\xi$, while the precise expression for c is model-dependent, where we defined the ratio of scales $\xi = v^2/f^2$. The limit $f \to \infty$ (i.e. $\xi \to 0$) describes the SM case, in which all NP effects decouple, while the opposite limit $f \to v$ is a Technicolor-like case, albeit with a composite scalar in the spectrum. Given the modified couplings of the Higgs with the SM gauge bosons, the elastic WW scattering amplitude for $E \gg m_W$ becomes

$$\mathcal{A}(\chi^1\chi^1 \to \chi^3\chi^3)_{MCHM} \simeq \frac{s}{v^2}\left(1 - a^2\frac{s}{s - m_H^2}\right) \overset{\sqrt{s} \gg m_H}{\longrightarrow} \xi\frac{s}{v^2} = \frac{s}{f^2} \; . \tag{3.7}$$

We see that the presence of a physical Higgs in the spectrum postpones the loss of perturbative unitarity in WW scattering to a scale $\Lambda_{CH} \sim 4\pi f = 4\pi v/\sqrt{\xi}$, and therefore increases the scale at which the contribution from composite resonances to the scattering is expected.[2] Having the scale f somewhat higher than the EW scale (by increasing the fine-tuning) allows these models to evade the bounds from the S parameter. Present bounds from S and from the measurement of the Higgs couplings require $\xi \lesssim 0.1$, which corresponds to $f \gtrsim 3v$.

3.1.1 Brief historical overview

After the first proposal of the composite Higgs setup by Georgi and Kaplan, the idea revived in the context of warped extra dimensional models at the end of the 90's, stimulated by the proposal of the Randall-Sundrum (RS) model [39] (also [106–108]). In these models the SM fields live on a 4-dimensional brane embedded in a 5d space-time, in which the fifth dimension has a warped geometry. This warping allows to obtain an exponential suppression of the EW scale with respect to the Planck scale. The AdS/CFT correspondence [40] allows to interpret these setups in terms of some strongly coupled conformal field theories (CFT), where the SM gauge and matter fields are external to the conformal sector [106].

The idea of dimensional deconstruction [109,110] allowed to construct purely 4d theories with analogous properties as 5d models. Little Higgs models [111,112] were among the first concrete 4d realizations which employed deconstructions to build models in which a light Higgs arises naturally as a pNGB of a spontaneously broken global symmetry.

Somewhat in parallel, another class of 5d models, known as gauge-Higgs unification models, was devised [113], in which the pNGB Higgs arises as the fifth component of the SM gauge fields living in the bulk of the extra dimension [114–117]. In this case, the finiteness of the Higgs potential is assured by the 5d gauge invariance, i.e. by the fact that the potential can only arise

---

[2]In this setup also the scattering involving the Higgs loses perturbative unitarity at the same scale, for example $\mathcal{A}(\chi^1\chi^1 \to hh)_{MCHM} \overset{\sqrt{s} \gg m_H}{\longrightarrow} (b - a^2)s/v^2 = \frac{s}{f^2}$. For a phenomenological study of this process in composite Higgs models see refs. [87,104,105].

from non-local Wilson lines wrapping the compactified 5th dimension. This eventually lead to the construction of the holographic composite Higgs models [41, 42] and the Minimal Composite Higgs Model with the custodially-preserving SO(5) → SO(4) symmetry breaking pattern [43].

The low-energy features of these models, including also the phenomenology of the first resonances, can be efficiently described by effective 4d theories [58, 73, 118]. In this case, a finite – and calculable – Higgs potential can be obtained by using the deconstruction idea and building multi-sites models as in ref. [119, 120] or by imposing some generalized Weinberg sum rules [1, 46].

Another class of possible UV completions of composite Higgs models is in the context of supersymmetric theories [3, 121, 122]. In these models the UV sensitivity of the effective Higgs potential is protected both by the pNGB nature and by supersymmetry (SUSY) [123–125]. SUSY can also offer tools to keep under some control the strongly coupled dynamics using Seiberg dualities [126]. This also allows to describe in a natural way the appearance of light top-partners [121].

In the rest of this thesis we concentrate on the low-energy effective 4d description of composite Higgs models. The strong connection of our approach to deconstructed models is described in appendix E.

3.2 A flavor paradigm: partial compositeness

Let us now review how the SM fermions can get a mass in this class of models. We follow closely the discussion presented in ref. [94]. The SM fermions are assumed to be elementary fields, not part of the new strongly coupled sector. However, since they need to feel EWSB, which takes place inside the strongly coupled sector, in order to get a mass, a mechanism which connects the elementary fermions with this sector is necessary.

In the simplest Technicolor models, SM fermion masses are generated through effective operators operators with a bilinear of SM fermions coupled to some composite scalar operator of the strong sector $\mathcal{O}_{TC}$, with the same quantum numbers of the Higgs field,

$$\mathcal{L} \supset \frac{g_{ETC}}{\Lambda_{ETC}^2}(\bar{f}_L f_R)\mathcal{O}_{TC} \ . \tag{3.8}$$

In the UV theory this operator is made of a bilinear of techniquarks, $\mathcal{O}_{TC} = (\bar{\psi}_{TC}\chi_{TC})$ and the term in eq. (3.8) is assumed to be generated at a higher scale $\Lambda_{ETC} \gg \Lambda_{TC}$ where some bigger *extended Technicolor* gauge group – containing both the full SM and the Technicolor gauge groups – is spontaneously broken. At lower energies the techniquarks condensate and the operator $\mathcal{O}_{TC}$ interpolates the Higgs field, breaking the EW symmetry and providing a mass term for the SM fermions $m_f \sim g_{ETC}\Lambda_{TC}^3/\Lambda_{ETC}^2$, as shown schematically in fig. 3.2(a). Since the operator in eq. (3.8) arises from gauge interactions, in order to explain the observed hierarchies in SM fermion masses it is necessary to embed the three families in the same ETC multiplet
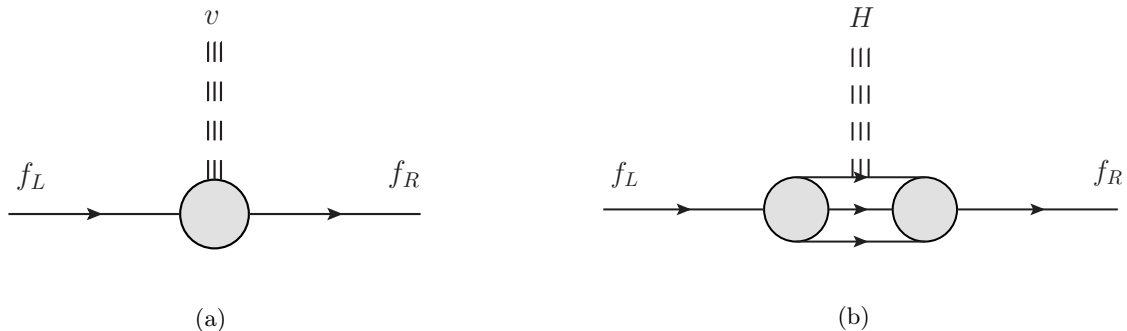
Figure 3.2: Technicolor (a) and partial compositeness (b) mechanisms for generating SM fermion masses.

and to arrange a complicated cascade of symmetry breakings at different scales. Requiring a perturbative g_{ETC} coupling, these breaking scales Λ_{ETC}^f are bounded for each fermion mass: $\Lambda_{ETC}^f \lesssim (\Lambda_{TC}^3/m_f)^{1/2}$. For example this scale is $\mathcal{O}(10\text{TeV})$ for the strange quark.

Such a low scale for this flavor mechanism poses a serious phenomenological problem. In fact, the same mechanism which generates the four-fermion operator discussed above, also generates four-fermion operators of SM fermions, $\mathcal{L} \supset g_{ETC}/\Lambda_{ETC}^2(\bar{f}_L f_R)(\bar{f}'_L f'_R)$. These operators induce flavor changing neutral currents and are very strongly constrained: $\Lambda_{ETC} \gtrsim 10^3 - 10^5\text{TeV}$, depending on the particular operator and its properties. This problem can be somewhat alleviated in *walking Technicolor* models, where one assumes that the coupling g_{TC} reaches a non-perturbative infrared fixed point when running from Λ_{ETC} down to Λ_{TC}, making the theory nearly conformal in this window. In this case the anomalous dimension γ of the operator $\mathcal{O}$ can become important, modifying the expression for the SM fermion masses to $m_f \sim \Lambda_{TC}(\Lambda_{TC}/\Lambda_{ETC})^{2+\gamma}$, allowing to increase the value of Λ_{ETC} if $\gamma < 0$. There are however many arguments which indicate that the anomalous dimension should be bounded $\gamma > -1$, which indicate that the flavor problem can only be somewhat alleviated but not completely solved. For a review see ref. [94] and references therein.

This kind of mechanism for generating quark masses was used in the first composite Higgs models, where $\Lambda_{TC} \to \Lambda \sim 4\pi f$. In this case the flavor model can be solved by increasing both scales Λ and Λ_{ETC}, albeit at the price of increasing the fine-tuning. By increasing Λ to very high scales one eventually recovers the SM, along with the original naturalness problem we set out to solve.

An alternative mechanism to provide masses to SM fermions was proposed by Kaplan in '91 [127] and then revived in extra-dimensional holographic Higgs models [128–130]. The idea consists in coupling linearly a single SM fermion to a fermonic operator of the strongly coupled

sector:

$$\mathcal{L} \supset \lambda_L \bar{f}_L \mathcal{O}_R^f + \lambda_R \bar{f}_R \mathcal{O}_L^f + h.c. \ , \tag{3.9}$$

where $\lambda_{L,R}$ are adimensional couplings. The fermionic operators need to have the same quantum numbers as the SM fermions they couple to, therefore for this mechanism to work it is necessary to have at least one fermionic operator for each SM fermion. These operators are assumed to be generated at some scale $\Lambda_{UV} \gg \Lambda$. When flowing down to Λ, the strong dynamics confines and $\bar{\mathcal{O}}_L^f \mathcal{O}_R^f$ interpolates the Higgs field, so that the terms in eq. (3.9) generate a Yukawa interaction for the SM fermion f and the composite Higgs, as depicted schematically in the right panel of fig. 3.2. Expanding for a large number of 'colors' N of the strongly coupled sector, a rough estimate for the fermion mass is

$$m_f \sim v \frac{\sqrt{N}}{4\pi} \lambda_L(\Lambda) \lambda_R(\Lambda) \ , \tag{3.10}$$

where the mixing parameters $\lambda_{L,R}$ should be evaluated at the scale Λ where the strong sector condenses and generates the Yukawa term. The couplings at this scale are related to the ones at the higher scale Λ_{UV} by the RG equation

$$\frac{d\lambda}{d \log \mu} = \gamma \lambda + c \frac{N}{16\pi^2} \lambda^3 + \dots \ , \tag{3.11}$$

where $\gamma = [\mathcal{O}] - 5/2$ is the anomalous dimension of the fermionic operator $\mathcal{O}$ and c is an $\mathcal{O}(1)$ coefficient. If λ is perturbative we can neglect higher order terms. Let us then assume that λ is perturbative at the high scale Λ_{UV} and study its evolution when flowing towards Λ. If $\gamma > 0$, λ decreases upon decreasing the scale, therefore the second term in eq. (3.11) is negligible and one gets $\lambda(\Lambda) = \lambda(\Lambda_{UV})(\Lambda/\Lambda_{UV})^{\gamma}$. If $\gamma < 0$ then λ increases when flowing towards Λ. In this case, if $c < 0$ then λ becomes non-perturbative. Instead, if c is positive then at a certain point the two terms in eq. (3.11) cancel and the flow reaches a fixed point near $\lambda \simeq \lambda_{fix} \simeq \sqrt{-\gamma/c}\, 4\pi/\sqrt{N}$, which is perturbative at large N.

Let us consider the case where both γ_L and γ_R are positive. In this case, using eq. (3.10) we get $m_f \sim v \frac{\sqrt{N}}{4\pi} (\Lambda/\Lambda_{UV})^{\gamma_L + \gamma_R}$. In contrast with the Technicolor case studied before, now the exponent of the suppression factor can be very close to zero without introducing new UV instabilities. This allows to increase arbitrarily the scale Λ_{UV}, even up to the Planck scale, while keeping Λ fixed. In this way all flavor violating operators generated by this UV flavor dynamics are strongly suppressed and thus can be safely neglected. Moreover, a large hierarchy between Λ and Λ_{UV} implies that $\mathcal{O}(1)$ differences in the anomalous dimensions $\gamma_{L,R}$ generate big hierarchies in SM fermion masses. In this way it is possible to explain naturally the big hierarchy in quark and lepton masses. The case with negative anomalous dimension, instead, can be used to explain the big value of the top mass, in fact if $\gamma_{L,R} < 0$ then $m_f \sim v \frac{4\pi}{\sqrt{N}} \sqrt{\gamma_L \gamma_R}$.

In this context the most important source of flavor-violating processes comes instead from the lower scale Λ, via the exchange of composite resonances coupled to the SM fermions via the

linear mixing terms of eq. (3.9). Eq. (3.10), however, suggests that light fermions – such as those of the first two generations – have small mixing couplings $\lambda_{L,R}$ with the composite sector. This implies that flavor changing processes involving light fermions, which are the most constraining processes, are automatically suppressed in this framework by the smallness of their mixing with the composite sector. However, sizable flavor-violating effects can still arise via the big mixing of the third family with the strong sector. This implies that a realistic scenario of flavor in the partial compositeness framework needs some flavor symmetry which protects against such processes [131].

3.2.1   Partial compositeness in CH models

The most important phenomenological consequence of the linear couplings in eq. (3.9) is the fact that the elementary SM fermions mix with composite fermion resonances in the strong sector. The composite operators $\mathcal{O}^f$ can excite from the vacuum a tower of heavy fermionic resonances with the same quantum numbers as the SM fermion f they couple to. Since these states are charged and massive even before EWSB, they are necessarily Dirac (i.e. vector-like) fermions.

Assuming that the first few states of this tower of resonances are somewhat below the strong coupling scale $\Lambda \sim 4\pi f$, it is possible to write a perturbative Lagrangian for the system with the mixing in eq. (3.9). For example, consider an elementary chiral field f_L and the respective massive fermion resonance Ψ:

$$\mathcal{L}_{ferm} = \bar{f}_L \slashed{\partial} f_L + \bar{\Psi}(\slashed{\partial} - m)\Psi + (\epsilon \bar{f}_L \Psi_R + h.c.) \ , \tag{3.12}$$

where ϵ is a mixing parameter with dimension of mass estimated to be of the order $\epsilon \sim \lambda f$. Given the above Lagrangian, the elementary fermion f_L mixes with Ψ_L by an angle

$$\tan\theta_L = \frac{\epsilon}{m} \ , \tag{3.13}$$

and the two eigenstates f'_L and Ψ' have masses

$$M_{\Psi'} = \sqrt{m^2 + \epsilon^2} \ , \qquad M_{f'} = 0. \tag{3.14}$$

Since here we did not include any elementary right-handed fermion, f' is still massless but now it is a mixture of the elementary and the composite states, hence it is a *partially composite* fermion. From eq. (3.13) we see that the bigger the mixing ϵ, the higher is the degree of compositeness. Therefore, since the mixing is big for heavy SM fermions, we expect those to be the ones with the higher degree of compositeness.

In the following sections we will show how complete models can be built following this principles, how they generate Yukawa interactions between the SM fermions and the composite Higgs and, finally, how these terms generate an effective potential for the Higgs.
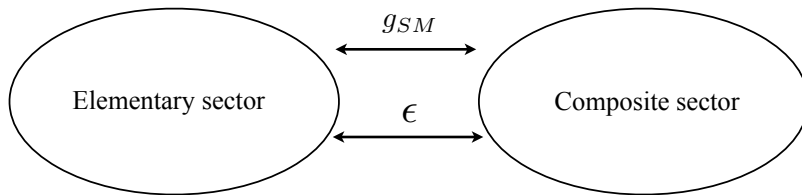
Figure 3.3:   Schematic representation of the structure of composite Higgs models.

3.3   The minimal composite Higgs model

Let us assume the existence of an unspecified strongly interacting sector, symmetric under global transformations of some group $\mathcal{G}$, spontaneously broken to a subgroup $\mathcal{H}$ by the condensate of the strong dynamics at a scale $f > v$.[3] The Higgs is assumed to be a composite pNGB of the spontaneous symmetry breaking pattern of the composite sector, together with the longitudinal polarizations of the W and Z bosons and the other heavy resonances. The elementary sector, instead, contains the transverse polarizations of the SM gauge bosons and the SM fermions. The global symmetry is also explicitly broken by gauging a subgroup $\mathrm{SU}(2)_L \times \mathrm{U}(1)_Y \subset \mathcal{H}$ and by Yukawa terms in the fermion sector. This explicit breaking terms are assumed to be the only ones which allow the elementary and composite sector to communicate, as depicted in fig. 3.3, and they generate, at one loop, a potential for the NGBs such that the Higgs takes a non-vanishing VEV and breaks the EW symmetry.

In order to avoid big tree-level corrections to the ρ parameter, eq. (1.18), the unbroken subgroup $\mathcal{H}$ should contain the custodial symmetry of the SM $\mathrm{SU}(2)_L \times \mathrm{SU}(2)_R \sim \mathrm{SO}(4)$. Moreover, since we aim to construct a model in which the complete Higgs doublet arises as NGB of the spontaneous symmetry breaking $\mathcal{G} \to \mathcal{H}$, the $\mathcal{G}/\mathcal{H}$ coset should contain *at least* four broken generators. The minimal symmetry breaking pattern satisfying these requirements is $\mathrm{SO}(5) \to \mathrm{SO}(4)$, which is at the basis of the minimal composite Higgs model [41, 43]. From this symmetry breaking four NGBs arise, which transform in the fundamental of $\mathrm{SO}(4)$, i.e. as a bidoublet $\mathrm{SU}(2)_L \times \mathrm{SU}(2)_R$, and can be identified with the components of the Higgs doublet. By enlarging the symmetry groups more NGBs arise. The next-to-minimal case is $\mathrm{SO}(6) \to \mathrm{SO}(5)$, where the NGBs are the Higgs doublet and a real singlet, which in some cases can be a stable particle and thus a potential dark matter candidate. In this thesis we concentrate on these two scenarios, a description of other non-minimal cases can be found in refs. [132, 133]

Let us now study in more detail the minimal scenario, postponing the discussion of the next-to-minimal model to chapter 4. We assume that the strong sector is invariant under the

---

[3]The strongly interacting sector should also be gauge-invariant under the $\mathrm{SU}(3)_c$ symmetry associated to color, but this is irrelevant for our considerations and will not be considered in what follows.

group $\mathcal{G} = \mathrm{SO}(5) \times \mathrm{U}(1)_X$, spontaneously broken to the subgroup $\mathcal{H} = \mathrm{SO}(4) \times \mathrm{U}(1)_X \sim$ $\mathrm{SU}(2)_L \otimes \mathrm{SU}(2)_R \otimes \mathrm{U}(1)_X$ [4] at some scale $f > v$. The SM EW gauge symmetry is identified as the subgroup $\mathcal{G}_{EW} = \mathrm{SU}(2)_L \otimes \mathrm{U}(1)_Y \subset \mathrm{SU}(2)_L \otimes \mathrm{SU}(2)_R \otimes \mathrm{U}(1)_X$, where the hypercharge is defined as

$$Y = T^{3_R} + X \ . \tag{3.15}$$

3.3.1   Basic construction and σ-model

For energies lower than the strong coupling scale $\Lambda \sim 4\pi f$, the dynamics of the NGBs can be described by an effective chiral Lagrangian. Callan, Coleman, Wess and Zumino [134, 135] (CCWZ) showed how to construct such Lagrangians for a generic coset, the main results are reviewed in appendix B.

The four NGBs $h^{\hat{a}}$ which arise from the $\mathrm{SO}(5) \rightarrow \mathrm{SO}(4)$ symmetry breaking pattern can be described by means of the matrix

$$U = \exp\left(i\frac{\sqrt{2}}{f}h^{\hat{a}}T^{\hat{a}}\right) \ , \tag{3.16}$$

which transforms under $\mathrm{SO}(5)$ as $U \rightarrow gUk^{\dagger}(g, h^{\hat{a}}(x))$, where k is a $\mathrm{SO}(4)$ transformation depending on g and on the space-time position through the NGB dependence. The $\mathrm{SO}(5)$ generators T^A are normalized so that in the fundamental representation $\mathrm{Tr}[T^A T^B] = \delta^{AB}$, where $A = a, \hat{a}$, and $a, \hat{a}$ denote the unbroken and broken generators ($a = 1, \ldots, 6$, $\hat{a} = 1, \ldots, 4$) respectively. Considering $\mathrm{SU}(2)_L \times \mathrm{SU}(2)_R \sim \mathrm{SO}(4)$, the unbroken generators can be further classified in those corresponding to the left and right subgroups: $a = (a_L, a_R)$, with $a_L = a, a_R = a + 3$ and $a = 1, 2, 3$. In the unitary gauge the NGBs can be taken in the form $h^{\hat{a}} = (0, 0, h, 0)$ and the matrix U reduces to

$$U = \begin{pmatrix} 1 & 0 & 0 & 0 & 0 \\ 0 & 1 & 0 & 0 & 0 \\ 0 & 0 & 1 & 0 & 0 \\ 0 & 0 & 0 & \cos\frac{h}{f} & -\sin\frac{h}{f} \\ 0 & 0 & 0 & \sin\frac{h}{f} & \cos\frac{h}{f} \end{pmatrix} . \tag{3.17}$$

The gauged CCWZ structures d_μ and E_μ introduced in appendix B are given by

$$iU^{\dagger}D_\mu U = d_\mu^{\hat{a}}T^{\hat{a}} + E_\mu^a T^a \ , \tag{3.18}$$

where $D_\mu = \partial_\mu - i(g_0 W_\mu^a T^{a_L} + g_0' B_\mu T^{3_R})$. Expanding in the number of fields, their first terms

---

[4]The $\mathrm{U}(1)_X$ factor is only needed to correctly reproduce the SM fermion hypercharges and does not play any role in the σ-model description.

are

$$
\begin{cases}
d_\mu^{\hat{a}} = & g_0 A_\mu^{\hat{a}} - \frac{\sqrt{2}}{f}(D_\mu h)^{\hat{a}} + \dots \\
E_\mu^{a} = & g_0 A_\mu^{a} + \frac{i}{f^2}(h \overset{\leftrightarrow}{D_\mu} h)^{a} + \dots
\end{cases} ,
\tag{3.19}
$$

where the SM gauging corresponds to

$$
A^{\hat{a}} = 0, \qquad A_\mu^{a_L} = W_\mu^{a}, \qquad A_\mu^{3_R} = \frac{g_0'}{g_0} B_\mu .
\tag{3.20}
$$

At the leading order in the chiral expansion, the Lagrangian describing the dynamics of the EW gauge fields and the NGBs is

$$
\mathcal{L}_{\text{MHCM}} = -\frac{1}{4} W_{\mu\nu}^{a_L} W^{a_L \mu\nu} - \frac{1}{4} B_{\mu\nu} B^{\mu\nu} + \frac{f^2}{4} \text{Tr}\,(d_\mu d^\mu) .
\tag{3.21}
$$

The explicit breaking of SO(5) due to the fact that only a subgroup of SO(5) is gauged by the EW gauge fields and the Yukawa terms for the fermions generates a potential for the Higgs through loop corrections. This potential features a non-vanishing vacuum expectation value for h which triggers the spontaneous breaking of the EW symmetry and gives mass to the SM fermions and gauge fields. With a little algebra, the last term in eq. (3.21) can be translated in the formalism of eq. (3.5), obtaining

$$
\mathcal{L}^{Higgs} = \frac{1}{2}(\partial_\mu h)^2 + \frac{f^2}{4} \text{Tr}\left[(D_\mu \Sigma)^\dagger D^\mu \Sigma\right] \sin^2 \frac{h}{f} .
\tag{3.22}
$$

Expanding this Lagrangian in the physical Higgs $h \to \langle h \rangle + h$ and defining

$$
\xi \equiv \frac{v^2}{f^2} = s_h^2 \equiv \sin^2 \frac{\langle h \rangle}{f} ,
\tag{3.23}
$$

we get the expression for the SM W, Z boson masses,

$$
m_W = \frac{g_0 f}{2} \sin \frac{\langle h \rangle}{f} = \frac{g_0 v}{2} , \qquad m_Z = \frac{m_W}{\cos \theta_W} \qquad \left(\text{where } \tan \theta_W = \frac{g_0'}{g_0}\right) ,
\tag{3.24}
$$

and for the a, b coefficients,

$$
a = \sqrt{1 - \xi}, \qquad b = 1 - 2\xi .
\tag{3.25}
$$

3.3.2 Partial compositeness and fermion embedding

In order to give mass to the SM fermions we adopt the partial compositeness scenario: the SM fields mix linearly with some fermonic operators of the composite dynamics with same quantum numbers. As described in sec. 3.2, we assume that such mixing terms arise from some flavor dynamics at a scale Λ_{UV} much higher than the spontaneous symmetry breaking scale f. It is thus reasonable to assume that the fermonic composite operators $\mathcal{O}^f$ belong to some linear representation $r_{\mathcal{G}}$ of the global symmetry group $\mathcal{G}$, therefore it transforms linearly under $g \in \mathcal{G}$: $\mathcal{O}^f \to g\mathcal{O}^f$. Since the SM fields are not in complete representations of $\mathcal{G}$, such

mixings will necessarily break explicitly the global symmetry. In order to write the mixing terms it is however convenient to embed the SM fields in the same representation of $\mathcal{O}^f$. At lower energies, where the symmetry is spontaneously broken, we render explicit the NGB dependence of these terms as $\mathcal{O}^f = U(x)\,\Psi(x)$ (see app. B), where $U(x)$ is the NGB matrix (3.17) and $\Psi(x)$ is a composite fermion beloning to some irreducible representation $r_{\mathcal{H}}$ of the unbroken subgroup $\mathcal{H}$. Any representation $r_{\mathcal{H}}$ can be "dressed" with the matrices U to get representations of $\mathcal{G}$. The choice of the representation $r_{\mathcal{G}}$, in which to embed the SM fields, and the representation of the composite fermions $r_{\mathcal{H}}$ is a source of model dependence, in particular the choice of the embedding of the elementary fields fixes the functional dependence of the effective Yukawa couplings of the Higgs with the SM fermions, hence the functional dependence in the effective potential and the deviation in the Higgs couplings.

We will not perform a systematic study of all possible $r_{\mathcal{G}}$'s here, but focus on the simplest case where $r_{\mathcal{G}}$ is the fundamental, **5**, of SO(5). The SM fields are then conveniently written in terms of spurion five-component fermions ξ_L and ξ_R, formally transforming in the fundamental of SO(5). The embedding of the SM quark doublets has to be different for the mixing terms responsible for the up-type or down-type quark masses:

$$\xi_L^u = \frac{1}{\sqrt{2}} \begin{pmatrix} b_L \\ -ib_L \\ t_L \\ it_L \\ 0 \end{pmatrix}_{2/3} , \quad \xi_R^u = \begin{pmatrix} 0 \\ 0 \\ 0 \\ 0 \\ t_R \end{pmatrix}_{2/3} , \quad \xi_L^d = \frac{1}{\sqrt{2}} \begin{pmatrix} t_L \\ it_L \\ -b_L \\ ib_L \\ 0 \end{pmatrix}_{-1/3} , \quad \xi_R^d = \begin{pmatrix} 0 \\ 0 \\ 0 \\ 0 \\ b_R \end{pmatrix}_{-1/3} ,$$

$$(3.26)$$

where the subscripts indicate the U(1)$_X$ charge needed to reproduce the correct hypercharge, eq. (3.15). With the above choice of fermion quantum numbers for the up-type embedding, b_L mixes with the bi-doublet component of the fermion resonance with $T_{3R} = T_{3L}$ and potentially large contributions to δg_b vanish [136].[5]

In order to obtain the possible structures of the low energy effective Lagrangian, when all the resonances have been integrated out, it is possible to write all the $\mathcal{G}$-invariants with the above spurions, the NGB matrix U and the projectors on the SO(4) irreducible representations, $P_Q = \mathrm{diag}(1,1,1,1,0)$ (fundamental), $P_S = \mathrm{diag}(0,0,0,0,1)$ (singlet). Recalling the transformation rule of U, $U \to gUk^\dagger(g, h^{\hat{a}}(x))$, where $g \in$ SO(5) and $k \in$ SO(4), we can write the following

---

[5]Such sizable corrections are instead present in the, even more minimal, case in which the elementary fermions are embedded in the spinorial representation **4** of SO(5). For this reason we do not consider this case.

SO(5) × U(1)$_X$ invariants:

$$\bar{\xi}_L^u U P_Q U^\dagger \gamma^\mu \xi_L^u = \bar{b}_L \gamma^\mu b_L + \left(1 - \frac{1}{2} s_h^2\right) \bar{t}_L \gamma^\mu t_L \ ,$$

$$\bar{\xi}_L^u U P_S U^\dagger \gamma^\mu \xi_L^u = \frac{1}{2} s_h^2 \bar{t}_L \gamma^\mu t_L \ ,$$

$$\bar{\xi}_L^d U P_Q U^\dagger \gamma^\mu \xi_L^d = \left(1 - \frac{1}{2} s_h^2\right) \bar{b}_L \gamma^\mu b_L + \bar{t}_L \gamma^\mu t_L \ ,$$

$$\bar{\xi}_L^d U P_S U^\dagger \gamma^\mu \xi_L^d = \frac{1}{2} s_h^2 \bar{b}_L \gamma^\mu b_L \ , \tag{3.27}$$

$$\bar{\xi}_R^u U P_Q U^\dagger \gamma^\mu \xi_R^u = s_h^2 \bar{t}_R \gamma^\mu t_R \ ,$$

$$\bar{\xi}_R^u U P_S U^\dagger \gamma^\mu \xi_R^u = (1 - s_h^2) \bar{t}_R \gamma^\mu t_R \ ,$$

$$\bar{\xi}_R^d U P_Q U^\dagger \gamma^\mu \xi_R^d = s_h^2 \bar{b}_R \gamma^\mu b_R \ ,$$

$$\bar{\xi}_R^d U P_S U^\dagger \gamma^\mu \xi_R^d = (1 - s_h^2) \bar{b}_R \gamma^\mu b_R \ ,$$

$$\bar{\xi}_L^u U P_Q U^\dagger \xi_R^u = \frac{i}{\sqrt{2}} c_h s_h \bar{t}_L t_R \ ,$$

$$\bar{\xi}_L^u U P_S U^\dagger \xi_R^u = -\frac{i}{\sqrt{2}} c_h s_h \bar{t}_L t_R \ ,$$

$$\bar{\xi}_L^d U P_Q U^\dagger \xi_R^d = \frac{i}{\sqrt{2}} c_h s_h \bar{b}_L b_R \ , \tag{3.28}$$

$$\bar{\xi}_L^d U P_S U^\dagger \xi_R^d = -\frac{i}{\sqrt{2}} c_h s_h \bar{b}_L b_R \ ,$$

where we evaluated U in the unitary gauge and omitted the trivial diagonal ones such as $\bar{\xi}_X \gamma^\mu \xi_X$. In general, all these operators are generated when the heavy fermions are integrated out, providing an effective Lagrangian for the SM fermions with a specific functional dependence on the Higgs field dictated by eqs. (3.27,3.28) (see eqs. (3.88,3.90)). Each of the above operators will be generated by the relevant mixing terms related to the specific spurion field, in particular the operators involving the ξ_X^u spurions will be generated by the top mixing while the ones involving ξ_X^d will be generated by the much smaller bottom quark mixing. The operators in eq. (3.27) provide a wave function normalization factor while those in eq. (3.28) generate the Yukawa interactions and – when the Higgs takes a VEV – a mass term for the SM fermions. In fact, from eq. (3.28) we can obtain the correction of the Higgs couplings to fermions by expanding the Higgs field around its vev $h \to f \arcsin(v/f) + h$:[6]

$$c_h s_h = \sqrt{\xi(1-\xi)} \left(1 + \frac{1-2\xi}{\sqrt{1-\xi}} \frac{h}{v} - 2\xi \frac{h^2}{v^2} + \mathcal{O}(h^3)\right) \ . \tag{3.29}$$

The first, constant, term in eq. (3.29) provides the mass for the SM fermion, while the second one is the single Higgs coupling to fermions. Comparing with eq. (3.6) we get

$$c = \frac{1-2\xi}{\sqrt{1-\xi}} \ . \tag{3.30}$$

---

[6]We neglect here small wave function normalization corrections.

We see that, differently from the SM, the pNGB nature of the Higgs implies the presence of interactions with more than one Higgs external leg, with a coupling suppressed by ξ.

3.4 Composite resonances

Generically, in strongly coupled theories conserved currents J_μ^α are expected to excite from the vacuum composite spin-1 resonances. This indeed happens in QCD, where the current corresponding to the unbroken $\mathrm{SU}(2)_I$ isospin symmetry excites the ρ_μ meson while the broken generators of the $\mathrm{SU}(2)_L \times \mathrm{SU}(2)_R/\mathrm{SU}(2)_I$ coset excite the axial vector a_μ. Therefore, we expect that also composite Higgs models present spin-1 composite resonances corresponding to the unbroken and broken generators of the $\mathcal{G} \to \mathcal{H}$ symmetry breaking pattern. These states are also important in restoring unitarity in the elastic NGB scattering before the cutoff scale $\Lambda \sim 4\pi f$. Moreover, as we discussed before, the partial compositeness mechanism predicts the presence of fermion resonances mixing linearly with the SM fermions.

According to the CCWZ formalism, the most general Lagrangian invariant under a non-linearly realized group $\mathcal{G}$, spontaneously broken to a linearly realized subgroup $\mathcal{H}$, should be written using the structures d_μ and the covariant derivative $\nabla_\mu = \partial_\mu - iE_\mu$ introduced before, that act on matter fields in representations of $\mathcal{H}$. Therefore, we expect the Lagrangian of the composite resonances to be just $\mathcal{H}$-invariant.

In this section we present how to construct generic Lagrangians for these composite resonances and show how they mix with the SM gauge bosons and fermions.

3.4.1 Spin-1 resonances

We assume that below the cut-off of the theory at $\Lambda \sim 4\pi f$, the theory contains spin-1 resonances parametrized by a mass $m_\rho \simeq g_\rho f$ and a coupling $1 < g_\rho < 4\pi$. The coupling g_ρ controls both the interactions among the resonances and the resonance-NGB interactions.

There are several ways to add vector resonances in a chiral Lagrangian. They have been shown to be all equivalent, once field redefinitions and the addition of local counterterms is taken into account [137]. Given our assumptions, the most useful set-up is a generalization of the so-called "hidden local symmetry" approach, where the resonances ρ_μ^L and ρ_μ^R, in representations $(\mathbf{3},\mathbf{1}) \oplus (\mathbf{1},\mathbf{3})$ of $\mathrm{SU}(2)_L \times \mathrm{SU}(2)_R$ respectively, transform non-linearly, while the resonances a_μ, forming $(\mathbf{2},\mathbf{2})$ representations of $\mathrm{SU}(2)_L \times \mathrm{SU}(2)_R$, transform homogeneously. With an abuse of language, for simplicity we will denote in the following the $\rho_\mu^{L,R}$'s and the a_μ as "vector" and "axial" resonances, respectively, although not all $\rho_\mu^{L,R}$ and not all a_μ actually transform under

parity as vector and axial gauge fields. Under a transformation $g \in \mathrm{SO}(5)$, we have

$$
\begin{cases}
\rho_\mu^L = \rho_\mu^{aL} T^{aL} & , \quad \rho_\mu^L \to h\rho_\mu^L h^\dagger + \frac{i}{g_{\rho_L}}(h\partial_\mu h^\dagger)^L, \\
\rho_\mu^R = \rho_\mu^{aR} T^{aR} & , \quad \rho_\mu^R \to h\rho_\mu^R h^\dagger + \frac{i}{g_{\rho_R}}(h\partial_\mu h^\dagger)^R, \\
a_\mu = a_\mu^{\hat{a}} T^{\hat{a}} & , \quad a_\mu \to h a_\mu h^\dagger,
\end{cases}
\tag{3.31}
$$

where $h = h(g, h^{\hat{a}})$. At leading order in derivatives, the most general Lagrangian allowed by eq.(3.31) for N_{ρ_L} multiplets in the $(\mathbf{3},\mathbf{1})$, N_{ρ_R} in the $(\mathbf{1},\mathbf{3})$ and N_a axial vectors in the $(\mathbf{2},\mathbf{2})$ is

$$
\mathcal{L}_g = \mathcal{L}^{v_L} + \mathcal{L}^{v_R} + \mathcal{L}^a,
\tag{3.32}
$$

where

$$
\begin{aligned}
\mathcal{L}^{v_L} &= \sum_{i=1}^{N_{\rho_L}} \left(-\frac{1}{4}\mathrm{Tr}\left(\rho_{L,\mu\nu}^i \rho_L^{i,\mu\nu}\right) + \frac{f_{\rho_L^i}^2}{2}\mathrm{Tr}\left(g_{\rho_L^i}\rho_{L,\mu}^i - E_\mu^L\right)^2 + \sum_{j<i}\frac{f_{\mathrm{mix}_{ij}}^2}{2}\mathrm{Tr}\left(g_{\rho_L^i}\rho_{L,\mu}^i - g_{\rho_L^j}\rho_{L,\mu}^j\right)^2 \right), \\
\mathcal{L}^{v_R} &= \mathcal{L}^{v_L}\;,\;\text{with } L \to R, \\
\mathcal{L}^a &= \sum_{i=1}^{N_a}\left(-\frac{1}{4}\mathrm{Tr}\left(a_{\mu\nu}^i a^{i\mu\nu}\right) + \frac{f_{a_i}^2}{2\Delta_i^2}\mathrm{Tr}\left(g_{a_i}a_\mu^i - \Delta_i d_\mu\right)^2 \right).
\end{aligned}
\tag{3.33}
$$

In eq.(3.33), $E_\mu^{L,R}$ are the $SU(2)_{L,R}$ components of E_μ. The field strengths and covariant derivatives are defined as

$$
\rho_{L,\mu\nu}^i = \partial_\mu \rho_{L,\nu}^i - \partial_\nu \rho_{L,\mu}^i - ig_{\rho_L^i}[\rho_{L,\mu}^i, \rho_{L,\nu}^i], \quad a_{\mu\nu} = \nabla_\mu a_\nu - \nabla_\nu a_\mu, \;\; \nabla = \partial - iE.
\tag{3.34}
$$

Note that for the axial vectors there is no need to add mass mixing terms, since one can always diagonalize the quadratic terms and bring the Lagrangian in the form above. It is useful to define the mass parameters

$$
m_{\rho_L^i}^2 = f_{\rho_L^i}^2 g_{\rho_L^i}^2, \quad m_{\rho_R^i}^2 = f_{\rho_R^i}^2 g_{\rho_R^i}^2, \quad m_{a_i}^2 = \frac{f_{a_i}^2 g_{a_i}^2}{\Delta_i^2},
\tag{3.35}
$$

keeping of course in mind that the actual masses for the ρ's in presence of mixing have to be obtained via a diagonalization of the quadratic terms. The mass terms in eq.(3.33) induce mixing terms between the vector resonances $\rho_{L,\mu}^i$ ($\rho_{R,\mu}^i$) and the SM gauge fields W (B), as expected by the partial compositeness scenario [118], generalized to more resonances. For $N_{\rho_L} = N_{\rho_R} = 1$, the actual mass eigenstates before EWSB are found by simple SO(2) rotations: $W_{aL} \to W_{aL}\cos\theta_g + \rho_{aL}\sin\theta_g$, $B \to B\cos\theta'_{g'} + \rho_{3R}\sin\theta_{g'}$ (and similar transformations for ρ_{aL} and ρ_{3R}), where $\tan\theta_g = g_0/g_{\rho_L}$, $\tan\theta_{g'} = g_0'/g_{\rho_R}$. Alternatively, for sufficiently heavy resonances, one can keep the original W and B fields and integrate out the resonances. The two descriptions are obviously equivalent, but depending on the problem at hand, one can be more convenient than the other.

We assume that the coefficients of higher dimensional operators are dictated by NDA, where g_ρ is treated as a "weak" coupling. This should in principle be contrasted to the recent *partial UV*

completion (PUVC) hypothesis, introduced in [105], according to which the couplings of higher dimensional operators should not exceed the σ model coupling, $g_* = \Lambda/f$, at the cutoff scale Λ. In particular, the NDA hypothesis puts more severe bounds on the values of the coefficients of the higher dimensional operators. For instance, let us consider as an illustration the $\mathcal{O}(p^4)$ operators Q_1 and Q_2 (in the notation of [105]), $Q_1 = \text{Tr}\,(\rho^{\mu\nu} i[d_\mu, d_\nu])$, $Q_2 = \text{Tr}\,(\rho^{\mu\nu} f_{\mu\nu}^+)$. The NDA and PUVC estimates of their couplings α_1 and α_2 are

$$\begin{aligned} \alpha_1^{(NDA)} &\simeq \frac{g_\rho}{16\pi^2}\,, & \alpha_1^{(PUVC)} &\leq \frac{1}{4\pi}\,, \\ \alpha_2^{(NDA)} &\simeq \frac{g g_\rho}{16\pi^2}\,, & \alpha_2^{(PUVC)} &\leq 1\,. \end{aligned} \tag{3.36}$$

We see that the two estimates are consistent with each other, but the PUVC hypothesis allows for larger coefficients.

Demanding a partial unitarization of $\mathcal{A}(\pi\pi \to \pi\pi)$ by the vector resonances allows to select a definite range in the values of f_ρ and f_a. For example, for one vector resonance ρ_μ in the adjoint of $SO(4)$, assuming left-right (LR) $\mathbf{Z}_2$ symmetry, from the Lagrangian in eq.(3.33) and eq.(3.21) one can obtain its contribution to the $\pi\pi$ scattering amplitude [105]. Neglecting the finite width of the resonance, one has

$$\mathcal{A}(\pi^a \pi^b \to \pi^c \pi^d) = A(s,t,u)\delta^{ab}\delta^{cd} + A(t,s,u)\delta^{ac}\delta^{bd} + A(u,t,s)\delta^{ad}\delta^{bc},$$
$$A(s,t,u) = \frac{s}{f^2}\left(1 - \frac{3}{2}a_\rho^2\right) - \frac{a_\rho^2}{2}\frac{m_\rho^2}{f^2}\left[\frac{s-u}{t-m_\rho^2} + \frac{s-t}{u-m_\rho^2}\right], \tag{3.37}$$

where $a_\rho \equiv f_\rho/f$ and s, t, u are the usual Mandelstam variables. From this formula one can check that ρ_μ unitarizes the scattering for $a_\rho = \sqrt{2/3}$. Assuming PUVC one obtains the bounds $a_\rho \sim 1$ and $f_a/f \equiv a_a \lesssim 1$, which we will typically assume in the following.

3.4.2 Spin-1/2 resonances

Let us now describe the composite fermion resonances responsible for providing a mass to the SM fermions. In the following we focus only on the top quark because it has the highest amount of mixing with the composite fermions, since its mass is – by far – the biggest among the SM fermions. As described in sec. 3.3.2, we need to embed the composite fermions in irreducible representations, $r_\mathcal{H}$ of $\mathcal{H}$. For simplicity we consider only the singlet and the fundamental $\mathbf{4} \sim (\mathbf{2}, \mathbf{2})$. Let us consider N_S and N_Q singlets and bi-doublets spin 1/2 resonances S_i and Q_j $(i = 1, \ldots, N_S, j = 1, \ldots, N_Q)$, with $U(1)_X$ charge $q_X = +2/3$. The two doublets contained in each Q_i have hypercharge 1/6 and 7/6 respectively, the first one therefore is the partner of the top doublet while the latter is an exotic fermion doublet which contains a fermion with electric charge $Q = 5/3$. From these fields, we can construct fermions transforming in the fundamental

of $\mathcal{G}$ as follows:

$$\sum_{a=1}^{4} U_{Aa} Q_{a,j}, \quad U_{A5} S_i, \quad A = 1, \ldots, 5, \tag{3.38}$$

where we have explicitly reported the SO(5) group indices. Each of the above two operators (3.38) can couple to the SM fermion fields, included in the spurions $\xi_{L,R}$ of eq. (3.26)[7].

As described in appendix B, the Lagrangian for non-linearly realized symmetries should include all local $\mathcal{H}$-invariant terms. The leading order Lagrangian for the SM and composite fermions is easily constructed:

$$\begin{aligned} \mathcal{L}_{f,0} = \ & \bar{q}_L i \not{D} q_L + \bar{t}_R i \not{D} t_R + \sum_{i=1}^{N_S} \bar{S}_i (i \not{\nabla} - m_{iS}) S_i + \sum_{j=1}^{N_Q} \bar{Q}_j (i \not{\nabla} - m_{iQ}) Q_j + \\ & \sum_{i=1}^{N_S} \left(\frac{\epsilon_{tS}^i}{\sqrt{2}} \bar{\xi}_R P_L U S_i + \epsilon_{qS}^i \bar{\xi}_L P_R U S_i \right) + \sum_{j=1}^{N_Q} \left(\frac{\epsilon_{tQ}^j}{\sqrt{2}} \bar{\xi}_R P_L U Q_i + \epsilon_{qQ}^j \bar{\xi}_L P_R U Q_i \right) + h.c., \end{aligned} \tag{3.39}$$

where a $\sqrt{2}$ factor in the definition of $\epsilon_{tS,tQ}^{i,j}$ has been introduced for later convenience and

$$\nabla_\mu = \partial_\mu - i E_\mu - i q_X g_0' B_\mu. \tag{3.40}$$

There are in general $3N_Q + 3N_S$ complex phases appearing in eq.(3.39), $2N_Q + 2N_S + 1$ of which can be reabsorbed by appropriate phase redefinitions of the fermion fields, for a total of $N_Q + N_S - 1$ physical phases. Therefore, without any loss of generality, we can take the vector masses m_{iS} and m_{jQ} to be real and positive. Along the lines of [119], it will be useful to rewrite the last row in (3.39) as

$$\sum_{i=1}^{N_S} \left(\bar{t}_R E_{tS}^i P_L U S_i + \bar{q}_L E_{qS}^i P_R U S_i \right) + \sum_{j=1}^{N_Q} \left(\bar{t}_R E_{tQ}^j P_L U Q_i + \bar{q}_L E_{qQ}^j P_R U Q_i \right) + h.c. \tag{3.41}$$

where the E's are spurion mixing terms, transforming as follows under the enlarged group $\text{SU}(2)_L^0 \times \text{U}(1)_R^0 \times \text{U}(1)_X^0 \times \text{SO}(5) \times \text{U}(1)_X$, eventually broken to G_{SM} by the spurion VEV's:

$$E_{tS}^i, E_{tQ}^j \sim (\mathbf{1}, 0, 2/3, \bar{\mathbf{5}}, -2/3), \quad E_{qS}^i, E_{qQ}^j \sim (\mathbf{2}, -1/2, 2/3, \bar{\mathbf{5}}, -2/3). \tag{3.42}$$

Couplings between spin 1/2 and spin 1 resonances and additional couplings to the σ-model fields d_μ and E_μ are easily constructed by recalling that $g_\rho \rho_\mu - E_\mu$, a_μ and d_μ, under SO(5), homogeneously transform according to local SO(4) transformations. The most general leading order couplings are the following (assuming LR symmetry):

$$\begin{aligned} \mathcal{L}_{f,int} = \sum_{\eta=L,R} \Big(& k_{ijk}^{V,\eta} \bar{Q}_j \gamma^\mu (g_{\rho^i} \rho_\mu^i - E_\mu) P_\eta Q_k + k_{ijkl}^{\text{mix}} \bar{Q}_i \gamma^\mu (g_{\rho^k} \rho_\mu^k - g_{\rho^l} \rho_\mu^l) P_\eta Q_j \\ & + k_{ikj}^{A,\eta} \bar{S}_i \gamma^\mu g_{a^k} a_\mu^k P_\eta Q_j + \sum_{i,j} k_{ij}^{d,\eta} \bar{S}_i \gamma^\mu d_\mu P_\eta Q_j + h.c. \Big), \end{aligned} \tag{3.43}$$

---

[7]We drop the u, d index since, unless explicitly stated, we assume always the embeddings for the up-type quarks.

where P_η are chiral projectors. The last term in eq. (3.43), in particular, can play an important role in the phenomenology of single production processes of top partners [138, 139] and in the fermion contributions to EW precision tests [86]. However, since they do not influence the scalar potential at one-loop, we neglect the terms in eq. (3.43) in the following.

The total fermion Lagrangian is obtained by summing eq. (3.39) with eq. (3.43):

$$\mathcal{L}_f = \mathcal{L}_{f,0} + \mathcal{L}_{f,int} \,. \tag{3.44}$$

The fermion Lagrangian (3.44) is easily generalized to include the couplings to other SM fermions. For instance, the bottom quark sector can be obtained by adding the b_R field and additional fermion singlet and bi-doublet resonances $S_i^{(d)}$ and $Q_j^{(d)}$, with $q_X = -1/3$. The latter mix to b_R and b_L by means of operators of the form $\bar{b}_{L/R} U S_{i,R/L}^{(d)}$ and $\bar{b}_{L/R} U Q_{j,R/L}^{(d)}$. These mixing affect the top sector, but they are safely negligible, given the smallness of the bottom mass. They also induce a non vanishing tree-level δg_b, which is however usually sub-dominant with respect to one-loop corrections coming from fermion mixing in the charge 2/3 (top) sector. It is then consistent to consider the Lagrangian (3.44), neglecting altogether the fermion resonances $S_i^{(d)}$ and $Q_j^{(d)}$.

It is useful to discuss in some more detail the simple case $N_S = N_Q = 1$. For simplicity let us take real mixing terms $\epsilon_{t,q/Q,S}$. We see from eq. (3.39) that before EWSB the LH top mixes with Q through the parameter ϵ_{qQ} and the RH top mixes with S through ϵ_{tS}, The degree of compositeness of the top quark can be measured by the angles $\theta_{L,R}$ [118] defined as:

$$\tan\theta_L = \frac{|\epsilon_{qQ}|}{m_Q} \,, \quad \tan\theta_R = \frac{|\epsilon_{tS}|}{\sqrt{2}m_S} \,. \tag{3.45}$$

The larger $\tan\theta_{L/R}$ is, the more $t_{L/R}$ is composite. For $s_h \ll 1$, the top mass is given by

$$M_{top} \simeq \frac{\sin\theta_L \sin\theta_R}{\sqrt{2}} \left| \frac{\epsilon_{qS}}{\epsilon_{qQ}} m_Q - \frac{\epsilon_{tQ}}{\epsilon_{tS}} m_S \right| s_h \,. \tag{3.46}$$

The physical masses of the fermion resonances, before EWSB, are the following:

$$M_0 = \frac{m_S}{\cos\theta_R} \,, \quad M_{1/6} = \frac{m_Q}{\cos\theta_L} \,, \quad M_{7/6} = m_Q \,, \tag{3.47}$$

where the subscripts 0, 1/6 and 7/6 denote the hypercharges of the singlet and of the two $SU(2)_L$ doublets forming the bi-doublet Q.

The case in which t_R is fully composite can be studied by assuming that t_R is a chiral massless fermion bound state coming from the compositTevatrone sector and directly identifying it as the RH component of the singlet fermion resonance S_R in eq.(3.39). In this way, t_R and S_L, and hence the parameters m_S, ϵ_{tS} and ϵ_{tQ}, should be removed from eq.(3.39). We will come back to this particularly simple model in section 3.8.

The total Lagrangian of the model is finally given by

$$\mathcal{L}_{Tot} = \mathcal{L}_{\sigma_g} + \mathcal{L}_g + \mathcal{L}_f \,. \tag{3.48}$$

3.5   Phenomenology of composite Higgs models

As we saw in the previous sections, composite Higgs models offer a rich phenomenology at colliders. The pNGB nature of the Higgs at a scale f not too far from the EW scale implies a definite pattern of deviations in the Higgs couplings to SM gauge bosons and fermions, which is largely independent on the details of the spectrum of the model.

For what regards searches of new particles, a rich spectrum of new states is predicted. On the one hand the presence of a strongly coupled sector at the few-TeV scale, the necessity of regularizing the SM gauge contribution to the Higgs potential and of curing the UV behavior of the NGB scattering amplitudes strongly suggests the presence of spin-1 resonances charged under the EW gauge group and mixing with the elementary SM gauge bosons at a scale of a few TeV. On the other hand, the partial compositeness mechanism predicts the presence of fermion top partners which, as we will show in section 3.7, are expected to be very near the $\sim 1\text{TeV}$ mass range.

Both the deviations in the Higgs couplings and the presence of these resonances produce also deviations in electroweak pseudo-observables such as the S and T oblique parameters and deviations in the Z boson couplings to the physical b quark. All these observables have been strongly constrained by LEP and impose strong indirect bounds on the new physics spectrum, albeit these constraints are more model-dependent.

In this section we discuss these phenomenological aspects of composite Higgs models in more detail, reviewing the constraints they offer on the models.

3.5.1   Higgs couplings deviations

As we saw, composite Higgs models predict $\mathcal{O}(\xi)$ deviations of the tree level Higgs couplings to gauge bosons and fermions w.r.t. their SM values, which implies deviations in the Higgs decay rates. In particular, in both minimal and next-to-minimal composite Higgs models with SM fermions embedded in the fundamental of $\mathcal{G}$ one has (see eqs. (3.25,3.30) for SO(5)/SO(4) and table F.1 for the SO(6)/SO(5) case)

$$\frac{\Gamma_{VV}}{\Gamma_{VV}^{SM}} = |a|^2 = 1 - \xi \;, \qquad \frac{\Gamma_{f\bar{f}}}{\Gamma_{f\bar{f}}^{SM}} = |c|^2 = \frac{(1-2\xi)^2}{1-\xi} \simeq 1 - 3\,\xi + \mathcal{O}(\xi^2) \;, \qquad (3.49)$$

with $V = W, Z$. It should be noted here that the ξ-dependence in the modified coupling of the Higgs with EW gauge bosons is model-independent,[8] whereas the coupling with fermions is modified according to the representation of $\mathcal{G}$ in which the SM fermions are embedded, as

---

[8]In general the couplings depend on the chosen parametrization of the coset, only when computing physical observables this parametrization-dependence is removed. See appendix F for a detailed discussion of this issue in the context of the next-to-minimal SO(6)/SO(5) model.

discussed in section 3.4.2. As in the previous construction of the models, we assume here that SM fermions are embedded in the fundamental **5** (or a symmetric **10**) of SO(5).[9] Loop-induced couplings – i.e. Higgs to gluons, photons and $Z\gamma$ – are also modified as an indirect consequence of the deviations in the tree-level Higgs couplings (see e.g. [141]):

$$\frac{\Gamma_{gg}}{\Gamma_{gg}^{SM}} \simeq 0.678 \left|1.28c_t - (0.07 - 0.1i)c_b\right|^2 = \frac{(1-2\xi)^2}{1-\xi} \simeq 1 - 3\,\xi + \mathcal{O}(\xi^2)\,, \tag{3.50}$$

$$\frac{\Gamma_{\gamma\gamma}}{\Gamma_{\gamma\gamma}^{SM}} \simeq 1.73 \left|0.97a - 0.21c_t\right|^2 = 1.73 \left(0.97\sqrt{1-\xi} - 0.21\frac{1-2\xi}{\sqrt{1-\xi}}\right)^2 \simeq 1 - 0.45\,\xi + \mathcal{O}(\xi^2)\,,$$

$$\frac{\Gamma_{Z\gamma}}{\Gamma_{Z\gamma}^{SM}} \simeq 0.51 \left|1.49a - 0.09c_t\right|^2 = 0.51 \left(1.49\sqrt{1-\xi} - 0.09\frac{1-2\xi}{\sqrt{1-\xi}}\right)^2 \simeq 1 - 0.87\,\xi + \mathcal{O}(\xi^2)\,,$$

where we specified the SM fermion included in the loop by the suffix t, b. For instance the Higgs coupling to gluons, whose value sets the Higgs production cross-section via gluon fusion, is dominated by the top triangle loop while the Higgs decays to $\gamma\gamma$ and to γZ is given by an interference of the top and the W contributions.

The proprieties of the Higgs boson, and in particular its couplings to each of the SM gauge bosons and fermions, are currently under investigation at the LHC. The couplings are measured by the ATLAS [142] and CMS [143] experiments considering the channels $h \to \gamma\gamma$, $h \to ZZ^*$ (with $ZZ^* \to 4l, 2l2\nu, 2l2q, 2l2\tau$), $h \to WW^*$ (with $WW^* \to l\nu l\nu, l\nu qq$), $h \to b\bar{b}$ and $h \to \tau^+\tau^-$ (with both leptonic and hadronic τ-decays). Since we aim to use this analysis also for the SO(6)/SO(5) model presented in chapter 4, in which the extra singlet NGB is a stable dark matter candidate, we study here also the possibility of a non-zero invisible decay branching ratio, $\mathrm{BR_{inv}}$, of the Higgs boson. This is strongly constrained by the fact that the rates associated to the channels listed above are compatible with the predictions of the SM [144,145]. In our analysis we perform a combined fit of all the data related to the Higgs searches under investigation at the LHC and the Tevatron taking into account both the modified Higgs couplings in eq. (3.49) and the invisible decay width. We perform a χ-square fit following ref. [141] (see also refs. [146–151] for similar analysis) and we present our results in figure 3.4. In the upper plot of figure 3.4 we show the result of a two-dimensional fit considering as free parameters both $\mathrm{BR_{inv}}$ and ξ [2]. Notice that larger values of $\mathrm{BR_{inv}}$ are allowed only if combined with small values of ξ. The reason is that a high value of ξ suppresses the Higgs production cross-section via gluon fusion, as immediately follows from the modified coupling g_{hgg} previously discussed. This suppression, in turn, gives a tighter bound on the invisible branching fraction since, intuitively, less Higgses than expected are produced [141]. In the lower panel of figure 3.4 we restrict our analysis to a one-dimensional fit obtained fixing either $\mathrm{BR_{inv}}$ or ξ to some given value. In the lower-left plot

---

[9]See ref. [140] for a special case, based on the non-compact global symmetry SO(4, 1), in which $g_{hVV} = g_{hVV}^{\mathrm{SM}}\sqrt{1+\xi}$.
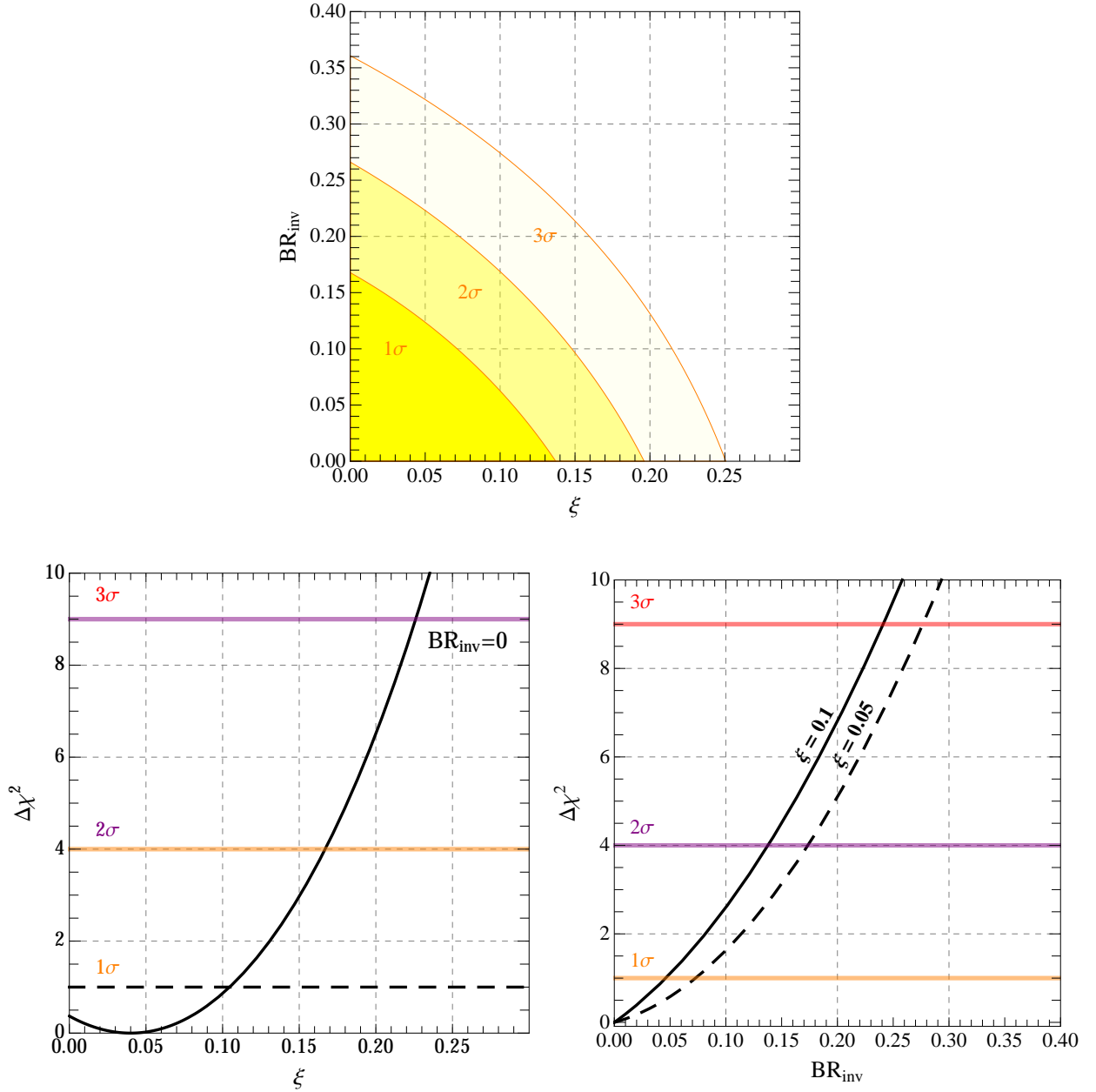
Figure 3.4: Results of the χ-square fit obtained considering all the Higgs searches under investigation at the LHC and the Tevatron (see ref. [141] for details).In the upper row we show the 1σ, 2σ and 3σ confidence regions obtained considering a two-dimensional fit of the data as a function of the invisible branching ratio and the parameter ξ. In the lower row we show the $\Delta\chi^2 = \chi^2 - \chi^2_{\min}$ distribution together with the corresponding 1σ, 2σ and 3σ confidence contours as a function of ξ (left panel) and the invisible branching ratio for a fixed value of ξ (right panel). The $\chi^2_{\min}$ is 51 in the lower left plot, and 52 (51) for $\xi = 0.1$ (0.05) in the lower right plot.

we fix $\mathrm{BR}_{\mathrm{inv}} = 0$, which is the case of the minimal composite Higgs model presented in this chapter, and find that a value of $\xi > 0.226$ is excluded at the 3σ level. In the lower-right plot, instead, we consider as free parameter only the invisible branching ratio, while we fix ξ to two benchmark values $\xi = 0.1$ and $\xi = 0.05$. For $\xi = 0.1$ ($\xi = 0.05$) we find that $\mathrm{BR}_{\mathrm{inv}} > 0.24$ ($\mathrm{BR}_{\mathrm{inv}} > 0.275$) is excluded at 3σ level.

3.5.2   Direct searches of composite resonances

Let us now focus on constraints from the LHC on the composite resonances present in our models, discussed in sections 3.4.1, 3.4.2. It is already well established that, in the context of composite pseudo-Nambu Goldstone Higgs models with partial compositeness, the measured values of the Higgs and top masses require the presence of top-partners with a mass below the TeV scale [1, 44–46]. The parameter scans we performed for our models (which are presented in the following sections, as well as for those in appendix D and for the next-to-minimal composite Higgs models discussed in chapter 4) confirm this fact, as can be seen from figures 3.8, 3.7, D.1, D.2, D.4, 4.3, 4.4. Moreover, in some interesting models, the spin-1 resonances are expected to be near (or even below) the ~ 2 TeV scale, see eqs. (3.104), (4.32) and figures D.1(b,d), D.2(a).

The present experimental bounds on spin-1 resonances and, more importantly, on spin-1/2 top partners are already able to rule out a relevant part of the parameter space of our models.

Vector resonances

Ref. [152] recently studied the bounds from direct searches at the LHC of spin-1 resonances introducing a simplified model with a triplet of $\mathrm{SU}(2)_L$ and presenting the bound in the (g_ρ, m_ρ) plane. Our model presents a more complicated spectrum of vector resonances: the adjoint of $\mathrm{SO}(4)$ (ρ_μ^a), with masses of the order m_ρ, contains a $(\mathbf{3}, \mathbf{1}) \oplus (\mathbf{1}, \mathbf{3})$ of $\mathrm{SU}(2)_L \otimes \mathrm{SU}(2)_R$ and the fundamental of $\mathrm{SO}(4)$ ($a_\mu^{\hat{a}}$), with mass m_a transforms as a bidoublet $(\mathbf{2}, \mathbf{2})$. In order to obtain experimental bounds on these states it would be necessary to perform a complete collider study of the model, including also possible chain decays involving composite fermions through the interactions of eq. (3.43), see ref. [153] for a recent phenomenological analysis of this issue. Since this is well beyond the purpose of this thesis we take at face value, as an approximate reference value of the experimental bound on these states, the result of ref. [152]. Fixing the two benchmark values of $\xi = 0.1, \ 0.05$ and taking for simplicity $f_\rho = f$, so that $m_\rho \simeq g_\rho f = g_\rho \frac{v}{\sqrt{\xi}}$, we get that the allowed region is approximately

$$m_\rho \gtrsim 1.8 \ (2.2) \ \text{TeV} \quad \text{for} \quad \xi = 0.1 \ (0.05) \ . \tag{3.51}$$

This is comparable with the bound one can extract from the tree-level contribution of the spin-1 resonances to the $\hat{S}$ parameter [59, 60] in eq. (3.85), assuming no correlation with other contri-

butions. In fact, from the constraint $\hat{S} \lesssim 2 \times 10^{-3}$ [83] one obtains a bound of $m_\rho \gtrsim 1.8$ (2.4) TeV for $f_\rho = f/\sqrt{2}$ ($= 2f$).

Top partners

Both ATLAS and CMS collaborations are providing bounds on pair produced top partners, studying different decay modes. The relevant searches for our models are those for colored vector-like fermions, X, with electric charge $Q = 5/3$ decaying in W^+t with BR$(X \to W^+t) = 100\%$ [154, 155] and for vector-like top partners T' with $Q = 2/3$ decaying into bW^+, tZ and th [156–158]. The $Q = 5/3$ fermion decays with unity probability to tW^+ when it is the lightest and masses $M_X < 800$ GeV are excluded at 95% C.L. by CMS [154]. The branching ratios of the T' in the three channels listed before are instead model-dependent and the 95% C.L. bound given in ref. [156] varies from ~ 680 GeV up to ~ 780 GeV. Applying the Equivalence Theorem gives a reference value, for the singlet branching ratios, of BR$(T' \to W^+b) \simeq 2$BR$(T' \to Zt) \simeq 2$BR$(T' \to ht) \simeq 50\%$ [138], in which case the bound is ~ 700 GeV. These analysis are always performed under the assumption that only one new state is present at low energy while the others are much heavier. This assumption is very strong and seldom realized in concrete models, including our case. For these reasons a complete analysis of the experimental results in order to adapt them to the realistic case would be needed, but is beyond the purpose of the present thesis.

In models which include more than one copy of resonances in the bidoublet or singlet representation of SO(4), we assume that the first copy is lighter than the others. This situation is often realized in realistic points in the parameter space. We then classify the parameter space of our models in three broad regions depending on the mass of the doublet which includes the exotic $Q = 5/3$ fermion, $M_{7/6}$, and the mass of the lightest SO(4) singlet, M_{S_1}. The first region is defined as $M_{S_1} \ll M_{7/6}$ (light singlet) in which case we expect that the bound on the singlet T' to be approximately valid since all other states are heavier. In the opposite case, $M_{7/6} \ll M_{S_1}$, the $Y = 7/6$ doublet is the lightest. Since the experimental bound on this state is the strongest, we still expect that it will put the strongest constraint on this region. Even though the precise value of the bound may differ from the one in the simplified model with only one resonance, for our purposes we take that as a reference value. The same argument applies also in the region where $M_{7/6} \sim M_{S_1}$. Therefore, as a first approximation we adopt the following constraints:

$$M_{7/6} \gtrsim 800 \text{ GeV} , \qquad M_{S_1} \gtrsim 700 \text{ GeV} . \tag{3.52}$$

Comparing these bounds with the spectrum obtained by our parameter scans, reported in figures 3.7, 3.8, D.1, D.2, D.4, 4.3, 4.4, we see that the models with lower tuning, $\xi = 0.1$, are already on the verge to be excluded by direct searches and also for $\xi = 0.05$ the bounds cut a sizable part of the parameter space of the models.

3.5.3 Electroweak precision tests

Electroweak precision tests (EWPT) put strong indirect constrains on new physics beyond the SM. In the context of composite Higgs models, the most relevant constraints come from the oblique $\hat{S}$ and $\hat{T}$ parameters, bounded by LEP1 at the per-mil level (see sec. 2.3.1 for a presentation of the EW oblique parameters). Constraints coming from the W and Y parameters [60] can be neglected in composite Higgs models because they are parametrically suppressed with respect to $\hat{S}$ by a factor $(g/g_\rho)^2$ [58], where by g_ρ here we indicate a generic coupling from the strong sector. A non-universal important bound comes from δg_b, the deviation of the $\bar{b}_L Z b_L$ coupling from its SM value. Imposing a custodial symmetry and a proper mixing of b_L with the fermion resonances allow to suppress the tree-level values of $\hat{T}$ and δg_b [136]. More precisely, in the (oblique) basis where the contributions to δg_b coming from vector resonance mixing (universal for any SM fermion) vanish, $\hat{T}$ exactly vanishes.

As we will show in the following, however, in our effective setup the contributions to these observables are not predictable with a sufficient degree of accuracy. Moreover, estimates suggest that the indirect bounds obtainable from EWPT are now of the same order as those which can be derived from Higgs couplings and from direct searches of heavy resonances.

$\hat{S}$ and $\hat{T}$ parameters

Let us now analyze in some detail the different contributions of this class of models to the electroweak $\hat{S}$ and $\hat{T}$ parameters. In general it is possible to disentangle an IR, calculable part, from the uncalculable part and use NDA and a spurionic analysis to estimate the size of the latter. More details on how to make such estimates can be found, e.g., in refs. [86, 119].

The IR contribution to the oblique EW oblique parameters arises from the modified couplings of the Higgs with the SM gauge bosons, due to the non-linearity of the pNGB dynamics [73]. This modification depends only on the symmetry breaking pattern. This can be computed by introducing running $\hat{S}$ and $\hat{T}$ parameters from the compositeness scale Λ, where the effect is generated, down to the Z boson mass scale, where the parameters are measured. In this way, for $\Lambda \gg \mu \simeq m_Z$, one obtains the "leading log" deviations to $\hat{S}$ and $\hat{T}$ due to a pNGB composite Higgs:

$$\hat{T}_H(m_Z) = -\frac{g'^2}{16\pi^2}\frac{3\xi}{2}\log\frac{\Lambda}{m_Z}\,, \qquad \hat{S}_H(m_Z) = \frac{g'^2}{16\pi^2}\frac{\xi}{6}\log\frac{\Lambda}{m_Z}\,. \qquad (3.53)$$

In the language of effective operators introduced in chapter 2, this corresponds to the RG contribution of the operator $\mathcal{O}_H$ (see table 2.1), generated at the scale Λ by the pNGB nature of the Higgs with a coefficient $1/f^2$ (i.e. $\hat{c}_H = \xi$) [58], to the $\hat{S}$ and $\hat{T}$ parameters, as reported in table 2.6 and figure 2.2(a). This IR contribution is also represented in fig. 3.5 (taken from ref. [86]) for different values of ξ.
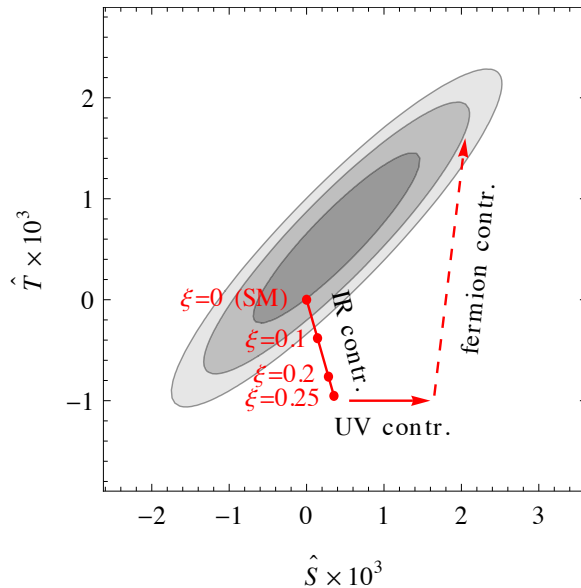
Figure 3.5:   Constraints on the $\hat{S}$ and $\hat{T}$ parameters as taken from ref. [86]. The grey ellipses represent the 68%, 95% and 99% CL contours from ref. [83]. In this plot we can recognize the IR contribution due to the deviations in the Higgs couplings as described in eq. (3.53), a UV contribution, such as the tree-level one from spin-1 resonances, and the fermion contribution.

Let us consider now the calculable and incalculable UV contributions, starting with $\hat{S}$. A tree level contribution to $\hat{S}$ is due to the exchange of heavy spin-1 resonances which mix with the SM electroweak gauge bosons. In our models this is given by (see sec. 3.6.2 for the derivation)

$$\Delta\hat{S}^{tree} \simeq 2\frac{m_W^2}{f^2} \left(\sum_{j=1}^{N_\rho} \frac{f_{\rho^j}^2}{m_{\rho^j}^2} - \sum_{i=1}^{N_a} \frac{f_{a_i}^2}{m_{a_i}^2} \right) \,, \tag{3.54}$$

The UV uncalculable gauge contribution to $\hat{S}$ is easily estimated by using NDA:

$$\Delta\hat{S}^{(NDA)} \sim \frac{1}{4\pi^2} \frac{m_W^2}{f^2} \,. \tag{3.55}$$

As expected, this is the value one gets from eq.(3.54) (modulo accidental cancellations or enhancements), when the vector and axial couplings approach 4π. Fermion resonances contribute to $\hat{S}$ at the loop level. A finite contribution, due to the mixing with the SM fermions, can be estimated as

$$\Delta\hat{S}_f \simeq \frac{N_c}{16\pi^2} \frac{\lambda^2 m_W^2}{m_f^2} \simeq \frac{N_c}{16\pi^2} \frac{m_W^2}{f^2} \frac{\epsilon^2}{m_f^2} \,. \tag{3.56}$$

For $\theta_{L,R} \sim \mathcal{O}(1)$ this is roughly of the same size of eq.(3.55). The authors of ref. [86] pointed out the presence of a logarithmically-divergent contribution due to derivative interactions between composite fermions and the Higgs, in particular those proportional to the k^d couplings in eq. (3.43) and the interactions with E_μ in the covariant derivative in eq. (3.39). This correction

can easily be the dominant one. While the k^d couplings could in principle be computed in explicit UV models, in our effective framework they do not contribute to the Higgs potential at one loop and therefore are arbitrary. This strongly limits our capability of computing contributions to the EW parameters.

The $\hat{T}$ parameter is a measure of breaking of the custodial symmetry. Since this is an exact symmetry of the strong sector, the only contribution to $\hat{T}$ will come from the mixing with the elementary sector and will be proportional either to the hypercharge coupling g' or to the fermion mixing. The NDA estimate for the uncalculable contribution to $\hat{T}$ coming exclusively from the gauge sector is

$$\Delta\hat{T}_g^{(NDA)} \sim \frac{m_W^2}{8\pi^2 f^2} \tan\theta_W^2 \,. \tag{3.57}$$

Eq.(3.57) also coincides with the NDA estimate for the contribution of the vector and axial resonances, because their couplings $g_\rho, g_a < 4\pi$ and their masses $m_\rho \simeq g_\rho f$, $m_a \simeq g_a f$, precisely compensate in the contribution to $\Delta\hat{T}$ to reproduce eq.(3.57). The uncalculable fermion contribution is easily shown to be sub-leading, in the limit of small mixing ϵ^i, and can be neglected. The calculable contribution to $\hat{T}$ due to the fermion resonances is given by (see e.g. the appendix of [159] for some explicit expressions of fermion contributions to $\hat{T}$)

$$\Delta\hat{T}_f \sim \frac{N_c}{8\pi^2} \frac{\lambda^4 f^2 s_h^2}{m_L^2} \,, \tag{3.58}$$

where λ is the Yukawa coupling between the top and a fermion resonance, $\lambda \sim \epsilon/f$, and m_f is its vector-like mass. We get

$$\frac{\Delta\hat{T}_f}{\Delta T_g^{(NDA)}} \sim \frac{N_c}{\pi} \cos^2\theta_W \frac{\epsilon^4}{f^2 m_L^2} \sim \frac{N_c}{\pi} \cos^2\theta_W \lambda_{top}^2 \,, \tag{3.59}$$

where in the last equality we have used eq.(3.46). The calculable fermion contribution is hence the dominant contribution to $\Delta\hat{T}$. A schematic representation of the possible contribution to $\hat{S}$ and $\hat{T}$ from composite Higgs models is showed in fig. 3.5, from ref. [86]. Since, as we saw, not all of these contributions are completely under control we do not present a fit of electroweak precision data for our models.

Deviation in the $Zb\bar{b}$ coupling

Let us now consider $\Delta\delta g_b$. We define by $\Delta\delta g_b$ the non-universal gauge coupling deviation due only to new physics, with the SM contribution (from loops) subtracted:

$$\Delta\delta g_b = \delta g_b - \delta g_{b,SM} \,, \tag{3.60}$$

where

$$g_{b,SM} = -\frac{1}{2} + \frac{1}{3}\sin^2\theta_W^2 \,, \quad \delta g_{b,SM} = \frac{\alpha_{em}}{16\pi\sin^2\theta_W} \frac{r(r^2 - 7r + 6 + (2 + 3r)\log r)}{(r - 1)^2} \,, \tag{3.61}$$

and $r \equiv \frac{M_{top}^2}{m_W^2}$, where M_{top} is the pole top mass, $M_{top} = 173.1$ GeV, not to be confused with M_{top} at the high scale, always taken around 150 GeV in this work. The calculable contribution we have computed arises from loops where a SM W is exchanged, δg_b^W, that can be estimated as

$$\delta g_b^W \simeq \frac{|\lambda|^4 v^2}{16\pi^2 m_L^2} \simeq \frac{|\epsilon|^4 s_h^2}{16\pi^2 f^2 m_L^2} \, . \tag{3.62}$$

In addition to that, we also have a calculable contribution where a vector resonance is exchanged in the loop, and the usual uncalculable contribution. The latter is estimated by NDA. It arises when the spurions (3.42) are inserted in the fermion bilinears. There are several local operators one can construct. For example, one contributing to δg_b is the following:

$$\frac{c_g}{f^4 (16\pi^2)^2}\left(\bar{q}_L E_{qQ}\gamma^\mu E_{qQ}^\dagger q_L\right)\sum_{\alpha=1}^{3}(\Sigma^t E_{qQ}^{\dagger,\alpha})(E_{qQ}^\alpha D_\mu \Sigma) = -\frac{c_g|\epsilon_{qQ}|^4 s_h^2}{4(16\pi^2)^2 f^4}\frac{g}{\cos\theta_W}\bar{q}_L \slashed{Z} q_L \tag{3.63}$$

with c_g an $\mathcal{O}(1)$ coefficient and α the $SU(2)_L^0$ index (see [119] for details), leading to

$$\delta g_b^{(NDA)} \sim \frac{|\epsilon_{qQ}|^4}{(16\pi^2)^2 f^4} s_h^2 \, , \tag{3.64}$$

which is sub-leading with respect to eq.(3.62). The one-loop deviations where a vector and a fermion resonance are exchanged in the loop are induced by the couplings in eq. (3.43). They are estimated to be

$$\delta g_b^\rho \simeq \frac{k^2 g_\rho^2 |\epsilon|^2 |\lambda|^2 v^2}{16\pi^2 m_L^2 m_\rho^2} \simeq \frac{k^2 |\epsilon|^4 s_h^2}{16\pi^2 f^2 m_L^2} \, , \tag{3.65}$$

where k generically represents the $\mathcal{O}(1)$ k coefficients in eq.(3.43). In general $\delta g_b^\rho \sim \delta g_b^W$ and both should be taken into account. However, δg_b^ρ depends on the couplings (3.43) that are otherwise irrelevant in our analysis.

The only tree-level correction to δg_b is due to the bottom quark mixing, and therefore is suppressed due to the smallness of the bottom mass with respect to the top one. Since we did not include these mixing terms in our computation of the potential, this contribution is arbitrary in our setup. However, we have checked for $N_S^{(u,d)} = N_Q^{(u,d)} = 1$ that this tree-level correction is typically 2-3 times smaller than δg_b^W.

3.6   The Higgs potential

In the previous sections we described in detail the tree-level effective Lagrangian of the composite Higgs model we study. We saw that the global symmetry $\mathcal{G}$ of the strong sector is explicitly broken in two sectors, in both cases due to mixing with the elementary SM fields. On the one hand the fact that only a subgroup of $\mathcal{G}$ is gauged by the EW gauge bosons selects a preferred direction in $\mathcal{G}$, which can also be seen as the fact that only some components of the spin-1 resonances mix with

the elementary SM gauge bosons. On the other hand the mixing terms between the elementary SM fermions and the composite fermion resonances breaks the global symmetry because the SM fermions are not in complete representations of $\mathcal{G}$. When a spontaneously broken global symmetry is explicitly broken by some small terms, the would-be NGBs acquire a non-vanishing potential, hence a mass term. Consider for example QCD with two flavors (up and down quarks only): the explicit breaking of the chiral symmetry $SU(2)_L \times SU(2)_R$ due to the quark masses generates a mass term for the Nambu-Goldstone bosons, i.e. the pions. In this case the breaking involves only the strongly coupled sector and therefore, in the language of chiral Lagrangians, the mass term for the pions is generated at tree-level by a chiral symmetry breaking operator.

In QCD, however, there is also another explicit breaking at play, due to the mixing with an elementary field: the photon. In fact, much like in the model we described in section 3.4.1, it is possible to write a Lagrangian for the spin-1 ρ_μ meson, which transforms in the adjoint of the unbroken $SU(2)_I$ of isospin, very similar to the one of eq. (3.33). The photon gauges a $U(1)_{em}$ subgroup of the unbroken $SU(2)_I$ and mixes linearly with the neutral ρ^0 meson. This linear mixing generates, at one loop, a potential for the charged pion, contributing to its mass and describing why the charged pion is slightly heavier than the neutral one (see e.g. ref. [94]).

In our models we assume that the strong sector is exactly symmetric under $\mathcal{G}$, therefore no tree-level potential term is present for the Higgs. However, the explicit breaking of the global symmetry due to the linear mixing between the elementary SM gauge bosons and fermions with the composite resonances induces, at one loop, an effective potential. Since all terms in the Lagrangian respect the EW gauge invariance, this potential affects only the physical Higgs h (and the scalar η in the SO(6)/SO(5) case).

When computing the one loop effective potential, since both the spin-1 and spin-1/2 lines are necessarily closed inside the loop, the contributions from the two breaking terms – gauge couplings g, g' and fermion mixings ϵ – act separately. For this reason we can consider separately the spin-1 and the spin-1/2 contributions to the potential.

The pNGB nature of the Higgs implies that its potential $V(h)$ depends on s_h only. Due to the contribution of particles whose masses vanish in the $s_h \to 0$ limit (such as the top, W and Z), the one-loop Higgs potential contains non-analytic terms of the form $s_h^4 \log s_h$ that do not admit a Taylor expansion around $s_h = 0$. In the phenomenological regions of interest, these terms do not lead to new features and are qualitatively but *not* quantitatively negligible [3]. However, they make an analytic study of the potential slightly more difficult. For this reason, we neglect them altogether in what follows and refer to the appendix C for a more refined analysis of the Higgs potential where they are included. For $s_h \ll 1$, we can therefore expand $V(h)$ up to quartic order and obtain

$$V(h) \simeq -\gamma\, s_h^2 + \beta\, s_h^4 + \mathcal{O}(s_h^6)\;. \tag{3.66}$$

The coefficients γ and β are induced by the explicit breaking of the shift symmetry: the gauge couplings g and g' in the gauge sector, the mixing terms ϵ in the fermion sector and possibly other terms coming from higher dimensional operators, not appearing in the Lagrangian (3.48).

The Higgs potential in our model is, strictly speaking, not calculable. There are generically two different contributions to γ and β that, with an abuse of language, we denote by IR and UV contributions. The IR contribution is the one coming from the leading operators defining our model (3.48), the UV contribution is the one coming from higher dimensional operators and physics at the cut-off scale. The explicit form of γ and β can be deduced, in the limit of small breaking terms, by a simple spurion analysis [119]. As expected from NDA, the IR contribution to γ and β shows generically quadratic and logarithmic divergencies, respectively. Instead of introducing as usual counterterms for such divergencies, leading to a loss of predictability in the Higgs sector, we can demand that the one-loop form factors defining the IR part of γ and β, that should be integrated over all energies scales, are peaked around the resonance masses and go to zero sufficiently fast at infinity. This is done by fulfilling some generalized Weinberg sum rules [1, 46]. In this way, the one-loop IR contribution to $V(h)$ can be made finite.

On the other hand, possible local operators contributing to the UV part of γ and β, coming purely from the gauge sector or the fermion sector, are for example[10]

$$c_g f^4 \sum_{a_L=1}^{3} \Sigma^t g T^{a_L} g T^{a_L} \Sigma = \frac{3}{4} c_g g^2 f^4 s_h^2 \equiv \gamma_g^{(NDA)} s_h^2 \,,$$

$$\frac{d_g}{16\pi^2} f^4 \big(\sum_{a_L=1}^{3} \Sigma^t g T^{a_L} g T^{a_L} \Sigma\big)^2 = \frac{9}{256\pi^2} d_g g^4 f^4 s_h^4 \equiv \beta_g^{(NDA)} s_h^4 \,.$$

$$c_f f^2 (E_{qS}\Sigma)(\Sigma^t E_{qS}^\dagger) = \frac{1}{2}|\epsilon_{qS}|^2 s_h^2 \equiv \gamma_f^{(NDA)} s_h^2 \,,$$

$$\frac{d_f}{16\pi^2} \Big((E_{qS}\Sigma)(\Sigma^t E_{qS}^\dagger)\Big)^2 = \frac{1}{64\pi^2}|\epsilon_{qS}|^4 s_h^4 \equiv \beta_f^{(NDA)} s_h^4 \,,$$

$$(3.67)$$

where $c_{g,f}$ and $d_{g,f}$ are estimated by NDA to be coefficients of $\mathcal{O}(1)$. By comparing $\gamma_g^{(NDA)}$ and $\beta_g^{(NDA)}$ with the typical values one gets from the IR contribution, once made calculable (such as eqs.(3.84) and (3.99) below), we see that $\gamma_{g,f}^{(NDA)} > \gamma_{g,f}$ and $\beta_{g,f}^{(NDA)} \simeq \beta_{g,f}$ so that calculability is still lost. In order to circumvent this problem, we assume here that the underlying UV theory is such that $\gamma^{(NDA)}$ and $\beta^{(NDA)}$ are sub-leading with respect to the IR part of γ and β, so that the Higgs potential is calculable and dominated at one-loop level by the fields in our

---

[10]The leading fermion local operators above were not considered in [119]. This is probably due to the fact that the free fermion composite Lagrangian has an obvious linearly realized $SO(5)$ symmetry when $m_{iQ} = m_{iS}$. In addition, when the mixing terms are taken to be equal, $\epsilon_{tS}^i = \epsilon_{tQ}^i$ and $\epsilon_{qS}^i = \epsilon_{qQ}^i$ (as in [119]), the whole Higgs field can be removed from the quadratic fermion Lagrangian by a field redefinition and hence vector mass insertions are needed to get a non-trivial one-loop potential. This is however an accident of the one-loop result and fermion operators like the ones in eq.(3.67) will be anyway generated at higher loop level.

model. The logic underlying the above assumption (that might seem too radical and strong) is that any theory where a symmetry mechanism is at work (not only collective breaking or extra space-time dimensions) to actually predict a calculable Higgs potential would automatically satisfy the above requirements and fall into our class of models, which can then be seen as a general parametrization of composite Higgs models. We denote the above assumption as the *Minimal Higgs Potential* (MHP) hypothesis. We have explicitly checked that deconstructed models present in the literature [119, 120] can be translated in our framework and it turns out that in this case the Weinberg sum rules are indeed satisfied due to the symmetries of the models. A dictionary between these models and our setup is presented in appendix E.

Having explained the philosophy of our perspective, we turn to the computation of the IR contribution of the one-loop Higgs potential, from now on simply denoted by the Higgs potential. First, we shift the NGBs, in this case the Higgs, with a constant background field h and a quantum field δh: $h \to h + \delta h$. Since, by assumption, the strong sector is exactly $\mathcal{G}$ invariant, loops of only the Higgs do not contain any explicit symmetry breaking term and therefore do not generate any contribution to the potential. We present in the following two different ways to compute the contribution to the potential due to the spin-1 and spin-1/2 fields.

3.6.1   Potential in dimensional regularization

Let us now show how the incalculability of the potential manifests itself when one uses dimensional regularization to regularize the quadratic and logarithmic divergencies, and how the Weinberg sum rules arise in this framework. The one loop Coleman-Weinberg potential can be easily obtained from the mass matrix in each sector (gauge and fermionic), keeping s_h as background fields. Let us parametrize the field-dependent mass terms for the spin-1 and spin-1/2 fields as

$$\mathcal{L}^{mass} = \frac{1}{2} V_\mu^i M_{V,ij}^2(s_h) V^{j\mu} - \left(\bar{\psi}_L^i M_{F,ij}(s_h) \psi_R^j + h.c. \right) , \tag{3.68}$$

where i, j run over all the fields in each sector and M_V^2 is a real symmetric matrix while M_F is a generic complex matrix. From these matrices one can obtain the singular values with a s_h background: $m_n(s_h)^2 > 0$, where n runs over all the states with a spin $s_n = 1, \frac{1}{2}$. These singular values can finally be used to obtain the one-loop effective potential. Regularizing the integral with dimensional regularization one has

$$
\begin{aligned}
V^{(1)}(s_h) &= \frac{1}{16\pi^2} \sum_n \frac{(-1)^{2s_n}(2s_n+1)}{4} m_n(s_h)^4 \left(\log \frac{m_n(s_h)^2}{Q^2} - k_{s_n} \right) \\
&= \frac{3}{64\pi^2} \text{Tr} \left[M_V^4(s_h) \left(\log \frac{M_V^2(s_h)}{Q^2} - k_1 \right) \right] \\
&\quad - \frac{2N_c}{64\pi^2} \text{Tr} \left[(M_F^\dagger M_F)^2(s_h) \left(\log \frac{(M_F^\dagger M_F)(s_h)}{Q^2} - k_{1/2} \right) \right] ,
\end{aligned}
\tag{3.69}
$$

where Q is the sliding scale and k_{s_n} are numerical factors which depend on the subtraction scheme used. We see that, in general, the potential is scale-dependent as well as scheme-dependent, which would imply the necessity to fix some boundary conditions at some scale, for example by matching with the measured Higgs mass and vacuum expectation value. This, however, would imply our impossibility to predict those values from our explicit models. To avoid this, we impose a set of generalized Weinberg sum rules by asking that $\mathrm{Tr}[M_V^4]$ and $\mathrm{Tr}[(M_F^\dagger M_F)^2]$ are independent on h

$$\text{WSR:} \quad \mathrm{Tr}\left[M_V^4(s_h)\right] \equiv \text{const} \quad \text{and} \quad \mathrm{Tr}\left[\left(M_F^\dagger(s_h)M_F(s_h)\right)^2\right] \equiv \text{const} . \tag{3.70}$$

Requiring this for both the s_h^2 and the s_h^4 dependences is equivalent to requiring the absence of UV divergencies in the computation of the γ and β coefficients.

While this method is very efficient for numerical computations, for analytic studies it is troublesome because of the difficulty of obtaining analytic field-dependent eigenvalues for the mass matrices, when the number of fields involved becomes high.

3.6.2 Form Factors analysis

The computation of the one-loop Coleman-Weinberg potential consists essentially in integrating out all fields at quadratic level, in the background of the scalar field of which we want to compute the potential. This process can be performed either in one single step, as presented above, or in two separate steps. One can first integrate out at tree-level the quadratic Lagrangian of the heavy spin 1 and 1/2 resonances, with no need to go to a mass basis, keeping the whole momentum dependence by introducing some form factors for the light fields, and then integrate at one-loop the remaining light degrees of freedom with the momentum-dependent form factors, usually with a cutoff regularization. This is a useful way to proceed because the pseudo-Goldstone nature of the Higgs field and the $\mathrm{SO}(5) \times \mathrm{U}(1)_X$ symmetries allow to fix in terms of a few form factors the form of the effective Lagrangian for the light states and encode there all the information of the heavy resonances, making it easier to perform approximations to obtain analytic results.

Gauge Contribution

In momentum space, the effective Lagrangian of the SM gauge fields up to quadratic order in the gauge fields and to any order in the Higgs field can be written in terms of some scalar form factors, functions of the momentum p^2, which correspond to the vacuum polarization amplitudes introduced in section 2.3.1:

$$\frac{P_t^{\mu\nu}}{2}\left(2\Pi_{W^+W^-}W_\mu^+W_\nu^- + \Pi_{W_3W_3}W_\mu^3W_\nu^3 + \Pi_{BB}B_\mu B_\nu + 2\Pi_{W_3B}W_\mu^3 B_\nu\right), \tag{3.71}$$

where $P_t^{\mu\nu} = \eta^{\mu\nu} - p^\mu p^\nu/p^2$ is the projector on the transverse field configurations and the Π's are form factors that also depend on the Higgs field. In particular, since we assume that the strong

sector – which we integrate out at tree level to obtain the Π's – is invariant under the custodial symmetry, the form factors will satisfy the relation $\Pi_{W^+W^-} = \Pi_{W_3W_3}$, which implies $\hat{T} = 0$ at tree level (2.22). The one-loop Higgs potential is easily computed from the above expression by taking the Landau gauge $\partial^\mu B_\mu = \partial^\mu W_\mu^a = 0$. In this gauge the longitudinal components of the gauge fields, as well as the ghosts, decouple and can be neglected. Integrating out the gauge fields and going to Euclidean momenta, one gets:

$$V_g(h) = \frac{3}{2} \int \frac{d^4 p_E}{(2\pi)^4} \left(2 \log \Pi_{W^+W^-}(-p_E^2) + \log \left(\Pi_{BB}(-p_E^2) \Pi_{W_3W_3}(-p_E^2) - \Pi_{W_3B}^2(-p_E^2) \right) \right). \tag{3.72}$$

To have an analytic understanding of the possible functional dependence on the Higgs field of the effective potential, it is useful to introduce spurionic gauge fields such that the whole $SO(5) \times U(1)_X$ group becomes gauged: $A_\mu = A_\mu^{\hat{a}} T^{\hat{a}} + A_\mu^{aL} T^{aL} + A_\mu^{aR} T^{aR}$. The most general $SO(5) \times U(1)_X$-invariant Lagrangian depending on the gauge fields and the NGB's, at the quadratic order in the gauge fields and in momentum space, is

$$\begin{aligned}\mathcal{L}^{eff} = \frac{P_t^{\mu\nu}}{2} \Big(&\Pi_0^X(p^2) X_\mu X_\nu + \Pi_0(p^2) \mathrm{Tr}[A_\mu A_\nu] + \Pi_1(p^2) \Sigma^t A_\mu A_\nu \Sigma + \\ &+ \Pi_{LR}(p^2) \left(\mathrm{Tr}[(U^\dagger A_\mu U)^L (U^\dagger A_\nu U)^L] - \mathrm{Tr}[(U^\dagger A_\mu U)^R (U^\dagger A_\nu U)^R] \right) \Big),\end{aligned} \tag{3.73}$$

where $(\ldots)^{L,R}$ implies the projection on the $(\mathbf{3}, \mathbf{1})$ and $(\mathbf{1}, \mathbf{3})$ irreducible representations inside the adjoint of $SO(4)$.[11] Switching off the spurionic fields, that is keeping only the components $A_\mu^{aL} = W_\mu^a$, $A_\mu^{3R} = c_X B_\mu$ and $X_\mu = s_X B_\mu$, where

$$c_X = \frac{g_X}{\sqrt{g_0^2 + g_X^2}} = \frac{g_0'}{g_0}, \quad s_X = \frac{g_0}{\sqrt{g_0^2 + g_X^2}}, \tag{3.74}$$

we obtain the most general effective Lagrangian for the gauge bosons in $SO(5)/SO(4)$ with the explicit dependence on the Higgs field:

$$\begin{aligned}\mathcal{L}^{eff} = \frac{P_t^{\mu\nu}}{2} \Big(&\Pi_0 W_\mu^a W_\nu^a + \Pi_1 \frac{s_h^2}{4} \left(W_\mu^1 W_\nu^1 + W_\mu^2 W_\nu^2 \right) + \\ &+ \Pi_B B_\mu B_\nu + \Pi_1 \frac{s_h^2}{4} \left(\frac{g_0'}{g_0} B_\mu - W_\mu^3 \right) \left(\frac{g_0'}{g_0} B_\nu - W_\nu^3 \right) + \\ &+ c_h \Pi_{LR} \left(W_\mu^a W_\nu^a - \frac{g_0'^2}{g_0^2} B_\mu B_\nu \right) \Big),\end{aligned} \tag{3.75}$$

---

[11]The term in the second line of (3.73) could be generated, for example, by the operator $O_3 = \left(\mathrm{Tr}[E_{\mu\nu}^L E^{L\,\mu\nu}] - \mathrm{Tr}[E_{\mu\nu}^R E^{R\,\mu\nu}] \right)$ [105], or directly in a model with vector resonances ρ_μ^L, ρ_μ^R without invariance under $L \leftrightarrow R$, see section 3.6.2.

where $\Pi_B = (s_X^2 \Pi_0^X + c_X^2 \Pi_0)$, $c_h = \cos\langle h\rangle/f$, and $g_0' = g_0 c_X$. From this Lagrangian one obtains

$$\Pi_{W^+ W^-} = \Pi_{W_3 W_3} = \Pi_0 + \frac{s_h^2}{4}\Pi_1 + c_h \Pi_{LR},$$

$$\Pi_{BB} = \Pi_B + c_X^2 \frac{s_h^2}{4}\Pi_1 - c_X^2 c_h \Pi_{LR}, \tag{3.76}$$

$$\Pi_{W_3 B} = -c_X \frac{s_h^2}{4}\Pi_1 \,.$$

The form factor $\Pi_{W_3 B}$ is related to the oblique $\hat{S}$-parameter, see eq. (2.22),

$$\hat{S} = -\frac{g}{g'}\Pi'_{W_3 B}(0) \simeq \frac{\langle s_h^2\rangle}{4}\Pi_1'(0) \,, \tag{3.77}$$

where the prime indicates a derivative with respect to p^2 and in the second step we approximated $g \simeq g_0$ and $g' \simeq g_0'$. It is well known that the bound on S provides one of the main phenomenological electroweak constraints on composite Higgs models, that requires $s_h^2 \ll 1$. As we will show below, a necessary condition to kill the quadratic divergence in the potential is to demand $\lim_{p_E \to \infty} \Pi_{LR} = 0$. In order to ensure this condition and to keep the model simple, in the following we impose a LR symmetry in the strong sector, that automatically implies $\Pi_{LR} = 0$.

The explicit expression of the form factors is obtained by integrating out the heavy vector resonances at tree-level and quadratic order (the one relevant at one-loop level). This is not straightforward to do for an arbitrary number of vector resonances, due to the last term in $\mathcal{L}^{v_L}$, eq.(3.33). Let us then set $f_{\text{mix}} = 0$ in the following (in ref. [1] we studied the effect of this term in the two vector case). In this simple case, we get

$$\Pi_1(p^2) = g_0^2 f^2 + 2g_0^2 p^2 \left[\sum_{i=1}^{N_a} \frac{f_{a_i}^2}{(p^2 - m_{a_i}^2)} - \sum_{j=1}^{N_\rho} \frac{f_{\rho^j}^2}{(p^2 - m_{\rho^j}^2)}\right],$$

$$\Pi_0(p^2) = -p^2 + g_0^2 p^2 \sum_{j=1}^{N_\rho} \frac{f_{\rho^j}^2}{(p^2 - m_{\rho^j}^2)}, \qquad \Pi_0^X(p^2) = -p^2 \,. \tag{3.78}$$

The physical SM gauge couplings are modified by the contribution of the resonances and given by (2.19):

$$g^2 = -\frac{g_0^2}{\Pi_0'(0)} = g_0^2\Big(1 + \sum_{j=1}^{N_\rho} \frac{g_0^2}{g_{\rho^j}^2}\Big)^{-1}, \qquad g'^2 = -\frac{g_0^2}{\Pi_B'(0)} = g_0'^2\Big(1 + \sum_{j=1}^{N_\rho} \frac{g_0'^2}{g_{\rho^j}^2}\Big)^{-1}, \tag{3.79}$$

where $\Pi' = d\Pi/dp^2$. It is straightforward to get from the above relations the form of the gauge

contribution to γ_g and β_g to the Higgs potential:[12]

$$\gamma_g = -\frac{3}{8(4\pi)^2} \int_0^\infty dp_E^2 \, p_E^2 \left(\frac{3}{\Pi_0} + \frac{c_X^2}{\Pi_B}\right) \Pi_1,$$

$$\beta_g = -\frac{3}{64(4\pi)^2} \int_{\mu_g^2}^\infty dp_E^2 \, p_E^2 \left(\frac{2}{\Pi_0^2} + \left(\frac{1}{\Pi_0} + \frac{c_X^2}{\Pi_B}\right)^2\right) \Pi_1^2. \tag{3.80}$$

For large Euclidean momenta, the form factors $\Pi_0 \propto \Pi_0^B \propto p_E^2$, while $\Pi_1 \propto p_E^0$, indicating that all higher terms in the s_h expansion are UV finite. On the other hand, γ_g and β_g are respectively quadratically and logarithmically divergent in the UV, in general. Their UV properties are fixed by the single form factor Π_1. Without imposing any condition, the form factor Π_1 goes to a constant at high energy and the potential diverges quadratically. However, the form-factor $\Pi_1(p^2)$ is an order parameter of the spontaneous symmetry breaking (being proportional to the difference of the form factors of gauge fields along the unbroken and broken generators [43]), so for energies much higher than the symmetry breaking scale f, it should go to zero, assuring that the potential should diverge only logarithmically. Imposing this condition, we obtain the first Weinberg sum rule [160]:

$$\lim_{p_E^2 \to \infty} g_0^{-2} \Pi_1(-p_E^2) = f^2 + 2\sum_{i=1}^{N_a} f_{a_i}^2 - 2\sum_{j=1}^{N_\rho} f_{\rho^j}^2 \equiv 0. \quad \text{(I)} \tag{3.81}$$

Demanding that Π_1 goes to zero faster than p_E^2 (finite potential) for large Euclidean momenta gives the second Weinberg sum rule:[13]

$$\lim_{p_E^2 \to \infty} g_0^{-2} p_E^2 \Pi_1(-p_E^2) = 2\sum_{i=1}^{N_a} f_{a_i}^2 m_{a_i}^2 - 2\sum_{j=1}^{N_\rho} f_{\rho^j}^2 m_{\rho^j}^2 \equiv 0. \quad \text{(II)} \tag{3.82}$$

Notice that the first sum rule requires the presence of at least one vector resonance ρ_μ, while the second sum rule requires at least one axial resonance a_μ. There is a qualitative difference between the Weinberg sum rules (I) and (II). While the former must be unavoidably imposed (at high energies the global symmetry is by assumption restored), the latter can be relaxed, leaving a mild logarithmic UV-sensitivity of the Higgs potential.[14] From eqs.(3.77) and (3.78), we get

---

[12]We have inserted the IR cut-off $\mu_g \simeq m_W$ to regulate a logarithmic divergence appearing in β_g. This is a spurious divergence arising from a non-analytic term in the potential in the $s_h \to 0$ limit and does not play an important role in what follows. We have checked that our results do not sensitively depend on the choice of μ_g. For a discussion on this non-analytic term see app. C.

[13]The sum rules (3.81) and (3.82) are also valid for the general case $f_{\text{mix}} \neq 0$ when $N_\rho = 2$.

[14]The second sum rule was originally derived by assuming that the broken and unbroken currents behave as free fields in the UV [160]. This assumption holds for asymptotically-free gauge theories but can break down if, say, the UV theory is a strongly interacting CFT. In particular, it has been pointed out in [161], where an approach similar to ours has been advocated in Higgsless models, that the second Weinberg sum rule does not hold in conformal Technicolor.

the tree-level contribution to the $\hat{S}$-parameter:

$$\Delta\hat{S} \simeq 2\frac{m_W^2}{f^2}\left(\sum_{j=1}^{N_\rho}\frac{f_{\rho^j}^2}{m_{\rho^j}^2} - \sum_{i=1}^{N_a}\frac{f_{a_i}^2}{m_{a_i}^2}\right) . \tag{3.83}$$

The explicit form of γ_g and β_g is readily computed for $N_\rho = N_a = 1$. Setting for simplicity $g' = 0$, $a_\rho = 1$ and expanding at leading order in $(g/g_\rho)^2$ (and in $\mu_g(= m_W)/m_\rho$ in β_g), we get

$$\gamma_g \simeq -\frac{9f^2g^2m_\rho^2\log 2}{64\pi^2}, \qquad \beta_g \simeq \frac{9f^4g^4}{1024\pi^2}\left(5 + \log\frac{m_W^2}{32m_\rho^2}\right). \tag{3.84}$$

For $N_\rho = N_a = 1$, when both eqs.(3.81) and (3.82) are imposed, ΔS can be rewritten as

$$\Delta\hat{S} = 2\frac{m_W^2}{m_\rho^2}\left(1 - \frac{f^2}{4f_\rho^2}\right) \tag{3.85}$$

and, as eq.(3.81) imposes $f_\rho > f/\sqrt{2}$, it is manifestly positive definite. As expected, for $s_h = 1$, eq.(3.85) agrees with the vector dominance estimate in Technicolor theories derived in [162]. In holographic 5d models, $\Delta\hat{S}$ is positive as well. For N_ρ or $N_a > 1$, on the other hand, $\Delta\hat{S}$ can in principle have any sign. Since as far as we know there is no general proof about the positivity of $\Delta\hat{S}$ (neither in Higgsless Technicolor theories nor in Composite Higgs Models) we will also consider, in the following, one model (with $N_\rho = 1$, $N_a = 2$) in the "exotic" region where $\Delta\hat{S}$ can be negative.

A possible constrain on the form factor Π_1 comes from the results of [163]. A straightforward generalization of the proof given there implies that any composite Higgs model, UV-completed by vector-like gauge theories, cannot give rise to EWSB without additional contributions to the Higgs potential (such as those given by fermion resonances). In other words, for $s_h < 1$, γ_g in eq.(3.80) should be negative definite. This condition (always satisfied in 5d models) is automatically satisfied when both (I) and (II) hold for $N_\rho = N_a = 1$ (see eq.(3.84)).[15] On the other hand, when N_ρ or $N_a > 1$, γ_g can be positive and induce EWSB by itself (although these regions are never found in our numerical scans).

Left-Right Asymmetric Case

Let us study in this section what are the consequences of having a LR asymmetric model. We consider the simplest example, with $N_{\rho_L} = N_{\rho_R} = 1$, which already shows all the important

---

[15]On the contrary, if one imposes only the sum rule (I), even for $N_\rho = N_a = 1$, γ_g (and ΔS) can have any sign.

aspects. From eq.(3.33) and eq.(3.76) we get:

$$
\begin{aligned}
\Pi_0(p^2) &= -p^2 + \frac{g_0^2 f_{\rho_L}^2 p^2}{2(p^2 - m_{\rho_L^2})} + \frac{g_0^2 f_{\rho_R}^2 p^2}{2(p^2 - m_{\rho_R^2})}, \\
\Pi_B(p^2) &= -p^2 + \frac{g_0'^2 f_{\rho_L}^2 p^2}{2(p^2 - m_{\rho_L^2})} + \frac{g_0'^2 f_{\rho_R}^2 p^2}{2(p^2 - m_{\rho_R^2})}, \\
\Pi_1(p^2) &= g_0^2 \left(f^2 - \frac{f_{\rho_L}^2 p^2}{p^2 - m_{\rho_L^2}} - \frac{f_{\rho_R}^2 p^2}{p^2 - m_{\rho_R^2}} \right), \\
\Pi_{LR}(p^2) &= \frac{g_0^2 f_{\rho_L}^2 p^2}{2(p^2 - m_{\rho_L^2})} - \frac{g_0^2 f_{\rho_R}^2 p^2}{2(p^2 - m_{\rho_R^2})}.
\end{aligned}
\tag{3.86}
$$

The form factor Π_{LR} goes to a constant for large Euclidean momenta, and it induces a quadratic divergence in the Higgs potential. Since the functional dependence related to this form factor is c_h, see eq.(3.75), this divergence is present at any order in the expansion for small s_h^2. Similarly to Π_1, Π_{LR} is an order parameter for the symmetry breaking and should hence go to zero at high energies. From the expression above we get

$$
5d \lim_{p_E \to \infty} \Pi_{LR}(-p_E^2) = \frac{g_o^2}{2} \left(f_{\rho_L}^2 - f_{\rho_R}^2 \right) - \frac{g_0^2}{2p_E^2} \left(f_{\rho_L}^2 m_{\rho_L}^2 - f_{\rho_R}^2 m_{\rho_R}^2 \right) + \mathcal{O}(p_E^{-4}).
\tag{3.87}
$$

Cancelling the quadratic and logarithmic divergence requires $f_{\rho_L} = f_{\rho_R}$ and $m_{\rho_L} = m_{\rho_R}$, respectively, which is equivalent in this case to impose a complete LR symmetry, for which $\Pi_{LR} = 0$ identically. Note that by adding more copies of vector resonances, however, one might be able to have a finite potential even without imposing a LR symmetry.

Fermion Contribution

Following a very similar approach to the one described for the gauge contribution to the potential, let us now consider the contribution due to SM fermions. In particular we focus on the top quark since its mixing with the strong sector is expected to be the dominant source of breaking of the global symmetry. The top quark effective Lagrangian up to quadratic order in the fermions and to any order in the Higgs field can be written, in momentum space, as

$$
\bar{t}_L \slashed{p} \, \Pi_{t_L} t_L + \bar{t}_R \slashed{p} \, \Pi_{t_R} t_R - \left(\bar{t}_L \Pi_{t_L t_R} t_R + h.c. \right),
\tag{3.88}
$$

resulting in the following contribution to the Higgs potential:

$$
V_f(h) = -2N_c \int \frac{d^4 p_E}{(2\pi)^4} \log \left(p_E^2 \Pi_{t_L}(-p_E^2) \Pi_{t_R}(-p_E^2) + \left| \Pi_{t_L t_R}(-p_E^2) \right|^2 \right).
\tag{3.89}
$$

Integrating out the fermion resonances S_i and Q_j, we get the following expression for the form factors (see eqs. (3.27,3.28)):

$$
\Pi_{t_L} = \Pi_Q + s_h^2 \Pi_{1Q}, \qquad \Pi_{t_R} = \Pi_S + s_h^2 \Pi_{1S}, \qquad \Pi_{t_L t_R} = i s_h c_h \Pi_{QS},
\tag{3.90}
$$

where

$$
\Pi_Q(p^2) \;=\; 1 - \sum_{j=1}^{N_Q} \frac{|\epsilon_{qQ}^j|^2}{p^2 - m_{jQ}^2}\,, \qquad \Pi_{1Q}(p^2) = -\frac{1}{2}\left(\sum_{i=1}^{N_S} \frac{|\epsilon_{qS}^i|^2}{p^2 - m_{iS}^2} - \sum_{j=1}^{N_Q} \frac{|\epsilon_{qQ}^j|^2}{p^2 - m_{jQ}^2} \right),
$$

$$
\Pi_S(p^2) \;=\; 1 - \sum_{i=1}^{N_S} \frac{|\epsilon_{tS}^i|^2}{2(p^2 - m_{iS}^2)}\,, \qquad \Pi_{1S}(p^2) = \frac{1}{2}\left(\sum_{i=1}^{N_S} \frac{|\epsilon_{tS}^i|^2}{p^2 - m_{iS}^2} - \sum_{j=1}^{N_Q} \frac{|\epsilon_{tQ}^j|^2}{p^2 - m_{jQ}^2} \right),
$$

$$
\Pi_{QS}(p^2) \;=\; \frac{1}{2}\left(\sum_{i=1}^{N_S} \epsilon_{tS}^{i*}\epsilon_{qS}^i \frac{m_{iS}}{p^2 - m_{iS}^2} - \sum_{j=1}^{N_Q} \epsilon_{tQ}^{j*}\epsilon_{qQ}^j \frac{m_{jQ}}{p^2 - m_{jQ}^2} \right). \tag{3.91}
$$

The top mass can be obtained either as the lightest singular value of the mass matrix of the $Q = 2/3$ fields in eq. (3.39), or from eq. (3.88) by finding the pole of the propagator:

$$
M_{top}^2 - \left. \frac{|\Pi_{t_L t_R}(M_{top}^2)|^2}{\Pi_{t_L}(M_{top}^2)\Pi_{t_R}(M_{top}^2)} \right|_{h=v,\eta=0} = 0\,, \tag{3.92}
$$

which, if the top is much lighter than the top partners, can be approximated as

$$
M_{top} \simeq \left. \frac{|\Pi_{t_L t_R}(0)|}{\sqrt{\Pi_{t_L}(0)\Pi_{t_R}(0)}} \right|_{h=v,\eta=0}. \tag{3.93}
$$

Similarly to the gauge case, for $s_h \ll 1$, we can expand V_f up to quartic order:

$$
V_f(h) \simeq -\gamma_f s_h^2 + \beta_f s_h^4, \tag{3.94}
$$

with

$$
\gamma_f = \frac{2N_c}{(4\pi)^2} \int_0^\infty dp_E^2\, p_E^2 \left(\frac{\Pi_{1Q}}{\Pi_Q} + \frac{\Pi_{1S}}{\Pi_S} + \frac{\Pi_{QS}^2}{p_E^2 \Pi_Q \Pi_S} \right),
$$

$$
\beta_f = \frac{N_c}{(4\pi)^2} \int_{\mu_f^2}^\infty dp_E^2\, p_E^2 \left(\left(\frac{\Pi_{QS}^2}{p_E^2 \Pi_Q \Pi_S} + \frac{\Pi_{1Q}}{\Pi_Q} + \frac{\Pi_{1S}}{\Pi_S} \right)^2 - \frac{2(p_E^2 \Pi_{1Q}\Pi_{1S} - \Pi_{QS}^2)}{p_E^2 \Pi_Q \Pi_S} \right). \tag{3.95}
$$

For large Euclidean momenta $\Pi_{Q,S} \propto p_E^0$, $\Pi_{1Q,1S} \propto p_E^{-2}$, $\Pi_{QS} \propto p_E^{-2}$. It then follows that the terms involving Π_{QS} in eq.(3.95) are all finite. The factor μ_f is an IR-cutoff curing a spurious logarithmic divergence arising from the non-analytic term in the potential. We fix it to be around the top mass (see footnote 12). All higher terms in the s_h expansion are UV finite. We can impose the fermion analogue of the Weinberg sum rules, demanding that the divergencies in γ_f and β_f above cancel. The cancellation of the logarithmic divergence in β_f requires

$$
\lim_{p_E^2 \to \infty} (-2)p_E^2 \frac{\Pi_{1S}}{\Pi_S} = \sum_{i=1}^{N_S} |\epsilon_{tS}^i|^2 - \sum_{j=1}^{N_Q} |\epsilon_{tQ}^j|^2 = 0\,.
$$

$$
\lim_{p_E^2 \to \infty} 2p_E^2 \frac{\Pi_{1Q}}{\Pi_Q} = \sum_{i=1}^{N_S} |\epsilon_{qS}^i|^2 - \sum_{j=1}^{N_Q} |\epsilon_{qQ}^j|^2 = 0\,. \tag*{(III) \qquad (3.96)}
$$

When eq.(3.96) is satisfied, the quadratic divergence in γ_f is automatically cancelled. Imposing the cancellation of the logarithmic divergence in γ_f requires the second condition

$$\lim_{p_E^2 \to \infty} 2p_E^4 \left(\frac{\Pi_{1S}}{\Pi_S} + \frac{\Pi_{1Q}}{\Pi_Q} \right) = \sum_{i=1}^{N_S} m_{iS}^2 \left(|\epsilon_{tS}^i|^2 - |\epsilon_{qS}^i|^2 \right) - \sum_{j=1}^{N_Q} m_{jQ}^2 \left(|\epsilon_{tQ}^j|^2 - |\epsilon_{qQ}^j|^2 \right) = 0 \quad \text{(IV)} . \quad (3.97)$$

It is useful to consider in some detail the case $N_Q = N_S = 1$, taking all the mixing parameters to be real, for simplicity. Assuming $m_S \neq m_Q$, a solution to eqs.(3.96) and (3.97) is

$$\epsilon_{tS} = \epsilon_{tQ} = \epsilon_{qS} = -\epsilon_{qQ} \equiv \epsilon . \quad (3.98)$$

Other solutions with different sign choices can also be considered. We take ϵ_{qQ} of opposite sign with respect to the other ϵ's so that the top mass is maximized, see eq.(3.46). The coefficients γ_f and β_f are now easily computed in analytic form, but the resulting expressions are too lengthy to be reported. For illustration, we just show here their approximate form in the limit of small mixing, $\theta_{L,R} \ll 1$. At leading order we get[16]

$$\gamma_f = \frac{N_c \epsilon^4}{32\pi^2} \frac{1 - x^2 + \left(x^2 + 2x + 2 \right) \log x^2}{x^2 - 1} , \qquad x = \frac{m_Q}{m_S} ,$$
$$\beta_f = \frac{N_c \epsilon^4}{32\pi^2} \frac{(1+x) \log x^2}{x - 1} . \quad (3.99)$$

Notice that the ϵ^4 behaviour of γ_f is an accident of the $N_Q = N_S = 1$ case, the typical scaling being $\propto \epsilon^2$.

The generalized Weinberg sum rules (I-IV) must be satisfied by any composite Higgs model where a symmetry mechanism is at work to realize the MHP hypothesis. They are clearly also satisfied in the notable case of five-dimensional theories, where locality in the extra dimension forbids any local Higgs potential to all orders in perturbation theory (thus implementing in full the MHP hypothesis). However, when one has to sum over an *infinite* set of fields, with increasing mass, such as in the 5d models, the sum rules written as in (I-IV) are not very useful. It is more convenient to first sum over the infinite set of fields and then take the limit of large euclidean momenta.[17] In doing that, one finds that the form factors such as Π_1, Π_{1S}, Π_{1Q} and Π_{QS} introduced before, all go to zero exponentially for $p_E \to \infty$. For instance, in the simplest set-up of a 5d theory on a flat interval of length L, one gets $\Pi_1(p_E) \propto p_E / \sinh(2Lp_E)$ (see e.g. [164] for an introduction and further examples).

---

[16]Contrary to the expansion in g/g_ρ in the gauge contribution (3.84), that is always a sufficiently accurate approximation, the explicit forms (3.99) are not always useful. When t_L and/or t_R significantly mix with the composite sector, different limits should be considered.

[17]The higher-dimensional symmetries demand that one has to sum over the whole infinite tower of states, despite the limited regime of validity of the 5d effective theory.

3.7   Light top partners for a light composite Higgs

Let us now analyze in detail the Higgs potential obtained in our framework and study what are the consequences, on the new physics spectrum, of imposing a successful electroweak symmetry breaking and the correct values of the top and Higgs masses.

The total Higgs potential up to $\mathcal{O}(s_h^4)$ is given by

$$V(h) = V_g(h) + V_f(h) = -\gamma s_h^2 + \beta s_h^4, \qquad (3.100)$$

where we have denoted $\gamma = \gamma_g + \gamma_f$ and $\beta = \beta_g + \beta_f$. For $\gamma \geq 0$ and $0 < \beta \geq \gamma/2$, the potential has three extrema: $s_h = 0$ (no EWSB), $s_h = 1$ (maximal EWSB) and

$$s_h^2 = \xi = \frac{\gamma}{2\beta}. \qquad (3.101)$$

The one at $\xi = 1$ should be discarded because it is outside the regime of validity of eq.(3.100) (and leads anyway to massless SM fermions, $\Pi_{t_L t_R} = 0$ in eq.(3.90)). The extremum (3.101) is a local minimum of the potential when $\gamma > 0$ and, at the same time, $\gamma < 2\beta$. Demanding a sufficiently small value of ξ, as suggested by the EWPT, requires to tune $\gamma < \beta$. The Higgs mass at the non trivial minimum (3.101) equals

$$m_H^2 = \frac{8\beta}{f^2}\xi\,(1 - \xi). \qquad (3.102)$$

It is very useful to parametrically understand what are (if any) the generic relations among the Higgs mass and the masses of the vector and fermion resonances.

From eq.(3.84), we see that the following parametric expressions for γ_g and β_g approximately hold:

$$\gamma_g \sim -\frac{g^2 f^2 m_\rho^2}{16\pi^2}, \qquad \beta_g \sim \frac{g^4 f^4}{16\pi^2} \sim |\gamma_g|\left(\frac{g}{g_\rho}\right)^2 \ll |\gamma_g|. \qquad (3.103)$$

For $\xi \ll 1$, using eqs.(3.101) and (3.102) we have

$$\frac{m_\rho^2}{m_H^2} \simeq \frac{4\pi^2}{g^2}\frac{|\gamma_g|}{\gamma}. \qquad (3.104)$$

Given the bounds coming from the $\hat{S}$ parameter and from direct searches (eq. (3.51)), we parametrically require $\gamma \ll |\gamma_g|$, as well as $\gamma \ll \beta$. This implies a fine-tuning at work, so that γ is small because the fermion and the gauge contribution compensate with each other, $\gamma_f \simeq -\gamma_g$. As we will shortly see, $|\gamma_f| \simeq |\beta_f|$, while $\beta_g \sim \gamma_g(g/g_\rho)^2$, implying that generally $\beta_g \ll \beta_f$ and can be neglected.

The fermion sector, with more different mass scales, is more involved. Before going into the details of the models, let us present some general – and rough – estimates. From eq. (3.102) we see that for a given ξ the Higgs mass depends only on the β parameter. This means that

the Higgs mass value at fixed ξ will depend largely only on the fermion sector. In the case of elementary t_L and t_R, which we are considering, the top mass goes like

$$M_{top} \sim \frac{\epsilon_L \epsilon_R}{M_f} s_h \,, \tag{3.105}$$

where $\epsilon_{L,R}$ are the mixing parameters for the $t_{L,R}$ quarks and M_f represents the mass of the lightest fermion resonances that couple to t_L and t_R. A simple NDA estimate of the top contribution to γ and β then gives

$$\gamma_f \sim \frac{N_c}{16\pi^2} \epsilon^2 M_f^2 \,, \qquad \beta_f \sim \frac{N_c}{16\pi^2} \epsilon^4 \,. \tag{3.106}$$

Using eqs. (3.105), (3.106) and (3.102) we obtain [3]

$$m_H^2 \sim \frac{N_c \epsilon^4}{2\pi^2 f^2} \xi \sim \frac{N_c}{2\pi^2} M_{top}^2 \frac{M_f^2}{f^2} \,. \tag{3.107}$$

This shows that the Higgs mass grows linearly with the top partners mass scale, in particular for a given ξ (i.e. f) we expect that the measured value of the Higgs mass should point to a specific range of masses for the top partners. In the rest of the chapter we focus on this prediction.

3.7.1   Estimates for the minimal model

For simplicity, we first consider the set-up where $N_\rho = N_a = N_S = N_Q = 1$, taking $a_\rho = 1$ and $g' = 0$. When the Weinberg sum rules (I-II) in the gauge sector are imposed, the axial mass and decay constant are completely determined in terms of the vector mass m_ρ, which is the only mass scale in the spin 1 sector, see eq. (3.84).

We choose to solve the sum rules (III-IV) as in eq.(3.98), so that the fermion sector is characterized by three mass scales: the mixing parameter ϵ and the vector masses m_S and m_Q. It is useful to parametrize the system in terms of $\omega_L \equiv \tan\theta_L$ and $\omega_R \equiv \tan\theta_R$, introduced in eq.(3.45), and one mass scale. We can split the fermion parameter space in $3 \times 3 = 9$ regions, $\omega_L \ll 1$ (elementary t_L), $\omega_L \simeq 1$ (semi-composite t_L), and $\omega_L \gg 1$ (fully composite t_L) and similarly for ω_R. We always take ω_L and ω_R to scale in a similar fashion, so that $\omega_L \simeq \omega_R$ for $(\omega_L \ll 1, \omega_R \ll 1)$ and $(\omega_L \gg 1, \omega_R \gg 1)$, and $\omega_L \omega_R \simeq 1$ for $(\omega_L \ll 1, \omega_R \gg 1)$ and $(\omega_L \gg 1, \omega_R \ll 1)$.[18] In each region we choose as mass scale the physical mass of the Lightest

---

[18]It is important to keep in mind that physically there is actually no way to take the formal parametric limit $\omega_{L,R} \to 0$ or $\omega_{L,R} \to \infty$, because, at fixed top mass, some fermion resonance mass becomes infinitely massive. The maximal value of a fermion mass in the effective theory should be less than $\Lambda = 4\pi f$, above which we should integrate out the heavy field. In light of that, the actual allowed range for $\omega_{L,R}$ is

$$\frac{1}{4\pi} \lesssim \omega_{L,R} \lesssim 4\pi \,. \tag{3.108}$$

ω_L \ ω_R	$\ll 1$	$\simeq 1$	$\gg 1$
$\ll 1$	$(M, \omega^4, \omega^4, \omega^4)$	$(M_0, 1, 1, 1)$	$(M_0, 1, 1, 1)$
$\simeq 1$	$(M_{7/6}, 1, 1, 1)$	$(M, 1, 1, 1)$	$(M, 1, 1, 1)$
$\gg 1$	$(M_{7/6}, \omega_L^2, \omega_L^4, \omega_L^4)$	$(M_{7/6}, \omega_L^2, \omega_L^4, \omega_L^4)$	$(M_{7/6}, 1, \omega_L^2, \omega_L^2)$

Table 3.1: Values of m_L, k_t, k_γ and k_β (in order) for the parametric limits of elementary, semi-composite and fully composite t_L, t_R. For simplicity, we have omitted the subscripts $0, 7/6$ on M, and L, R on ω, when not necessary.

Fermion Resonance (LFR), denoted by m_L, as given by eq.(3.47). This is always either M_0 or $M_{7/6}$. We then define the parameters

$$M_{top}^2 \equiv k_t(\omega_L, \omega_R) m_L^2 \xi, \quad \gamma_f \equiv \frac{N_c m_L^4}{16\pi^2} k_\gamma(\omega_L, \omega_R), \quad \beta_f \equiv \frac{N_c m_L^4}{16\pi^2} k_\beta(\omega_L, \omega_R). \quad (3.109)$$

We report in table 1 the parametric dependence of k_t, k_γ and k_β on ω_L and ω_R, as well as m_L, in each region. Notice that the table is not symmetric under the exchange $\omega_L \leftrightarrow \omega_R$ and $m_Q \leftrightarrow m_S$, because of the presence of the bi-doublet with $Y = 7/6$, whose mass is $M_{7/6} = m_Q$, independently of ω_L and ω_R. Given the mixing parameters and ξ, everything else is parametrically determined, namely m_ρ, m_L and m_H. In particular, we have

$$m_\rho^2 \simeq \frac{N_c M_{top}^2}{4 m_W^2} \frac{k_\gamma}{k_t^2 \xi} M_{top}^2, \quad m_H^2 \simeq \frac{g^2 N_c M_{top}^2}{8\pi^2 m_W^2} \frac{k_\beta}{k_t^2} M_{top}^2, \quad m_L^2 = \frac{M_{top}^2}{k_t \xi}, \quad (3.110)$$

$$\frac{m_\rho^2}{m_H^2} \simeq \frac{2\pi^2}{g^2 \xi} \frac{k_\gamma}{k_\beta}, \quad \frac{m_\rho^2}{m_L^2} \simeq \frac{N_c M_{top}^2}{4 m_W^2} \frac{k_\gamma}{k_t}, \quad \frac{m_H^2}{m_L^2} \simeq \frac{g^2 N_c M_{top}^2}{8\pi^2 m_W^2} \frac{k_\beta}{k_t} \xi. \quad (3.111)$$

In all regions, except $(\omega_L \ll 1, \omega_R \ll 1)$ and $(\omega_L \gg 1, \omega_R \gg 1)$, $k_\beta/k_t^2 \sim 1$ and the Higgs is parametrically determined in terms of M_{top} to be quite light (below the LEP bound, taking eq.(3.110) literally).[19] In all these regions, for reasonably natural values of ξ (say, $\xi \simeq 1/10$), the LFR (singlet T' or the exotic fermion X contained in the $Y = 7/6$ doublet, depending on the region) is always light, of order $1/\sqrt{\xi}$ times the top mass, or even too light, of order $1/(\omega_L \sqrt{\xi})$, with $\omega_L \gg 1$. For $(\omega_L \gg 1, \omega_R \gg 1)$ the Higgs is heavier and yet the fermion resonance Q_7 is light. Finally, when $(\omega_L \ll 1, \omega_R \ll 1)$, both the Higgs and the resonance masses (vector and fermion) increase as $1/\omega^2$. In all regions, $k_\beta = k_\gamma$, implying that m_ρ/m_H is independent of the fermion sector and determined, at fixed ξ. Finally, since $k_{\beta,\gamma} \geq k_t$ in all regions, we can conclude that *a light Higgs implies light fermion and vector resonances*. The latter are always heavier than

---

[19]Needless to say, the considerations above are quite schematic and are only valid parametrically. They are not accurate enough for a more quantitative description.

the former, as can be seen from eq.(3.111) that, taken literally, predict vector masses roughly twice heavier than fermion masses. The converse is not always true. In particular, for a strongly composite top, we can have light fermion resonances and an heavy Higgs.[20]

3.7.2 Generalizing to non-minimal scenarios

Let us now consider the generalizations to models with multi vector and fermion resonances. When more spin 1 resonances are considered, a too large $\hat{S}$ parameter can be circumvented by either some tuning between the axial and vector resonances or by an increase in the vector resonance mass. For illustration, let us consider how the latter situation can be realized with 2 vectors and 1 axial resonance (see section 3.7.3 and appendix D for a discussion of a model based on this gauge sector). For simplicity, we take $f_{\rho^1} = f_{\rho^2} = f$ and $f_{mix} = 0$. Imposing the sum rules (I) and (II) allows to determine m_a and f_a as a function of f and of the two vector masses m_{ρ^1} and m_{ρ^2}. A simple calculation gives as leading expression in an expansion in $(g/g_\rho)^2$

$$\gamma_g = -\frac{9f^2 g^2 m_\rho^2}{64\pi^2}\left((1+x^2)\log\left(\frac{2}{3}(1+x^2)\right) - 2x^2\log x\right), \tag{3.112}$$

where $m_\rho = m_{\rho^1}$ and $x = m_{\rho^2}/m_{\rho^1}$. For an appropriate range in x, the coefficient multiplying $f^2 g^2 m_\rho^2$ in eq.(3.112) can be significantly smaller than the one in eq.(3.84). At fixed γ_f, this implies the possibility of increasing m_ρ and hence decreasing the value of $\Delta\hat{S}$ within the allowed range. One can also check that in the case of 2 axials and 1 vector resonance, $\Delta\hat{S}$ can be made small when one of the two axial resonances is quite light (see eq.(D.4)).

When more fermion resonances are involved, N_Q and/or N_S greater than one, the analysis is greatly complicated by the large number of parameters involved. The main qualitative feature, as already mentioned, comes from γ_f that for small mixing terms scales as ϵ^2. This implies that parametrically $\gamma_f \gg \beta_f$, in tension with eq.(3.101), that would favour regions where $\gamma \ll \beta$. On the other hand, a larger γ_f is welcome, because it implies a larger γ_g (in order to tune $\gamma_f + \gamma_g$ to be small) and hence spin one resonance masses heavy enough to keep $\Delta\hat{S}$ under control, although at the expense of a higher fine-tuning. We still expect the Higgs to be light when the LH and RH top are substantially composite ($\epsilon_i \gtrsim m_i$) and at least one fermion resonance, barring accidental cancellations, to be light and parametrically related to the top mass by $m_L^2 \sim M_{top}^2/\xi$. On the other hand, when we approach the region of an elementary top, both the Higgs mass and the fermion resonances related to the top become heavy. We then expect that the implication light Higgs $\rightarrow$ light fermion resonances continue to apply. These arguments are also supported by the

---

[20] The direct link between m_H and m_ρ can be problematic for these minimal models with just one resonance. In fact, a more detailed analysis reveals that m_ρ is always below 2 TeV for a 125 GeV Higgs mass (see eqs.(D.1)-(D.3) and fig. D.1 (b,d) in appendix E), leading generally to a too large $\hat{S}$ parameter and to a tension with the bound from direct searches reported in eq. (3.51).
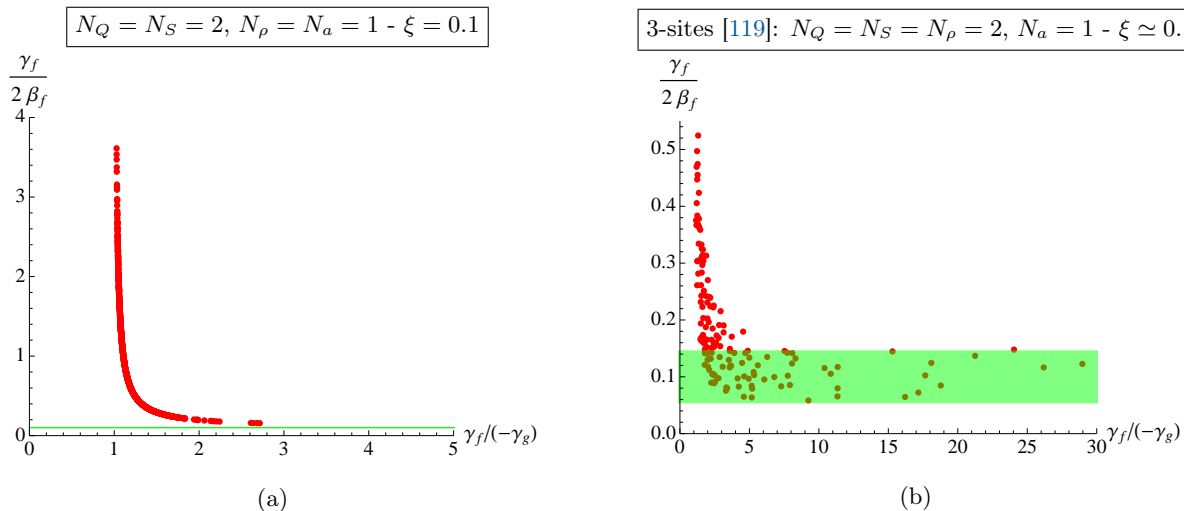
Figure 3.6: Values of $\gamma_f/(-\gamma_g)$ versus $\gamma_f/(2\beta_f)$, that is the value of ξ one would get by neglecting the gauge contribution to the Higgs potential. The points are obtained by a numerical scan, requiring $m_H \in [100, 150]$ GeV. (a) The range of the parameters is taken as follows: $m_{iQ}, m_{iS} \in [0, 8f]$, $\theta_{qQ}, \theta_{tQ}, \theta_{qS}, \theta_{tS} \in [0, 2\pi]$, $a_\rho \in [1/\sqrt{2}, 2]$. ϵ_t, as defined in eq.(D.5), has been obtained by fixing M_{top} while m_ρ by fixing ξ. The green line represents $\xi = 0.1$. In most of the points $\gamma_g \simeq -\gamma_f$ and it is never possible to go in the region where $\gamma_f \gg -\gamma_g$. (b) The range of the parameters is taken, in the notation of [119], as follows: $g_*, \tilde{g}_* \in [0, 8]$, $M_Q, M_S, m, \Delta \in [0, 8f]$, $y_R/(\sqrt{2}y_L) \in [0.3, 0.6]$ and y_L has been obtained fixing M_{top}, cutting for $\xi \in [0.05, 0.15]$. The green band represents the actual values of $\xi \in [0.05, 0.15]$. In most of the points still $\gamma_g \simeq -\gamma_f$, but now there is a region where the gauge contribution is negligible.

estimate in eq. (3.107). We will provide more accurate estimates of the relation among Higgs and fermion resonance masses in the next section, where we consider in more detail some specific classes of models.

Non-minimal models with more vectors and fermions allow the possibility to tune $\xi \ll 1$ in a different way. Since with more vectors, as we have just seen, the estimate (3.103) does not necessarily hold, there is the possibility to have $\gamma_f \gg |\gamma_g|$ (and yet heavy enough vector resonances), so that the whole gauge contribution to the Higgs potential is sub-leading with respect to the fermion one. All the tuning is at work in the fermion sector to get $\gamma_f \simeq 2\xi\beta_f \ll \beta_f$. This is possible, in the region of small mixing, if *both* the coefficients of the leading quadratic and next-to-leading quartic terms in the mixing in γ_f are tuned to be small, so that $\gamma_f \ll \beta_f$. In such regions a double tuning is at work, needed to get a small hierarchy between v and f. See fig. 3.6 for a comparison between the multi-fermion and multi-gauge model (e.g. the 3-sites theory of [119]), where this kind of tuning can occur, and the multi fermion (but minimal-gauge) model.

3.7.3   Three Examples of Selected Models

The framework introduced in the previous sections opens up a huge set of possibilities for model building. In fact, not only the number of spin 1 and spin 1/2 resonances to be introduced below the cutoff is free, but also the Weinberg sum rules have often physically different possible solutions. Studying in detail each of these models is well beyond the scope of this work and, as the simplest cases are already able to produce working models which display all the interesting aspects, we focus in the following on the case where $N_Q, N_S, N_\rho, N_a \leq 2$. A schematic presentation of the results for all the different cases will be presented in the appendix D. The simplest realization of our framework, that is the model with $N_\rho = N_a = N_Q = N_S = 1$ described in section 3.7 and in appendix D, does not grossly pass the EWPT for $m_H \in [100, 150]$, GeV because of a too large tree-level $\hat{S}$ parameter, induced by (relatively) too light vector resonances, $m_\rho \lesssim 2$ TeV, as can be seen in fig. D.1 (b, d). This is a direct consequence of the first relation in eq.(3.111) and of the fact that $k_\gamma \simeq k_\beta$ in this model.

A straightforward way to circumvent this problem is to add more freedom either in the gauge sector or in the fermionic sector. In the rest of this section we consider three models. The first two, in our opinion, offer the best compromise between simplicity and viability, that is $N_\rho = 2$, $N_a = N_Q = N_S = 1$ and $N_S = 2$, $N_Q = N_\rho = N_a = 1$. The third one is actually the simplest possible model, with $N_\rho = N_Q = 1$ and $N_a = N_S = 0$. Here the composite sector is assumed to contain a massless chiral bound state, identified with the RH top quark. As we will see, this model is not realistic because it predicts a too light Higgs, but it is a counterexample to the statement that a light Higgs predicts light fermion resonances.

For the first two models presented here and those in the appendix D we have performed a scan of the parameters imposing the generalized Weinberg sum rules, setting the ratio $v^2/f^2 = \xi = 0.1, 0.2$ and requiring a light Higgs boson, $m_H \in [100, 150]$ GeV. In all our scans we set the top mass (roughly at the TeV scale) to be $M_{top}(\text{TeV}) \simeq 150$ GeV [21].

Direct search bounds on the fermion resonance masses should be taken into account. The present available experimental constraints are discussed in section 3.5.2. The plots presented in this chapter, however, use only an older (and weaker) bound on the exotic fermion X with electric charge $Q = 5/3$ coming from the CMS bound on double production of B' resonances $(Q = -1/3)$ decaying to $W^- t$, $m_{B'} > 611$ GeV [165], which also applies to the X search (the signature of the final state is two pairs of same-sign di-leptons in both cases, also the efficiency of the cuts is approximately the same):

$$M_{7/6} > 611 \text{ GeV} . \tag{3.113}$$

---

[21] This value is obtained by considering the running of the top Yukawa coupling in the SM from the top mass energy scale, where it is measured, to the scale of the top partners $\sim$ TeV, where it is generated.
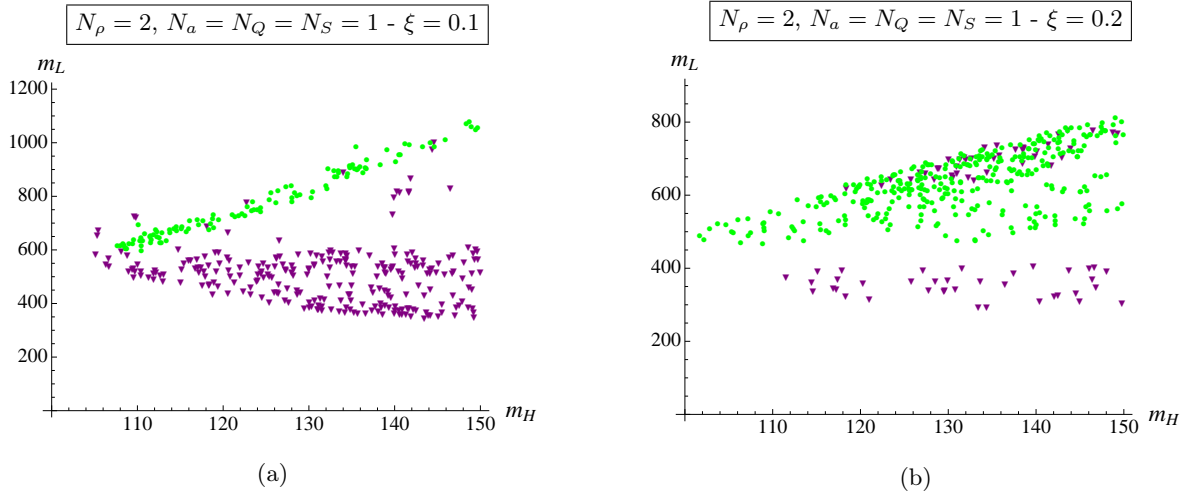
Figure 3.7:   Mass of the LFR (in GeV), before EWSB, as a function of the Higgs mass (in GeV). The green circles represent the points where the LFR is the singlet T' while if it is the exotic X with charge $5/3$ then they are represented by purple triangles. The masses m_Q, m_{ρ_1} and m_{ρ_2} are taken in the range $[0, 8f]$, $a_{\rho_1}, a_{\rho_2} \in [1/2, 2]$ and $a_{\mathrm{mix}} \in [0, 5]$; ϵ and m_S have been obtained by fixing M_{top} and ξ.

In appendix D we also comment on the models where the generalized second Weinberg sum rules are relaxed and the Higgs potential is logarithmically divergent.

Two-vector model

The models with $N_\rho = 2$, $N_a = N_Q = N_S = 1$, are the simplest models passing the EWPT within our set-up. A similar model with $N_\rho = N_Q = N_S = 1$ and $N_a = 2$, considered in the appendix D, also pass the EWPT, but it is theoretically less motivated than the $N_\rho = 2$, $N_a = 1$ case. Indeed, while the gauge sector of the latter can be realized, for instance, in a deconstructed model (such as the 3-sites model of [119]), the former appears to be more exotic and unconventional. For this reason, we have decided to focus on the $N_\rho = 2$, $N_a = 1$ model in the following. We assume invariance under LR symmetry, so that Π_{LR} in the last row of eq.(3.75) vanishes. In the fermion sector we take eq.(3.98) to satisfy the two sum rules (3.96) and (3.97), and keep $m_S \neq m_Q$. This solution allows us to explore both the regions of parameter space where the LFR is a T' or X.

As explained in section 3.7, adding a second vector resonance allows for a higher overall mass scale for the vectors, keeping γ_g fixed, and alleviate the constraints coming from the S parameter. This can be explicitly seen in the approximation $f_{\mathrm{mix}} = 0$ and $f_{\rho_1} = f_{\rho_2} = f$, where we obtain the expression (3.112) for γ_g, which is negative in the range $0.4 \lesssim x \equiv m_{\rho^2}/m_{\rho^1} \lesssim 2.5$ and positive otherwise. It is therefore possible to tune $x \simeq 2.5$ (or $x \simeq 0.4$) and at the same time increase m_{ρ^1} to keep γ_g fixed. A posteriori, the numerical scan shows that $a_{\mathrm{mix}} \equiv f_{\mathrm{mix}}/f \lesssim 0.3$, so that the approximation used above is valid.

The fermion sector of this model is simple enough that it is not hard to write simple analytic formulas for the top and Higgs mass, that go beyond the parametric estimate given in section 4. In particular, this allows us to explicitly check that a light Higgs requires light fermion resonances. Let us first consider the elementary $t_{L,R}$ region, with $\omega_{L,R} < 1$. In this region, at leading order in $\omega_L \sim \omega_R$, we have

$$M_{top}^2 \simeq \frac{1}{2} m_S^2 \omega_R^2 (\omega_L + \sqrt{2}\omega_R)^2 \xi = \frac{1}{4} \epsilon^4 \frac{(m_Q + m_S)^2}{m_Q^2 m_S^2} \xi \,. \tag{3.114}$$

Using eq.(3.102) for $\xi \ll 1$ and expanding β_f at leading order in $\omega_{L,R}$, we immediately get

$$m_H^2 \simeq \frac{N_c}{\pi^2 f^2} \frac{m_S^4 \omega_R^4 (\omega_L + \sqrt{2}\omega_R)^2 \xi}{2\omega_R^2 - \omega_L^2} \log\left(\frac{2\omega_R^2}{\omega_L^2}\right) = \frac{N_c}{\pi^2 f^2} \frac{m_Q^2 m_S^2}{m_Q^2 - m_S^2} \log\left(\frac{m_Q^2}{m_S^2}\right) M_{top}^2 \,, \tag{3.115}$$

where in the last relation we have used eqs.(3.45) and (3.114). It is straightforward to derive from eq.(3.115) an upper bound for the LFR mass m_L:

$$m_L \leq \frac{\pi f}{\sqrt{N_c}} \frac{m_H}{M_{top}} \simeq 1.2 \left(\frac{0.1}{\xi}\right)^{1/2} \text{ TeV} \,. \tag{3.116}$$

Let us now consider the region $\omega_L < 1$, $\omega_R \simeq 1$ (elementary t_L, semi-composite t_R, often found in the numerical scan). In this region the LFR is necessarily T', with $m_L = M_0 \simeq \sqrt{2}m_S$. Expanding in $\omega_L < 1$, we have

$$M_{top}^2 \simeq \frac{m_L^2}{4} \xi \,,$$
$$m_H^2 \simeq \frac{N_c}{8\pi^2 f^2} m_L^2 \left(\log \xi^{-1} + 8 \log\left(\frac{m_Q^2}{m_S^2}\right) + \log 4 - 1 \right) M_{top}^2 \,, \tag{3.117}$$

and gives the upper bound

$$m_L \leq \frac{2\sqrt{2}\pi f}{\sqrt{N_c}\sqrt{\log \xi^{-1}}} \frac{m_H}{M_{top}} \simeq 2.2 \text{ TeV} \quad \text{for } \xi = 0.1 \,. \tag{3.118}$$

We performed the parameter scan for a light Higgs, both for $\xi = 0.1$ and $\xi = 0.2$. We show in fig. 3.7 the relation between the LFR mass, m_L, and the Higgs mass, m_H, in the light Higgs region, obtained by a numerical scan over the parameter space. The bounds in eq. (3.52) rule out most of the region with a light X. As explained above, the vector masses can be arbitrarily heavy, so passing the constraints on the $\hat{S}$ parameter is not an issue for this model. Also in this case, the tuning to get a successful EWSB is between the gauge and the fermion contribution to the Higgs potential, γ_g and γ_f.

Two-singlet model

Adding a second composite fermion, singlet of SO(4), is the minimal choice to go beyond the simplest setup in the fermionic sector. This is already enough to increase γ_f and therefore to obtain heavier vector resonances and smaller tree-level contribution to the $\hat{S}$ parameter.
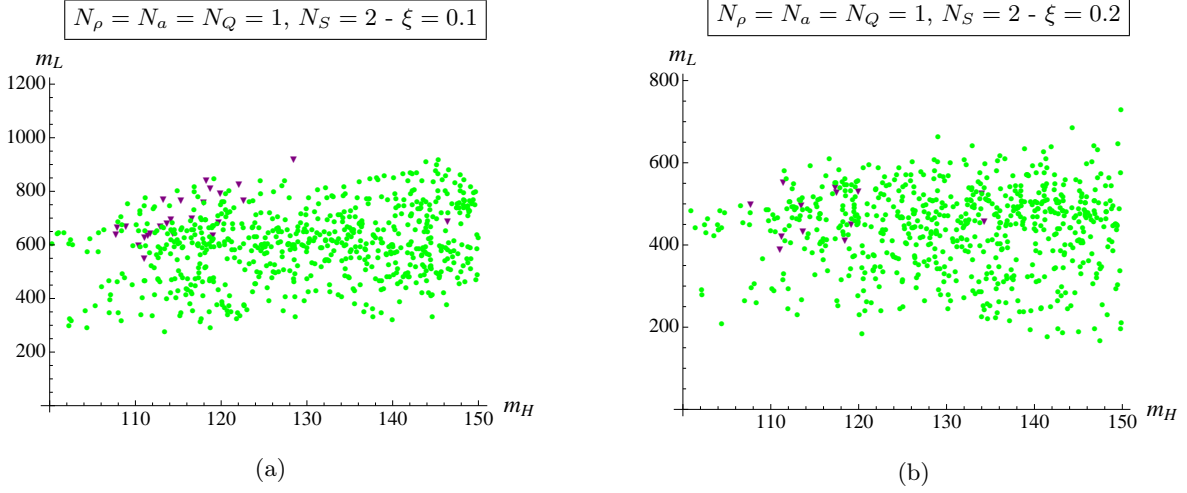
Figure 3.8: Mass of the LFR (in GeV), before EWSB, as a function of the Higgs mass (in GeV). The green circles represent the singlet T' while the purple triangles represent the fermion X. All the fermion masses are taken in the range $[0, 6f]$, the angles $\theta_q, \theta_t \in [0, 2\pi]$ and $a_\rho \in [1/\sqrt{2}, 2]$. The mixing ϵ_t and the mass m_ρ have been obtained by fixing M_{top} and ξ respectively.

The fermionic Lagrangian we start with is the one of eq.(3.39) with $N_Q = 1$, $N_S = 2$. The most general solution to the first fermionic sum rule, eq.(3.96), is given in terms of two angles and two mixings:

$$\epsilon_{qQ} = \epsilon_q \qquad \vec{\epsilon}_{qS} = (\epsilon_q \cos\theta_q, \ \epsilon_q \sin\theta_q),$$
$$\epsilon_{tQ} = \epsilon_t \qquad \vec{\epsilon}_{tS} = (\epsilon_t \cos\theta_t, \ \epsilon_t \sin\theta_t). \tag{3.119}$$

We can solve eq.(3.97) for one of the remaining parameters, say ϵ_q, in terms of the remaining ones, obtaining

$$\epsilon_q = \epsilon_t \sqrt{\frac{m_Q^2 - m_{1S}^2 \cos^2\theta_t - m_{2S}^2 \sin^2\theta_t}{m_Q^2 - m_{1S}^2 \cos^2\theta_q - m_{2S}^2 \sin^2\theta_q}}. \tag{3.120}$$

Once we impose this relation, for small mixing ϵ_t we have $\gamma_f \propto \epsilon_t^2$ and $\beta_f \propto \epsilon_t^4$, in contrast to the 1-singlet case where $\gamma_f, \beta_f \propto \epsilon^4$. In particular, we get

$$\gamma_f \propto \epsilon_t^2 (m_Q^2 - m_{1S}^2)(m_Q^2 - m_{2S}^2)(m_{2S}^2 - m_{1S}^2)(\cos 2\theta_q - \cos 2\theta_t). \tag{3.121}$$

This implies that γ_f can be enhanced with respect to the estimate in eq.(3.99). However γ_g cannot increase too much, leading otherwise to too heavy vector resonances, and hence the enhancement of γ_f should be kept small. This is confirmed by the numerical scan where we get small deviations from the exact cancellation. In this simple, yet fundamental, observation lies the reason why this model, like all the ones with more fermionic resonances, is able to pass the EWPT.

Let us consider a specific region in parameter space selected by EWSB, where $\epsilon_q \sim \epsilon_t \sim \epsilon$, $m_Q \sim m_{2S} \sim M$, $\theta_q \sim \pi$ and $\theta_t \sim 0$, with both m_{1S} and ϵ much smaller than M. In this region the coefficient of the ϵ_t^2 term in γ_f is suppressed. We get

$$\gamma_f \simeq \frac{N_c}{32\pi^2}\epsilon^4\left(\log\frac{M^2}{m_L^2} - 1\right) = \frac{N_c}{32\pi^2}\epsilon^4 b_\gamma,$$

$$\beta_f \simeq \frac{N_c}{32\pi^2}\epsilon^4\left(\log\frac{M^2}{m_L^2} + \frac{\epsilon^4}{8m_L^4}\left(\log\frac{m_L^2}{\mu_f^2} - 1\right)\right) = \frac{N_c}{32\pi^2}\epsilon^4 b_\beta, \tag{3.122}$$

$$M_{top}^2 \simeq \frac{\xi}{4}\frac{\epsilon^4}{m_L^2},$$

where μ_f is the IR regulator of the spurious IR divergence arising from β_f (see eq.(3.95) and footnote 12) and m_L denotes the mass of the LFR, that is clearly the singlet S_1 in this region: $m_L \simeq \sqrt{m_{S_1}^2 + \epsilon^2/2}$. From these relations we obtain the estimate

$$m_L \simeq f\sqrt{\frac{\pi}{b_\beta}\frac{m_H}{M_{top}}}. \tag{3.123}$$

Since $b_\beta > \log\frac{M^2}{m_L^2} \gtrsim 2$ for at least $M > 3m_L$, the singlet has an upper bound of $m_L \lesssim 800$ GeV for $\xi = 0.1$. We therefore obtain that also in this case *a light Higgs boson implies light fermionic resonances*. For both $\xi = 0.1$ and 0.2 we find that the singlet is the LFR, with a mass in the range $\sim 300 - 800$ GeV, see fig.3.8. A sizable portion of this region is now excluded by the bound in eq. (3.52) from direct searches of double production of T' resonances, in particular the model for $\xi = 0.2$ is now completely excluded. Even though the bulk of the points show a vector mass in the same range as in the minimal model, there are nevertheless points with bigger values of m_ρ so that the model can pass the EWPT

3.8   A Counter-Example: a Light Higgs and Heavy Resonances

Let us now consider a qualitatively different setup. We modify the picture presented in sec. 3.3 by assuming that the right-handed top quark is part of the composite sector. Such a choice, which differentiates the third family with respect to the first two, could be justified by the fact that the top is much heavier than the other SM fermions. Since composite states should be in complete representations of SO(4), if we assumed that the doublet q_L was part of the composite sector, then we should have added other light states in order to complete a representation of SO(4) (in particular another doublet), which is not observed. Moreover, bounds from the measurement of the $Zb\bar{b}$ coupling do not allow to assume a composite RH bottom quark. The only available possibility is then to consider a composite RH top quark in a (chiral) singlet representation of SO(4). As in the previous sections we embed the LH top doublet in a **5** of SO(5), ξ_L, with $X = 2/3$.
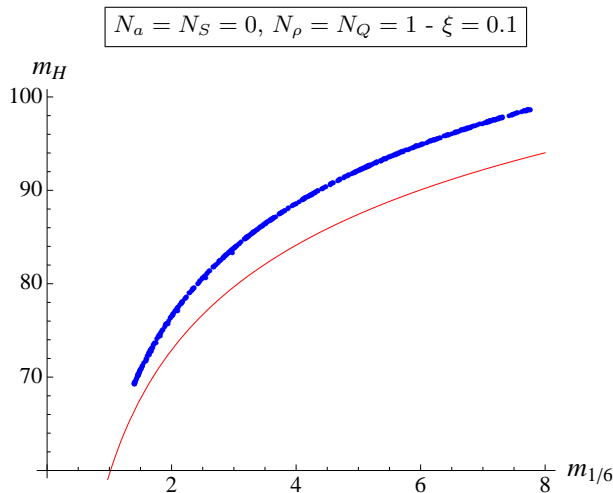
Figure 3.9:   Higgs mass (in GeV) as a function of the $Y = 1/6$ doublet mass (in TeV) in the composite t_R model, for $\xi = 0.1$. The blue points are obtained by a numerical scan, while the thin red line represents the analytic estimate eq.(3.127). The two results are compatible, up to a $\sim 5\%$ error, due to the expansion for small ξ in eq.(3.127). In the numerical scan, the mass m_Q has been taken in the range $[0, 10f]$, while the mixing parameter ϵ has been obtained by fixing M_{top}.

In order to provide a mass to the top the mixing term $\epsilon \, \bar{\xi}_L U t_R$ would be sufficient since it would give $M_{top} \simeq \epsilon s_h$, however the Higgs potential in this model would be quadratically divergent and therefore we would not be able to compute the Higgs mass. To cure this issue let us add some composite top partners and estimate the expected values of the Higgs mass in this class of models [3]. We can easily estimate $\beta \sim \frac{N_c}{16\pi^2} \, \epsilon^4$ and therefore the Higgs mass

$$M_H^2 \simeq \frac{N_c \epsilon^4}{2\pi^2 f^2}\xi \simeq \frac{N_c}{2\pi^2} M_{top}^2 \frac{M_{top}^2}{v^2} \simeq (36\text{GeV})^2. \tag{3.124}$$

We see that, at this level of approximation, the Higgs mass is independent of the details of the models and too light.

Let us now construct an explicit model in order to confirm this estimate. In order to cure the quadratic divergence in the Higgs potential it is sufficient to add one composite fermion in the bidoublet representation, Q, while no singlet fields S are needed, $N_S = 0$. The leading fermion Lagrangian is[22]

$$\mathcal{L}_{f,0} = \bar{q}_L i \not{D} q_L + \bar{t}_R i \not{\nabla} t_R + \bar{Q}(i\not{\nabla} - m_Q)Q + \epsilon_{qS}\bar{\xi}_L U t_R + \epsilon_{qQ}\bar{\xi}_L U Q_R + h.c.. \tag{3.125}$$

The Weinberg sum rules (III) and (IV) obtained in section 3 do not apply in this case with

---

[22]One might think that the Lagrangian (3.125) can be obtained from eq.(3.39) with $N_Q = N_S = 1$, in the limit $\epsilon_{tS,tQ} \to \infty$, in which case the singlet becomes ultra-heavy and can be integrated out. This is however not the case, because the Weinberg sum rule (III) would imply $\epsilon_{qS,qQ} \to \infty$, and hence a ultra-heavy doublet as well.

$N_S = 0$, but the expressions for the form factors and the 1-loop Higgs potential are particularly simple. Demanding the cancellation of the quadratic divergence in the fermion sector requires $|\epsilon_{qQ}| = |\epsilon_{qS}| \equiv \epsilon$. Requiring also the cancellation of the logarithmic divergence in γ_f would imply $\epsilon = 0$, which of course is not a viable possibility. This is not an issue because we are interested mostly in computing the Higgs mass, which is finite in this case. Keeping the logarithmic divergence, as we explained in section 3.6.1, means that γ is scale-dependent and therefore one has to fix ξ via some observation, rendering it not calculable. We then proceed by assuming a given value for ξ and computing only β. Since $\beta_g \ll \beta_f$, we can completely neglect the gauge sector.[23] In this approximation, and at first order in ξ, we obtain the expression for the Higgs and top masses:

$$M_H^2 \simeq \frac{N_c}{8\pi^2} \frac{\epsilon^4 m_Q^4}{f^2 m_{1/6}^4} \xi \left(\log \frac{m_{1/6}^2}{\mu_f^2} - 1 \right), \qquad M_{top}^2 \simeq \frac{\epsilon^2 m_Q^2}{2 m_{1/6}^2} \xi, \qquad (3.126)$$

where $m_{1/6}^2 = m_Q^2 + \epsilon^2$ is the physical mass of the composite $Y = 1/6$ doublet before EWSB. From these expressions we get the estimate for the Higgs mass as

$$M_H \simeq \sqrt{\frac{N_c}{2\pi^2}} \frac{M_{top}^2}{v} \sqrt{\log \frac{m_{1/6}^2}{\mu_f^2} - 1} \simeq 36 \sqrt{\log \frac{m_{1/6}^2}{\mu_f^2} - 1} \text{ GeV}, \qquad (3.127)$$

which is in very good agreement with eq. (3.124). As can be noticed immediately, the Higgs is always too light ($M_H \simeq 90$ GeV for $m_{1/6} \simeq 6$ TeV). This conclusion has also been checked by a numerical scan of the model, which gives results in agreement with the estimate above, see fig. 3.9. In this model the LFR is χ, with a mass (before EWSB) $M_{7/6} = m_Q$. It is interesting to notice that a light Higgs *does not* imply a light fermionic resonance, at least for models with a chiral composite sector. In this class of models a heavier value for the Higgs mass can of course be obtained by adding to the model other sources of explicit breaking of the global symmetry. For example this is the case of the SUSY pNGB Higgs model with a composite t_R studied in ref. [121], where the extra symmetry breaking terms are required by anomaly cancellation and for the absence of unwanted massless non-SM states.

3.9   Summary

In this chapter we constructed an effective theory in which the Higgs arises as a composite pseudo-NGB of a spontaneously broken global symmetry of a strongly coupled sector at the ~few TeV scale and in which the SM fermions (the top quark in particular) get a mass via the partial compositeness mechanism. Assuming that some vector and fermion resonances are somewhat

---

[23]Since ξ is not calculable, we can also relax the Weinberg sum rule (II) in the gauge sector, in which case we can assume that no axial resonance is present at all.

lighter than the typical strong coupling scale Λ, we included those states in the effective theory and computed their contribution to the Higgs potential, which allowed us to link the Higgs mass with the properties – the mass in particular – of these states. In order to have a calculable potential in our effective approach, we introduce the Minimal Higgs Potential hypothesis. That is, we require that the contribution to the potential from dynamics at the cutoff is subleading and we regulate the quadratic and logarithmic divergencies of the calculable contribution by imposing suitable generalized Weinberg sum rules.

After constructing various realizations of the models with different content of composite resonances, sec. 3.4, we were able to show that in such composite Higgs models, the measured value of the Higgs mass implies the presence of light (sub-TeV) fermion top partners, sec. 3.7. The LHC constraints on these states, described in section 3.5.2, are already able to exclude a big part of the parameter space of the models. We expect that the next run of the LHC at 14TeV will be able to cover completely all the parameter space of these natural models.

CHAPTER 4

A Composite Dark Matter Model

As already mentioned in the previous chapter, the next-to-minimal symmetry breaking pattern for composite Higgs models is $\mathrm{SO}(6) \to \mathrm{SO}(5)$, which includes five NGBs in the spectrum. Under the custodial subgroup $\mathrm{SU}(2)_L \times \mathrm{SU}(2)_R$ they transform as a bidoublet, $(\mathbf{2}, \mathbf{2})$, plus a singlet $(\mathbf{1}, \mathbf{1})$, which are identified respectively with the Higgs doublet H and a real singlet η. This scalar singlet can be made stable by introducing a symmetry under a parity P_η.

This opens up the possibility for this new particle to be a dark matter (DM) candidate. In this chapter we study this issue. We construct the models following very closely the approach described in the previous chapter, i.e. we introduce spin-1 and spin-1/2 resonances which mix linearly with the SM fields, and then we compute the effective potential for the Higgs and the DM candidate by assuming the MHP hypothesis and curing the UV sensitivity by suitable generalized Weinberg sum rules. In this way we are be able to link the properties of the DM candidate (mass and couplings), relevant to the astrophysical constraints, to the resonance spectrum, and study how the LHC bounds on these resonances and the Higgs couplings affect the DM properties. This chapter is based on the work done in ref. [2], where we extended the results of ref. [166].

4.1   A composite Dark Matter model

In this section we present a Composite DM model in which both the Higgs doublet H and the scalar singlet DM particle η arise as composite pNGBs, characterized by the NGB *decay constant* f, from a spontaneous symmetry breaking due to the dynamics of a new strongly coupled sector, lying at a high scale $\Lambda \sim 4\pi f$. The scenario considered here is based on the $\mathrm{SO}(6) \to \mathrm{SO}(5)$ symmetry breaking pattern. The singlet η is stable thanks to a parity P_η under which

$$\eta \to -\eta \; . \tag{4.1}$$

The main difference between this case and models in which η is an elementary scalar (see, e.g., refs. [167–169]) comes from derivative interactions between η and H. The universality of the leading-order chiral Lagrangian implies that these interactions depend only on the symmetry

breaking pattern and on the scale f. As showed in the previous chapter, fit of the Higgs couplings, EW precision observables and bounds from direct searches of composite resonances constrain the scale f to be somewhat higher than the EW scale, $v^2/f^2 \lesssim 0.2$. We can therefore expand the chiral Lagrangian for the NGBs in powers of $(|H|^2, \eta^2)/f^2$; up to dimension-6 terms one has [166]

$$\mathcal{L}^{kin} \simeq |D_\mu H|^2 + \frac{1}{2}(\partial_\mu \eta)^2 + \frac{1}{2f^2}\left(\partial_\mu |H|^2 + \frac{1}{2}\partial_\mu \eta^2\right)^2 . \tag{4.2}$$

As for the MCHM, in order to provide a mass to SM fermions we assume the *partial compositeness* mechanism. Upon integrating out the heavy fermions, the SM Yukawa interactions are generated, along with higher order interaction terms. Considering, for example, the bottom quark, up to dimension-6 terms the effective Yukawa Lagrangian can be written as

$$\mathcal{L}^{Yuk,b} \simeq -y_b \bar{q}_L H b_R \left(1 - \kappa_{hb}\frac{|H|^2}{f^2} - \kappa_{\eta b}\frac{1}{2}\frac{\eta^2}{f^2} + \dots\right) + h.c. , \tag{4.3}$$

and similarly for the other SM fermions. In our explicit model all the coefficients $\kappa_{hf} = \kappa_{\eta f} = 1$, where in general they depend on the choice of embedding of the SM fermions in (incomplete) SO(6) representations and on the parametrization of the SO(6)/SO(5) coset, as discussed in detail in appendix F.

As we saw in section 3.6, the mixing term between elementary and composite fields generate an effective potential for the pNGBs at the quantum level. Assuming invariance under the parity in eq. (4.1), the most general scalar potential, up to dimension 4 terms, is

$$V(H, \eta)_{\text{eff}} = \mu_h^2 |H|^2 + \frac{\mu_\eta^2}{2}\eta^2 + \lambda_h |H|^4 + \frac{\lambda_\eta}{4}\eta^4 + \lambda |H|^2 \eta^2 , \tag{4.4}$$

where λ is often dubbed *Higgs portal coupling* [170]. Assuming that $0 < -\mu_h^2 < \lambda_h f^2$ and $\mu_\eta^2 - \lambda\frac{\mu_h^2}{\lambda_h} > 0$, this potential has a minimum for

$$\langle H \rangle = \left(0, \frac{v}{\sqrt{2}}\right)^t, \quad \langle \eta \rangle = 0, \quad \text{where} \quad v^2 = -\frac{\mu_h^2}{\lambda_h} \equiv \xi f^2 \simeq (246 \text{ GeV})^2 . \tag{4.5}$$

The masses of the physical fields h and η, being h the Higgs boson, are given by

$$m_H^2 = 2\lambda_h v^2(1 - \xi) , \qquad m_\eta^2 = \mu_\eta^2 + \lambda v^2 , \tag{4.6}$$

where the $(1 - \xi)$ factor in the Higgs mass is a correction due to a wave function normalization effect, see eq. (4.12) in the next subsection.

Following the discussion of chapter 3 we render the scalar potential calculable by assuming the *Minimal Higgs Potential* hypothesis and we impose generalized Weinberg sum rules in order to remove the quadratic and logarithmic sensitivity to the cutoff. At one loop, the only composite states which contribute to the scalar potential are those that mix with the elementary SM particles, breaking the global SO(6) symmetry with such mixings. Such states are the spin-1/2

top partners and composite spin-1 resonances, with masses of the order $m_\rho^2 \ll \Lambda^2$, which mix with the SM EW gauge bosons.

The main aim of the rest of this section is to build explicit models in order to study the allowed range of the DM mass and Higgs portal coupling in realistic cases which, in particular, correctly describe both the top and Higgs mass and which still evade the bounds from direct searches of top partners at the LHC.

4.1.1   Structure and symmetries of the $\mathbf{SO}(6)/\mathbf{SO}(5)$ coset

Let us review here the basic structure of next-to-minimal Composite Higgs models where the strong sector enjoys a global symmetry $\text{SO}(6) \otimes \text{U}(1)_X$[1] spontaneously broken to the subgroup $\text{SO}(5) \otimes \text{U}(1)_X$ at a scale f [45, 132, 166]. Due to this spontaneous symmetry breaking, the low energy theory has 5 NGBs, which transform in the fundamental, $\mathbf{5}$, of SO(5). The custodial symmetry group is contained in the unbroken group, $\text{SO}(4) \sim \text{SU}(2)_L \otimes \text{SU}(2)_R \subset \text{SO}(5)$, and the NGBs transform as a $\mathbf{4} \oplus \mathbf{1} \sim (\mathbf{2}, \mathbf{2}) \oplus (\mathbf{1}, \mathbf{1})$ of the custodial group. Here and in the following we describe the five broken SO(6)/SO(5) generators as $T^{\hat{a}}$, with $\hat{a} = 1, \ldots, 5$. The 10 unbroken generators of SO(5), T^a, can be divided in the 6 generators of the $SO(4)$ custodial subgroup, $T^{a_{L,R}}$ with $a_{L,R} = 1, 2, 3$, and the 4 generators of the SO(5)/SO(4) coset, T^α with $\alpha = 1, \ldots, 4$ (see eq. (F.1) in appendix F for the explicit definition of the generators). The SM EW gauge symmetry is identified as the subgroup $\mathcal{G}_{EW} = \text{SU}(2)_L \otimes \text{U}(1)_Y \subset \text{SU}(2)_L \otimes \text{SU}(2)_R \otimes \text{U}(1)_X$, where the hypercharge is defined as $Y = T^{3_R} + X$.

The NGBs can be described by the Σ field

$$\Sigma = \frac{1}{f}\left(h_1, h_2, h_3, h_4, \eta, \sqrt{f^2 - h^2 - \eta^2}\right) , \tag{4.7}$$

where $h^2 = \sum_{i=1}^{4} h_i^2$ and where h_i and η live in the region $\sqrt{h^2 + \eta^2} \leq f$.[2] The usual Higgs doublet can can be constructed as $H = \frac{1}{\sqrt{2}}(h_1 + ih_2, h_3 + ih_4)^t$. In the unitary gauge $h_1(x) = h_2(x) = h_4(x) = 0$ and $h(x) \equiv h_3(x)$. See Appendix F for more details.

The chiral Lagrangian can be written in an expansion in derivatives over the cutoff. The leading term, with two derivatives, can be written as

$$\mathcal{L}^{kin} = \frac{f^2}{2}(D_\mu \Sigma)^t D^\mu \Sigma , \tag{4.8}$$

where $D_\mu = \partial_\mu - i\left(g_0 W_\mu^{a_L} T^{a_L} + g_0' B_\mu Y\right)$ and $f > v$ is the symmetry breaking scale, that is the only parameter of the leading order chiral Lagrangian. To eq. (4.8) one should add the kinetic

---

[1] The U(1)$_X$ factor is needed in order to correctly reproduce the SM fermion hypercharges.

[2] The effect of this constraint is negligible at any order in perturbation theory and therefore does not have any effect in any of the computation we perform in this work. In appendix F we will explicitly show the relations to other parametrizations used in the literature.

term for the elementary SM EW gauge bosons (we neglect QCD here since it does not play an important role in our discussion)[3]

$$\mathcal{L}^{gauge} = -\frac{1}{4} W_{\mu\nu}^a W^{a\mu\nu} - \frac{1}{4} B_{\mu\nu} B^{\mu\nu} \ , \tag{4.9}$$

In the unitary gauge, the chiral Lagrangian in eq. (4.8) reads

$$\begin{aligned}
\frac{f^2}{2}(D_\mu \Sigma)^t D^\mu \Sigma &= \frac{1}{2}\left[(\partial_\mu h)^2 + (\partial_\mu \eta)^2 + \frac{(h\partial_\mu h + \eta\partial_\mu \eta)^2}{f^2 - h^2 - \eta^2}\right] \\
&+ \frac{h^2}{8}\left\{g_0^2\left[(W_\mu^1)^2 + (W_\mu^2)^2\right] + (g_0' B_\mu - g_0 W_\mu^3)^2\right\} \ .
\end{aligned} \tag{4.10}$$

The SM gauge boson masses are given by

$$m_W^2 = \frac{g_0^2}{4}\langle h\rangle^2 \ , \qquad m_Z^2 = \frac{(g_0^2 + g_0'^2)}{4}\langle h\rangle^2 \ . \tag{4.11}$$

This fixes the EW scale $v = \langle h\rangle \equiv f\sqrt{\xi} \simeq 246$ GeV. Given that in the vacuum $\langle \eta\rangle = 0$, it is immediate to see that the canonically normalized fields, in this parametrization, are

$$h \to v + \sqrt{1-\xi}\, h_{phys} \ , \qquad \eta \to \eta_{phys} \ . \tag{4.12}$$

The parity $\eta \to -\eta$, which keeps this scalar stable, corresponds to the operator

$$P_\eta = \mathrm{diag}(1,1,1,1,-1,1) \in \mathrm{O}(6) \ , \tag{4.13}$$

and is an accidental symmetry of the leading order chiral Lagrangian, eq. (4.10). Higher derivative terms (such as the Wess-Zumino-Witten term) in general break this symmetry. As we want this scalar to be a viable DM candidate, we assume that this is a symmetry of the whole strong sector, that is we take the symmetry breaking pattern to be $\mathrm{O}(6) \to \mathrm{O}(5)$ [166].

Another symmetry of eq. (4.10), very relevant for the η phenomenology, is a $\mathrm{SO}(2)_\eta \simeq \mathrm{U}(1)_\eta$ generated by $T^{\hat{5}}$ which rotates the fifth and sixth components of Σ and under which η shifts. If the fermion mixings also respect this symmetry then η remains an exact NGB, thus its mass and couplings from the potential vanish.

4.1.2   Composite resonances Lagrangian

The Lagrangian of the spin-1 and spin-1/2 resonances which mix with the SM gauge bosons and fermions is completely analogous to the one for the MCHM described in section 3.4. Let us briefly review it adapting it to the $\mathrm{SO}(6)/\mathrm{SO}(5)$ coset.

---

[3] Our convention for the field strength is $W_{\mu\nu} = \partial_\mu W_\nu - \partial_\nu W_\mu - ig_0[W_\mu, W_\nu]$ and $B_{\mu\nu} = \partial_\mu B_\nu - \partial_\nu B_\mu$, where $W_\mu \equiv W_\mu^{a_L} T^{a_L}$.

Vector Lagrangian

Let us consider spin-1 fields in the adjoint, $\rho_\mu = \rho_\mu^a T^a \in \mathbf{10}$, and in the fundamental, $a_\mu = a_\mu^{\hat{a}} T^{\hat{a}} \in \mathbf{5}$ of SO(5). For simplicity we limit ourself to one copy only of each resonance. At leading order in the number of derivatives, the Lagrangian for these fields, assumed to be lighter than the cutoff, is

$$\mathcal{L}^{spin-1} = -\frac{1}{4}\mathrm{Tr}\left[\rho_{\mu\nu}^2\right] + \frac{f_\rho^2}{2}\mathrm{Tr}\left[(g_\rho\rho_\mu - E_\mu)^2\right] - \frac{1}{4}\mathrm{Tr}\left[a_{\mu\nu}^2\right] + \frac{f_a^2}{2\Delta^2}\mathrm{Tr}\left[(g_a a_\mu - \Delta d_\mu)^2\right] \ . \quad (4.14)$$

Let us also define the masses $m_\rho = f_\rho g_\rho$, $m_a = f_a \frac{g_a}{\Delta}$. As we see, this Lagrangian is formally identical to the one in eq (3.33), but it should be kept in mind that the field content is different.

Fermion Lagrangian

In order to give mass to the SM fermions we adopt the partial compositeness scenario. The choice of the representation of SO(6) in which to embed the SM fields is a source of model dependence, in particular the characteristics of the scalar one-loop potential and the preservation of P_η and of $U(1)_\eta$ depend on the choice of the embedding of the third generation of quarks. It has been shown in ref. [166] that, since $[P_\eta, T^{\hat{5}}] \neq 0$, the only way in which both symmetries can be respected by the mixing terms is if the SM fermions are embedded in representations of SO(6) with vanishing $U(1)_\eta$ charge.

In the following we focus on the embedding of the SM doublets q_L, ℓ_L in the bi-doublet inside the $\mathbf{6}$, with $P_\eta = +1$ and which preserves $U(1)_\eta$, and the right-handed fermions u_R, d_R, e_R in the parity even singlet inside the $\mathbf{6}$, that is its sixth component with non-zero $U(1)_\eta$ charge. The charge under $U(1)_X$ is fixed by requiring the correct hypercharge. The embedding of the SM doublets has to be different for the mixing terms responsible for the up-type or down-type quark masses:

$$\xi_L^u = \frac{1}{\sqrt{2}}\begin{pmatrix} b_L \\ -ib_L \\ t_L \\ it_L \\ 0 \\ 0 \end{pmatrix}_{2/3} , \quad \xi_R^u = \begin{pmatrix} 0 \\ 0 \\ 0 \\ 0 \\ 0 \\ t_R \end{pmatrix}_{2/3} , \quad \xi_L^d = \frac{1}{\sqrt{2}}\begin{pmatrix} t_L \\ it_L \\ -b_L \\ ib_L \\ 0 \\ 0 \end{pmatrix}_{-1/3} , \quad \xi_R^d = \begin{pmatrix} 0 \\ 0 \\ 0 \\ 0 \\ 0 \\ b_R \end{pmatrix}_{-1/3} , \quad (4.15)$$

where the subscript indicate the X charge.[4] We embed the SM lepton doublets and singlets in the same way as ξ_L^d and ξ_R^d but with $U(1)_X$ charges $X_{\ell_L} = X_{e_R} = -1$.

---

[4]In section 4.4.2 the couplings between DM and the first two generations of quarks will be extremely important for our phenomenological analysis in the context of DM direct detection. In order to be as general as possible, therefore, we will consider also different embedding w.r.t. eq. (4.15).

Let us briefly comment on the case in which the right handed top quark is embedded in a **15** of SO(6), in order to preserve the U(1)$_\eta$ symmetry. In this case the breaking of this symmetry, and therefore the contribution to the η potential, comes only from the bottom quark, assuming its right chirality is embedded in the **6**. Since the bottom mixings to the composite sector are much smaller than those of the top, we expect that in this case the singlet is much lighter, $m_\eta \lesssim \mathcal{O}(10)$ GeV. From the expression of the DM mass in eq. (4.6), assuming $\mu_\eta^2 > 0$, this implies that also the coupling λ is generically small: $\lambda \lesssim 10^{-3}$. In this case the bound from the Higgs invisible width is able to exclude such a framework for any value of $\xi \gtrsim 0.05$. For this reason, we will not further consider this possibility in the rest of this paper.

Let us now focus on the fermion partners responsible to give mass to the top quark, since the mixing terms with these fermions provide the leading contributions to the effective potential. We assume that the right-handed top is an elementary state, as all the other SM fermions. We introduce N_F vector-like composite fermions in the fundamental, $F \in \mathbf{5}$ with $X = \frac{2}{3}$ (each contains two doublets $F_{1/6} \in (\mathbf{2}, \frac{1}{6})$, $F_{7/6} \in (\mathbf{2}, \frac{7}{6})$ and one singlet $F_5 \in (\mathbf{1}, \frac{2}{3})$ under SU(2)$_L \times$ U(1)$_Y$), and N_S vector-like singlets, $S \in \mathbf{1}$, of SO(5), with $X = Y = \frac{2}{3}$. We embed the SM fermions in the **6** of SO(6). The leading Lagrangian for the top sector, relevant for the computation of the one-loop effective potential, is given by

$$
\begin{aligned}
\mathcal{L}_f = & \ \bar{q}_L i \slashed{D} q_L + \bar{t}_R i \slashed{D} t_R + \sum_{i=1}^{N_S} \bar{S}_i (i \slashed{\nabla} - m_{iS}) S_i + \sum_{j=1}^{N_F} \bar{F}_j (i \slashed{\nabla} - m_{jF}) F_j \\
& + \sum_{i=1}^{N_S} \left(\epsilon_{tS}^i \bar{\xi}_R P_L U S_i + \epsilon_{qS}^i \bar{\xi}_L P_R U S_i \right) + \sum_{j=1}^{N_F} \left(\epsilon_{tF}^j \bar{\xi}_R P_L U F_j + \epsilon_{qF}^j \bar{\xi}_L P_R U F_j \right) + h.c. \ ,
\end{aligned}
\tag{4.16}
$$

where $P_{L,R} = \frac{1 \mp \gamma^5}{2}$ are chirality projectors and

$$
\nabla_\mu = \partial_\mu - i E_\mu - i q_X g_0' B_\mu \ .
\tag{4.17}
$$

In general at the same order in the expansion in derivatives it is possible to write other invariants which do not involve the elementary fields, analogous to those of eq. (3.43). Even if they can be phenomenologically important, since they do not contribute to the pNGB potential at one-loop we neglect them in the following.

4.2   Analysis of the potential and parameter scans

In this section we present the main results of this approach, focusing the discussion on the analysis of the one-loop effective potential for the h and η scalars. All the details of the computation, including the explicit formulae for the form factors, are the same as in the minimal case presented in section 3.6, therefore we will be very brief here presenting only the most relevant

results. Analytical approximations and full numerical results are explicitly computed using two benchmark values for the parameter $\xi = v^2/f^2$, namely $\xi = 0.1$, corresponding to $f \simeq 800$ GeV, and $\xi = 0.05$, corresponding to $f \simeq 1.1$ TeV.

4.2.1   Vector contribution

The gauge sector, described by the Lagrangian of eq. (4.14), contributes to the potential only via the h^2 dependence, therefore only to the μ_h^2 and λ_h coefficients of eq. (4.4). In general, this contribution is quadratically divergent. We require the cancellation of this quadratic divergence by imposing the sum rule

$$(\text{WSR 1})_{gauge} \quad : \qquad \frac{f^2}{2} + f_a^2 - f_\rho^2 = 0 \; , \tag{4.18}$$

while the logarithmic divergence is removed requiring

$$(\text{WSR 2})_{gauge} \quad : \qquad f_a^2 m_a^2 = f_\rho^2 m_\rho^2 \; . \tag{4.19}$$

We use these two sum rules to express f_a and m_a in terms of the other parameters; note that this fixes all the parameters of the a_μ fields relevant for the effective potential, since only the combination g_a^2/Δ enters in the potential. The sum rule of eq. (4.18) requires a bound $f_\rho > f/\sqrt{2}$, that is compatible with the *partial UV completion* (PUVC) criterion introduced in ref. [105] which predicts $f_\rho \sim f$.

In order to obtain a simple analytic expression for the gauge contribution to the potential let us take $g' = 0$, $f_\rho = f$ and expand for $g^2 \ll 1$. We obtain

$$(\mu_h^2)^g \simeq \frac{9g^2 f^2 m_\rho^2}{32\pi^2} \log 2 \; , \qquad (\lambda_h)^g \simeq -\frac{9g^4 f^4}{256\pi^2} \left(\log \frac{32 m_\rho^2}{m_W^2} - 5 \right) \; . \tag{4.20}$$

4.2.2   Fermion contribution

In general, the fermion sector contributes to all the coefficients of the potential in eq. (4.4). To cure the quadratic divergence we impose the sum rules

$$(\text{WSR 1})_{ferm} \quad : \quad \begin{cases} \sum\limits_{j=1}^{N_F} |\epsilon_{qF}^j|^2 = \sum\limits_{i=1}^{N_S} |\epsilon_{qS}^i|^2 \; , \\[2ex] \sum\limits_{j=1}^{N_F} |\epsilon_{tF}^j|^2 = \sum\limits_{i=1}^{N_S} |\epsilon_{tS}^i|^2 \; . \end{cases} \tag{4.21}$$

In order to cancel the residual logarithmic divergence we further require

$$
(\text{WSR 2})_{ferm} \; : \;
\begin{cases}
\displaystyle\sum_{j=1}^{N_F} m_{jF}^2 |\epsilon_{qF}^j|^2 = \sum_{i=1}^{N_S} m_{iS}^2 |\epsilon_{qS}^i|^2 \; , \\[3mm]
\displaystyle\sum_{j=1}^{N_F} m_{jF}^2 |\epsilon_{tF}^j|^2 = \sum_{i=1}^{N_S} m_{iS}^2 |\epsilon_{tS}^i|^2 \; .
\end{cases}
\tag{4.22}
$$

The rest of the section is devoted to analyze in more detail two specific models. First we consider the minimal scenario which allows to enforce both sum rules and to reproduce the top mass, that is with only one fundamental F and one singlet S. Then we study the next-to-minimal scenario, in which we add a second singlet, since it allows more freedom in exploring the parameter space of these composite Higgs models.

Minimal case: $N_F = N_S = 1$

In this minimal model it is straightforward to obtain the mass spectrum of the top partners before EWSB from the Lagrangian of eq. (3.39). The SM top is massless at this level, the singlet S gets a mass $M_S^2 = m_S^2 + |\epsilon_{tS}|^2$, the doublet $F_{1/6}$ has a mass $M_{1/6}^2 = m_F^2 + |\epsilon_{qF}|^2$ while the other doublet, $F_{7/6}$, and the other singlet, F_5, are degenerate with a mass $M_{7/6} = M_{F_5} = m_F$. After EWSB the fermions with same electric charge mix and these masses shift by an amount of the order $\mathcal{O}(v\epsilon/m)$. From eq. (3.93) we obtain the top mass, at leading order for small ξ, [1]

$$
M_{top} \simeq \frac{|\epsilon_{qF}\epsilon_{tS}|}{\sqrt{2}M_{1/6}M_S} \left| m_S \frac{\epsilon_{tF}}{\epsilon_{tS}} + m_F \frac{\epsilon_{qS}}{\epsilon_{qF}} \right| \sqrt{\xi} \; .
\tag{4.23}
$$

In this minimal setup, the first sum rule is solved by imposing

$$
|\epsilon_{qF}|^2 = |\epsilon_{qS}|^2 \equiv \epsilon_Q^2 \qquad \text{and} \qquad |\epsilon_{tF}|^2 = |\epsilon_{tS}|^2 \equiv \epsilon_T^2 \; .
\tag{4.24}
$$

The second sum rule further fixes

$$
m_F = m_S = m \; ,
\tag{4.25}
$$

where we used the field basis where the masses are real and positive. Assuming for simplicity that the mixing parameters are real, the only solution (up to field redefinition) for which the potential does not vanish is

$$
\epsilon_{qF} = \epsilon_{qS} = \epsilon_Q \; , \qquad \epsilon_{tF} = \epsilon_{tS} = \epsilon_T \; .
\tag{4.26}
$$

In this case, it turns out that

$$
\frac{(\mu_\eta^2)^f}{f^2} = \lambda_\eta^f = 0 \; , \qquad \lambda^f = \lambda = -\frac{(\mu_h^2)^f}{f^2} \; .
\tag{4.27}
$$

Since μ_η^2 does not receive any contribution neither from the gauge sector nor from the fermion sector, it vanishes and therefore the singlet will be light (its mass is ξ-suppressed, as the Higgs mass, eq. (4.6)).

In this simple model it is straightforward to obtain exact analytic formulae for these coefficients, however in order to get an understanding of the behavior of this model it is useful to make some approximations. For example assuming big mixings, that is $m^2 \ll M_{1/6}^2, M_S^2$, we get $M_{top}^2 \simeq 2m^2\xi$ and

$$\lambda = \lambda^f = -\frac{(\mu_h^2)^f}{f^2} \simeq \frac{1}{2}\lambda_h^f \simeq \frac{N_c M_{top}^2}{4\pi^2 v^2} \frac{M_{1/6}^2 M_S^2}{f^2(M_{1/6}^2 - M_S^2)} \log \frac{M_{1/6}^2}{M_S^2} \; , \tag{4.28}$$

which is evidently always positive. The top mass fixes $m = M_{7/6} \sim 350$ GeV which, as we showed in section 3.5.2, is experimentally excluded, therefore this region is strongly disfavored. In the opposite limit, that is $\epsilon_Q^2, \epsilon_T^2 \ll m^2$, we obtain $M_{top}^2 \simeq 2\xi\epsilon_Q^2\epsilon_T^2/m^2$ and

$$\lambda = \lambda^f = -\frac{(\mu_h^2)^f}{f^2} \simeq \frac{1}{2}\lambda_h^f \simeq \frac{N_c M_{top}^2}{4\pi^2 v^2} \frac{m^2}{f^2} \; . \tag{4.29}$$

In this case, the scale of the top partner masses m has to be smaller than $\sim 1.5f \simeq 1.2$ (1.6) TeV for $\xi = 0.1$ (0.05), in order to reproduce the correct Higgs mass. We have checked numerically that, indeed, the relation $\lambda^f \simeq \frac{1}{2}\lambda_h^f$ holds, up to $\mathcal{O}(20\%)$ corrections, in all the parameter space. This fact, using eq. (4.6) and the fact that the gauge contribution to λ_h is always negligible, allows us to conclude that in this model, for a given ξ, the Higgs mass fixes both the DM mass and portal coupling

$$m_\eta \simeq \frac{1}{2}m_H \simeq 63 \text{ GeV} \; , \quad \text{and} \quad \lambda = \frac{m_\eta^2}{v^2} \simeq \frac{1}{4}\frac{m_H^2}{v^2} \simeq 0.065 \; . \tag{4.30}$$

Let us finally discuss how ξ can be tuned to realistic values, in particular our benchmark values $\xi = 0.1, 0.05$. From the relation $-\frac{(\mu_h^2)^f}{f^2} \simeq \frac{1}{2}\lambda_h^f$ and eq. (4.6) we get

$$\xi \simeq \frac{1}{2} - \frac{(\mu_h^2)^g}{m_H^2}2\xi \; , \tag{4.31}$$

where we neglected the gauge contribution to λ_h since it is always negligible with respect to the fermionic one. The gauge contribution to μ_h^2 is therefore necessary in order to reduce ξ. Eq. (4.20) allows to fix the composite vector mass as a function of the Higgs mass (for a given value of f_ρ/f, which has been set to 1 in this example)

$$m_\rho \sim \sqrt{\frac{2}{\log 2}} \frac{\pi}{3} \frac{m_H}{m_W} \frac{v}{\sqrt{\xi}} \simeq 2 \text{ TeV} \qquad \text{(for } \xi = 0.1) \; . \tag{4.32}$$

From eq. (4.31) we see that, in absence of the gauge contribution, the natural value of ξ would be ~ 0.5. Therefore, we can estimate the amount of tuning needed to get a smaller value with the simple relation
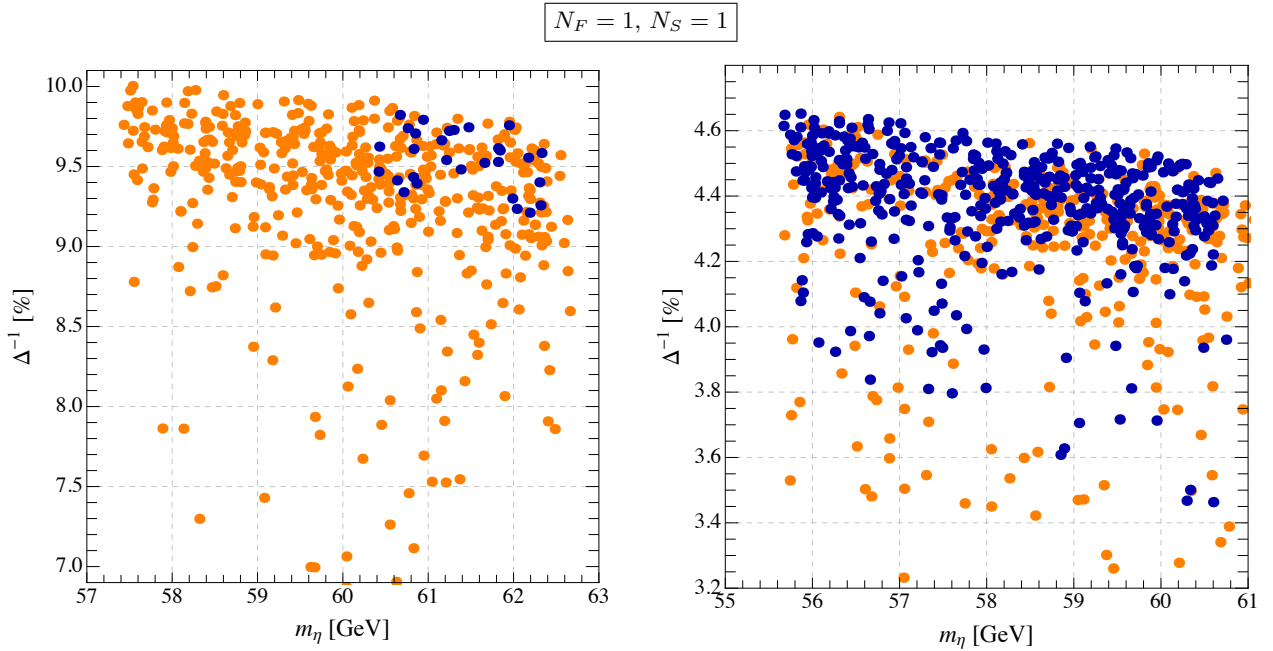
$$\Delta \sim \frac{1}{2\xi} \; , \tag{4.33}$$

Figure 4.1: Here we show the distribution of the fine-tuning Δ, computed summing in quadrature the logarithmic derivatives of ξ with respect to all the free parameters of the model after imposing the Weinberg sum rules, versus m_η. The left plot is for $\xi = 0.1$ while the right one is for $\xi = 0.05$. All the points here reproduce the correct top and Higgs masses. The blue points pass the direct searches bounds described in section 4.3.2, the orange ones do not.

that is, a $\sim 20\%$ tuning for $\xi = 0.1$. Such a low amount of tuning in this model is due to the fact that the extreme simplicity of the model after imposing the Weinberg sum rules fixes $-\frac{(\mu_h^2)^f}{f^2}$ to be of the same order (actually, a factor of 2 smaller) of λ_h, see eqs. (4.28, 4.29). This and the relations in eq. (4.27) are non-generic features of these kind of models: in general the mass term in the potential is expected to be generated at quadratic order in the mixings while the self-coupling term only at quartic order, so that $\left|\frac{(\mu_h^2)^f}{f^2 \lambda_h^f}\right|$ would be naturally much bigger than 1 and therefore the needed amount of tuning much larger. For this reason, in order to assess with more generality the viability of these DM model, in the next section we study also a non-minimal model, in which this more generic feature is indeed present.

To verify the conclusions obtained by our analytic study, we performed a numerical parameter scan of the model, extracting randomly the parameters $f_\rho \in [\frac{1}{\sqrt{2}} f, 2f]$, $\epsilon_T \in [0.2f, 6f]$, $m \in [0, 6f]$ and obtaining ϵ_Q by requiring the correct top mass at the TeV scale $M_{top}(1\ \text{TeV}) \simeq 155$ GeV. The vector mass m_ρ finally has been fixed by requiring the desired value of ξ (we took as benchmark points $\xi = 0.1$ and $\xi = 0.05$). After computing the full potential with the chosen parameters, we selected only the points with a Higgs mass between 120 GeV and 130 GeV.[5] As can be seen from

---

[5]This loose interval has been chosen in order to obtain a sufficient number of points from the scan and because

fig. 4.1, our scan confirms the analytical estimations presented above, in particular the relation in eq. (4.30), within a few percent deviation. For each point of the scan we computed the fine tuning in ξ adding in quadrature the logarithmic derivatives of ξ with respect to all the free parameters of the model after fixing the Weinberg sum rules (that is $c_i \in \{f_\rho/f, m_\rho, m, \epsilon_T, \epsilon_Q\}$),

$$\Delta = \sqrt{\sum_i \left(\frac{\partial \log \xi}{\partial \log c_i}\right)^2} \, , \tag{4.34}$$

and found that $\Delta^{-1} \simeq 10\%$ for $\xi = 0.1$ and $\Delta^{-1} \simeq 5\%$ for $\xi = 0.05$, confirming the estimate of eq. (4.33).

Next-to-minimal case: $N_F = 1$, $N_S = 2$

Let us now move to discuss the next-to-minimal scenario with one fundamental and two fermionic singlets. Also in this model, the mass spectrum before EWSB can be easily obtained from eq. (3.39). The mass of the fields in the fundamental is the same as in the previous model, while the two singlets now have a mass

$$M_{S_{1,2}}^2 = \frac{1}{2}\left\{\widetilde{m}^2 \mp \sqrt{\widetilde{m}^2 - 4\left[m_{1S}^2 m_{2S}^2 + (\epsilon_{tS}^1)^2 m_{2S}^2 + (\epsilon_{tS}^2)^2 m_{1S}^2\right]}\right\} \, , \tag{4.35}$$

where we defined $\widetilde{m}^2 \equiv m_{1S}^2 + m_{2S}^2 + (\epsilon_{tS}^1)^2 + (\epsilon_{tS}^2)^2$. In the limit where m_{2S} is much bigger than the other masses, these two expressions reduce to $M_{S_{X=1,2}}^2 \simeq m_{XS}^2 + (\epsilon_{tS}^X)^2$. From eq. (3.93) we get the top mass, at leading order in $\xi \ll 1$

$$M_{top} \simeq \frac{\sqrt{\xi}\epsilon_{qF}^1 \epsilon_{tS}^1 \epsilon_{tS}^2 \left|\frac{m_{1S}m_{2S}\epsilon_{tF}^1}{\epsilon_{tS}^1 \epsilon_{tS}^2} + \frac{m_F}{\epsilon_{qF}}\left(\frac{m_{1S}\epsilon_{qS}^2}{\epsilon_{tS}^1} + \frac{m_{2S}\epsilon_{qS}^1}{\epsilon_{tS}^2}\right)\right|}{\sqrt{2}M_{F_{1/6}}\sqrt{(M_{S_2}^2 + M_{S_2}^2)^2 - (M_{S_2}^2 - M_{S_2}^2)^2}} \, . \tag{4.36}$$

In this case the most general solution to the first sum rule is (assuming real mixings)

$$(\text{WSR 1})_{ferm} : \begin{cases} \epsilon_{qF} = \epsilon_Q \, , & \epsilon_{qS}^1 = \epsilon_Q \cos\theta \, , & \epsilon_{qS}^2 = \epsilon_Q \sin\theta \, , \\ \epsilon_{tF} = \epsilon_T \, , & \epsilon_{tS}^1 = \epsilon_T \cos\phi \, , & \epsilon_{tS}^2 = \epsilon_T \sin\phi \, . \end{cases} \tag{4.37}$$

After imposing this, the second sum rule becomes

$$(\text{WSR 2})_{ferm} : \begin{cases} m_F^2 = m_{1S}^2 \cos^2\theta + m_{2S}^2 \sin^2\theta \, , \\ m_F^2 = m_{1S}^2 \cos^2\phi + m_{2S}^2 \sin^2\phi \, . \end{cases} \tag{4.38}$$

Solving these two conditions in terms of m_{2S} and ϕ, up to arbitrary signs, we get

$$(\text{WSR 2})_{ferm} : \begin{cases} m_{2S} = \frac{1}{\sin\theta}\sqrt{m_F^2 - m_{1S}^2 \cos^2\theta} \, , \\ \sin\phi = \sin\theta \, . \end{cases} \tag{4.39}$$

---

a $\mathcal{O}(5)$ GeV deviation in m_H does not have a significant relevance in our models. Moreover, we expect some small correction to m_H^2 to arise from the bottom quark mixing, which we didn't include in the scan.

Without loss of generality we take $m_{2S} > m_{1S}$. This and eq. (4.39) imply that the relation $m_F^2 > m_{1S}^2$ has to be satisfied.

In this model, from our numerical parameter scans, we find two characteristic regions depending on the values of m_F and $\sin\theta$. In the limit of small m_F, that is of big mixing terms, the DM quadratic term μ_η^2 goes to zero, so the DM mass is expected to be of the order of the Higgs mass, and, like in the minimal model, the other coefficients are related by $\mathcal{O}(1)$ factors:

$$\lambda = \lambda^f = -\frac{(\mu_h^2)^f}{f^2} \simeq \frac{1}{2}\lambda_h^f \simeq \frac{N_c m_F^2}{8\pi^2 f^4}(9 + 7|\sin\theta|)\frac{\epsilon_Q^2 \epsilon_T^2}{\epsilon_Q^2 - \epsilon_T^2}\log\frac{\epsilon_Q^2}{\epsilon_T^2} \, , \tag{4.40}$$

where we fixed $m_{1S} = m_F/2$ in order to respect the bound from the second sum rule and to simplify the expression. In this region this model behaves like the minimal model discussed in the previous section, in particular we expect the DM mass to be $m_\eta \sim 63$ GeV and the coupling $\lambda \sim 6 \times 10^{-2}$, eq. (4.30). A similar result is obtained by expanding for small mixings ϵ_Q and ϵ_T (in order to obtain simple analytic expressions) and going in the $\sin\theta \to 1$ limit, due to a term proportional to $\log\sin^2\theta$ in the leading term in μ_h^2 and μ_η^2, as in eq. (4.41). In this case we exactly reproduce the relations of eq. (4.29), and therefore the same conclusions apply.

A different region is reached (always in an expansion for small mixings) in the limit of big $m_F \gg f$ and small $\sin\theta \ll 1$, that is with a hierarchy $m_{2S} \gg m_F \gg m_{1S} \sim f$. In this case we obtain

$$\begin{aligned}
(\mu_h^2)^f &\simeq -\frac{N_c}{8\pi^2}\frac{m_F^2(\epsilon_Q^2 - 2\epsilon_T^2)}{f^2}\log\frac{1}{\sin^2\theta} \, , \\
\mu_\eta^2 &\simeq \frac{N_c}{4\pi^2}\frac{m_F^2\epsilon_T^2}{f^2}\log\frac{1}{\sin^2\theta} \, , \\
\lambda_h^f &\simeq \frac{N_c}{16\pi^2 f^4}\left[-2(\epsilon_Q^2 - 2\epsilon_T^2)^2 + (\epsilon_Q^4 + 4\epsilon_T^4)\log\frac{m_F^2}{m_S^2}\right] \, , \\
\lambda &\simeq \frac{N_c}{4\pi^2}\frac{\epsilon_T^2}{f^4}\left(\epsilon_Q^2 - 2\epsilon_T^2 + \epsilon_T^2\log\frac{m_F^2}{m_S^2}\right) \, .
\end{aligned} \tag{4.41}$$

In this case the DM mass can be arbitrarily high (for big m_F and small $\sin\theta$), while in order to obtain the correct EW scale, that is to suppress $(\mu_h^2)^f$, it is necessary to tune $\epsilon_Q^2 \sim 2\epsilon_T^2$. If this tuning is avoided here, then the gauge contribution to μ_h^2 has to provide the necessary cancellation, which will imply higher values of the vector mass m_ρ than the case in eq. (4.32). In both cases, we expect the tuning in this region to be higher than in the cases examined previously, for which the expected tuning is as in eq. (4.33). Taking $\epsilon_Q^2 \sim 2\epsilon_T^2$, from the expression for λ_h in eq. (4.41) we can fix ϵ_T by requiring the correct Higgs mass and then substitute this in the formula for λ. We obtain

$$\lambda \simeq \frac{m_H^2}{4v^2} \simeq 0.065 \, , \tag{4.42}$$
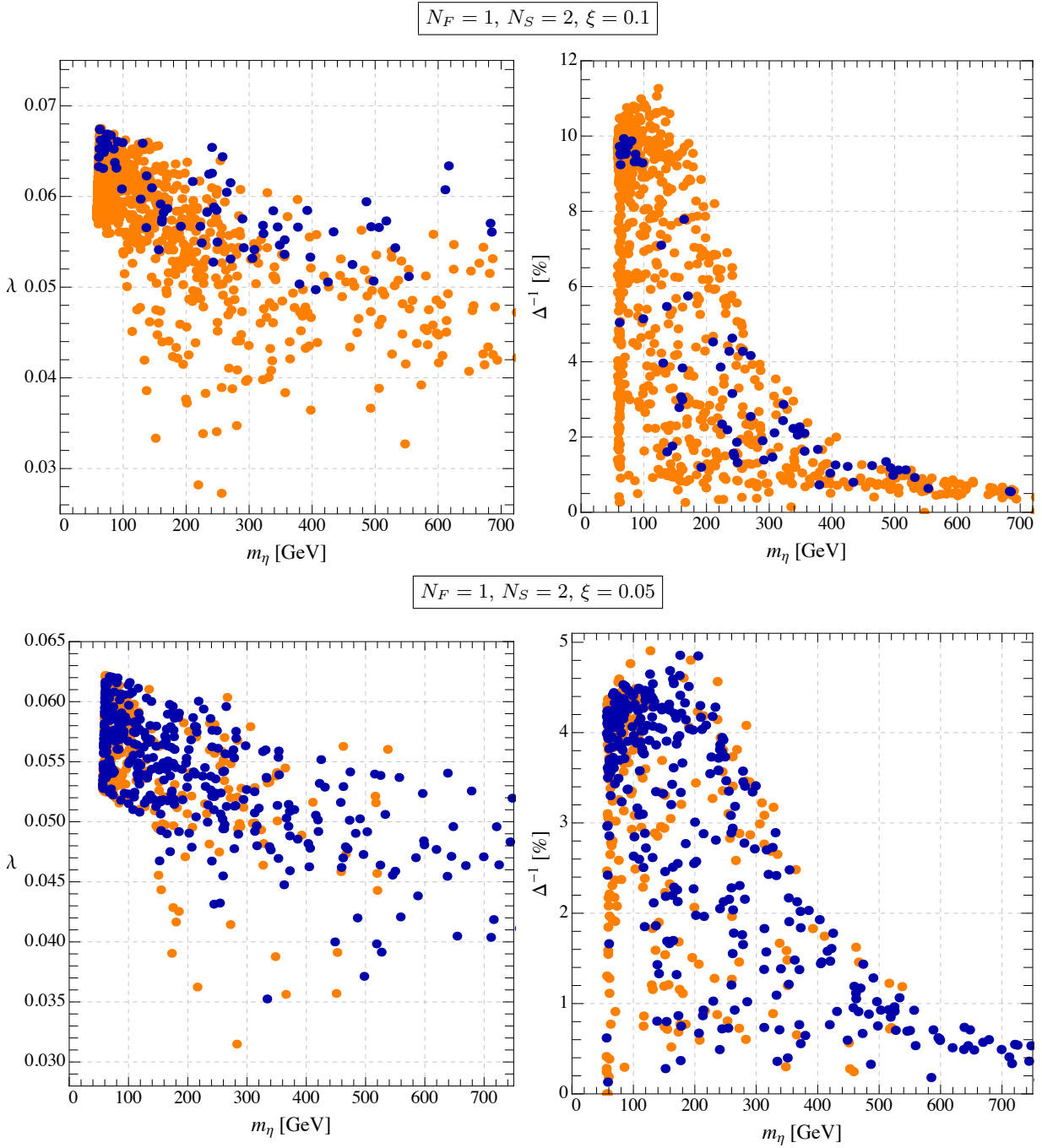
which is the same value we obtained in the minimal model.

Figure 4.2: In the left column we show the distribution of the points obtained from the scan of the next-to-minimal model in the (m_η, λ) plane, while in the right column we show the distribution of the fine-tuning Δ, computed summing in quadrature the logarithmic derivatives of ξ with respect to all the parameters of the model, versus m_η. The upper row is for $\xi = 0.1$ while the lower one for $\xi = 0.05$. All the points here reproduce the correct top and Higgs masses. The blue points pass the direct searches bounds described in section 4.3.2, the orange ones do not.

Also in this case we performed a numerical parameter scan of the model, extracting randomly $f_\rho \in [\frac{1}{\sqrt{2}}f, 2f]$, $\epsilon_T \in [0.2f, 6f]$, $m_S \in [0, 8f]$, $m_F \in [m_S, 8f]$, $\theta \in [0, \frac{\pi}{2}]$ and obtaining ϵ_Q by

requiring the correct top mass at the TeV scale $M_{top}(1 \text{ TeV}) \simeq 155$ GeV. As in the minimal model, the vector mass m_ρ has been fixed by requiring $\xi = 0.1$ (or 0.05) and we selected only the points with a Higgs mass between 120 GeV and 130 GeV. From these scans we observe that, even when relaxing the tuning condition $\epsilon_Q^2 \sim 2\epsilon_T^2$, the value of the coupling λ remains always of the same order of magnitude, that is in the range $3 \times 10^{-2} \lesssim \lambda \lesssim 7 \times 10^{-2}$, while the DM mass can vary from $m_\eta \sim m_H/2$ up to $m_\eta \sim \mathcal{O}(700)$ GeV, see figure 4.2.

Computing the fine-tuning as presented in the minimal model, we find that for $m_\eta \lesssim 200$ GeV most of the points present $\Delta^{-1} \sim \xi$ with a tail of points with $\Delta^{-1} \lesssim 0.5\%$, as can be seen in the right panels of figure 4.2. Increasing m_η the fine-tuning increases: for $m_\eta \simeq 600$ GeV we have $0.5\% \lesssim \Delta^{-1} \lesssim 1\%$.

Relaxing the second Weinberg sum rules

In order to assess the generality of our prediction for $\lambda \sim 6 \times 10^{-2}$, which we obtain both in the minimal and in the next-to-minimal models presented above, we also consider a generalization of the next-to-minimal model in which we impose only eq. (4.37), relaxing the second Weinberg sum rules of eq. (4.39), which renders the effective potential incalculable. In particular, relaxing the second sum rules leaves a logarithmic divergence (i.e. a scale dependence) in μ_h^2 and μ_η^2. On the other hand, the quartic couplings λ, λ_h and λ_η are still scale-independent and therefore calculable. As a consequence, both ξ and m_η^2 can not be explicitly computed in this case but need to be fixed as boundary conditions.

Since we are mostly interested in the range of λ given the measured Higgs mass, we performed a parameter scan of this model fixing $\xi = 0.1$ and extracting randomly $\epsilon_T \in [0.2f, 6f]$, $m_{1S}, m_F \in [0, 8f]$, $m_{2S} \in [m_{1S}, 8f]$, $\theta \in [0, \frac{\pi}{2}]$, $\phi \in [0, \frac{\pi}{2}]$ and obtaining ϵ_Q by requiring the correct M_{top}.[6] For each point we computed λ and m_H and selected only the points with m_H between 120 GeV and 130 GeV. As shown in the left panel of figure 4.3, we obtain that λ ranges from $\sim 3 \times 10^{-2}$ and $\sim 8 \times 10^{-2}$, with the distribution of the points peaked near $\lambda \sim 6 \times 10^{-2}$, thus confirming the range obtained in the cases where both Weinberg sum rules were being imposed. The DM mass m_η, not being calculable, is in this case a free parameter.

4.3 Phenomenological analysis – part I: LHC

In this section we analyze the constraints placed on the parameter space of our Composite DM model by the LHC. In section 4.3.1 we discuss the bound on the invisible Higgs decay width, while in section 4.3.2 we consider direct searches of composite resonances.

---

[6]We took into consideration only the fermion sector, since the gauge contribution to the Higgs mass is always negligible due to the g^4 factor as well as a numerical suppression, see eq. (4.20).
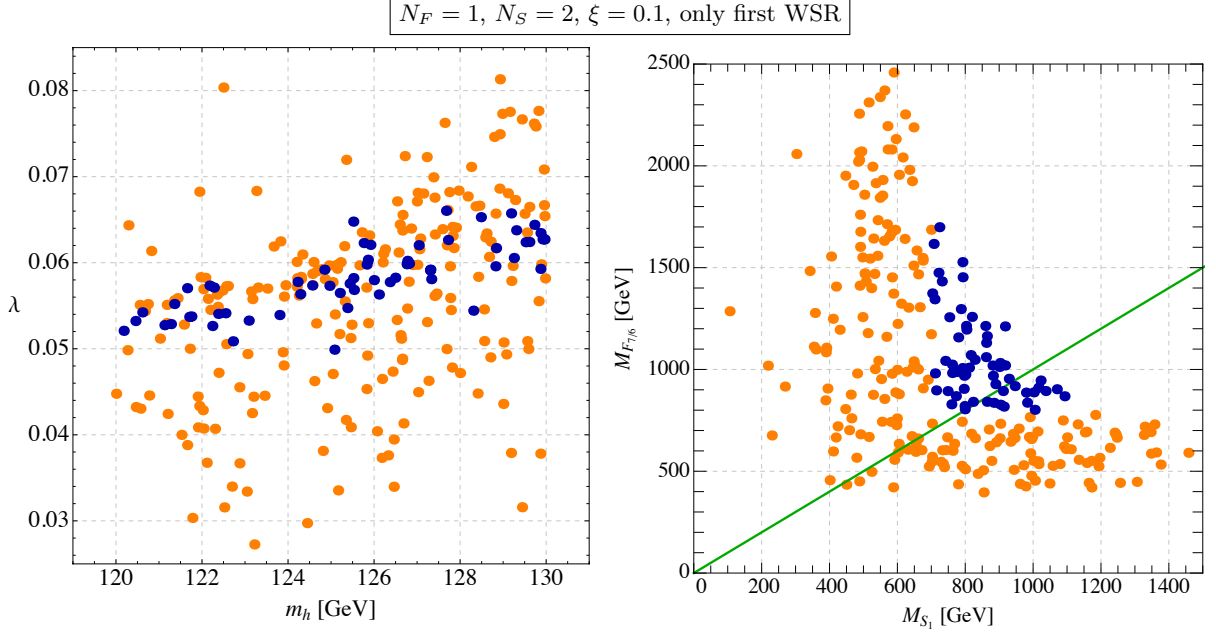
Figure 4.3: In the left plot we show the points obtained from the parameter scan in the model with $N_S = 2$, $N_F = 1$ relaxing the second Weinberg sum rules, in the (m_H, λ) plane. In the right one we show the lightest top partner masses, the green line is a reference line for $M_{F_{7/6}} = M_{S_1}$. The blue points pass the direct searches bounds described in section 4.3.2, the orange ones do not.

4.3.1 Invisible Higgs decay width

If $m_\eta < m_h/2$, the Higgs boson can decay invisibly into two DM particles. The invisible decay width corresponding to this process is given by [166]

$$\Gamma_{\text{inv}}(h \to \eta\eta) = \frac{v^2}{32\pi m_H} \left(\frac{m_H^2 \xi}{v^2 \sqrt{1-\xi}} - 2\lambda\sqrt{1-\xi} \right)^2 \sqrt{1 - \frac{4m_\eta^2}{m_H^2}} \, \theta(m_H - 2m_\eta) \ . \qquad (4.43)$$

This can be rephrased in terms of the following invisible branching ratio

$$\text{BR}_{\text{inv}} \equiv \frac{\Gamma_{\text{inv}}(h \to \eta\eta)}{\Gamma_{\text{SM}}^\xi + \Gamma_{\text{inv}}(h \to \eta\eta)} \ , \qquad (4.44)$$

where Γ_{SM}^ξ is the decay width of the Higgs boson into SM particles obtained including the deviations of the Higgs couplings in eqs. (3.49, 3.50). Writing explicitly BR_{inv} as a function of the DM mass and the Higgs portal coupling – using eqs. (4.43, 4.44) – it is possible to draw an exclusion curve in the plane (m_η, λ) using the constraint on BR_{inv} described in section 3.5.1 (figure 3.4). We will show this bound in section 4.5, together with all the other phenomenological constraints that we will derive in the following sections.

4.3.2   Direct searches of composite resonances

Let us now apply to this model the experimental constraints from direct searches at the LHC of spin-1 and spin-1/2 resonances presented in section 3.5.2.

The spectrum of spin-1 resonances in this next-to-minimal model is the following: the adjoint of $SO(5)$ (ρ_μ^a), with masses of the order m_ρ, contains a $(\mathbf{3}, \mathbf{1}) \oplus (\mathbf{1}, \mathbf{3}) \oplus (\mathbf{2}, \mathbf{2})$ of $SU(2)_L \otimes SU(2)_R$ while the fundamental of $SO(5)$ ($a_\mu^{\hat{a}}$), with mass m_a, contains $(\mathbf{2}, \mathbf{2}) \oplus (\mathbf{1}, \mathbf{1})$. We apply to m_ρ the approximate bound of eq. (3.51), albeit for a completely consistent bound a dedicated collider study would be necessary.

Also for the top partners of this model, in particular the doublet $F_{7/6}$ and the lightest singlet S_1, we apply the constraints of eq. (3.52). In this case, the difference between the minimal and the next-to-minimal composite Higgs model is the presence of another fermion as part of the fundamental of $\mathcal{H}$. In particular the field F, in the $\mathbf{5}$ of SO(5), includes – other than the bidoublet – also a singlet F_5 which is degenerate in mass with the $F_{7/6}$ doublet. This field is odd under the parity P_η, which implies that it does not mix with the top and that its only allowed two-body decay channel is $F_5 \to t\eta$, where η is stable and detected only as missing energy. Although the study of this decay can be a promising source of new bounds, in the work presented here we do not research further this direction. Aside from this point, as described in section 3.52 we expect that the constraints on the top partners would be dominated by the bound from searches of $F_{7/6}$ since it provides the strongest bound.

In figure 4.4 we present the results of the parameter scans we performed for the two models (the minimal in the upper row, the next-to-minimal in the lower one) showing the points which reproduce the correct top and Higgs masses, as well as the desired value of ξ, in the plane ($M_{S_1}, M_{F_{7/6}}$). The blue (orange) points are those which pass (do not pass) the bounds of eqs. (3.51, 3.52) while the green is a reference for the two regions specified before. We see that the models with lower tuning, $\xi = 0.1$, are already on the verge to be excluded by direct searches and also for $\xi = 0.05$ the bounds cut a sizable part of the parameter space of the models.

4.4   Phenomenological analysis – part II: astrophysics

In this section we analyze all the relevant bounds placed on the parameter space of our Composite DM model by the most constraining DM searches currently ongoing in high-energy astrophysics. In section 4.4.1 we discuss the DM relic abundance, while in section 4.4.2 we analyze the result of the LUX experiment in the context of direct detection of DM particles. In section 4.4.3 we study indirect detection experiments, focusing in particular on the measurement of the antiproton energy spectrum.
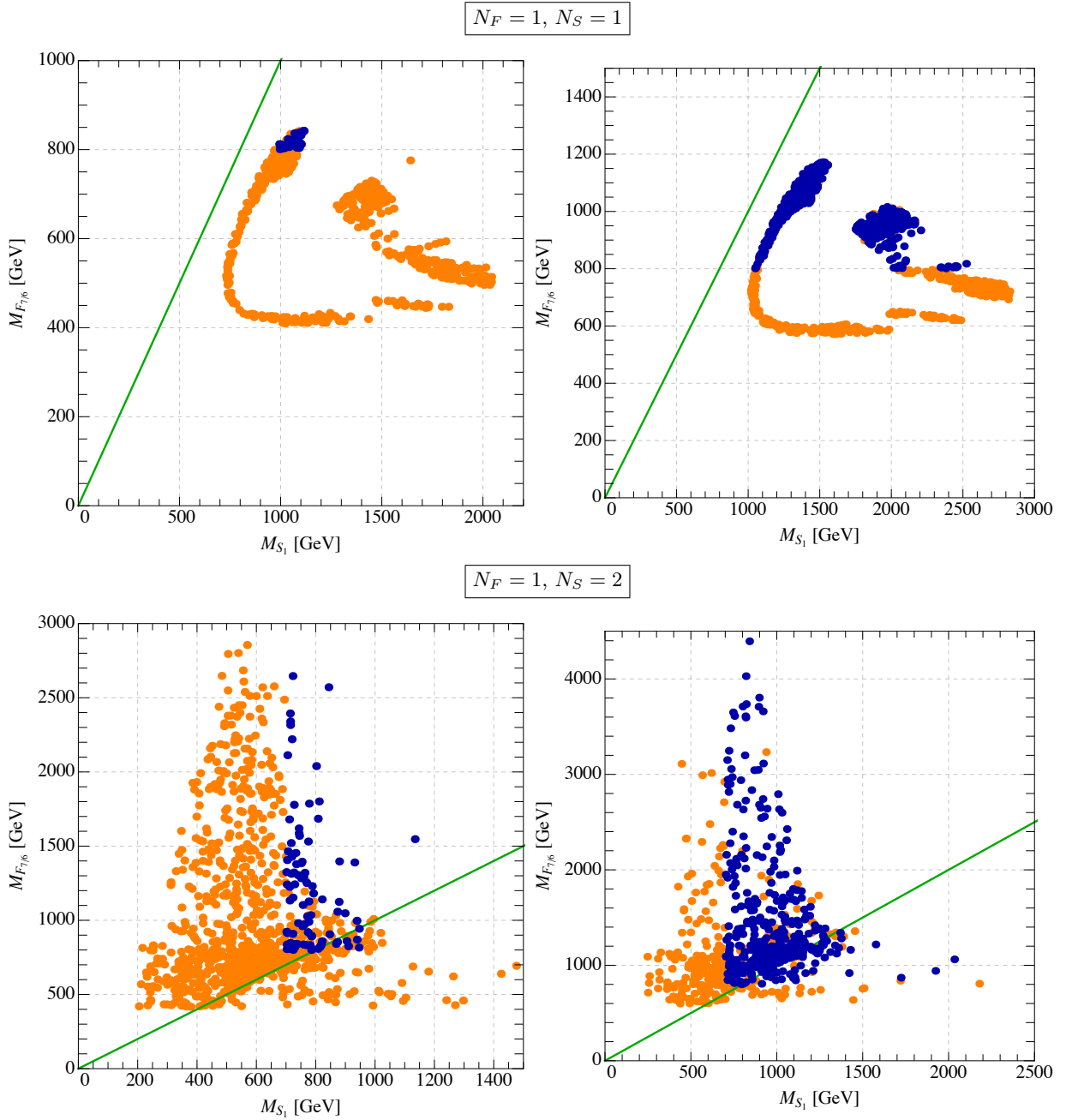
Figure 4.4:   In the upper (lower) row we show the lightest top partner masses (before EWSB) in the minimal (next-to-minimal) model with for $\xi = 0.1$ [0.05] in the left [right] plot. The points reproduce the correct top and Higgs masses, up to a ~ 5 GeV tolerance on m_H. The blue points pass the selection while the orange ones are excluded by direct searches of top partners and vector resonances, eqs. (3.51, 3.52). The green line is a reference for $M_{F_{7/6}} = M_{S_1}$.

4.4.1   Relic density

The DM scenario considered here is the standard one for Weakly Interacting Massive Particles (WIMP), in which the η DM candidate is a weakly-interacting cold thermal relic. According

to this paradigm, in the early Universe DM particles are kept in thermal equilibrium with the other species in the thermal bath because processes in which a pair of DM particles annihilate occur at the same rate as those in which they are created. As the Universe expands and cools, however, the thermal energy is no longer enough to produce the massive DM particles with a fast enough rate and also their number density dilutes due to the expansion of the Universe, making more and more rare the annihilation process. This brings the DM particles out of the thermal equilibrium and their number density "freezes-out", that is scales in the same way as the entropy density.

The evolution of the DM number density $n(x)$ during the expansion of the Universe, being $x \equiv m_\eta/T$ where T is the temperature, is quantitatively described using a Boltzmann equation. In terms of the yield $\mathrm{Y}(x) = n(x)/s(x)$, where $s(x)$ is the entropy density, this equation reads

$$\frac{d\mathrm{Y}}{dx} = -Z(x)\left[\mathrm{Y}^2(x) - \mathrm{Y}_{\mathrm{eq}}^2(x)\right] , \tag{4.45}$$

where

$$Z(x) \equiv \sqrt{\frac{\pi}{45}}\frac{m_\eta M_{\mathrm{PL}}}{x^2}\sqrt{g_*(T)}\langle\sigma v_{\mathrm{rel}}\rangle(x) , \tag{4.46}$$

$M_{\mathrm{PL}} = 1.22 \times 10^{19}$ GeV is the Planck mass and $g_*(T)$ is the number of relativistic degrees of freedom. The thermally averaged annihilation cross-section is given by

$$\langle\sigma v_{\mathrm{rel}}\rangle(x) = \int_{4m_\eta^2}^{\infty} ds \frac{s\sqrt{s - 4m_\eta^2}K_1(\sqrt{s}/T)}{16Tm_\eta^4 K_2^2(m_\eta/T)} \sigma v_{\mathrm{rel}}(s) , \tag{4.47}$$

where s is the center of mass energy squared, $K_{\alpha=1,2}$ are the modified Bessel functions of second kind and $\sigma v_{\mathrm{rel}}(s)$ is the total annihilation cross-section times relative velocity of two DM particles. At the equilibrium

$$\mathrm{Y}_{\mathrm{eq}}(x) = \frac{45}{4\pi^4}\frac{x^2}{h_{\mathrm{eff}}(T)}K_2(x) , \tag{4.48}$$

where $h_{\mathrm{eff}}(T)$ is the effective entropy.[7] The integration of the Boltzmann equation gives the yield today, Y_0, which is related to the DM relic density through

$$\Omega_\eta h^2 = \frac{2.74 \times 10^8 m_\eta \mathrm{Y}_0}{\mathrm{GeV}} , \tag{4.49}$$

where $\Omega_\eta \equiv \rho_\eta/\rho_{\mathrm{c}}$ is the ratio between the energy density of DM and the critical energy density of the Universe and $h \equiv H_0/(100$ km/s/Mpc$)$ is the reduced value of the present Hubble parameter. We solved numerically the Boltzmann equation in eq. (4.45), requiring to reproduce the value observed by the Planck collaboration, $\Omega_{\mathrm{DM}}h^2 = 0.1199 \pm 0.0027$ (68% C.L.) [172].

---

[7]Solving numerically the Boltzmann equation, we keep the temperature dependence both in $g_*(T)$ and $h_{\mathrm{eff}}(T)$ (see ref. [171]).
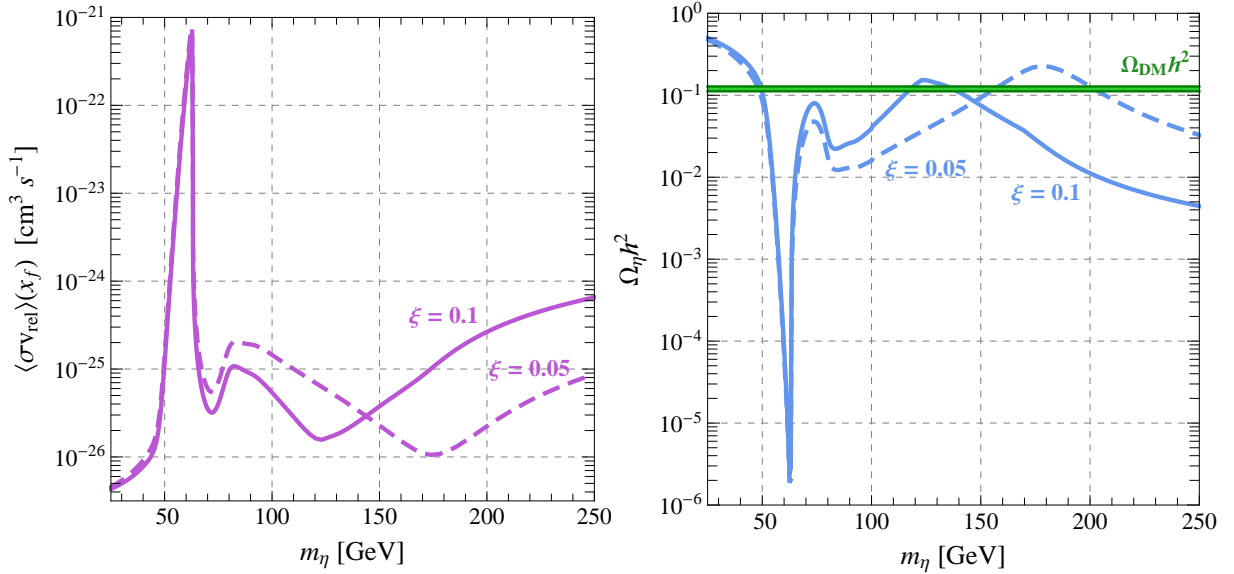
Figure 4.5: Left panel: thermally averaged annihilation cross-section $\langle \sigma v_{\text{rel}} \rangle(x)$ evaluated at the typical freeze-out temperature for a weakly-interacting DM particle, namely $T_f = m_\eta / x_f$ with $x_f = 20$. Right panel: DM relic density $\Omega_\eta h^2$ in eq. (4.49) compared with the 3σ interval measured by the Planck collaboration (green band). We show two different values $\xi = 0.1$ (solid line) and $\xi = 0.05$ (dashed line) while we fix $\lambda = 0.065$ as suggested by eqs. (4.30, 4.42).

In our analysis we included the annihilation processes $\eta\eta \to \bar{f}f$, $\eta\eta \to W^+W^-$, $\eta\eta \to ZZ$, $\eta\eta \to hh$. The relevant SM fermions entering in the computation are the bottom and the top quark. Moreover, below the kinematical threshold for the annihilation into two on-shell gauge bosons, we also include the three-body processes $\eta\eta \to WW^*$, $\eta\eta \to ZZ^*$. Given the great precision reached by the measurement of the relic abundance, in fact, the inclusion of these radiative effects is mandatory in order to obtain an accurate matching [173].[8] Let us now discuss the results of our analysis from a more quantitative point of view.

In the left panel of figure 4.5 we plot the thermally averaged annihilation cross-section at the freeze-out epoch, i.e. assuming $x_f = 20$, as a function of the DM mass m_η, for the benchmark values $\xi = 0.1$ and $\xi = 0.05$. We fix $\lambda = 0.065$, as suggested by eqs. (4.30, 4.42). Going from small to large values for the DM mass m_η it is possible to recognize the Higgs resonance ($m_\eta \approx 63$ GeV), the two-body threshold for annihilation into two on-shell W bosons ($m_\eta \approx 80$ GeV) and the effect of the momentum-dependent interactions of the chiral Lagrangian in eq. (4.2). The latter, growing proportionally to the square of the total energy in the c.o.m., becomes important for large values of the DM mass enhancing the annihilation cross-section. Finally, the dip around 130 GeV for $\xi = 0.1$ (180 GeV for $\xi = 0.05$) corresponds to the value of m_η that solves the equation

---

[8]See refs. [174, 175] for a more general discussion about the role of radiative corrections for the computation of the relic abundance.

$s - 2\lambda\xi(1-\xi)/v^2 = 0$, with $s = 4m_\eta^2/(1-v_{\rm rel}^2/4)$ and $v_{\rm rel} \approx 1/2$ at the freeze-out. This condition corresponds to an accidental cancellation between the derivative and the λ contribution to the η-η-h vertex (see appendix F and ref. [166]).

In the right panel of figure 4.5 we plot, as a function of the DM mass m_η, the value of the relic density in eq. (4.49) compared with the 3σ interval measured by the Planck collaboration. As before, we take $\xi = 0.1$ and $\xi = 0.05$, with $\lambda = 0.065$. At the qualitative level the result can be understood bearing in mind that a naïve but useful approximated solution of the Boltzmann equation is given by

$$\frac{\Omega_\eta h^2}{0.1199} \simeq \frac{3 \times 10^{-26} \text{ cm}^3\text{s}^{-1}}{\langle \sigma v_{\rm rel} \rangle(x_f)} \ . \tag{4.50}$$

As a consequence the relic abundance retraces, upside down, the same contour of the thermally averaged annihilation cross-section.

In section 4.5 we will present our numerical results for the computation of the relic density from a more general viewpoint as contour plot in the plane (m_η, λ). In this way we will be able to compare the region of the parameter space in which the model can reproduce the observed value of the relic abundance with the other constraints analyzed in the rest of this paper.

4.4.2 Direct detection

WIMP Dark Matter particles present in the galactic halo can scatter elastically with matter in the Earth. Experiments for direct detection of DM aim to detect such rare DM scatterings with a target nucleus of a detector by measuring the nuclear recoil energy. To reduce the natural background these experiments place their detectors beneath the Earth surface. The LUX experiment has recently reported the most stringent limit on the spin-independent DM-nucleon elastic cross-section $\sigma_{\rm SI}$ [176].

In our model the spin-independent DM-nucleon elastic cross-section is generated by two types of diagrams. On the one hand, the η-η-h vertex in the chiral Lagrangian in eq. (4.2) generates a tree-level contribution via the exchange in the t-channel of the Higgs boson which, in turn, couples to quarks and gluons inside the nucleon. On the other one, the Yukawa Lagrangian in eq. (4.3) contains a contact interaction between DM and quarks proportional to $(m_q/f^2)\eta^2\bar{q}q$. Note that in both cases we have a scalar-mediated interaction with quarks, i.e. the interactions involving quarks are always proportional to the scalar operator $m_q\bar{q}q$. The momentum transfer in these processes is given by $q^2 = -2m_{\rm Xe}E_{\rm re} \ll m_H^2$ (where the mass of a nucleus of Xenon is $m_{\rm Xe} = 121$ GeV while for the typical kinetic recoil energy one has $E_{\rm re} \sim$ few keV), therefore it is possible to integrate out the Higgs and to neglect the effect of the derivative interactions. It is then possible to describe the DM interaction via a single operator and a few parameters a_q:

$$\mathcal{L}_\eta^{\rm DD} \supset \sum_q a_q m_q \eta^2 \bar{q}q \ , \tag{4.51}$$

In order to write down explicitly these coefficients in our model, we need to specify the contact interactions between DM and the first two generations of quarks. Since the computation of the spin-independent elastic cross-section is the only place in which these interactions play an important phenomenological role, we decided to distinguish between two cases

$$\text{Case 1}: \qquad a_{q=u,d,c,s} = \frac{\lambda(1-2\xi)}{m_H^2} \;, \quad a_{q=t,b} = \frac{\lambda(1-2\xi)}{m_H^2} + \frac{\xi}{2(1-\xi)v^2} \;, \qquad (4.52)$$

$$\text{Case 2}: \qquad a_{q=u,d,c,s,t,b} = \frac{\lambda(1-2\xi)}{m_H^2} + \frac{\xi}{2(1-\xi)v^2} \;. \qquad (4.53)$$

In the first case – eq. (4.52) – we set to zero the contact interaction between η and all the quarks belonging to the first two generations. This setup can be easily realized, for instance, considering the embedding of the right handed quarks of the first two generations into the **15** of $SO(6)$. The only non-zero contribution to $a_{q=u,d,c,s}$, as a consequence, arises from the t-channel exchange of the Higgs boson. The coefficients $a_{q=t,b}$ receive, in addition to the term generated by the t-channel exchange of the Higgs, an extra contact interaction from the Yukawa Lagrangian in eq. (4.3); according to the discussion in section 4.1.2, this contribution has been computed assuming the embedding of the bottom and top quark into the fundamental representation **6** of $SO(6)$. In the second case – eq. (4.53) – we assumed non-zero contact interactions also for the quarks belonging to the first two generations, adopting the same embedding into the **6** of $SO(6)$ characterizing the top-bottom sector.

Given the operator in eq. (4.51), the spin-independent DM-nucleon elastic cross-section mediated by scalar interactions can always be parametrized as

$$\sigma_{\text{SI}} = \frac{1}{\pi} \left(\frac{m_{\text{N}}}{m_\eta + m_{\text{N}}} \right)^2 \frac{[Zf_p + (A-Z)f_n]^2}{A^2} \;, \qquad (4.54)$$

where $m_{\text{N}} = (m_n + m_p)/2 = 938.95$ MeV is the nucleon mass while Z and $A-Z$ are the number of protons and neutrons inside the nucleus, with $Z = 54$ and $A = 130$ for a nucleus of Xenon. In eq. (4.54) f_p and f_n describe the coupling between DM and, respectively, protons and neutrons. They are given by

$$f_{n,p} = \sum_{q=u,d,s} f_{T_q}^{(n,p)} a_q m_{n,p} + \frac{2}{27} f_{T_G} \sum_{q=c,b,t} a_q m_{n,p} \;, \qquad (4.55)$$

where for the nuclear matrix elements we take [177,178] $f_{T_u}^{(n)} = 0.026$, $f_{T_d}^{(n)} = 0.020$, $f_{T_u}^{(p)} = 0.020$, $f_{T_d}^{(p)} = 0.026$, $f_{T_s}^{(n,p)} = 0.043$, and $f_{T_G} = 1 - f_{T_u}^{(n,p)} - f_{T_d}^{(n,p)} - f_{T_s}^{(n,p)} = 0.911$.

We show our results in figure 4.6. In the left panel we compare the spin-independent elastic cross-section computed in our model with the bound set by the LUX experiment. Following our choice of benchmark values, we plot σ_{SI} for $\lambda = 0.065$ and for $\xi = 0.1$, $\xi = 0.05$. Moreover, for definiteness, we show only the setup corresponding to eq. (4.52). The bound of LUX turns out
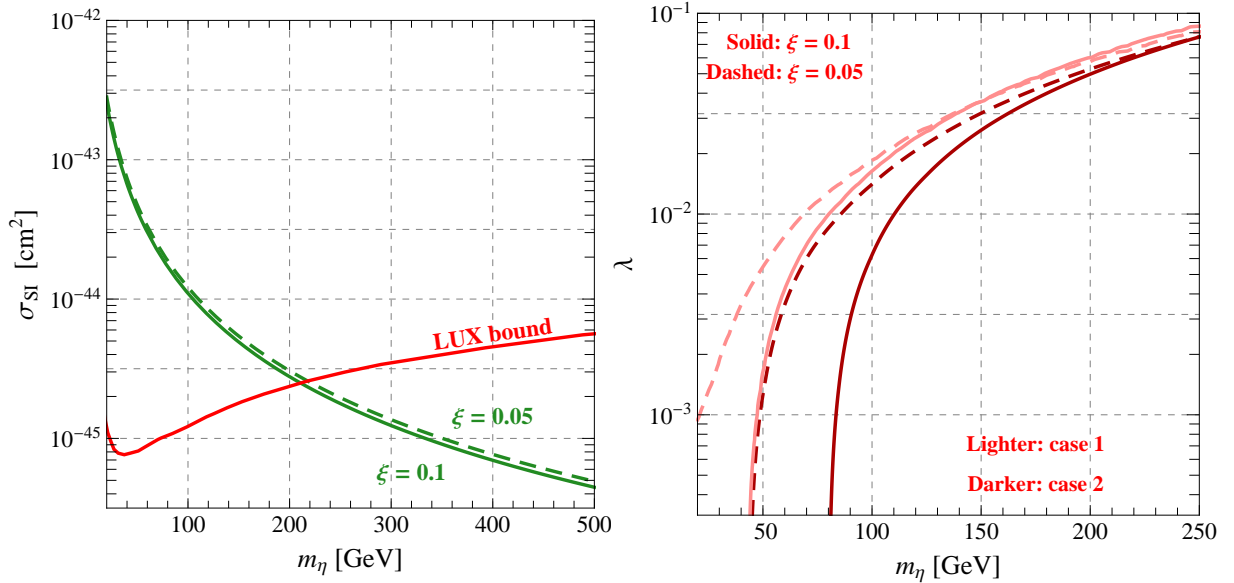
Figure 4.6: Left panel: comparison between the spin-independent elastic cross-section σ_{SI} in eq. (4.54) and the bound extracted by the LUX experiment (the region above the red line is excluded). We plot the value of σ_{SI} corresponding to $\lambda = 0.065$ limited to case 1 in eq. (4.52), with $\xi = 0.1$ (green solid line) and $\xi = 0.05$ (green dashed line). Right panel: region of the parameter space (m_η, λ) excluded by the LUX experiment. We show the corresponding bound for $\xi = 0.1$ (red solid line) and $\xi = 0.05$ (red dashed line), considering both case 1 in eq. (4.52) (lighter red) and case 2 in eq. (4.53) (darker red).

to be very stringent, and only values of DM mass larger than 200 GeV are allowed. The two lines for $\xi = 0.1$ and $\xi = 0.05$ are almost indistinguishable. The difference between these two values, in fact, starts to be significant when $\lambda(1 - 2\xi)/m_H^2 < \xi/2(1 - \xi)v^2$, i.e. for $\lambda \lesssim 10^{-2}$. In the right panel of figure 4.6 we illustrate the difference between case 1 and case 2 in eqs. (4.52, 4.53) showing the bound of the LUX experiment in the parameter space (m_η, λ), both for $\xi = 0.1$ and $\xi = 0.05$. For small values of λ, i.e. $\lambda \lesssim 10^{-2}$, the role of the additional contact interactions in case 2 starts to be significant, pushing the excluded region towards larger values of DM mass if compared with those allowed in case 1. For $m_\eta \gtrsim 150$ GeV, where the LUX bound can exclude only large values of $\lambda \gtrsim 10^{-2}$ in order to compensate the m_η^{-2} suppression in σ_{SI}, the difference between case 1 and case 2 is less relevant.

In section 4.5 we will use the result in the right panel of figure 4.6 in order to combine the bound of LUX with all the other phenomenological constraints under investigation in our analysis.

4.4.3 Indirect detection

DM annihilation into lighter SM particles can still occur in regions of relatively high DM density in the halo of the Milky Way galaxy. This process leads, eventually, to a flux of stable particles

– e.g. photons, positrons, antiprotons and neutrinos – that could be detectable from Earth [179,180]. The major task that has to be addressed in order to detect such signal is to understand, for each of the stable species mentioned above, the contribution of the astrophysical background, mostly originated from the interactions of ultra high-energy cosmic rays of extragalactic origin with the interstellar medium in the Galaxy. In this context, the measurement of the antiproton flux plays a central role because it offers the best signal-to-background ratio (including different spectra features) and because the astrophysical background for antiprotons is moderately under control.

The balloon-borne experiment BESS [181] and the space-based experiment PAMELA [182] have measured with good precision the antiproton energy spectrum in the energy range from 0.1 GeV up to about 180 GeV. A further improvement is expected when the antiproton data collected by the AMS-02 experiment will be released. The measured rate agrees well with standard background estimate; this result, as a consequence, can be used to set limits on the yield of antiprotons from exotic sources like DM annihilation.

The number of antiproton per unit energy, time and volume produced by DM annihilation is given by the following source term

$$Q_{\bar{p}} = \frac{1}{2} \left[\frac{\rho_{\text{DM}}(r)}{m_\eta} \right]^2 \langle \sigma v_{\text{rel}} \rangle_0 \left. \frac{dN}{dE} \right|_{\bar{p}} , \tag{4.56}$$

where $\langle \sigma v_{\text{rel}} \rangle_0$ is the thermally averaged annihilation cross-section times relative velocity describing DM annihilation today and $dN/dE|_{\bar{p}}$ is the antiproton energy spectrum per DM annihilation. This is given by

$$\left. \frac{dN}{dE} \right|_{\bar{p}} = \sum_f \text{BR}_f \times \left. \frac{dN}{dE} \right|_{\bar{p}}^f , \tag{4.57}$$

where the sum runs over all the possible final states $\eta\eta \to f$ that are kinematically allowed for a given value of DM mass m_η (we included the three-body annihilation processes $\eta\eta \to WW^*$, ZZ^* below the kinematical threshold for the annihilation into two on-shell gauge bosons). In eq. (4.57) $dN/dE|_{\bar{p}}^f$ is the number of antiprotons per each annihilation into the finale state $\eta\eta \to f$ whose branching ratio is given by BR_f. Concerning the DM halo profile $\rho_{\text{DM}}(r)$ we adopted three different possibilities, namely the Einasto [183], NFW [184] and Isothermal [185] profiles. We then propagated the antiprotons produced by DM annihilation considering for definiteness two different propagation models among those described in refs. [186], i.e. the KOL and CON propagation models. The comparison between these two different choices should give an idea of the uncertainties affecting the propagation of charged particles in the Galaxy. Finally, comparing the DM antiproton signal with the background generated using the same propagation models, we were able to 3σ extract exclusion curves for $\langle \sigma v_{\text{rel}} \rangle_0$. For more details on our approach see ref. [2].
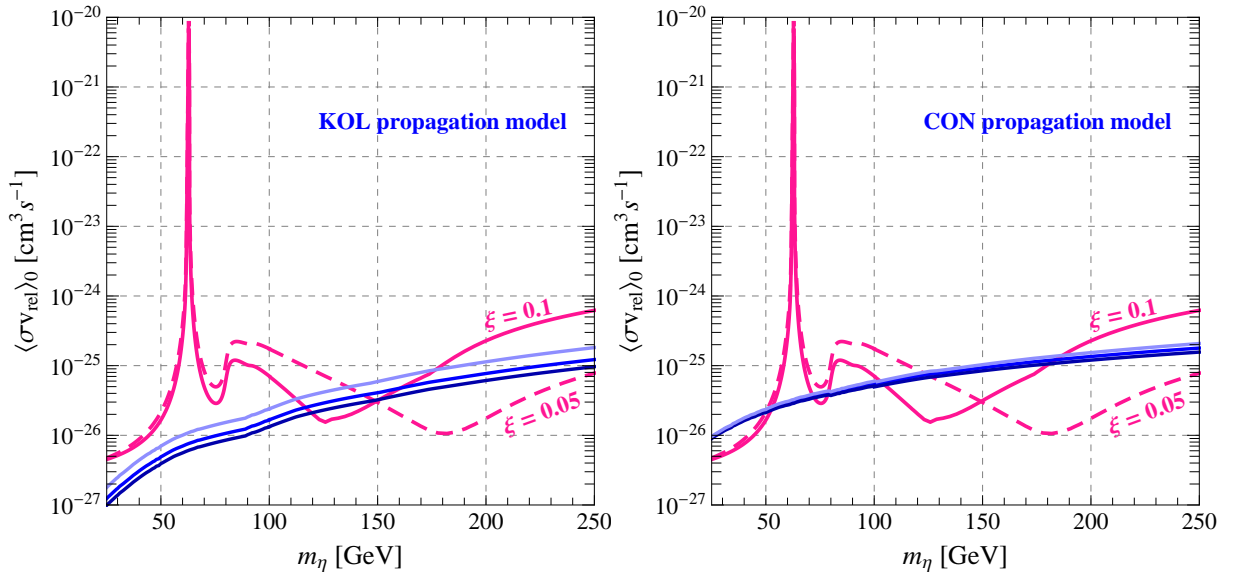
Figure 4.7: Bounds on the thermally averaged annihilation cross-section times relative velocity $\langle \sigma v_{\rm rel} \rangle_0$ obtained using the antiproton flux measured by the PAMELA experiment. The region above the blue lines is excluded at 3σ level. We show the bounds obtained using two different models for the propagation of charged cosmic rays in the Galaxy, namely the KOL (left panel) and CON (right panel) propagation models. In both cases we plot three lines corresponding to different DM density profiles, namely – from bottom to top – Einasto (darker blue), NFW (blue), Isothermal (lighter blue). We also show the value of $\langle \sigma v_{\rm rel} \rangle_0$ for $\xi = 0.1$ (pink solid line) and $\xi = 0.05$ (pink dashed line), with $\lambda = 0.065$.

In figure 4.7 we show the bounds on $\langle \sigma v_{\rm rel} \rangle_0$ obtained using this procedure, considering both the KOL (left panel) and CON (right panel) propagation models (the three shades of blue lines correspond to the three DM profiles mentioned above). For comparison, we also plot the value of $\langle \sigma v_{\rm rel} \rangle_0$ using the two benchmark values $\xi = 0.1$ and $\xi = 0.05$, with $\lambda = 0.065$. In both cases it is clear that the antiproton bound provides a stringent constraint on the annihilation cross-section. In section 4.5 we will present the antiproton bound as contour plot in the plane (m_η, λ) considering both the KOL and CON propagation models but focusing only on the NFW profile for definiteness.

4.5   Results

Here we combine all the constraints obtained in our phenomenological analysis for the Composite DM model studied in this chapter. We present our results in figure 4.8 in the plane (m_η, λ). The green strip reproduces the correct amount of relic abundance as measured by the Planck collaboration [172] (section 4.4.1). In the same plot we also show the bounds placed by the LUX experiment [176] in the context of direct detection of DM (section 4.4.2), the PAMELA experiment [182] in the context of indirect detection of DM (section 4.4.3) and the LHC experiment

considering the invisible decay width of the Higgs (section 4.3.1). On top of this, we superimpose the results of the scans performed in section 4.2 analyzing the effective potential, dividing the points among those which pass or not the bounds from direct searches of top partners and vector resonances at the LHC described in section 4.3.2. We consider the two benchmark values $\xi = 0.1$ and $\xi = 0.05$.

Let us now describe in detail the features present in figure 4.8. The region of the parameter space reproducing at 3σ the correct value of the relic density is covered by the green strip. Considering DM annihilation, the interactions between η and the Higgs boson described by the chiral Lagrangian in eq. 4.2 grow with the DM mass and decrease with the scale f. For $\xi = 0.1$ (0.05) and $m_\eta \gtrsim 180$ (250) GeV these annihilations become too efficient, thus leading to a value of relic density that is too small to match the observed one.[9] The funnel-shaped region that stretches towards this limit value $m_\eta \approx 180$ (250) GeV corresponds to the condition $s - 2\lambda\xi(1-\xi)/v^2 = 0$ with $s = 4m_\eta^2/(1 - v_{\rm rel}^2/4)$ and $v_{\rm rel} \approx 1/2$, where an accidental cancellation between the derivative and the λ contribution to the η-η-h vertex partially counterbalances the growth of the cross-section discussed before. On the basis of this observation, and in order to keep our discussion as clear as possible, let us divide the plane (m_η, λ) in three parts: the low-mass region $m_\eta \lesssim m_H/2$, the resonant region $m_\eta \approx m_H/2$ and the funnel-shaped region defined above.

For $\xi = 0.1$, the region $m_\eta \lesssim m_H/2$ is ruled out by a combination of LHC and LUX bounds. On the one hand, as soon as the invisible decay channel $h \to \eta\eta$ is kinematically allowed, $\Gamma_{\rm inv}(h \to \eta\eta)$ easily dominates over the SM contribution $\Gamma_{\rm SM}^{\xi=0.1} \approx 3$ MeV (eqs. (4.43, 4.44)); on the other one, the LUX experiment reaches in this region its best sensitivity. Decreasing ξ, however, reduces the strength of the η-η-h interaction for low values of λ. Therefore, for $\xi = 0.05$ a combination of LHC and LUX bound rules out only values of $\lambda \gtrsim 7 \times 10^{-3}$ in the $m_\eta \lesssim m_H/2$ region; this bound can be further pushed towards lower values $\lambda \simeq 10^{-3}$ considering non-zero contact interactions between η and light quarks (see section 4.4.2 and eq. (4.53)).

The resonant region $m_\eta \simeq m_H/2$ cannot be ruled out by constraints on the invisible branching ratio or the spin-independent elastic DM-nucleon cross-section since in the first case $\rm BR_{inv} \to 0$ if $m_\eta \to m_H/2$ while in the second one $-q^2 \ll m_H^2$. Around the Higgs resonance, however, DM particles mostly annihilate into $b\bar{b}$ pairs, producing a large antiproton signal that is ruled out by the bound extracted from the local antiproton flux measured by the PAMELA experiment. This conclusion is still valid regardless the astrophysical uncertainties plaguing the propagation of charged particles in the Galaxy and the DM density profile and for both values of ξ considered

---

[9]It is worth noting that this is a distinctive feature of the composite model. In the singlet scalar extension of the SM, in which the derivative interactions are absent, it is always possible to increase the value of λ in order to reproduce the correct relic density for large DM masses.

here. Note that for $\xi = 0.1$ the antiproton bound, at least adopting the KOL propagation models, can also rule out the right boundary of the funnel-shaped region (i.e. the vertical line corresponding to $m_\eta \simeq 80$ GeV).

As far as the bottleneck of the funnel-shaped region is concerned, the bound from antiproton cannot be applied since the accidental cancellation that characterizes this region also suppresses DM annihilations today ($v_{\rm rel} \approx 0$). On the contrary the spin-independent DM-nucleon elastic cross-section, relying on a different kinematic w.r.t. the annihilation process, does not suffer from the same cancellation and, as a consequence, the funnel-shaped region turns out to be ruled out by the LUX experiment for $\xi = 0.1$ and strongly constrained for $\xi = 0.05$, in particular the upper half part of the region. For $\xi = 0.05$ a viable candidate of DM, therefore, sits on the strip of the analyzed parameter space (m_η, λ) that spans values from $m_\eta \simeq 100$ GeV, $\lambda \simeq 3 \times 10^{-4}$ up to $m_\eta \simeq 200$ GeV, $\lambda \simeq 6 \times 10^{-2}$.

Finally, we also show in the right panels of figure 4.8 the result of the numerical parameter scans performed in the next-to-minimal scenario discussed in section 4.2.2. We do not show here the result for the minimal case since it predicts a very narrow region in this plane which is also contained in the next-to-minimal one. Both for $\xi = 0.1$ and $\xi = 0.05$, the points reproducing the correct top and Higgs masses, as expected from eq. (4.42), lie around the value $\lambda \simeq 0.065$ and vary between $m_\eta \sim m_H/2$ and $m_\eta \sim 700$ GeV; moreover the points with $m_\eta \lesssim 200$ GeV, shown in the plot, have the smaller amount of tuning, see figure 4.2.

For $\xi = 0.1$ all the points which provide the correct DM abundance lie in the region excluded by LUX or by the antiproton flux measurements. Moreover, most of the points are also disfavored by direct searches of top partners and vector resonances at the LHC. In conclusion we find that – remarkably – the entire region of the (m_η, λ) plane in which the model can accommodate a realistic DM candidate is ruled out by our phenomenological analysis.

For the smaller value of ξ considered here, $\xi = 0.05$, the constraints from direct searches at LHC are substantially alleviated. The favored region of the parameter space lies close to the bound imposed by DM direct detection experiments, $m_\eta \simeq 200$ GeV and $\lambda \simeq 6 \times 10^{-2}$. In this regard it should be noted that if we assume non-zero contact interactions between η and light quarks the bound becomes even more stringent (red dot-dashed line in figure 4.8). In any case – including or not this theoretical uncertainty – we expect that this region will be definitely covered in the near future by direct detection experiments.
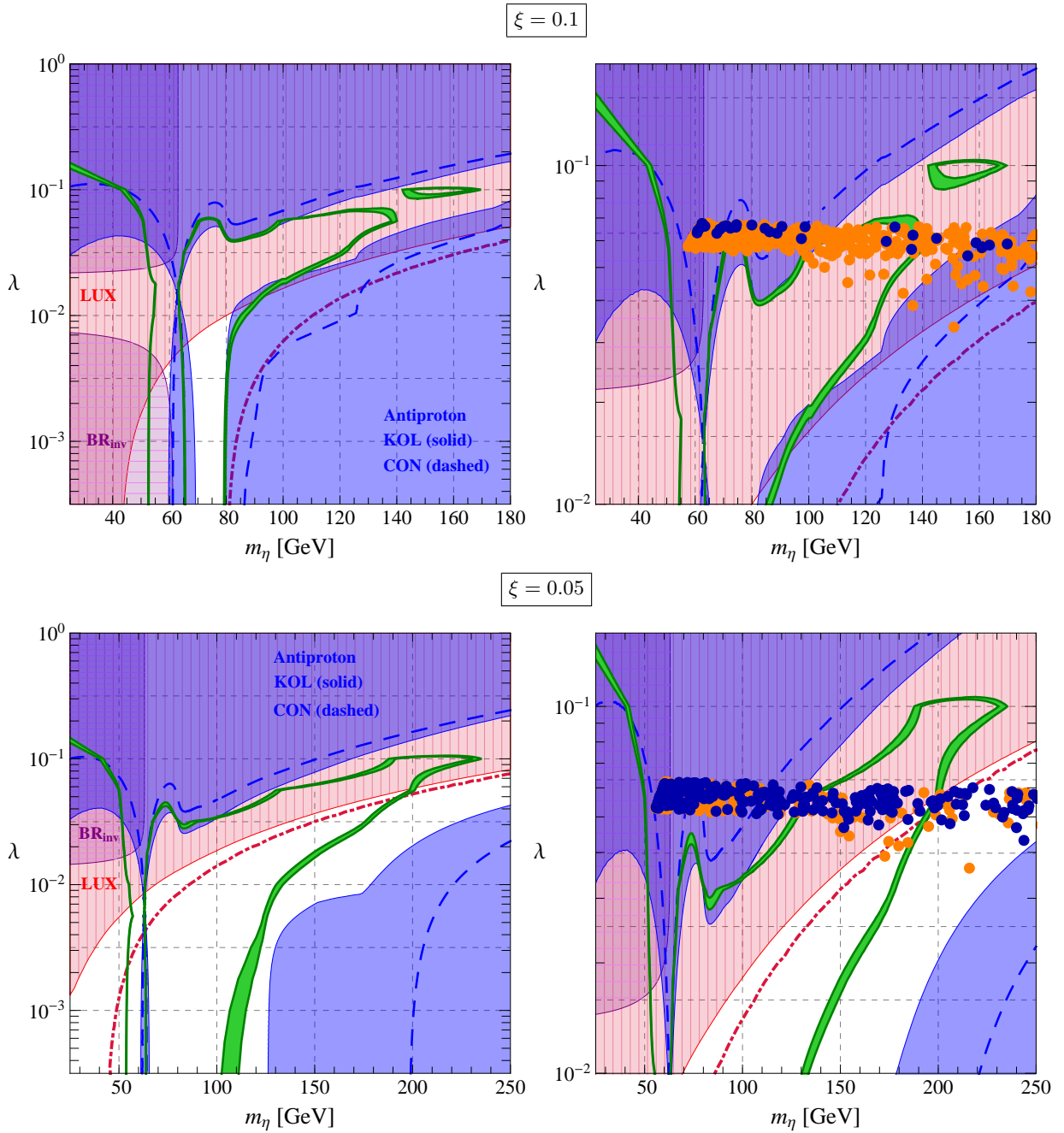
Figure 4.8:   Green line: 3σ contour reproducing the correct DM relic abundance. Red region (vertical meshes): region excluded by the LUX experiment at 95% C.L. assuming case 1 in eq. (4.52) while the red dot-dashed line represents the bound assuming case 2 in eq. (4.53). Purple region (horizontal meshes): region excluded by the LHC at 3σ considering the bound on the invisible Higgs branching ratio. Blue region (no meshes): region excluded at 3σ by the PAMELA measurement of the antiproton flux (solid line: KOL propagation model; dashed line: CON propagation models). In the upper (lower) plot we use $\xi = 0.1$ (0.05). In the right panel we zoom on a specific window of values for λ, and we superimpose the result of the scan performed in section 4.3.2. All the points reproduce the correct top and Higgs masses; the orange points are excluded by direct searches of top partners and vector resonances, while the blue points pass the selection.

CHAPTER 5

Neutrino Mixing and CP Violation

The observation of neutrino mixing implied that neutrinos are massive and that they mix among themselves. The rich experimental program in neutrino physics, culminating with the 2012 measurement of the reactor angle θ_{13} at the Daya Bay experiment [187, 188], allowed us to know with fairly good precision the value of all three neutrino mixing angles. However, on the experimental side, other than measuring with even better accuracy the mixing angles, there are still very important open questions to be addressed. Are neutrinos Dirac or Majorana fermions? What is the value of the leptonic CP violating phase (or phases, in the Majorana case) and the ordering of neutrino masses?

On the theory side, understanding the observed pattern of neutrino masses and mixings is a very challenging problem, part of the quest to understand the origin of flavor of SM fermions. In this chapter, after a brief presentation of the basic aspects of neutrino mixing, we shall study the predictions of a particular class of neutrino mixing models. In particular we will see how, in this setup, the Dirac CP violating phase can be sharply predicted in terms of the three neutrino mixing angle, making this class of models testable at future experiments. The work presented here is based on refs. [6, 7]. For a complete presentation on neutrino physics we refer to the classic review [189] (see also the relevant chapter in ref. [190]).

5.1   Neutrino masses

In the SM neutrinos are massless because it is not possible to write a renormalizable and gauge invariant operator which provides a mass term for the neutrinos ν_L^i inside the lepton doublets ℓ_L^i. Going beyond the SM, however, it is straightforward to include a mass term for these particles. The fact that neutrinos are neutral opens up the possibility of having two different kind of mass terms: Dirac or Majorana. Let us briefly describe in the following how these two mechanisms work, at least in their simplest implementation.

Dirac Neutrinos

Adding to the SM spectrum a set of three right-handed (RH) neutrinos completely neutral under the SM gauge group, $\nu_R^i = (\mathbf{1}, \mathbf{1})_0$, allows to write a Yukawa interaction analogous to the ones in eq. (1.14):

$$\mathcal{L}^D = -y_\nu^{ij} \bar{\ell}_L^i H^c \nu_R^j + h.c. \ . \tag{5.1}$$

Upon EWSB, this Lagrangian provides Dirac mass terms to neutrinos given by

$$\mathcal{L}_{m_\nu}^D = -\bar{\nu}_L^i m_\nu^{ij} \nu_R^j + h.c. \ , \tag{5.2}$$

where $m_\nu = y_\nu v \sqrt{2}$. In this case the smallness of neutrino masses is achieved just by fixing the Yukawa couplings y_ν to very small values. No explanation for the hierarchy between these couplings and the other Yukawa couplings in the SM is present.

In general the matrix m_ν is not diagonal, implying that each lepton number L_i is not conserved by itself, however in this case the sum of the three lepton numbers L is a conserved quantum number (L is however anomalous at the quantum level, while only the $B - L$ combination remains conserved), see sec. 1.1.1. As in the quark case, the Dirac mass matrix m_ν can be diagonalized by a biunitary transformation:

$$m_\nu = U_{\nu_L} m_\nu^{\text{diag}} U_{\nu_R}^\dagger, \tag{5.3}$$

where U_{ν_L}, U_{ν_R} are 3×3 unitary matrices.

Majorana Neutrinos

A Majorana neutrino mass term can instead be obtained, without enlarging the field content of the SM, only with the left-handed (LH) neutrinos. Assuming that the lepton number is just an accidental low-energy symmetry and that the SM is only an effective theory (see chapter 2), then it is possible to write non-renormalizable operators which violate L and provide a neutrino Majorana mass. In fact, at scaling dimension-5 the only gauge-invariant operator that can be written with the SM field content is the Weinberg operator [56]

$$\mathcal{L}_5 = -\frac{y_\nu^{ij}}{\Lambda_L} (\bar{\ell}_L i\sigma^2 H^c)(H^\dagger i\sigma^2 \ell_L^c) \ , \tag{5.4}$$

where $\ell_L^c = C\bar{\ell}_L^t$ (C is the charge-conjugation matrix), $i\sigma^2 = \epsilon$ is the 2×2 antisymmetric tensor and Λ_L is the UV scale at which this operator is generated, i.e. the scale of the dynamics which breaks the lepton number. When the Higgs takes a VEV , this operator provides a Majorana mass term for the neutrinos

$$\mathcal{L}_{m_\nu}^M = -\bar{\nu}_L^i m_\nu^{ij} \nu_L^{j\,c} + h.c. \ , \tag{5.5}$$

where $m_\nu = y_\nu v^2/\Lambda_L$. This mass matrix, complex and symmetric, can be diagonalized by a congruent transformation introducing only one unitary matrix U_ν:

$$m_\nu = U_{\nu_L} m_\nu^{\text{diag}} U_{\nu_L}^t \ . \tag{5.6}$$

Since the lepton number is a good symmetry of the SM, we expect $\Lambda_L \gg v$, which suppresses the neutrino masses. The value of Λ_L necessary to reproduce the neutrino masses is

$$\Lambda_L \simeq 0.6 \left(\frac{y_\nu}{1}\right) \left(\frac{0.1\text{eV}}{m_\nu}\right) \times 10^{15} \text{ GeV} \ , \tag{5.7}$$

which, for $\mathcal{O}(1)$ values of the y_ν couplings is very near to the scale at which the SM gauge couplings become similar. This is a strong hint to the possibility that the dynamics responsible for generating neutrino masses could be tightly linked to grand unified theories (GUT). This suppression of the neutrino masses due to a very high scale is known as *see-saw* mechanism. Note that by relaxing the assumption of having $\mathcal{O}(1)$ Yukawa couplings it would also be possible to lower the scale Λ_L down to the TeV scale, or even to lower values. While many studies of sterile neutrinos rely on this approach, in the rest of the thesis we will assume that Λ_L is a very high scale, near to the GUT scale.

In terms of UV degrees of freedom, the operator in eq. (5.4) can be obtained by integrating out at tree-level a set of singlet right-handed neutrinos (type 1 see-saw), scalar triplets under $\text{SU}(2)_L$ (type 2) or right-handed fermion triplets (type 3). In particular, the presence of singlet right-handed heavy neutrinos ν_R is one of the predictions of many GUTs, for example based on the gauge group $\text{SO}(10)$. For our discussion of neutrino mixing, however, the details of the UV dynamics generating the Weinberg operator are not important and therefore we take eq. (5.4) as our starting point.

5.2   Neutrino Mixing

As we saw in chapter 1, after EWSB in the SM the charged leptons acquire a mass matrix m_e given by (1.14)

$$\mathcal{L}_{m_e} = -\bar{e}_L^i m_e^{ij} e_R^j \ . \tag{5.8}$$

The complex matrix m_e can by diagonalized by a biunitary transformation

$$m_e = U_{e_L} m_e^{\text{diag}} U_{e_R}^\dagger \ , \tag{5.9}$$

where $U_{e_{L,R}}$ are unitary matrices. As in the quark sector, the misalignment of the mass matrices of the charged leptons and the neutrinos does not allow to simultaneously diagonalize the charged lepton and the neutrino mass matrices in a gauge invariant way. For example, one can choose to

diagonalize the charged lepton mass matrix by a gauge-invariant transformation in flavor space $\ell_L \to U_{e_L}\ell_L$, $e_R \to U_{e_R}e_R$, obtaining (in the Majorana case)

$$\mathcal{L}_{m_{\text{leptons}}} = -\bar{e}_L m_e^{\text{diag}} e_R - \bar{\nu}_L U_{\text{PMNS}} m_\nu^{\text{diag}} U_{\text{PMNS}}^t \nu_L^c \,, \tag{5.10}$$

(in the Dirac case one can also transform the RH neutrino $\nu_R \to U_{\nu_R}\nu_R$ and the last term in eq. (5.10) is substituted by $-\bar{\nu}_L U_{\text{PMNS}} m_\nu^{\text{diag}} \nu_R$) where U_{PMNS} is the unitary Pontecorvo-Maki-Nakagawa-Sakata (PMNS) neutrino mixing matrix, given by

$$U_{\text{PMNS}} = U_{e_L}^\dagger U_{\nu_L} \,. \tag{5.11}$$

It should be noticed that if the neutrino were massless then this mixing matrix would not be physical since it would always be possible to rotate the three neutrinos so that $U_{\text{PMNS}} = \mathbf{1}$. This means that any evidence of neutrino mixing implies that neutrinos are massive. Similarly to the CKM matrix V_{CKM} (1.16), the PMNS matrix U_{PMNS} has three physical angles and one physical CP-violating (CPV) phase. In the case of Majorana masses there are two further physical CPV phases. In the widely used standard parametrisation [190], U_{PMNS} is expressed in terms of the solar (θ_{12}), atmospheric (θ_{23}) and reactor (θ_{13}) neutrino mixing angles and one Dirac (δ) and two Majorana [191] (α_{21} and α_{31}) CPV phases:

$$U_{\text{PMNS}} \equiv U = V(\theta_{12}, \theta_{23}, \theta_{13}, \delta)\, Q(\alpha_{21}, \alpha_{31})\,, \tag{5.12}$$

where

$$V = \begin{pmatrix} 1 & 0 & 0 \\ 0 & c_{23} & s_{23} \\ 0 & -s_{23} & c_{23} \end{pmatrix} \begin{pmatrix} c_{13} & 0 & s_{13}e^{-i\delta} \\ 0 & 1 & 0 \\ -s_{13}e^{i\delta} & 0 & c_{13} \end{pmatrix} \begin{pmatrix} c_{12} & s_{12} & 0 \\ -s_{12} & c_{12} & 0 \\ 0 & 0 & 1 \end{pmatrix}\,, \tag{5.13}$$

$$Q = \text{diag}(1, e^{i\alpha_{21}/2}, e^{i\alpha_{31}/2})\,, \tag{5.14}$$

and we have used the standard notation $c_{ij} \equiv \cos\theta_{ij}$, $s_{ij} \equiv \sin\theta_{ij}$ with $0 \leq \theta_{ij} \leq \pi/2$, $0 \leq \delta < 2\pi$ and, in the case of interest for our analysis, $0 \leq \alpha_{j1} < 4\pi$, $j = 2, 3$. If CP invariance holds, we have $\delta = 0, \pi$, and $\alpha_{21(31)} = 0, \pi, 2\pi, 3\pi$ [192].

5.2.1 Neutrino oscillations

Let us now briefly review the basics of neutrino oscillations. The concept of neutrino flavor is related to the production and detection mechanisms via the charged weak current (CC). For example ν_e is the neutrino produced in CC processes current together with e^+, or the one which produces an e^- when interacting with something via a CC process, and analogously for ν_μ and ν_τ. This fixes the flavor basis $|\nu_\ell\rangle$. Neutrino mixing arises because this basis is not aligned with the basis of the mass eigenstates $|\nu_i\rangle$:

$$\nu_i = \sum_{\ell = e, \mu, \tau} U_{\ell i}\, \nu_\ell\,, \qquad i = 1, 2, 3\,, \tag{5.15}$$

where $U = U_{\text{PMNS}}$ is the PMNS mixing matrix, eq. (5.11), and each ν_i is a mass eigenstates with mass m_i. Assuming that a neutrino of flavor ν_ℓ is generated by some CC process with an energy E and that it travels (in the vacuum) a distance L, where it interacts with a detector capable of observing also other flavors $\nu_{\ell'}$, the probability of observing a flavor ℓ' is (see e.g. ref. [190])

$$P(\nu_\ell \to \nu_{\ell'}) = \sum_i |U_{\ell'i}|^2 |U_{\ell i}|^2 + 2\sum_{i>j} |U_{\ell'i}U_{\ell i}^* U_{\ell j}U_{\ell'j}^*| \cos\left(\frac{\Delta m_{ij}^2}{2E}L - \phi_{\ell'\ell;ij}\right) , \qquad (5.16)$$

where $\Delta m_{ij}^2 = m_i^2 - m_j^2$ and $\phi_{\ell'\ell;ij} = \arg\left(U_{\ell'i}U_{\ell i}^* U_{\ell j}U_{\ell'j}^*\right)$. In the case of antineutrino oscillation one gets

$$P(\bar\nu_\ell \to \bar\nu_{\ell'}) = \sum_i |U_{\ell'i}|^2 |U_{\ell i}|^2 + 2\sum_{i>j} |U_{\ell'i}U_{\ell i}^* U_{\ell j}U_{\ell'j}^*| \cos\left(\frac{\Delta m_{ij}^2}{2E}L + \phi_{\ell'\ell;ij}\right) . \qquad (5.17)$$

As a consequence of CPT invariance, these probabilities satisfy $P(\nu_\ell \to \nu_{\ell'}) = P(\bar\nu_{\ell'} \to \bar\nu_\ell)$. If neutrino mixing would satisfy the CP symmetry then $P(\nu_\ell \to \nu_{\ell'}) = P(\bar\nu_\ell \to \bar\nu_{\ell'})$, therefore a measure of CP violation is given by the asymmetry

$$A_{CP}^{(\ell'\ell)} \equiv P(\nu_\ell \to \nu_{\ell'}) - P(\bar\nu_\ell \to \bar\nu_{\ell'}) = 4\sum_{i>j} \text{Im}\left(U_{\ell'i}U_{\ell i}^* U_{\ell j}U_{\ell'j}^*\right) \sin\frac{\Delta m_{ij}^2}{2E}L . \qquad (5.18)$$

As a consequence of the unitarity of U, these asymmetries are the same in all three cases, up to a sign difference:

$$A_{CP}^{(\mu e)} = -A_{CP}^{(\tau e)} = A_{CP}^{(\tau\mu)} = 4J_{CP}\left(\sin\frac{\Delta m_{32}^2}{2E}L + \sin\frac{\Delta m_{21}^2}{2E}L + \sin\frac{\Delta m_{13}^2}{2E}L\right) , \qquad (5.19)$$

where J_{CP} is the Jarlskog invariant [193–195]

$$J_{CP} = \text{Im}\left(U_{\mu 3}U_{e3}^* U_{e2}U_{\mu 2}^*\right) . \qquad (5.20)$$

The presence of matter in the path of the neutrinos can induce some relevant effects which change qualitatively the picture of neutrino oscillations. These effects are particularly important for understanding the solar neutrino mixing, the atmospheric and long baseline accelerator neutrinos which pass through the earth. We will not discuss these effects here, for a review see e.g. refs. [189, 190].

5.2.2 Present status of neutrino mixing data

The neutrino oscillation data, accumulated over many years, allowed to determine the parameters which drive the solar and atmospheric neutrino oscillations, Δm_{21}^2, θ_{12} and $|\Delta m_{31}^2| \cong |\Delta m_{32}^2|$, θ_{23}, with a good precision (see, e.g., [196]).

Parameter	Best fit	1σ range	2σ range	3σ range
$\sin\theta_{13}$	0.154	0.147 - 0.160	0.140 - 0.166	0.133 - 0.172
$\sin^2\theta_{12}$	0.308	0.291 - 0.325	0.275 - 0.342	0.259 - 0.359
$\sin^2\theta_{23}$ (NH)	0.425	0.398 - 0.454	0.376 - 0.506	0.357 - 0.641
$\sin^2\theta_{23}$ (IH)	0.437	0.408 - 0.496 $\oplus$ 0.531 - 0.610	0.384 - 0.637	0.363 - 0.659
δ (NH)	4.37	3.52 - 5.40	0.00 - 0.346 $\oplus$ 2.76 - 6.28	—
δ (IH)	4.24	3.02 - 5.00	0.00 - 0.126 $\oplus$ 2.04 - 6.28	—

Table 5.1: Summary of the results of the global fit of the PMNS mixing angles taken from [196](v1 version) and used in our analysis. The results on the atmospheric neutrino angle θ_{23} and on the Dirac CPV phase δ depend on the type of neutrino mass hierarchy. The values of $\sin^2\theta_{23}$ and δ obtained in both the cases of normal hierarchy (NH) and inverted hierarchy (IH) are shown.

Furthermore, there were spectacular developments in the last 1.5 years in what concerns the angle θ_{13} (see, e.g., [190]). They culminated in 2012 with a high precision determination of $\sin^2 2\theta_{13}$ in the Daya Bay experiment with reactor $\bar{\nu}_e$ [187, 188]:

$$\sin^2 2\theta_{13} = 0.089 \pm 0.010 \pm 0.005\,. \tag{5.21}$$

Similarly the RENO, Double Chooz, and T2K experiments reported, respectively, 4.9σ, 2.9σ and 3.2σ evidences for a non-zero value of θ_{13} [197–199], compatible with the Daya Bay result. Most recently, during the Neutrino 2014 conference, Daya Bay announced the most precise determination of θ_{13} [200] to date, after 621 days of data taking:

$$\sin^2 2\theta_{13} = 0.084 \pm 0.005\,. \tag{5.22}$$

The high precision measurement on θ_{13} described above and the fact that θ_{13} turned out to have a relatively large value, have far reaching implications for the program of research in neutrino physics (see, e.g., [190]). After the successful measurement of θ_{13}, the determination of the absolute neutrino mass scale, of the type of the neutrino mass spectrum, of the nature – Dirac or Majorana – of massive neutrinos, as well as getting information about the status of CP violation in the lepton sector, are the most pressing and challenging problems and the highest priority goals of the research in the field of neutrino physics.

A global analysis of the neutrino oscillation data presented at the Neutrino 2012 International Conference, was performed in [201]. An updated version of the fit with 2013 data added has been published in [196] and will be used in the following. The results on $\sin^2\theta_{12}$, $\sin^2\theta_{23}$ and $\sin^2\theta_{13}$ obtained in [196], which play important role in our further discussion, are given in table 5.1. An inspection of table 5.1 shows that, in addition to the nonzero value of θ_{13}, the new feature which seems to be suggested by the current global neutrino oscillation data is a sizeable deviation of the

angle θ_{23} from the value $\pi/4$. This trend is confirmed by the results of the subsequent analysis of the global neutrino oscillation data performed in [202], however the significance of the deviation is still too small to say anything definite.

Regarding the absolute neutrino mass scale, bounds can be obtained both directly from experiments in the lab measuring β decay of radioactive nuclei and indirectly via cosmological measurements of the CMB anisotropies and Large Scale Structures. The most recent bounds are approximately

$$
\begin{aligned}
m_\nu &\lesssim 2\text{eV} \quad \text{(lab, from tritium decay) ,} \\
\sum_i m_{\nu_i} &< 0.2 - 1\text{eV} \quad \text{(cosmo) .}
\end{aligned}
\tag{5.23}
$$

5.3 Hints of an organizing principle

While neutrino masses and mixings may or may not look anarchical, the hierarchy of charged lepton masses suggests an ordered origin of lepton flavour. Given the wide spectrum of specific theoretical models, which essentially allows to account for any pattern of lepton masses and mixings, we would like to consider here the consequence for lepton mixing of simple, general assumptions on its origin.

In fact, although $\theta_{13} \neq 0$, $\theta_{23} \neq \pi/4$ and $\theta_{12} \neq \pi/4$, the deviations from these values are small, in fact we have $\sin\theta_{13} \cong 0.16 \ll 1$, $\pi/4 - \theta_{23} \cong 0.07$ and $\pi/4 - \theta_{12} \cong 0.20$, where we have used the relevant best fit values in table 5.1. The value of θ_{13} and the magnitude of deviations of θ_{23} and θ_{12} from $\pi/4$ suggest that the observed values of θ_{13}, θ_{23} and θ_{12} might originate from certain "symmetry" values which undergo relatively small (perturbative) corrections as a result of the corresponding symmetry breaking. This idea was and continues to be widely explored in attempts to understand the pattern of mixing in the lepton sector (see, e.g., [6, 7, 203–214]. Given the fact that the PMNS matrix is a product of two unitary matrices, $U = U_e^\dagger U_\nu$ (5.11), it is usually assumed that U_ν has a specific form dictated by a symmetry which fixes the values of the three mixing angles in U_ν that would differ, in general, by perturbative corrections from those measured in the PMNS matrix, while U_e (and symmetry breaking effects that we assume to be subleading) provide the requisite corrections. A variety of symmetry forms of U_ν have been explored in the literature on the subject (see, e.g., [215]). In the present study we will consider three widely used forms.

i) Tribimaximal Mixing (TBM) [216]:

$$
U_{\text{TBM}} = \begin{pmatrix} \sqrt{\frac{2}{3}} & \sqrt{\frac{1}{3}} & 0 \\ -\sqrt{\frac{1}{6}} & \sqrt{\frac{1}{3}} & \sqrt{\frac{1}{2}} \\ \sqrt{\frac{1}{6}} & -\sqrt{\frac{1}{3}} & \sqrt{\frac{1}{2}} \end{pmatrix} ;
\tag{5.24}
$$

ii) Bimaximal Mixing (BM) [217, 218]:

$$
U_{\mathrm{BM}} = \begin{pmatrix}
\frac{1}{\sqrt{2}} & \frac{1}{\sqrt{2}} & 0 \\[2mm]
-\frac{1}{2} & \frac{1}{2} & \frac{1}{\sqrt{2}} \\[2mm]
\frac{1}{2} & -\frac{1}{2} & \frac{1}{\sqrt{2}}
\end{pmatrix} ;
\tag{5.25}
$$

iii) the form of U_ν resulting from the conservation of the lepton charge $L' = L_e - L_\mu - L_\tau$ of the neutrino Majorana mass matrix (LC) [219]:

$$
U_{\mathrm{LC}} = \begin{pmatrix}
\frac{1}{\sqrt{2}} & \frac{1}{\sqrt{2}} & 0 \\[2mm]
-\frac{c_{23}^\nu}{\sqrt{2}} & \frac{c_{23}^\nu}{\sqrt{2}} & s_{23}^\nu \\[2mm]
\frac{s_{23}^\nu}{\sqrt{2}} & -\frac{s_{23}^\nu}{\sqrt{2}} & c_{23}^\nu
\end{pmatrix} ,
\tag{5.26}
$$

where $c_{23}^\nu = \cos\theta_{23}^\nu$ and $s_{23}^\nu = \sin\theta_{23}^\nu$.

We would like to notice here that if $U_e = \mathbf{1}$, $\mathbf{1}$ being the unity 3×3 matrix, we have:

i) $\theta_{13} = 0$ in all three cases of interest of U_ν;

ii) $\theta_{23} = \pi/4$, if U_ν coincides with U_{TBM} or U_{BM}, while θ_{23} can have an arbitrary value if U_ν is given by U_{LC};

iii) $\theta_{12} = \pi/4$, for $U_\nu = U_{\mathrm{BM}}$ or U_{LC}, while $\theta_{12} = \sin^{-1}(1/\sqrt{3})$ if $U_\nu = U_{\mathrm{TBM}}$.

Thus, the matrix U_e has to generate corrections

i) leading to $\theta_{13} \neq 0$ compatible with the observations in all three cases of U_ν considered;

ii) leading to the observed deviation of θ_{12} from $\pi/4$ in the cases of $U_\nu = U_{\mathrm{BM}}$ or U_{LC}.

iii) leading to the sizable deviation of θ_{23} from $\pi/4$ for $U_\nu = U_{\mathrm{TBM}}$ or U_{BM}, if it is confirmed by further data that $\sin^2\theta_{23} \cong 0.40$.

In the following we investigate quantitatively what are the "minimal" forms of the matrix U_e in terms of the number of angles and phases it contains, that can provide the requisite corrections to U_{TBM}, U_{BM} and U_{LC} so that the angles in the resulting PMNS matrix have values which are compatible with those derived from the current global neutrino oscillation data, table 5.1. In particular, we introduce the two types of "minimal" charged lepton "rotation" matrix U_e, with "standard" and "inverse" ordering. The two differ by the order in which the 12 and 23 rotations appear in U_e and will be defined more precisely in the following section.

5.3.1   General Setup

As we have indicated above, we are interested in the possibility that the θ_{13} mixing angle originates because of the contribution of the charged lepton sector to lepton mixing. This assumption needs a precise definition.

We assume that the neutrino contribution U_ν to the PMNS matrix U in eq. (5.11) has $U_{13}^\nu = 0$, so that the PMNS angle θ_{13} vanishes in the limit in which the charged lepton contribution U_e can be neglected, $U_e = \mathbf{1}$. This is a prediction of a number of theoretical models. As a consequence, U_ν can be parameterized as

$$U_\nu = \Psi_\nu R_{23}(\theta_{23}^\nu) R_{12}(\theta_{12}^\nu) \Phi_\nu, \tag{5.27}$$

where $R_{ij}(\theta)$ is a rotation by an angle θ in the ij block and Ψ_ν, Φ_ν are diagonal matrices of phases. We will in particular consider specific values of θ_{12}^ν and, in certain cases, of θ_{23}^ν, representing the predictions of well known models, such as those presented in eqs. (5.24-5.26).

The above assumption on the structure of U_ν is not enough to draw conclusions on lepton mixing: any form of U can still be obtained by combining U_ν with an appropriate charged lepton contribution $U_e = U_\nu U^\dagger$. However, the hierarchical structure of the charged lepton mass matrix allows to motivate a form of U_e similar to that of U_ν, with $U_{13}^e = 0$, so that we can write: [1]

$$U_e = \Psi_e R_{23}^{-1}(\theta_{23}^e) R_{12}^{-1}(\theta_{12}^e) \Phi_e. \tag{5.28}$$

In fact, the diagonalisation of the charged lepton mass matrix gives rise to a value of U_{13}^e that is small enough to be negligible for our purposes, unless the hierarchy of masses is a consequence of correlations among the entries of the charged lepton mass matrix or the value of the element $(m_E)_{31}$, contrary to the common lore, happens to be sizable. In such a scheme, with no 13 rotation neither in the neutrino nor in the charged lepton sector, the PMNS angle θ_{13} is generated purely by the interplay of the 23 and 12 rotations in eqs. (5.27) and (5.28).

While the assumption that U_{13}^e is small, leading to eq. (5.28), is well motivated, textures leading to a sizeable U_{13}^e are not excluded. In such cases, it is possible to obtain an "inverse ordering" of the R_{12} and R_{23} rotations in U_e:

$$U_e = \Psi_e R_{12}^{-1}(\theta_{12}^e) R_{23}^{-1}(\theta_{23}^e) \Phi_e. \tag{5.29}$$

In the following, we will also consider such a possibility.

5.3.2   Standard Ordering

Consider first the standard ordering in eq. (5.28). We can then combine U_ν and U_e in eqs. (5.27) and (5.28) to obtain the PMNS matrix. When doing that, the two 23 rotations, by the θ_{23}^ν and θ_{23}^e angles, can be combined into a single 23 rotation by an angle $\hat\theta_{23}$. The latter angle is not necessarily simply given by the sum $\hat\theta_{23} = \theta_{23}^\nu + \theta_{23}^e$ because of the possible effect of the phases in Ψ_ν, Ψ_e (see further, eq. (G.3)). Nevertheless, the combination $R_{23}(\theta_{23}^e) \Psi_e^* \Psi_\nu R_{23}(\theta_{23}^\nu)$

---

[1]The use of the inverse in eqs. (5.28) and (5.29) is only a matter of convention. This choice allows us to lighten the notation in the subsequent expressions.

entering the PMNS matrix is surely a unitary matrix acting on the 23 block and, as such, it can be written as $\Omega_\nu R_{23}(\hat{\theta}_{23})\Omega_e$, where $\Omega_{\nu,e}$ are diagonal matrices of phases and $\hat{\theta}_{23} \in [0, \pi/2]$. Moreover, we can write $\Omega_\nu R_{23}(\hat{\theta}_{23})\Omega_e = \Omega'_\nu \Phi R_{23}(\hat{\theta}_{23})\Omega'_e$, where $\Phi = \text{diag}(1, e^{i\phi}, 1)$ and $\Omega'_{\nu,e}$ are diagonal matrices of phases that commute with the 12 transformations and either are unphysical or can be reabsorbed in other phases. The PMNS matrix can therefore be written as [6]

$$U = PR_{12}(\theta^e_{12})\Phi R_{23}(\hat{\theta}_{23})R_{12}(\theta^\nu_{12})Q, \tag{5.30}$$

where the angle $\hat{\theta}_{23}$ can have any value, P is a diagonal matrix of unphysical phases, Q contains the two Majorana CPV phases, and $\Phi = \text{diag}(1, e^{i\phi}, 1)$ contains the only Dirac CPV phase. The explicit relation between the physical parameters $\hat{\theta}_{23}$, ϕ and the original parameters of the model (θ^ν_{23}, θ^e_{23}, and the two phases in $\Psi = \Psi^*_e \Psi_\nu$) can be useful to connect our results to the predictions of specific theoretical models. We provide it in app. G.

The observable angles in the standard PMNS parametrization are given by

$$\begin{aligned} \sin\theta_{13} &= |U_{e3}| = \sin\theta^e_{12} \sin\hat{\theta}_{23}, \\ \sin^2\theta_{23} &= \frac{|U_{\mu3}|^2}{1 - |U_{e3}|^2} = \sin^2\hat{\theta}_{23}\frac{\cos^2\theta^e_{12}}{1 - \sin^2\theta^e_{12}\sin^2\hat{\theta}_{23}}, \\ \sin^2\theta_{12} &= \frac{|U_{e2}|^2}{1 - |U_{e3}|^2} = \frac{\left|\sin\theta^\nu_{12}\cos\theta^e_{12} + e^{i\phi}\cos\theta^\nu_{12}\cos\hat{\theta}_{23}\sin\theta^e_{12}\right|^2}{1 - \sin^2\theta^e_{12}\sin^2\hat{\theta}_{23}}. \end{aligned} \tag{5.31}$$

The rephasing invariant related to the Dirac CPV phase, J_{CP} (5.20), in the standard parametrization is given by

$$J_{CP} = \text{Im}\left\{U^*_{e1}U^*_{\mu3}U_{e3}U_{\mu1}\right\} = \frac{1}{8}\sin\delta\sin 2\theta_{13}\sin 2\theta_{23}\sin 2\theta_{12}\cos\theta_{13}. \tag{5.32}$$

At the same time, in the parametrization given in eq. (5.30), we get:

$$J_{CP} = -\frac{1}{8}\sin\phi\sin 2\theta^e_{12}\sin 2\hat{\theta}_{23}\sin\hat{\theta}_{23}\sin 2\theta^\nu_{12}. \tag{5.33}$$

The relation between the phases ϕ and δ present in the two parametrisations is obtained by equating eq. (5.32) and eq. (5.33) and taking also into account the corresponding formulae for the real part of $U^*_{e1}U^*_{\mu3}U_{e3}U_{\mu1}$. To leading order in $\sin\theta_{13}$, one finds the approximate relation $\delta \simeq -\phi$ (see further eqs. (5.44), (5.45) and eqs. (5.49) and (5.50) for the exact relations).

In the simplest case, considered in ref. [6], the charged lepton corrections to neutrino mixing are dominated only by the angle θ^e_{12} and $\hat{\theta}_{23}$ is fixed at the maximal value $\hat{\theta}_{23} = \pi/4$. In this case the atmospheric mixing angle would be given by

$$\sin^2\theta_{23} = \frac{1}{2}\frac{1 - 2\sin^2\theta_{13}}{1 - \sin^2\theta_{13}} \cong \frac{1}{2}\left(1 - \sin^2\theta_{13}\right), \quad \text{where} \quad \sin\theta_{13} = \frac{1}{\sqrt{2}}\sin\theta^e_{12}. \tag{5.34}$$

This in turn would imply that the deviation from maximal atmospheric neutrino mixing corresponding to the observed value of θ_{13} is relatively small, as shown in fig. 5.1.
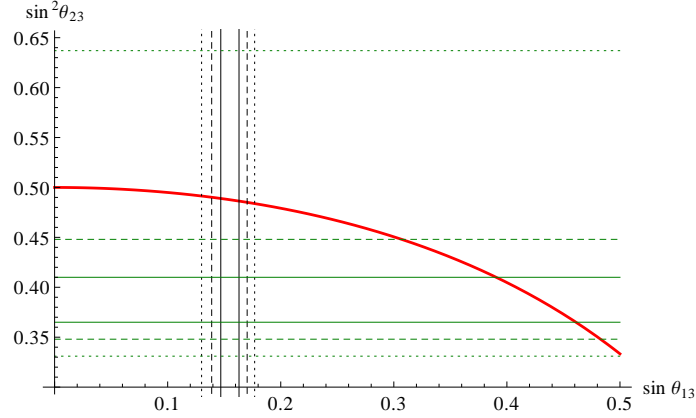
Figure 5.1: The thick red line corresponds to the relation in eq.(5.34). The black and green lines show the $1\sigma, 2\sigma, 3\sigma$ contours (solid, dashed and dotted lines, respectively) for $\sin\theta_{13}$ and $\sin^2\theta_{23}$, as obtained in [196] (see table 5.1).

Since the data seems to suggest a possible larger deviation from maximal atmospheric mixing [196, 201], we also consider the case in which $\hat{\theta}_{23}$ is essentially free. A deviation of $\hat{\theta}_{23}$ from $\pi/4$ can occur in models in which $\theta^\nu_{23} = \pi/4$ (BM, TBM) because of the charged lepton contribution to $\hat{\theta}_{23}$, or in models in which θ^ν_{23} itself is not maximal (LC). This allows to account for a sizable deviation of θ_{23} from the value $\pi/4$. As for the neutrino angle θ^ν_{12}, we will consider two cases:

- *bimaximal* mixing (BM): $\theta^\nu_{12} = \dfrac{\pi}{4}$ (as also predicted by models with approximate conservation of $L' = L_e - L_\mu - L_\tau$);

- *tri-bimaximal* mixing (TBM): $\theta^\nu_{12} = \sin^{-1}\dfrac{1}{\sqrt{3}}$.

Recently, ref. [220] extended this analysis also to the case in which θ^ν_{12} is related to the golden ratio and to the hexagonal mixing case (i.e. $\theta^\nu_{12} = \pi/6$), both of which can be obtained in explicit models with discrete symmetries.

Since in the approach we are following the four parameters of the PMNS matrix (the three measured angles θ_{12}, θ_{23}, θ_{13} and the CPV Dirac phase δ) will be expressed in terms of only three parameters (the two angles θ^e_{12}, $\hat{\theta}_{23}$ and the phase ϕ), the values of θ_{12}, θ_{23}, θ_{13} and δ will be correlated. More specifically, δ can be expressed as a function of the three angles, $\delta = \delta(\theta_{12}, \theta_{23}, \theta_{13})$, and its value will be determined by the values of the angles. As a consequence, the J_{CP} factor also will be a function of θ_{12}, θ_{23} and θ_{13}, which will allow us to obtain predictions for the magnitude of the CP violation effects in neutrino oscillations using the current data on $\sin^2\theta_{12}$, $\sin^2\theta_{23}$ and $\sin\theta_{13}$.

We note first that using eq. (5.31) we can express $\sin^2\theta_{23}$ in terms of $\sin^2\hat{\theta}_{23}$ and $\sin^2\theta_{13}$:

$$\sin^2\theta_{23} = \frac{\sin^2\hat{\theta}_{23} - \sin^2\theta_{13}}{1 - \sin^2\theta_{13}} . \tag{5.35}$$

It follows from these equations that $\hat{\theta}_{23}$ differs little from θ_{23} (it is somewhat larger). Further, using eqs. (5.31) and (5.35), we can express $\sin^2 \theta_{12}$ in terms of θ^ν_{12}, θ_{23}, θ_{13} and ϕ:

$$\sin^2 \theta_{12} = \left(1 - \cos^2 \theta_{23} \cos^2 \theta_{13}\right)^{-1} \left[\sin^2 \theta^\nu_{12} \sin^2 \theta_{23} + \cos^2 \theta^\nu_{12} \cos^2 \theta_{23} \sin^2 \theta_{13}\right.$$

$$\left. + \tfrac{1}{2} \sin 2\theta^\nu_{12} \sin 2\theta_{23} \sin \theta_{13} \cos \phi\right] . \tag{5.36}$$

As we have already indicated, we will use in the analysis which follows two specific values of $\theta^\nu_{12} = \pi/4$ (BM or LC); $\sin^{-1}(1/\sqrt{3})$ (TBM). Equation (5.36) will lead in each of the two cases to a new type of "sum rules", i.e., to a correlation between the value of θ_{12} and the values of θ_{23}, θ_{13} and ϕ. In the case of bimaximal and tri-bimaximal θ^ν_{12}, the sum rules have the form:

$$\text{BM}: \quad \sin^2 \theta_{12} = \frac{1}{2} + \frac{1}{2} \frac{\sin 2\theta_{23} \sin \theta_{13} \cos \phi}{1 - \cos^2 \theta_{23} \cos^2 \theta_{13}} \tag{5.37}$$

$$\cong \frac{1}{2} + \cot \theta_{23} \sin \theta_{13} \cos \phi \left(1 - \cot^2 \theta_{23} \sin^2 \theta_{13} + \mathcal{O}(\cot^4 \theta_{23} \sin^4 \theta_{13})\right) , \tag{5.38}$$

$$\text{TBM}: \quad \sin^2 \theta_{12} = \frac{1}{3} \left(2 + \frac{\sqrt{2} \sin 2\theta_{23} \sin \theta_{13} \cos \phi - \sin^2 \theta_{23}}{1 - \cos^2 \theta_{23} \cos^2 \theta_{13}}\right) \tag{5.39}$$

$$\cong \frac{1}{3} \left[1 + 2\sqrt{2} \cot \theta_{23} \sin \theta_{13} \cos \phi \left(1 - \cot^2 \theta_{23} \sin^2 \theta_{13}\right)\right.$$

$$\left. + \cot^2 \theta_{23} \sin^2 \theta_{13} + \mathcal{O}(\cot^4 \theta_{23} \sin^4 \theta_{13})\right] . \tag{5.40}$$

The expressions for $\sin^2 \theta_{12}$ in eqs. (5.37) and (5.39) are exact, while those given in eqs. (5.38) and (5.40) are obtained as expansions in the small parameter $\cot^2 \theta_{23} \sin^2 \theta_{13}$. The latter satisfies $\cot^2 \theta_{23} \sin^2 \theta_{13} \lesssim 0.052$ if $\sin^2 \theta_{23}$ and $\sin^2 \theta_{13}$ are varied in the 3σ intervals quoted in table 5.1. To leading order in $\sin \theta_{13}$ the sum rule in eq. (5.38) was derived in ref. [206].

We note next that since θ_{12}, θ_{23} and θ_{13} are known, eq. (5.36) allows us to express $\cos \phi$ as a function of θ_{12}, θ_{23} and θ_{13} and to obtain the range of possible values of ϕ. Indeed, it follows from eqs. (5.37) and (5.39) that

$$\text{BM}: \quad \cos \phi = -\frac{\cos 2\theta_{12} \left(1 - \cos^2 \theta_{23} \cos^2 \theta_{13}\right)}{\sin 2\theta_{23} \sin \theta_{13}} , \tag{5.41}$$

$$\text{TBM}: \quad \cos \phi = \frac{\left(3 \sin^2 \theta_{12} - 2\right) \left(1 - \cos^2 \theta_{23} \cos^2 \theta_{13}\right) + \sin^2 \theta_{23}}{\sqrt{2} \sin 2\theta_{23} \sin \theta_{13}} . \tag{5.42}$$

Taking for simplicity for the best fit values of the three angles in the PMNS matrix $\sin^2 \theta_{12} = 0.31$, $\sin^2 \theta_{23} = 0.43$ and $\sin \theta_{13} = 0.16$ (see table 5.1), we get:

$$\cos \phi \cong -1.0 \ \text{(BM)}; \qquad \cos \phi \cong -0.20 , \ \text{(TBM)}. \tag{5.43}$$

Equating the imaginary and real parts of $U^*_{e1} U^*_{\mu 3} U_{e3} U_{\mu 1}$ in the standard parametrisation and in the parametrisation under discussion one can obtain a relation between the CPV phases δ and

ϕ. We find for the BM case ($\theta_{12}^{\nu} = \pi/4$):

$$\sin\delta = -\frac{\sin\phi}{\sin 2\theta_{12}}, \tag{5.44}$$

$$\cos\delta = \frac{\cos\phi}{\sin 2\theta_{12}} \left(\frac{2\,\sin^2\theta_{23}}{\sin^2\theta_{23}\cos^2\theta_{13} + \sin^2\theta_{13}} - 1 \right). \tag{5.45}$$

Since, as can be easily shown,

$$\sin 2\theta_{12} = \left(1 - 4\frac{\cot^2\theta_{23}\sin^2\theta_{13}\cos^2\phi}{(1 + \cot^2\theta_{23}\sin^2\theta_{13})^2} \right)^{\frac{1}{2}}, \tag{5.46}$$

we indeed have to leading order in $\sin\theta_{13}$, $\sin\delta \cong -\sin\phi$ and $\cos\delta \cong \cos\phi$.

The expressions for $\sin\delta$ and $\cos\delta$ in eqs. (5.44) and (5.45) are exact. It is not difficult to check that we have $\sin^2\delta + \cos^2\delta = 1$. Using the result for $\cos\phi$, eq. (5.41), we can get expressions for $\sin\delta$ and $\cos\delta$ in terms of θ_{12}, θ_{23} and θ_{13}. We give below the result for $\cos\delta$:

$$\cos\delta = -\frac{1}{2\sin\theta_{13}}\cot 2\theta_{12}\tan\theta_{23}\left(1 - \cot^2\theta_{23}\sin^2\theta_{13}\right). \tag{5.47}$$

Numerically we find for $\sin^2\theta_{12} = 0.31$, $\sin^2\theta_{23} = 0.43$ and $\sin\theta_{13} = 0.16$:

$$\sin\delta \cong 0, \quad \cos\delta \cong -1. \tag{5.48}$$

Therefore, we have $\delta \simeq \pi$. For fixed $\sin^2\theta_{12}$ and $\sin\theta_{13}$, $|\cos\delta|$ increases with the increasing of $\sin^2\theta_{23}$. However, $\sin^2\theta_{23}$ cannot increase arbitrarily since eq. (5.37) and the measured values of $\sin^2\theta_{12}$ and $\sin^2\theta_{13}$ imply that the scheme with bimaximal mixing under discussion can be self-consistent only for values of $\sin^2\theta_{23}$, which do not exceed a certain maximal value. The latter is determined taking into account the uncertainties in the values of $\sin^2\theta_{12}$ and $\sin\theta_{13}$ in section 3, where we perform a statistical analysis using the data on $\sin^2\theta_{23}$, $\sin^2\theta_{12}$, $\sin\theta_{13}$ and δ as given in [196].

In a similar way we obtain for the TBM case ($\theta_{12}^{\nu} = \sin^{-1}(1/\sqrt{3})$):

$$\sin\delta = -\frac{2\sqrt{2}}{3}\frac{\sin\phi}{\sin 2\theta_{12}}, \tag{5.49}$$

$$\cos\delta = \frac{2\sqrt{2}}{3\sin 2\theta_{12}}\cos\phi\left(-1 + \frac{2\sin^2\theta_{23}}{\sin^2\theta_{23}\cos^2\theta_{13} + \sin^2\theta_{13}}\right)$$

$$+ \frac{1}{3\sin 2\theta_{12}}\frac{\sin 2\theta_{23}\sin\theta_{13}}{\sin^2\theta_{23}\cos^2\theta_{13} + \sin^2\theta_{13}}. \tag{5.50}$$

The results for $\sin\delta$ and $\cos\delta$ we have derived are again exact and, as can be shown, satisfy $\sin^2\delta + \cos^2\delta = 1$. Using the above expressions and the expression for $\sin^2\theta_{12}$ given in eq. (5.39) and neglecting the corrections due to $\sin\theta_{13}$, we obtain $\sin\delta \simeq -\sin\phi$ and $\cos\delta \simeq \cos\phi$. With

the help of eq. (5.42) we can express $\sin\delta$ and $\cos\delta$ in terms of θ_{12}, θ_{23} and θ_{13}. The result for $\cos\delta$ reads:

$$\cos\delta = \frac{\tan\theta_{23}}{3\sin 2\theta_{12}\sin\theta_{13}}\left[1 + \left(3\sin^2\theta_{12} - 2\right)\left(1 - \cot^2\theta_{23}\sin^2\theta_{13}\right)\right].\qquad(5.51)$$

For the best fit values of $\sin^2\theta_{12} = 0.31$, $\sin^2\theta_{23} = 0.39$ and $\sin\theta_{13} = 0.16$, we find:

$$\sin\delta \cong \pm 0.998\,, \quad \cos\delta \cong -0.066\,.\qquad(5.52)$$

Thus, in this case $\delta \simeq \pi/2$ or $3\pi/2$. For $\sin^2\theta_{23} = 0.50$ and the same values of $\sin^2\theta_{12}$ and $\sin^2\theta_{13}$ we get $\cos\delta \cong -0.096$ and $\sin\delta \cong \pm 0.995$.

The fact that the value of the Dirac CPV phase δ is determined (up to an ambiguity of the sign of $\sin\delta$) by the values of the three mixing angles θ_{12}, θ_{23} and θ_{13} of the PMNS matrix, eqs. (5.47) and (5.51), are the most striking predictions of the scheme considered with standard ordering and bimaximal and tri-bimaximal mixing in the neutrino sector. For the best fit values of θ_{12}, θ_{23} and θ_{13} we get $\delta \cong \pi$ and $\delta \cong \pi/2$ or $3\pi/2$ in the cases of bimaximal and tri-bimaximal mixing, respectively. These results imply also that in the scheme with standard ordering under discussion, the J_{CP} factor which determines the magnitude of CP violation in neutrino oscillations is also a function of the three angles θ_{12}, θ_{23} and θ_{13} of the PMNS matrix:

$$J_{CP} = J_{CP}(\theta_{12}, \theta_{23}, \theta_{13}, \delta(\theta_{12}, \theta_{23}, \theta_{13})) = J_{CP}(\theta_{12}, \theta_{23}, \theta_{13})\,.\qquad(5.53)$$

This allows to obtain predictions for the range of possible values of J_{CP} using the current data on $\sin^2\theta_{12}$, $\sin^2\theta_{23}$ and $\sin\theta_{13}$. We present these predictions in section 3. The predictions we derive for δ and J_{CP} will be tested in the experiments searching for CP violation in neutrino oscillations, which will provide information on the value of the Dirac phase δ.

Let us finally point out that such a scheme with "standard ordering" and TBM mixing was realized in a self-consistent model of lepton flavor based on T' symmetry in ref. [221]. In particular, the same prediction for δ was obtained.

5.3.3 Inverse Ordering

As anticipated, we also study for completeness the case where the diagonalisation of the charged lepton mass matrix gives rise to the inverse ordering in eq. (5.29). The PMNS matrix, in this case, can be written as [205]

$$U = R_{23}(\tilde{\theta}_{23}^e)R_{12}(\tilde{\theta}_{12}^e)\Psi R_{23}(\theta_{23}^\nu)R_{12}(\theta_{12}^\nu)\tilde{Q},\qquad(5.54)$$

where unphysical phases have been eliminated, $\tilde{Q}$ contains the two Majorana phases, and $\Psi = \mathrm{diag}(1, e^{i\psi}, e^{i\omega})$. Unlike in the case of standard ordering, it is not possible to combine the 23 rotation in the neutrino and charged lepton sector and describe them with a single parameter, $\hat{\theta}_{23}$.

After fixing θ_{23}^{ν} and θ_{12}^{ν}, we therefore have, in addition to the Majorana phases, four independent physical parameters, two angles and two phases, one more with respect to the case of standard ordering. In particular, it is not possible anymore to write the mixing matrix in terms of one physical Dirac CPV phase only. Thus, in this case the four parameters of the PMNS matrix (the three angles θ_{12}, θ_{23} and θ_{13} and the Dirac CPV phase δ) will be expressed in terms of the four parameters of the inverse ordering parametrisation of the PMNS matrix, eq. (5.54). We have for $\sin\theta_{13}$, $\sin\theta_{23}$ and $\sin\theta_{12}$:

$$
\begin{aligned}
\sin\theta_{13} &= \tilde{s}_{12}^{e} s_{23}^{\nu}, \\
\sin\theta_{23} &= s_{23}^{\nu} \frac{\left| (t_{23}^{\nu})^{-1}\tilde{s}_{23}^{e} + e^{i(\psi-\omega)}\tilde{c}_{12}^{e}\tilde{c}_{23}^{e} \right|}{\sqrt{1 - (\tilde{s}_{12}^{e}s_{23}^{\nu})^2}}, \\
\sin\theta_{12} &= s_{12}^{\nu} \frac{\left| \tilde{c}_{12}^{e} + e^{i\psi}(t_{12}^{\nu})^{-1}\tilde{s}_{12}^{e}c_{23}^{\nu} \right|}{\sqrt{1 - (\tilde{s}_{12}^{e}s_{23}^{\nu})^2}}.
\end{aligned}
\tag{5.55}
$$

Given that the expressions for θ_{23} and θ_{13} do not depend on the value of θ_{12}^{ν}, they will be the same for bimaximal and tri-bimaximal mixing (in both cases $\theta_{23}^{\nu} = \frac{\pi}{4}$):

$$
\sin\theta_{13} = \frac{\sin\tilde{\theta}_{12}^{e}}{\sqrt{2}},
\tag{5.56}
$$

$$
\sin^2\theta_{23} = \frac{1}{2}\frac{1 + \sin 2\tilde{\theta}_{23}^{e}\sqrt{\cos 2\theta_{13}}\cos\omega' - 2\sin^2\theta_{13}\cos^2\tilde{\theta}_{23}^{e}}{\cos^2\theta_{13}}
\tag{5.57}
$$

$$
\cong \frac{1}{2}\left(1 + \sin 2\tilde{\theta}_{23}^{e}\cos\omega' - \cos 2\tilde{\theta}_{23}^{e}\sin^2\theta_{13} + \mathcal{O}(\sin^4\theta_{13})\right),
\tag{5.58}
$$

where the phase $\omega' = \psi - \omega$. For each value of the phase ψ, any value of θ_{13} and θ_{23} in the experimentally allowed range at a given C.L., can be reproduced for an appropriate choice of ω', θ_{12}^{e} and θ_{23}^{e}. This is not always the case for the solar neutrino mixing angle θ_{12}, as we will see in sec. 5.5. Using eqs. (5.56), $\sin^2\theta_{12}$ can be expressed in terms of θ_{13} and ψ as follows:

- *bimaximal* mixing (BM$_{\text{IO}}$), $\theta_{12}^{\nu} = \frac{\pi}{4}$:

$$
\sin^2\theta_{12} = \frac{1}{2\cos^2\theta_{13}}\left(1 + 2\sin\theta_{13}\sqrt{\cos 2\theta_{13}}\cos\psi - \sin^2\theta_{13}\right)
\tag{5.59}
$$

$$
\simeq \frac{1}{2} + \sin\theta_{13}\cos\psi + \mathcal{O}(\sin^5\theta_{13});
\tag{5.60}
$$

- *tri-bimaximal* mixing (TBM$_{\text{IO}}$), $\theta_{12}^{\nu} = \sin^{-1}\frac{1}{\sqrt{3}}$:

$$
\sin^2\theta_{12} = \frac{1}{3\cos^2\theta_{13}}\left(1 + 2\sqrt{2}\sin\theta_{13}\sqrt{\cos 2\theta_{13}}\cos\psi\right)
\tag{5.61}
$$

$$
\simeq \frac{1}{3}(1 + \sin^2\theta_{13}) + \frac{2\sqrt{2}}{3}\sin\theta_{13}\cos\psi + \mathcal{O}(\sin^4\theta_{13}).
\tag{5.62}
$$

The expressions for $\sin^2 \theta_{12}$ in eqs. (5.59) and (5.61) are exact, while those given in (5.60) and (5.62) are obtained as expansions in $\sin^2 \theta_{13}$ in which the terms up to $\mathcal{O}(\sin^4 \theta_{13})$ and $\mathcal{O}(\sin^3 \theta_{13})$, respectively, were kept. This together with eq. (5.60) and the 3σ ranges of allowed values of $\sin^2 \theta_{12}$ and $\sin \theta_{13}$ quoted in table 5.1 suggests that the bimaximal mixing scheme considered by us can be compatible with the current (3σ) data on $\sin^2 \theta_{12}$ and $\sin \theta_{13}$ only for a very limited interval of negative values of $\cos \psi$ close to (-1).

It follows from eqs. (5.59) and (5.61) that the value of $\cos \psi$ is determined by the values of the PMNS angles θ_{12} and θ_{13}. At the same time, $\sin^2 \theta_{23}$ depends on two parameters: ω' and θ_{23}^e. This implies that the values of ω' and θ_{23}^e are correlated, but cannot be fixed individually using the data on $\sin^2 \theta_{23}$.

It is not difficult to derive also the expressions for the J_{CP} factor in terms of the inverse ordering parameters in the two cases of values of θ_{12}^ν of interest:

$$\text{BM}: \quad J_{CP} \simeq -\frac{\sin \theta_{13}}{4} \left(\sin \psi \cos 2\tilde{\theta}_{23}^e + \sin \omega' \cos \psi \sin 2\tilde{\theta}_{23}^e \right) + \mathcal{O}(\sin^2 \theta_{13}), \tag{5.63}$$

$$\text{TBM}: \quad J_{CP} \simeq -\frac{\sin \theta_{13}}{3\sqrt{2}} \left(\sin \psi \cos 2\tilde{\theta}_{23}^e + \sin \omega' \cos \psi \sin 2\tilde{\theta}_{23}^e \right) + \mathcal{O}(\sin^2 \theta_{13}). \tag{5.64}$$

We have not discussed here the LC case (conservation of the lepton charge $L' = L_e - L_\mu - L_\tau$) as it involves five parameters (θ_{23}^e, θ_{12}^e, θ_{23}^ν, and two CPV phases). At the same time, the "minimal" LC case with $\theta_{23}^e = 0$ is equivalent to the standard ordering case with BM mixing (i.e., with $\theta_{12}^\nu = \pi/4$) analised in detail in the previous subsection.

As in the case of the standard ordering, to obtain the CPV phase δ of the standard parametrisation of the PMNS matrix from the variables of these models, that is the function $\delta = \delta(\psi, \omega, \tilde{\theta}_{23}^e, \theta_{13})$, we equate the imaginary and real parts of $U_{e1}^* U_{\mu3}^* U_{e3} U_{\mu1}$ in the two parametrisations.

5.4 Results with Standard Ordering

In the numerical analysis presented here, we use the data on the neutrino mixing parameters obtained in the global fit of ref. [196] to constrain the mixing parameters of the setup described in section 5.3.1. Our goal is first of all to derive the allowed ranges for the Dirac phase δ, the J_{CP} factor and the atmospheric neutrino mixing angle parameter $\sin^2 \theta_{23}$. We also obtain the allowed values of $\sin^2 \theta_{12}$ and $\sin^2 \theta_{13}$. We start by considering the standard ordering setup, and in particular the two different choices for the angle θ_{12}^ν: $\theta_{12}^\nu = \pi/4$ (BM and LC), $\theta_{12}^\nu = \sin^{-1}(1/\sqrt{3})$ (TBM).

We construct the likelihood function and the χ^2 for both schemes of bimaximal and tri-bimaximal mixing as described in appendix H, using as parameters for this model $\sin \theta_{13}$, $\sin^2 \theta_{23}$
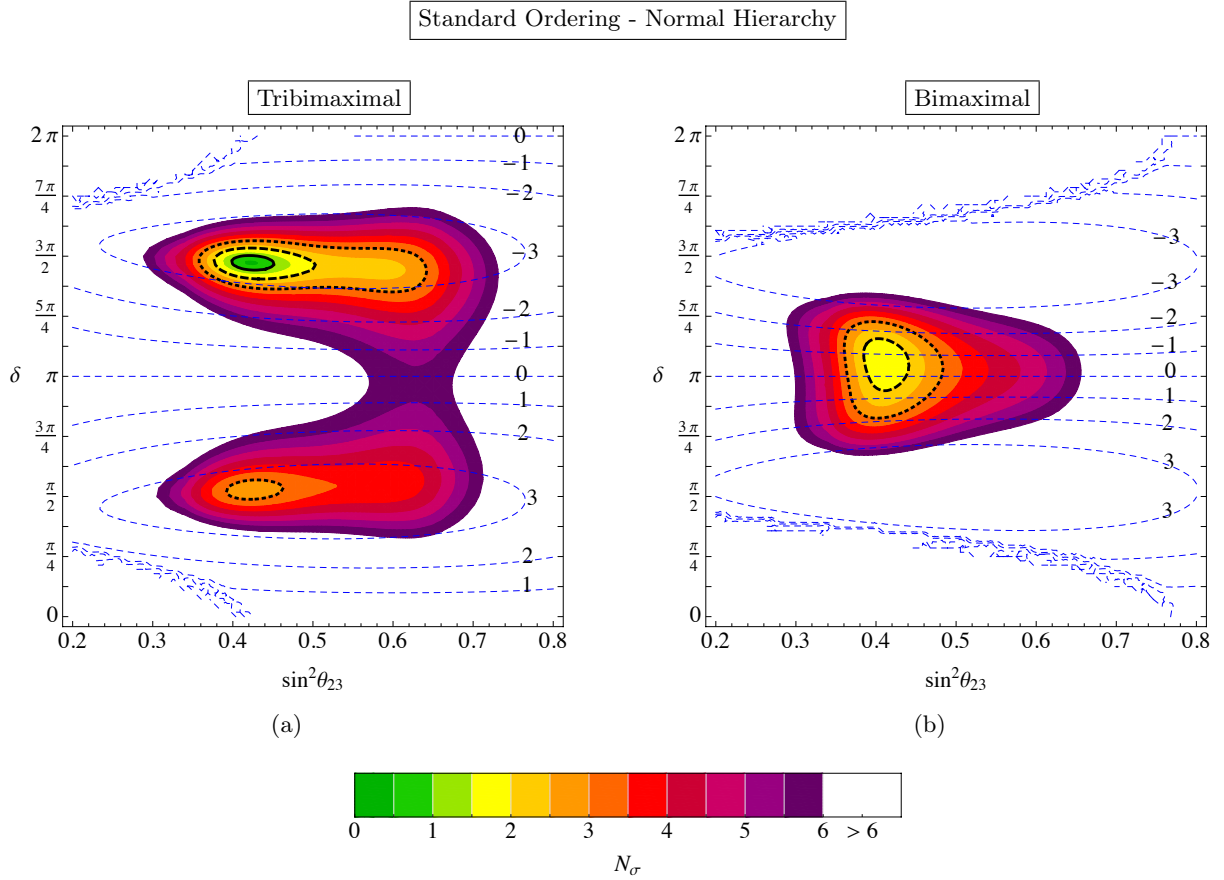
Figure 5.2: Contour plots for $N_\sigma = \sqrt{\chi^2}$ in the standard ordering setup and normal hierarchy of neutrino masses. The value of the reactor angle θ_{13} has been marginalized. The solid, dashed and dotted thick lines represent respectively the $1\sigma, 2\sigma$ and 3σ contours. The dashed blue lines are contours of constant $|J_{CP}|$ in units of 10^{-2}.

and δ, and exploiting the constraints on $\sin^2\theta_{12}$, $\sin^2\theta_{23}$, $\sin^2\theta_{13}$ and on δ obtained in ref. [196].

In fig. 5.2 we show the contours of $N_\sigma = \sqrt{\chi^2}$ in the $(\sin^2\theta_{23}, \delta)$ plane, where the value of $\sin\theta_{13}$ has been marginalized. The blue dashed lines represent the contours of constant J_{CP} (in units of 10^{-2}). In figs. 5.3 and 5.4, starting from the same likelihood function, we show the bounds on the neutrino mixing parameters and J_{CP} in each scheme, both for normal and inverted neutrino mass hierarchy. These bounds are obtained minimizing the χ^2 in the parameter space of the model, keeping as a constraint the value of the corresponding parameter. To make a direct comparison of the bounds obtained in the scheme considered by us with the general bounds obtained in the global fit in ref. [196], we show the results from ref. [196] with thin dashed lines. Thus, the thin dashed lines in fig. 5.4 are the bounds on J_{CP} obtained using directly the results of the global fit [196] and eq. (5.32), and represent the present status of our knowledge on this
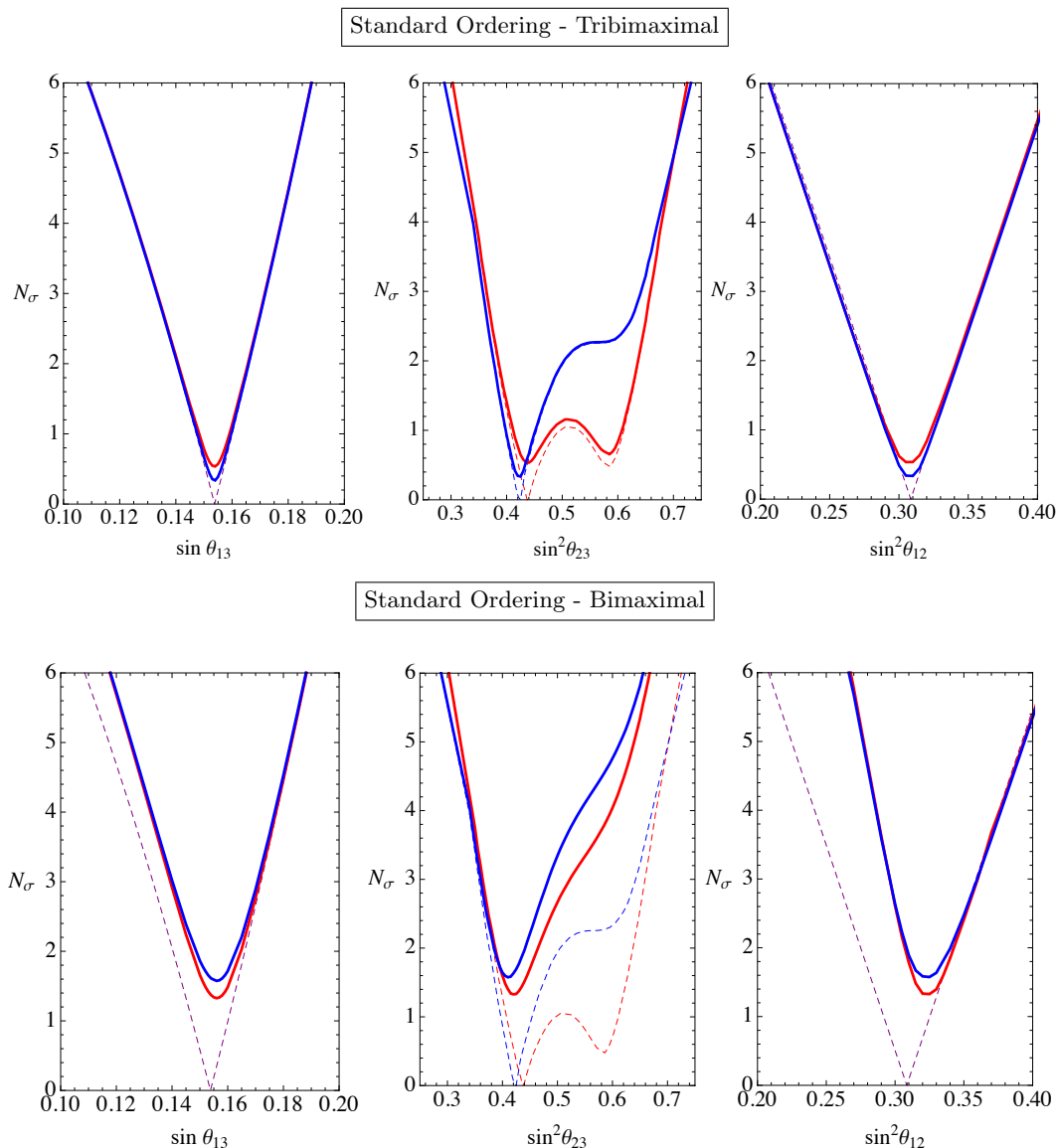
Figure 5.3: N_σ as a function of each mixing angle for the TBM and BM models in the standard ordering setup. The dashed lines represent the results of the global fit reported in ref. [196] while the thick ones represent the results we obtain in our setup. Blue lines are for normal hierarchy while the red ones are for inverted hierarchy (we used purple when the two bounds are approximately identical). These bounds are obtained minimizing the value of N_σ in the parameter space for fixed value of the showed mixing angle.
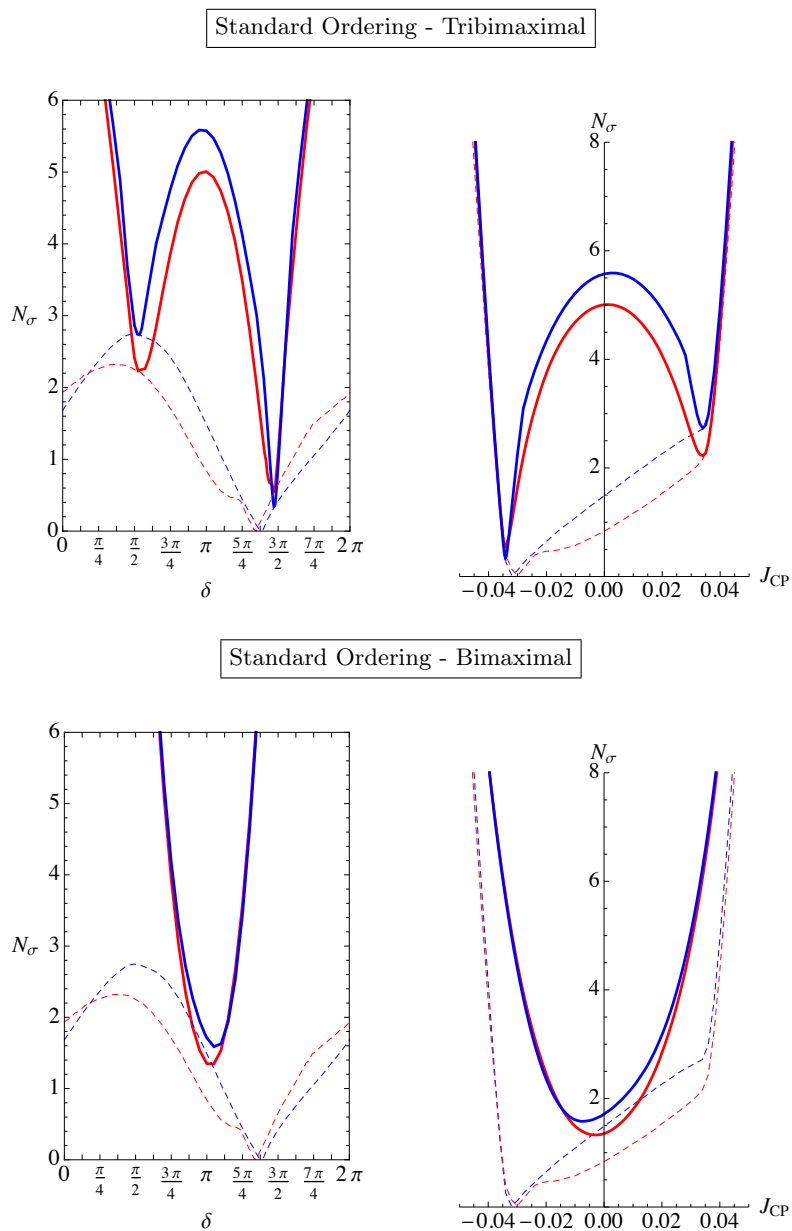
Figure 5.4: N_σ as a function of δ and J_{CP} for the TBM and BM models in the standard ordering setup. The dashed lines represent the results of the global fit reported in [196] while the thick ones represent the results we obtain in our setup. Blue lines are for normal hierarchy while the red ones are for inverted hierarchy. These bounds are obtained minimizing the value of N_σ in the parameter space for a fixed value of δ (left plots) or J_{CP} (right plots).

observable assuming the standard 3-neutrino mixing setup [2]. The thick solid lines represent the results obtained in the scheme with standard ordering considered. The blue and red color lines correspond respectively to the cases of normal and inverted neutrino mass hierarchy; in the case when the two bounds are essentially identical we used purple color lines.

From figs. 5.2 and 5.3 we see that both the tribimaximal and bimaximal cases are well compatible with data. The $\sim 1.5\sigma$ difference between the minimum of N_σ in the two cases is due to the fact that the bound on δ obtained in ref. [196] favours values of $\delta \sim 3\pi/2$ (see table 5.1), which is indeed the value needed in the tri-bimaximal mixing scheme ($|\cos\delta| \ll 1$), while the bimaximal mixing scheme prefers $\delta \sim \pi$ (see Subsection 5.3.2).

The results we obtain for $\sin^2\theta_{12}$, $\sin^2\theta_{23}$ and $\sin^2\theta_{13}$ (i.e., the best fit values and the 3σ ranges) in the case of tri-bimaximal mixing are similar to those given in ref. [196]. In contrast, our results for the Dirac phase δ and, correspondingly, for the J_{CP} factor, are drastically different. For the best fit values and the 3σ allowed ranges [3] of δ and J_{CP} we find (see also section 5.2):

$$\text{NH}: \quad \delta \cong 4.63 \cong \frac{3\pi}{2}, \quad 1.53 \lesssim \delta \lesssim 1.80, \quad \text{or} \tag{5.65}$$

$$4.24 \lesssim \delta \lesssim 4.92, \tag{5.66}$$

$$\text{IH}: \quad \delta \cong 4.62 \cong \frac{3\pi}{2}, \quad 1.45 \lesssim \delta \lesssim 2.10, \quad \text{or} \tag{5.67}$$

$$4.03 \lesssim \delta \lesssim 4.94, \tag{5.68}$$

$$\text{NH}: \quad J_{CP} \cong -0.034, \quad 0.032 \lesssim J_{CP} \lesssim 0.036, \quad \text{or} \tag{5.69}$$

$$-0.038 \lesssim J_{CP} \lesssim -0.028, \tag{5.70}$$

$$\text{IH}: \quad J_{CP} \cong -0.034, \quad 0.027 \lesssim J_{CP} \lesssim 0.037, \quad \text{or} \tag{5.71}$$

$$-0.039 \lesssim J_{CP} \lesssim -0.024. \tag{5.72}$$

The 3σ intervals of allowed values of δ (J_{CP}) in eqs. (5.65) and (5.67) (eqs. (5.69) and (5.71)) are associated with the local minimum at $\delta \cong \pi/2$ ($J_{CP} \cong 0.034$) in table. 5.4 upper left (right) panel, while those given in eqs. (5.66) and (5.68) (eqs. (5.70) and (5.72)) are related to the absolute minimum at $\delta \cong 3\pi/2$ ($J_{CP} \cong -0.034$).

A degeneracy with respect to $J_{CP} \to -J_{CP}$, or $\delta \to (2\pi - \delta)$, which stems from the fact that the phase ϕ enters into the expressions for the mixing angles only via its cosine, see eqs. (5.37) and (5.39), is broken by the explicit bound on δ given in ref. [196], which is graphically represented in fig. 5.4 by the asymmetry of the dashed lines showing that negative values of J_{CP} are favored at the 2σ level.

---

[2] More refined bounds on J_{CP} in the standard parametrisation of the PMNS matrix could be obtained by the authors of ref. [196], using the full likelihood function.

[3] These ranges are obtained imposing: $\sqrt{\Delta\chi^2} = \sqrt{N_\sigma^2 - (N_\sigma^{min})^2} \equiv 3$.

		Best fit	3σ range
TBM	J_{CP} (NH)	-0.034	$-0.038 \div -0.028 \oplus 0.032 \div 0.036$
	J_{CP} (IH)	-0.034	$-0.039 \div -0.024 \oplus 0.027 \div 0.037$
	δ (NH)	4.63	$1.53 \div 1.80 \oplus 4.24 \div 4.92$
	δ (IH)	4.62	$1.45 \div 2.10 \oplus 4.03 \div 4.94$
	$\sin\theta_{13}$	0.15	$0.13 \div 0.17$
	$\sin^2\theta_{23}$ (NH)	0.43	$0.36 \div 0.64$
	$\sin^2\theta_{23}$ (IH)	0.44	$0.36 \div 0.66$
	$\sin^2\theta_{12}$	0.31	$0.26 \div 0.36$
BM	$J_{CP}(NH)$	-0.008	$-0.026 \div 0.022$
	$J_{CP}(IH)$	-0.003	$-0.025 \div 0.023$
	δ (NH)	3.35	$2.50 \div 3.92$
	δ (IH)	3.22	$2.47 \div 3.88$
	$\sin\theta_{13}$	0.16	$0.14 \div 0.17$
	$\sin^2\theta_{23}$ (NH)	0.41	$0.35 \div 0.50$
	$\sin^2\theta_{23}$ (IH)	0.42	$0.36 \div 0.55$
	$\sin^2\theta_{12}$	0.32	$0.29 \div 0.36$

Table 5.2: Best fit and 3σ ranges in the standard ordering setup. When not explicitly indicated otherwise, the result applies both for normal hierarchy and inverted hierarchy of neutrino masses.

As figs. 5.2 and 5.4 show, in the case of tri-bimaximal mixing, the CP conserving values of $\delta = 0; \pi; 2\pi$ are excluded with respect to the best fit CP violating values $\delta \cong \pi/2; 3\pi/2$ at more than 5σ. Correspondingly, $J_{CP} = 0$ is also excluded with respect to the best-fit values $J_{CP} \simeq (-0.034)$ and $J_{CP} \simeq 0.034$ at more than 5σ. It follows from eqs. (5.65) - (5.72) (see also table 5.2) that the 3σ allowed ranges of values of both δ and J_{CP} form rather narrow intervals. These are the most striking predictions of the scheme with standard ordering and tri-bimaximal mixing under investigation.

We obtain different results assuming bimaximal mixing in the neutrino sector. Although in this case the best fit values of $\sin^2\theta_{23}$ and $\sin^2\theta_{13}$ practically coincide with those found in [196], the 3σ allowed intervals of values of $\sin^2\theta_{12}$ and especially of $\sin^2\theta_{23}$ and δ differ significantly from those given in [196].

For the best fit values and the 3σ intervals of $\sin^2\theta_{12}$ and $\sin^2\theta_{23}$ we get (see also table 5.2):

$$\sin^2\theta_{12} \cong 0.32, \quad 0.29 \lesssim \sin^2\theta_{12} \lesssim 0.36 \,; \tag{5.73}$$

$$\text{NH}: \quad \sin^2\theta_{23} \cong 0.41, \quad 0.35 \lesssim \sin^2\theta_{23} \lesssim 0.50 \,; \tag{5.74}$$

$$\text{IH}: \quad \sin^2\theta_{23} \cong 0.42, \quad 0.36 \lesssim \sin^2\theta_{23} \lesssim 0.55 \,. \tag{5.75}$$

As in [196], we find for the best fit value of δ and J_{CP}: $\delta \cong \pi$ and $J_{CP} \cong 0$. However, the 3σ range of δ and, correspondingly, of J_{CP}, we obtain differ from those derived in [196]:

$$\text{NH}: \quad 2.50 \lesssim \delta \lesssim 3.92; \quad -0.026 \lesssim J_{CP} \lesssim 0.022 \,. \tag{5.76}$$

$$\text{IH}: \quad 2.47 \lesssim \delta \lesssim 3.88; \quad -0.025 \lesssim J_{CP} \lesssim 0.023 \,. \tag{5.77}$$

We see, in particular, that also in this case the Dirac CPV phase δ is constrained to lie in a narrow interval around the value $\delta \simeq \pi$. This and the constraint $\sin^2\theta_{23} \lesssim 1/2$ are the most important predictions of the scheme with standard ordering and bimaximal neutrino mixing.

5.5 Results with the Inverse Ordering

The case of inverse ordering is qualitatively and quantitatively different from the case of standard ordering. For given values of θ_{12}^ν, θ_{23}^ν, the number of parameters is the same as in the PMNS matrix. Still, not all values of U can be obtained, as we shall see.

The constraints on the reactor and atmospheric neutrino mixing angles are the same for bimaximal and tri-bimaximal mixing and can be derived directly from eq. (5.56). For any given value of the phase ψ, any values of θ_{13} and θ_{23} in the ranges

$$0 \leq \sin\theta_{13} \leq \frac{1}{\sqrt{2}},$$
$$0 \leq \sin^2\theta_{23} \leq \frac{\cos 2\theta_{13}}{\cos^4\theta_{13}} \simeq 1 + \mathcal{O}(\sin^2\theta_{13}), \tag{5.78}$$

can be obtained by an appropriate choice of ω', θ_{12}^e and θ_{23}^e. Clearly, the range of values allowed for θ_{13} and θ_{23} covers the full experimentally allowed range. The solar neutrino mixing angle can now be expressed in terms of θ_{13} and ψ as in eq. (5.56). Any value of θ_{12} in the interval

$$\text{BM}_{IO}:$$
$$\frac{1}{2}\frac{1 - 2\sin\theta_{13}\sqrt{\cos 2\theta_{13}} - \sin^2\theta_{13}}{\cos^2\theta_{13}} \leq \sin^2\theta_{12} \leq \frac{1}{2}\frac{1 + 2\sin\theta_{13}\sqrt{\cos 2\theta_{13}} - \sin^2\theta_{13}}{\cos^2\theta_{13}}, \tag{5.79}$$

$$\text{TBM}_{IO}:$$
$$\frac{1}{3}\frac{1 - 2\sqrt{2}\sin\theta_{13}\sqrt{\cos 2\theta_{13}}}{\cos^2\theta_{13}} \leq \sin^2\theta_{12} \leq \frac{1}{3}\frac{1 + 2\sqrt{2}\sin\theta_{13}\sqrt{\cos 2\theta_{13}}}{\cos^2\theta_{13}}, \tag{5.80}$$

can then be obtained for an appropriate choice of ψ. At leading order in $\sin\theta_{13}$ these bounds become

$$\text{BM}_{IO}: \quad \frac{1}{2} - \sin\theta_{13} \lesssim \sin^2\theta_{12} \lesssim \frac{1}{2} + \sin\theta_{13},$$
$$\text{TBM}_{IO}: \quad \frac{1}{3} - \frac{2\sqrt{2}}{3}\sin\theta_{13} \lesssim \sin^2\theta_{12} \lesssim \frac{1}{3} + \frac{2\sqrt{2}}{3}\sin\theta_{13}. \tag{5.81}$$

Given the experimental bounds on the PMNS angles found in the global fit [196], see table 5.1, one can immediately notice that while the tri-bimaximal case is perfectly compatible with the data, the bimaximal case has a $\sim 2\sigma$ tension in the prediction of the solar neutrino mixing angle parameter $\sin^2\theta_{12}$.

As was done for the standard ordering case, we construct the likelihood function and the χ^2 for both models as described in appendix H, exploiting the constraints on $\sin^2\theta_{12}$, $\sin^2\theta_{23}$, $\sin^2\theta_{13}$ and on δ obtained in [196], and using in this case as parameters $\sin\theta_{13}$, $\sin\theta_{23}^e$ and the phases ψ and ω. We show in figs. 5.5 and 5.6 the bounds on the neutrino mixing angles and the J_{CP} factor both in the cases of bimaximal and tri-bimaximal mixing in the neutrino sector, and for normal and inverted neutrino mass hierarchy.

From fig. 5.5, we see that in the case of tribimaximal mixing (upper row), the intervals of allowed values of the PMNS mixing angles obtained in the model under discussion and in the global fit performed in [196] coincide. This is a consequence of the fact that the 4D parameter space of the model considered completely overlaps with the experimentally allowed parameter space in the PMNS parametrisation and therefore it does not give any additional constraint. It is consistent with the analytic bounds reported above as well.

In the case of bimaximal mixing instead (fig. 5.5 lower row), only a portion of the relevant PMNS parameter space is reachable, a fact that is reflected in the bounds on $\sin^2\theta_{12}$ given in eq. (5.81). Values of θ_{12} in the upper part of its present experimental range are favoured in this case.

In both cases of tri-bimaximal and bimaximal mixing from the neutrino sector, the bounds on $\sin^2\theta_{13}$ and $\sin^2\theta_{12}$ corresponding to the normal and inverted neutrino mass hierarchy are approximately identical, while they differ for the atmospheric neutrino mixing angle and for the J_{CP} factor.

Considering the expressions for J_{CP} in eqs. (5.63) and (5.64) and fig. 5.6, we see that within $\sim 2\sigma$ from the best-fit point, every value in the range

$$\left|J_{CP}^{BM}\right| \lesssim \frac{\sin\theta_{13}^{+2\sigma}}{4} \sim 0.041, \qquad \left|J_{CP}^{TBM}\right| \lesssim \frac{\sin\theta_{13}^{+2\sigma}}{3\sqrt{2}} \sim 0.039, \tag{5.82}$$

is allowed, where we have used the 2σ upper bound on $\sin\theta_{13}$ from table 5.1. As a consequence, we cannot make more specific predictions about the CP violation due to the Dirac phases δ in this case. This is an important difference with respect to the standard ordering scheme where,
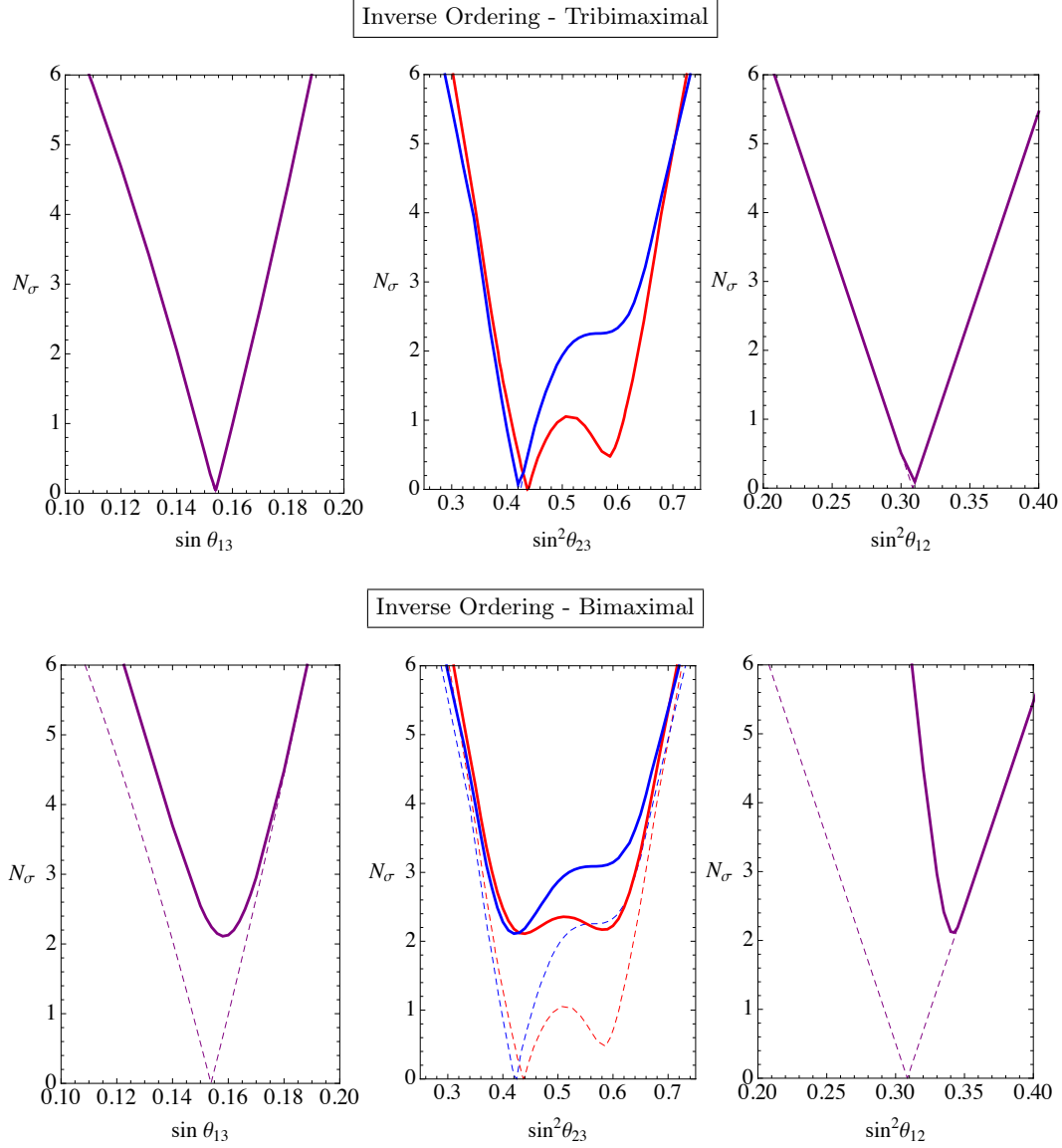
Figure 5.5: N_σ as a function of each mixing angle for the TBM and BM models with the inverse ordering setup. The dashed lines represent the results of the global fit reported in [196] while the thick ones represent the results we obtain in our setup. Blue lines are for normal hierarchy while the red ones are for inverted hierarchy (we use purple when the two bounds are approximately identical). These bounds are obtained minimizing the value of N_σ in the parameter space for fixed value of the showed mixing angle.
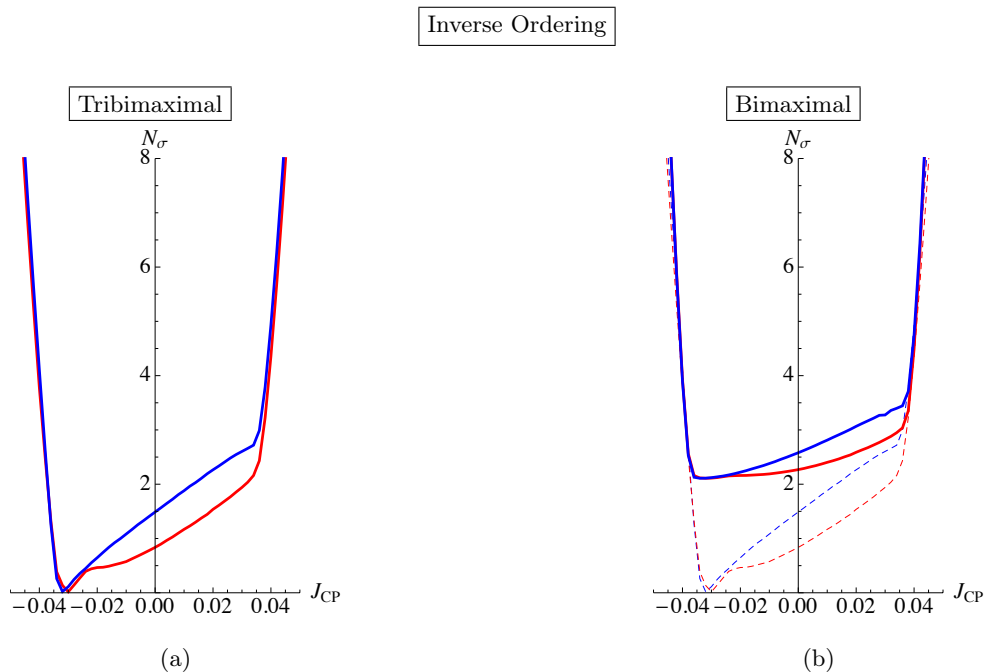
Figure 5.6: N_σ as a function of J_{CP} for the TBM and BM models in the inverse ordering setup. The dashed lines represent the results of the global fit reported in [196] while the thick ones represent the results we obtain in our setup. Blue lines are for normal neutrino mass hierarchy while the red ones are for inverted hierarchy. These bounds are obtained minimizing the value of N_σ in the parameter space for a fixed value of J_{CP}.

in the tri-bimaximal mixing case, relatively large values of the $|J_{CP}|$ factor lying in a narrow interval are predicted at 3σ and, in the bimaximal mixing case, δ is predicted to lie at 3σ in a narrow interval around the value of $\delta \sim \pi$.

5.6 Relation between θ_{12}^e and θ_{13} in GUTs

Let us now focus, for simplicity, on the standard ordering case with $\hat{\theta}_{23} = \pi/4$, i.e. we assume that the charged lepton rotation matrix is dominated only by the θ_{12}^e angle. We would like to study the possibility of generating a θ_{12}^e large enough to induce a θ_{13} in the experimentally allowed range, in the context of an SU(5) SUSY Grand Unified Theory (GUT). The unification assumption is powerful because it allows to relate the charged lepton and down quark Yukawa matrices λ_E and λ_D. If all the Yukawa entries were generated by renormalizable operators and the MSSM Higgs fields were embedded in **5** and **5̄** representations only, we would have $\lambda_{ji}^E = \lambda_{ij}^D$, leading to wrong predictions for the fermion mass ratios. In the general case one has instead $\lambda_{ji}^E = \alpha_{ij}\lambda_{ij}^D$. The Clebsh-Gordan (CG) coefficients α_{ij} depend on the operators from which the Yukawa entries arise. Such values can be constrained to belong to a finite set of rational

Operator Dimension	α_{ij}
4	1
	-3
5	-1/2
	1
	$\pm 3/2$
	-3
	9/2
	6
	9
	-18

Table 5.3:   Summary of possible SU(5) predictions for the CG coefficients α_{ij}. Numbers are taken from [222], where also the corresponding operators are listed.

numbers at the price of assuming that each Yukawa entry comes at least dominantly from a single renormalizable or non-renormalizable SU(5) operator[4]. In this case, the possible values of the α_{ij} coefficients are listed in table 5.3, see also ref. [222].

The θ_{12}^e angle is obtained from the diagonalization of the 12 block of the charged lepton Yukawa matrix after the 23 block has been diagonalized. Let us denote such 12 blocks in the charged lepton and down quark sectors (in the RL convention in which the Yukawa interactions are written with the left-handed fields on the right) as

$$
\hat{\lambda}_{[12]}^D = \begin{pmatrix} a & b' \\ b & c \end{pmatrix} \qquad \hat{\lambda}_{[12]}^E = \begin{pmatrix} \alpha a & \beta b \\ \beta' b' & \gamma c \end{pmatrix}. \tag{5.83}
$$

In the following we will assume that the entries in eq. (5.83) can be approximated with the corresponding entries of $\lambda^{E,D}$, in which case the coefficients α, β, β', γ are still bound to take one of the values in table 5.3 (the rotation used to diagonalize the 23 sector can have a sizeable effect on the coefficient γ and, if the charged lepton contribution to θ_{23} from U_{23}^e is sizeable, on the coefficient β).

We would like to determine the values of the coefficients α, β, β', γ allowed by data, and in particular capable to account for the measured value of θ_{13} (see table 5.1). Not all the values of the coefficients are allowed, in principle. The observables to be described are in fact

$$
\theta_{13}, \quad |V_{us}|, \quad \frac{m_e}{m_\mu}, \quad \frac{m_d}{m_s}, \quad \frac{m_\mu}{m_s}, \tag{5.84}
$$

---

[4]This could not be the case, for example, if SU(5) is embedded in SO(10) or a larger unified group.

Input Parameter	Value	Assumed error distribution
m_e/m_μ	$(4.7362 - 4.7369) \times 10^{-3}$ [223]	Uniform
m_μ/m_s	$2.48 - 7.73$ [222]	Uniform
m_s/m_d	18.9 ± 0.8 [224]	Gaussian
$|V_{us}|$	0.2252 ± 0.0009 [190]	Used uniform in $|V_{us}| \pm \Delta$
$\sin\theta_{13}$	$0.140 - 0.166$ (2σ) [196]	Gaussian

Table 5.4: List of input parameters used in our analysis

and for given α, β, β', γ, the five experimental inputs above depend on the four real variables $|b/c|$, $|b'/c|$, $|a/c|$, ω, where the phase ω is defined by $ac(bb')^* = e^{i\omega}|acbb'|$. The explicit dependence is given by the following relations

$$\tan\theta_{12}^e = \left| \frac{\beta'b'}{\gamma c} \left(1 - \left| \frac{\beta b}{\gamma c} \right|^2 \right) + \frac{\beta b^*}{\gamma c^*} \frac{\alpha a}{\gamma c} \right| \tag{5.85a}$$

$$|V_{us}| = \left| \frac{b}{c} \left(1 - \left| \frac{b'}{c} \right|^2 - \frac{1}{2} \left| \frac{b}{c} \right|^2 \right) + \frac{b'^*}{c^*} \frac{a}{c} \right| \pm \Delta \tag{5.85b}$$

$$\frac{m_e}{m_\mu} = \left| \frac{\alpha}{\gamma} \frac{a}{c} - \frac{\beta\beta'}{\gamma^2} \frac{bb'}{c^2} \right| \left(1 - \frac{\beta^2|b|^2 + \beta'^2|b'|^2}{\gamma^2|c|^2} \right) \tag{5.85c}$$

$$\frac{m_d}{m_s} = \left| \frac{a}{c} - \frac{bb'}{c^2} \right| \left(1 - \frac{|b|^2 + |b'|^2}{|c|^2} \right) \tag{5.85d}$$

$$\frac{m_\mu}{m_s} = |\gamma| \left(1 + \frac{(\beta^2 - \gamma^2)|b|^2 + (\beta'^2 - \gamma^2)|b'|^2}{2|c|^2\gamma^2} \right), \tag{5.85e}$$

where Δ takes into account the possibility of a model-dependent contribution to $|V_{us}|$ from the up quark sector and is assumed to be in the range $|\Delta| < \sqrt{m_u/m_c} \approx 0.045$. The experimental inputs used for the quantities on the LHS are listed in table 5.4. The relations above are approximated and are accurate up to corrections of order λ^4, if $|b/c| \lesssim |b'/c| \lesssim \lambda$, $|a/c| \lesssim \lambda^2$.

Besides the general case in eq. (5.83), we will also consider the case in which $a = 0$ and the symmetric case in which $|\lambda_{12}^D| = |\lambda_{21}^D|$ and $|\lambda_{12}^E| = |\lambda_{21}^E|$, as they arise in many models of fermion masses. Note that the symmetry condition implies $b = \pm b'$ and $\beta = \beta'$.

5.6.1   Procedure

Before we come to the results we briefly discuss the procedure we implemented. Since only the ratios $|a/c|$, $|b/c|$, and $|b'/c|$ enter when computing the experimental inputs, we have set in our forthcoming numerical analysis $|c| = 1$. We can also always perform a phase redefinition of the fields such that all the remaining coefficients are real and positive and the only physical phase is in c, so that $c = \exp(i\,\omega)$.

For each possible combination of Clebsh-Gordan (CG) coefficients we diagonalized exactly

both the mass matrices, using the expressions for the observables in eq. (5.84) in terms of a, b, b', ω, of which the relations in eq. (5.85) are the expansion at NLO. Then we determined numerically a solution for these parameters such that all the experimental inputs are satisfied. We extracted the values for these inputs randomly following the distributions given in table 5.4. We repeated this procedure until one solution is found. If, after a large number of attempts, no solution is found, we discard this combination of CG coefficients. For the viable CG coefficients we obtained by this procedure a distribution for θ_{13}, from which we computed the mean value and the standard deviation. To obtain $\sin\theta_{13}$ from $\sin\theta_{12}^e$ we have assumed that θ_{23} in the neutrino sector is maximal for simplicity. Given the uncertainties on the other input variables, this is a good approximation.

Note that eq. (5.85e) fixes γ to lie in the range of the observed m_μ/m_s. Therefore we used this equation only to reduce the possible values of γ to -3, $9/2$ and 6, cf. table 5.4. The GUT scale ratio m_μ/m_s depends strongly on low energy SUSY threshold corrections (see e.g. ref. [225]) and in principle one can use them to push this ratio to more extreme values, but in simple SUSY breaking scenarios these are the only plausible values [222].

5.6.2 Results

We restrict the following analysis to some well motivated cases. In order to choose the allowed and excluded cases we use the present 2σ bound, $0.140 < \sin\theta_{13} < 0.166$ (see table 5.1 [196]). Note also the recent Daya Bay measurement, eq. (5.22), which sets the stringent 2σ interval $0.137 < \sin\theta_{13} < 0.155$.

Results for Renormalizable Operators Only

$\{\alpha, \beta, \beta', \gamma\}$	$\{a, b, b', \omega\}$	$\sin\theta_{13}$
$\{-3, 1, -3, -3\}$	$\{0.0151, 0.220, 0.189, -2.81\}$	0.130 ± 0.013

Table 5.5: Possible CG coefficients with Yukawa couplings coming only from renormalizable operators. We also show typical values for the entries of $\hat{\lambda}_D$, where c is normalised to one, and we give the prediction for $\sin\theta_{13}$ inlcuding its 1σ standard deviation.

We start our discussion with the case in which the Yukawa couplings come only from renormalizable operators. This case is very restrictive as there are only two possible CG coefficients, which are $\alpha_{ij} = 1$, if the Higgs sits in a $\bar{\mathbf{5}}$ of SU(5), and $\alpha_{ij} = -3$, if the Higgs sits in a $\overline{\mathbf{45}}$ of SU(5) [226]. There is only one combination which is marginally in agreement with the experimental data when including the uncertainty in the prediction. It is shown in table 5.5, where we give in addition typical values for the entries of $\hat{\lambda}_D$ and the prediction for $\sin\theta_{13}$.

Results without Representations larger than the Adjoint

$\{\alpha, \beta, \beta', \gamma\}$	$\{a, b, b', \omega\}$	$\sin\theta_{13}$
$\{6, 1, 6, 6\}$	$\{0.0155, 0.281, 0.259, 0.278\}$	0.175 ± 0.009
$\{6, -3/2, 6, 6\}$	$\{0.0134, 0.247, 0.184, -2.77\}$	0.137 ± 0.014

Table 5.6: Possible CG coefficients with Higgs fields in representations not larger than the adjoint. We also show typical values for the entries of $\hat{\lambda}_D$, where c is normalised to one, and we give the prediction for $\sin\theta_{13}$ inlcuding its 1σ standard deviation.

The next case we consider is the one in which the Yukawa couplings are generated by a dimension five operator, with all fields sitting in a representation not larger than the adjoint. This concerns also the messenger sector of a possible UV completion. Especially the Georgi-Jarlskog factor of -3 [226] is here not possible anymore. There are only three α_{ij} left, which are 1, $-3/2$, and 6, giving two valid combinations as listed in table 5.6, where we give again typical values for the parameters and the predictions for $\sin\theta_{13}$, including its standard deviation.

Results for $a = 0$

$\{\beta, \beta', \gamma\}$	$\{b, b'\}$	$\sin\theta_{13}$
$\{-1/2, 6, 6\}$	$\{0.251, 0.240\}$	0.164 ± 0.013

Table 5.7: Possible Clebsch Gordan coefficients with a texture zero in the 11 element, $a = 0$. We also show typical values for the entries of $\hat{\lambda}_D$, where c is normalised to one, and we give the prediction for $\sin\theta_{13}$ inlcuding its 1σ standard deviation.

Let us now consider the scenario in which we have a texture zero in the 11 element, $a = 0$. This can be motivated by having a flavon vacuum alignment, which has a zero in this position or having a Froggat-Nielsen mechanism at work, which puts there a zero or suppresses this element very strongly. For the CG coefficients we take all the possible values in table 5.3. In this case we end up with only one possible combination showed in table 5.7. Note that in this case there are no physical phases.

Results for Symmetric Mass Matrices

In the (anti-)symmetric case $|\lambda_{12}^D| = |\lambda_{21}^D|$ and $|\lambda_{12}^E| = |\lambda_{21}^E|$, which implies $b = \pm b'$ and $\beta = \beta'$, we find 5 possible combinations listed in table 5.8. Such a mass matrix is generated, if the 12 and the 21 entries are coming from the same operator. Note that by choosing the unphysical phases appropriately we can always make $b = b'$.

$\{\alpha, \beta, \gamma\}$	$\{a, b, \omega\}$	$\sin\theta_{13}$
$\{-3/2, -3, -3\}$	$\{0.115, 0.233, -0.0736\}$	0.164 ± 0.007
$\{6, -3, -3\}$	$\{0.0186, 0.205, -3.08\}$	0.139 ± 0.001
$\{9, -3, -3\}$	$\{0.0142, 0.212, -3.04\}$	0.144 ± 0.003
$\{-18, 9/2, 9/2\}$	$\{0.0117, 0.209, -3.05\}$	0.149 ± 0.003
$\{-18, 6, 6\}$	$\{0.0133, 0.211, -3.08\}$	0.143 ± 0.003

Table 5.8: Possible Clebsch-Gordan coefficients with a symmetric mass matrix and the resulting prediction for $\sin\theta_{13}$.

This case cannot be combined with any other case. If we restrict ourselves to certain operators or choose $a = 0$, no combination remains viable.

5.7 Summary and Conclusions

We considered the possibility that the neutrino mixing angle θ_{13} arises from the interplay of 12 and 23 rotations in the neutrino (U_ν) and charged lepton (U_e) contributions to the PMNS neutrino mixing matrix ($U = U_e^\dagger U_\nu$). We considered two possible orderings of 12 and 23 rotations in U_e, the "standard", $U_e \sim R_{23}^e R_{12}^e$, and the "inverse", $U_e \sim R_{12}^e R_{23}^e$, while keeping the standard ordering in the neutrino sector, $U_\nu \sim R_{23}^\nu R_{12}^\nu$. In order to be able to accommodate a possible deviation of the atmospheric neutrino mixing angle θ_{23} from $\pi/4$, we allowed the charged lepton 23 rotation angle (and possibly the neutrino one, in the standard case) to assume arbitrary values. We considered the cases in which U_ν is in the bimaximal or tri-bimaximal form, or in the form resulting from the conservation of the lepton charge $L_e - L_\mu - L_\tau$ (LC). We took, of course, all relevant physical CP violation (CPV) phases into account.

The case of standard ordering turns out to be particularly interesting. The PMNS matrix can be parameterized in terms of the charged lepton and neutrino 12 rotation angles, θ_{12}^e and θ_{12}^ν, an effective 23 rotation angle, $\hat{\theta}_{23} \approx \theta_{23}$, and a CPV phase ϕ. Once θ_{12}^ν is fixed to the bimaximal (LC) or tri-bimaximal value, the number of parameters reduces to three, and the Dirac phase δ in the PMNS matrix can be predicted in terms of the PMNS solar, atmospheric and reactor neutrino mixing angles θ_{12}, θ_{23} and θ_{13}. Moreover, the range of possible values of the PMNS angles turns out to be constrained.

In the tri-bimaximal case, the Dirac CPV phase δ is predicted to have a value $\delta \approx 3\pi/2$ or $\delta \approx \pi/2$ (with the former favored at $\sim 2\sigma$), implying nearly maximal CP violation in neutrino oscillations, while in the bimaximal (and LC) case we find $\delta \approx \pi$ and, consequently, the CP violation effects in neutrino oscillations are predicted to be small. The present data have a mild preference for the TBM option (see table 5.1 and, e.g., fig. 5.4). Moreover, θ_{23} is predicted to

be below $\pi/4$ in the bimaximal case, which is also in agreement with the indications from the current global neutrino oscillations data. In the set-up considered by us, the $\theta_{23} > \pi/4$ solution of the global fit analysis in [196, 201] is disfavored.

The case of inverse ordering is qualitatively and quantitatively very different. Fixing U_ν to the bimaximal or tri-bimaximal form is not sufficient to obtain a prediction: the number of free physical parameters in this case is four – two angles and two CPV phases. Still, not all values of the four physical parameters in the PMNS matrix, θ_{12}, θ_{23}, θ_{13} and δ, can be reached in this parameterization. In the tri-bimaximal case, the ranges of parameters that can be reached overlaps with the experimental ranges, so that no predictions can be made. In the bimaximal case, however, this is not the case. One obtains, in fact, the approximate relation $\sin^2 \theta_{12} \gtrsim 1/2 - \sin\theta_{13}$, which is barely compatible with the data. As a consequence, i) there is a tension in the above relation that worsen the quality of the fit, and ii) values of θ_{12} in the upper part of its present experimental range are preferred. In both cases, no predictions for the Dirac CPV phase δ can be made. We did not consider here the LC case as it involves, in general, five parameters, while its "minimal" version, corresponding to setting $\theta_{23}^e = 0$, is equivalent to the standard ordering case with BM mixing (i.e., with $\theta_{12}^\nu = \pi/4$).

The fact that the value of the Dirac CPV phase δ is determined (up to an ambiguity of the sign of $\sin\delta$) by the values of the three PMNS mixing angles, θ_{12}, θ_{23} and θ_{13}, eqs. (5.47) and (5.51), are the most striking predictions of the scheme considered with standard ordering and bimaximal (LC) and tri-bimaximal mixing in the neutrino sector. As we have already indicated, for the best fit values of θ_{12}, θ_{23} and θ_{13} we get $\delta \cong \pi$ and $\delta \cong 3\pi/2$ in the cases of bimaximal and tri-bimaximal mixing, respectively. These results imply also that in the scheme with standard ordering we have discussed, the J_{CP} factor which determines the magnitude of CP violation in neutrino oscillations, is also a function of the three mixing angles: $J_{CP} = J_{CP}(\theta_{12}, \theta_{23}, \theta_{13}, \delta(\theta_{12}, \theta_{23}, \theta_{13})) = J_{CP}(\theta_{12}, \theta_{23}, \theta_{13})$. This allowed us to obtain predictions for the range of possible values of J_{CP} using the current data on $\sin^2 \theta_{12}$, $\sin^2 \theta_{23}$ and $\sin\theta_{13}$, which are given in eqs. (5.65) - (5.71) and eqs. (5.76) - (5.77). For a recent work on using this strategy to predict the Majorana phases see ref. [220].

The predictions for $\sin^2 \theta_{23}$, and for δ and J_{CP} we have obtained in the scheme with standard ordering and bimaximal (or LC) or tri-bimaximal form of U_ν will be tested by the neutrino oscillation experiments able to determine whether $\sin^2 \theta_{23} \lesssim 0.5$ or $\sin^2 \theta_{23} > 0.5$, and in the experiments searching for CP violation in neutrino oscillations.

Finally, restricting ourselves to the simple case in which the only contribution from charged leptons is the 12 rotation, we studied the predicted values of θ_{13} in SU(5) Grand Unified theories, where the 12 rotation in the charged lepton sector is related to the Cabibbo angle in the CKM matrix and to some ratios of quark and lepton masses, depending on the particular type of

operator which generates the Yukawas. After performing a scan over all possible combinations of Clebsh-Gordan coefficients, only a few of them are compatible with the present measurement of the reactor angle, as can be seen from tables 5.5, 5.6, 5.7, 5.8.

APPENDIX A

Redundant operators and field redefinitions

To compute the anomalous dimension matrix of the set of 13 operators we are interested in,

$$\{\mathcal{O}_H, \mathcal{O}_T, \mathcal{O}_B, \mathcal{O}_W, \mathcal{O}_{2B}, \mathcal{O}_{2W}, \mathcal{O}_{BB}, \mathcal{O}_{WW}, \mathcal{O}_{WB}, \mathcal{O}_{3W}, \mathcal{O}_{2G}, \mathcal{O}_{GG}, \mathcal{O}_{3G}\} \ , \qquad \text{(A.1)}$$

we compute the one-loop effective action generated by those operators. One important feature of this kind of computation is the appearance of counterterms corresponding to operators which are not in our basis: the computation *does not know* our choice of basis. Working in the background field gauge assures that the structure of these counterterms is gauge-invariant, therefore they can be written as some gauge-invariant dim-6 operators. However, this does not imply that the coefficient of the counterterms should be also gauge-invariant, in fact at this stage many terms are ξ-dependent, which reflects the fact that the computation is not physical at this point. A possible way to obtain physical results is to consider some physical process and include all one-loop contributions: both those from operators in the basis and those from loop-generated ones. When this process is completed, the result has to be gauge-independent. Another way for dealing with this, without the need of considering physical observables, is to 'rotate' back this loop-generated redundant operators into the basis we are working with. The completeness of the basis assures that this is always possible. After this process, which will be described in this appendix for the subset of operators we consider, the final anomalous dimension matrix has to be gauge-independent. This subtlety is well known and, for instance, it also appears in the context of non-relativistic QCD, where the running of the Wilson coefficients is gauge independent only when the redundancy of different operators is taken into account [227]. This has also been recently stressed again in ref. [75].

The relevant redundant operators that are radiatively generated by those in eq. (A.1) are:

$$
\begin{aligned}
&\mathcal{O}_r = |D_\mu H|^2 \, |H|^2 \,, && \mathcal{O}_{K4} = |D^2 H|^2 \,, \\[4pt]
&\mathcal{O}_{LL}^{(3)L_1} = (\bar{L}_L \sigma^a \gamma^\mu L_L)(\bar{L}_L \sigma^a \gamma^\mu L_L)\,, && \mathcal{O}_L^{(3)L_1} = i(H^\dagger \sigma^a \overset{\leftrightarrow}{D}_\mu H)\bar{L}_L^1 \sigma^a \gamma^\mu L_L^1 \,, \\[4pt]
&\mathcal{O}_{LL}^{L_1} = (\bar{L}_L \gamma^\mu L_L)(\bar{L}_L \gamma^\mu L_L)\,, && \mathcal{O}_R^{e_1} = i(H^\dagger \overset{\leftrightarrow}{D}_\mu H)(\bar{e}_R^1 \gamma^\mu e_R^1)\,, \\[4pt]
&\mathcal{O}_{RR}^{(8)u_1 d_1} = (\bar{u}_R \gamma^\mu T^A u_R)(\bar{d}_R \gamma^\mu T^A d_R)\,, && \mathcal{O}_{RR}^{e_1} = (\bar{e}_R \gamma^\mu e_R)(\bar{e}_R \gamma^\mu e_R)\,, \\[4pt]
&\mathcal{O}_{K3L}^{F_i} = \tfrac{1}{2} \bar{F}_L^i \left(\slashed{D} D^2 + D^2 \slashed{D}\right) F_L^i \,, && \mathcal{O}_{K3R}^{f_i} = \tfrac{1}{2} \bar{f}_R^i \left(\slashed{D} D^2 + D^2 \slashed{D}\right) f_R^i \,, \\[4pt]
&\mathcal{O}_{WL}^{F_i} = g D^\nu W_{\mu\nu}^a (\bar{F}_L^i \sigma^a \gamma^\mu F_L^i)\,, && \mathcal{O}_{WL}^{\prime F_i} = g \widetilde{W}_{\mu\nu}^a i \bar{F}_L^i \sigma^a \gamma^\mu D^\nu F_L^i \,, \\[4pt]
&\mathcal{O}_{BL}^{F_i} = g' D^\nu B_{\mu\nu} (\bar{F}_L^i \gamma^\mu F_L^i)\,, && \mathcal{O}_{BL}^{\prime F_i} = g' \widetilde{B}_{\mu\nu} i \bar{F}_L^i \gamma^\mu D^\nu F_L^i \,, \\[4pt]
&\mathcal{O}_{BR}^{f_i} = g' D^\nu B_{\mu\nu} (\bar{f}_R^i \gamma^\mu f_R^i)\,, && \mathcal{O}_{BR}^{\prime f_i} = g' \widetilde{B}_{\mu\nu} i \bar{f}_R^i \gamma^\mu D^\nu f_R^i \,, \\[4pt]
&\mathcal{O}_{GL}^{Q_i} = g_s D^\nu G_{\mu\nu}^A (\bar{Q}_L^i T^A \gamma^\mu Q_L^i)\,, && \mathcal{O}_{GL}^{\prime Q_i} = g_s \widetilde{G}_{\mu\nu}^A i (\bar{Q}_L^i T^A \gamma^\mu D^\nu Q_L^i)\,, \\[4pt]
&\mathcal{O}_{GR}^{q_i} = g_s D^\nu G_{\mu\nu}^A (\bar{q}_R^i T^A \gamma^\mu q_R^i)\,, && \mathcal{O}_{GR}^{\prime q_i} = g_s \widetilde{G}_{\mu\nu}^A i (\bar{q}_R^i T^A \gamma^\mu D^\nu q_R^i)\,,
\end{aligned}
\tag{A.2}
$$

By *relevant* we mean those radiatively generated redundant operators that modify the Wilson coefficient of the operators in eq. (A.1) when the former operators are redefined into operators in our basis, defined in Section 2.1.

A.1   Anomalous dimension matrix

Below we present in three different tables the anomalous dimension matrix of the operators in eq. (A.1) as well as the relevant redundant operators generated by them, eq. (A.2), at the order stated in eq. (2.10). We work with arbitrary ξ in the background field gauge (see eq. (2.11)) and use dimensional regularization. All the contributions given in Tables A.1, A.2 and A.3 below arise from one-particle-irreducible Feynman diagrams, i.e. it is the one-loop renormalization of the Effective Action. We have defined

$$
\gamma_{c_i} = 16\pi^2 \frac{dc_i}{d\log\mu}\,, \quad \beta_g = \frac{dg}{d\log\mu}
\tag{A.3}
$$

and

$$
\gamma_H = -N_c y_t^2 + \frac{1}{4}\left(3[3 - \xi_W]g^2 + [3 - \xi_B]g'^2\right)\,, \quad \gamma_W = -\frac{1}{g}\beta_g = \left(\frac{43}{6} - \frac{4}{3}N_G\right)g^2\,,
$$
$$
\gamma_G = -\frac{1}{g_s}\beta_{g_s} = \left(11 - \frac{4}{3}N_G\right)g_s^2\,, \quad \gamma_B = -\frac{1}{g'}\beta_{g'} = \left(-\frac{1}{6} - \frac{20}{9}N_G\right)g'^2\,,
\tag{A.4}
$$

in the background field gauge. $N_G = 3$ is the number of generations.

In Table A.1 we display the contributions of $\mathcal{O}_H$, $\mathcal{O}_r$ and $\mathcal{O}_T$ to the running of the Wilson coefficients of the operators in eq. (A.1). The contributions not shown are either zero or proportional to the Yukawa coupling y_l of any fermion lighter than the top. Notice that in Table A.1

	c_H	c_r	c_T
γ_{c_H}	$28\lambda + 12y_t^2 - 3\left(\frac{5}{2}g^2 + g'^2\right)$	$\frac{3}{2}\left(2g^2 + g'^2\right) - 4\lambda$	$8\lambda - 6g^2 - \frac{3}{2}g'^2$
γ_{c_T}	$\frac{3}{2}g'^2$	$-\frac{3}{2}g'^2$	$12\lambda + 12y_t^2 + \frac{9}{2}g^2$
γ_{c_B}	$-\frac{1}{3}$	$\frac{1}{3}$	$-\frac{5}{3}$
γ_{c_W}	$-\frac{1}{3}$	$\frac{1}{3}$	$-\frac{1}{3}$
γ_{c_r}	$4\lambda - 3g^2$	$20\lambda + 12y_t^2 - \frac{3}{2}\left(g^2 + g'^2\right)$	$-4\lambda + 3g^2 - 6g'^2$

Table A.1: Anomalous dimension matrix. Further contributions of $\mathcal{O}_H$, $\mathcal{O}_r$ and $\mathcal{O}_T$ to other operators in eq. (A.1) and eq. (A.2) are either zero or proportional to the Yukawa coupling of any fermion lighter than the top. The dashed line separates the anomalous dimension of the operators in our basis from that of the redundant operators.

	c_{BB}	c_{WW}	c_{WB}	c_{3W}
γ_{c_H}	$6g'^4$	$18g^4$	$6g'^2 g^2$	0
γ_{c_T}	0	0	0	0
γ_{c_B}	0	0	0	0
γ_{c_W}	0	0	0	$2g^2$
$\gamma_{c_{2B}}$	0	0	0	0
$\gamma_{c_{2W}}$	0	0	0	$4g^2$
$\gamma_{c_{BB}}$	$\frac{g'^2}{2} - \frac{9g^2}{2} + 6y_t^2 + 12\lambda$	0	$3g^2$	0
$\gamma_{c_{WW}}$	0	$-\frac{3g'^2}{2} - \frac{5g^2}{2} + 6y_t^2 + 12\lambda$	g'^2	$\frac{5}{2}g^2$
$\gamma_{c_{WB}}$	$2g'^2$	$2g^2$	$-\frac{g'^2}{2} + \frac{9g^2}{2} + 6y_t^2 + 4\lambda$	$-\frac{g^2}{2}$
$\gamma_{c_{3W}}$	0	0	0	$24g^2 - 2\gamma_W$
γ_{c_r}	$6g'^4$	$18g^4$	$6g'^2 g^2$	0
$\gamma_{c_{WL}^{Q,L}}$	0	0	0	g^2

Table A.2: Anomalous dimension matrix. Further contributions of $\mathcal{O}_{BB}, \mathcal{O}_{WW}, \mathcal{O}_{WB}$ and $\mathcal{O}_{3W}$ to other operators in eq. (A.1) and eq. (A.2) are either zero or proportional to the Yukawa coupling of fermions lighter than the top. The dashed line separates the anomalous dimension of the operators in our basis from that of the redundant operators.

	c_B	c_W	c_{2B}	c_{2W}
γ_{c_H}	$\frac{3}{4}g'^2\left(g'^2+4g^2\right)$	$\frac{3}{4}g^2\left(3g^2+4g'^2\right)-6\lambda g^2$	$-\frac{3}{8}g'^2\left(g'^2+4g^2\right)$	$-\frac{3}{8}g^2\left(g^2(3+2\xi_W)+4g'^2\right)+3\lambda g^2$
γ_{c_T}	$-\frac{9}{4}g'^2g^2-6\lambda g'^2$	$-\frac{9}{4}g'^2g^2$	$\frac{9}{8}g'^2g^2+3\lambda g'^2$	$\frac{9}{8}g'^2g^2$
γ_{c_B}	$\frac{g'^2}{6}+6y_t^2$	$\frac{g^2}{2}$	$-\frac{g'^2}{12}$	$-\frac{g^2}{4}$
γ_{c_W}	$\frac{g'^2}{6}$	$\frac{11}{2}g^2+6y_t^2$	$-\frac{g'^2}{12}$	$-g^2\left(\frac{1}{4}+3\xi_W\right)$
$\gamma_{c_{2B}}$	$-\frac{2}{3}g'^2$	0	$-2\gamma_B$	0
$\gamma_{c_{2W}}$	0	$-\frac{2}{3}g^2$	0	$g^2\left(\frac{59}{3}-3\xi_W\right)-2\gamma_W$
$\gamma_{c_{BB}}$	0	0	0	0
$\gamma_{c_{WW}}$	0	0	0	0
$\gamma_{c_{WB}}$	0	0	0	0
$\gamma_{c_{3W}}$	0	0	0	0
γ_{c_r}	$\frac{3}{2}g'^2\left(2g'^2-g^2\right)+6\lambda g'^2$	$\frac{3}{2}g^2\left(6g^2-g'^2\right)+30\lambda g^2$	$\frac{3}{4}g'^2\left(g^2-2g'^2\right)-3\lambda g'^2$	$-\frac{3}{4}g^2\left(2g^2(3-\xi_W)-g'^2\right)-15\lambda g^2$
$\gamma_{c_{K4}}$	$-g'^2$	$-3g^2$	$\frac{g'^2}{2}$	$\frac{3}{2}g^2$
$\gamma_{c_L^{(3)Q,L}}$	0	$\frac{3}{4}g^4$	0	$\frac{3}{4}g^4\xi_W$
$\gamma_{c_L^{Q,L}}$	0	0	0	0
$\gamma_{c_R^{u,d,e}}$	0	0	0	0
$\gamma_{c_{K3L}^{Q,L}}$	0	0	$-Y_F^2g'^2$	$-\frac{3}{4}g^2$
$\gamma_{c_{K3R}^{u,d,e}}$	0	0	$-Y_f^2g'^2$	0
$\gamma_{c_{WL}^{Q,L}}$	$\mathcal{O}\left(y_i\right)$	$\mathcal{O}\left(y_i\right)$	$-\frac{5}{12}Y_F^2g'^2$	$-\frac{21}{16}g^2-\frac{3}{2}\xi_Wg^2$
$\gamma_{c_{BL}^{Q,L}}$	$\mathcal{O}\left(y_i\right)$	$\mathcal{O}\left(y_i\right)$	$-\frac{5}{6}Y_F^3g'^2$	$-Y_F\frac{5}{8}g^2$
$\gamma_{c_{BR}^{u,d,e}}$	$\mathcal{O}\left(y_i\right)$	$\mathcal{O}\left(y_i\right)$	$-\frac{5}{6}Y_f^3g'^2$	0
$\gamma_{c_{WL}'^{Q,L}}$	$\mathcal{O}\left(y_i\right)$	$\mathcal{O}\left(y_i\right)$	$-\frac{1}{2}Y_F^2g'^2$	$-\frac{3}{8}g^2$
$\gamma_{c_{BL}'^{Q,L}}$	$\mathcal{O}\left(y_i\right)$	$\mathcal{O}\left(y_i\right)$	$-Y_F^3g'^2$	$-\frac{3}{4}Y_Fg^2$
$\gamma_{c_{BR}'^{u,d,e}}$	$\mathcal{O}\left(y_i\right)$	$\mathcal{O}\left(y_i\right)$	$-Y_f^3g'^2$	0
$\gamma_{c_{LL}^{(3)F}}$	0	0	$-\frac{3}{2}g^2(g'Y_F)^2$	$\frac{3}{8}g^2(g^2(1+\xi_W)-4(g'Y_F)^2)$
$\gamma_{c_{LL}^{F}}$	0	0	$-6(g'Y_F)^4$	$-\frac{9}{8}g^4$
$\gamma_{c_{RR}^{f}}$	0	0	$-6(g'Y_f)^4$	0

Table A.3: Contributions of the operators $\mathcal{O}_B, \mathcal{O}_W, \mathcal{O}_{2B}$ and $\mathcal{O}_{2W}$ to the anomalous dimension matrix of the operators in eq. (A.1) and eq. (A.2). By y_i we denote the Yukawa coupling of any fermion. The dashed line separates the anomalous dimension of the operators in our basis from that of the redundant operators.

	c_{2G}	c_{GG}	c_{3G}	c_{2B}	c_{2W}
$\gamma_{c_{2G}}$	$\frac{1}{2}g_s^2(59-9\xi_G)-2\gamma_G$	0	$6g_s^2$	0	0
$\gamma_{c_{GG}}$	0	$-\frac{3}{2}g'^2-\frac{9}{2}g^2+12\lambda+6y_t^2$	0	0	0
$\gamma_{c_{3G}}$	0	0	$36g_s^2-2\gamma_G$	0	0
$\gamma_{c_{RR}^{ud}}$	$-12g_s^2(g'^2Y_uY_d)$	0	0	$-12(g'^2Y_uY_d)^2$	0
$\gamma_{c_{RR}^{(8)ud}}$	$\frac{1}{2}g_s^4(9\xi_G-1)$	0	0	$-12g_s^2(g'^2Y_uY_d)$	0
$\gamma_{c_{K3L}^Q}$	$-\frac{4}{3}g_s^2$	0	0	Table A.3	Table A.3
$\gamma_{c_{K3R}^{u,d}}$	$-\frac{4}{3}g_s^2$	0	0	Table A.3	0
$\gamma_{c_{GR}^{u,d}}$	$-g_s^2(\frac{9}{2}\xi_G+\frac{37}{9})$	0	$3g_s^2$	$-\frac{5}{6}(g'Y_{u,d})^2$	0
$\gamma_{c_{GL}^Q}$	$-g_s^2(\frac{9}{2}\xi_G+\frac{37}{9})$	0	$3g_s^2$	$-\frac{5}{6}(g'Y_Q)^2$	$-\frac{5}{8}g^2$
$\gamma_{c_{WL}^Q}$	$-\frac{5}{9}g_s^2$	0	0	Table A.3	Table A.3
$\gamma_{c_{BL}^Q}$	$-\frac{10}{9}g_s^2Y_Q$	0	0	Table A.3	Table A.3
$\gamma_{c_{BR}^{u,d}}$	$-\frac{10}{9}g_s^2Y_{u,d}$	0	0	Table A.3	0
$\gamma_{c_{GR}^{\prime u,d}}$	$-\frac{4}{3}g_s^2$	0	0	$-(g'Y_{u,d})^2$	0
$\gamma_{c_{GL}^{\prime Q}}$	$-\frac{4}{3}g_s^2$	0	0	$-(g'Y_Q)^2$	$-\frac{3}{4}g^2$
$\gamma_{c_{WL}^{\prime Q}}$	$-\frac{2}{3}g_s^2$	0	0	Table A.3	Table A.3
$\gamma_{c_{BL}^{\prime Q}}$	$-\frac{4}{3}g_s^2Y_Q$	0	0	Table A.3	Table A.3
$\gamma_{c_{BR}^{\prime u,d}}$	$-\frac{4}{3}g_s^2Y_{u,d}$	0	0	Table A.3	0

Table A.4: Contributions of the operators $\mathcal{O}_{2G},\mathcal{O}_{GG},\mathcal{O}_{3G},\mathcal{O}_{2B}$ and $\mathcal{O}_{2W}$ to the anomalous dimension of the operators in eq. (A.1) and eq. (A.2). The dashed line separates the anomalous dimension of the operators in our basis from that of the redundant operators.

we have gone beyond the strictly necessary computations to obtain the anomalous dimension matrix and also included the contributions of the operator $\mathcal{O}_r$, that is redundant with respect to our basis; their contributions can be used for an important crosscheck, described in Appendix B of ref. [4].

In Table A.2 we show the contributions of $\mathcal{O}_{BB}, \mathcal{O}_{WW}, \mathcal{O}_{WB}$ and $\mathcal{O}_{3W}$ to the running of the operators in eq. (A.1). The c_{3W} self-renormalization has been extracted from the result of ref. [69]. The contributions of these operators to the running of the redundant ones in eq. (A.2) that we have not written are either zero or proportional to light fermion Yukawas y_l.

Lastly, in Table A.3 we show the contributions of $\mathcal{O}_B, \mathcal{O}_W, \mathcal{O}_{2B}$ and $\mathcal{O}_{2W}$ to the running of any of the operators in eq. (A.1) and eq. (A.2). We have indicated by $\mathcal{O}\left(y_l\right)$ those contributions that *at most* are expected to be proportional to the Yukawa coupling of a fermion lighter than the top. As can be noted from Table A.3, the contribution of $\mathcal{O}_{2W}$ to the running of $\mathcal{O}_H$, $\mathcal{O}_r$, $\mathcal{O}_W$, $\mathcal{O}_{2W}$, $O_L^{(3)F_i}$, $\mathcal{O}_{WL}^{F_i}$ and $\mathcal{O}_{LL}^{(3)F_i}$ is ξ-dependent. In section A.2 we show that upon redefining the redundant operators in terms of operators in our basis the ξ dependence vanishes.

Table A.4 reports the contributions of $\mathcal{O}_{2G}, \mathcal{O}_{GG}, \mathcal{O}_{3G}, \mathcal{O}_{2B}$ and $\mathcal{O}_{2W}$ to the anomalous dimension of the (redundant) operators in eq. (A.1) and eq. (A.2), as needed to derive the anomalous dimension matrix of the dim-6 bosonic operators with gluons of our basis (see Table 2.7).

A.2   Removal of the radiatively-generated redundant operators

Let us now discuss how to deal with each operator in eq. (A.2) and their effect on the operators of eq. (A.1). The easiest way to deal with the redundant operator $\mathcal{O}_{BR}'^{f_i} = g'\widetilde{B}_{\mu\nu}i\bar{f}_R^i\gamma^\mu D^\nu f_R^i$ [57] is by means of the identity[1]

$$\gamma^\mu\gamma^\nu\gamma^\rho = g^{\mu\nu}\gamma^\rho + g^{\nu\rho}\gamma^\mu - g^{\mu\rho}\gamma^\nu + i\epsilon^{\mu\nu\rho\sigma}\gamma_\sigma\gamma^5\,; \tag{A.5}$$

one finds

$$\begin{aligned}
g'\widetilde{B}_{\mu\nu}\bar{f}_R\gamma^\mu iD^\nu f_R &= \frac{g'}{4}\bar{f}_R i\left(\gamma_\mu\gamma_\nu\slashed{D} + \overleftarrow{\slashed{D}}\gamma_\mu\gamma_\nu\right)f_R g'\widetilde{B}^{\mu\nu} \\
&+ ig'\bar{f}_R\gamma_\rho\gamma_\mu\gamma_\nu f_R D^\rho\widetilde{B}^{\mu\nu}\,.
\end{aligned} \tag{A.6}$$

Then, using the fermion's EoM

$$\begin{aligned}
\frac{g'}{4}\bar{f}_R i\left(\gamma_\mu\gamma_\nu\slashed{D} + \overleftarrow{\slashed{D}}\gamma_\mu\gamma_\nu\right)f_R g'\widetilde{B}^{\mu\nu} &= \frac{1}{4}g'y_f i\bar{F}_L\sigma_{\mu\nu}f_R Hg'\widetilde{B}^{\mu\nu} + \text{h.c.} \\
&= \frac{1}{4}g'y_f\bar{F}_L\sigma_{\mu\nu}f_R Hg'B^{\mu\nu} + \text{h.c.} \equiv \frac{1}{4}\mathcal{O}_{DB}^f\,, \tag{A.7}
\end{aligned}$$

---

[1]We use the conventions of *Peskin & Schroeder* textbook.

which is a *dipole* operator, where $\sigma^{\mu\nu} \equiv \frac{i}{2}[\gamma^\mu, \gamma^\nu]$; using again eq. (A.5) in the second term of the right hand side of eq. (A.6)

$$ig'\bar{f}_R\gamma_\rho\gamma_\mu\gamma_\nu f_R D^\rho \widetilde{B}^{\mu\nu} \;\; = \;\; 2g'\bar{f}_R\gamma_\sigma f_R D_\rho B^{\sigma\rho} = 2\mathcal{O}^f_{BR}\,. \tag{A.8}$$

Therefore, Eqs. (A.6)-(A.8) and analogous manipulations, are equivalent to the following shifts $(c_i \to c_i + \delta c_i)$ in the following Wilson coefficients:

$$\delta c^F_{WL} = 2c'^F_{WL}\,, \quad \delta c^F_{BL} = 2c'^F_{BL}\,, \quad \delta c^f_{BR} = 2c'^f_{BR}, \quad \delta c^Q_{GL} = 2c'^Q_{GL}, \quad \delta c^q_{GR} = 2c'^q_{GR}\,. \tag{A.9}$$

The Wilson coefficient of the dipole operators are also shifted, see eq. (A.7), however, we can not conclude that the dipoles are renormalized by the set of bosonic operators we considered because we did not compute direct contributions, those coming from one-particle-irreducible diagrams.

Then, for the operator $\mathcal{O}^{f_i}_{K3R}$, consider the field redefinition $\delta f_i = -\frac{c^{f_i}_{K3R}}{2\Lambda^2}D^2 f_i$, that removes $\mathcal{O}^{f_i}_{K3R}$ from the Lagrangian while generates the operator

$$-\frac{c^{f_i}_{K3R}y_{f_i}}{2\Lambda^2}D_\mu\bar{F}_{iL}D^\mu\left(f_{iR}H\right) + \text{h.c.} = -\frac{c^{f_i}_{K3R}y_{f_i}}{2\Lambda^2}[D_\mu\bar{F}_{iL}\gamma^\mu\gamma^\nu D^\nu\left(f_{iR}H\right)$$
$$-\frac{1}{2}\bar{F}_{iL}X_{\mu\nu}\sigma^{\mu\nu}f_{iR}H + \text{h.c.}]\,, \tag{A.10}$$

where $X_{\mu\nu} = g'Y_{F_i}B_{\mu\nu} + gW^a_{\mu\nu}\tau^a + g_sG^A_{\mu\nu}T^a$, being τ^a and T^A the $SU(2)_L$ and $SU(3)_c$ generators in the fundamental representation, respectively. Then, by inserting the fermion's EoM in the first operator in the right hand side of eq. (A.10) one gets operators of the type $\mathcal{L}_{\text{Yuk}}|H|^2$ and the operator $y_{f_i}\mathcal{O}^{f_i}_R \equiv y_{f_i}i(H^\dagger\overset{\leftrightarrow}{D}_\mu H)\bar{f}^i_R\gamma^\mu f^i_R$; we do not care about the latter (proportional to y_{f_i}) since our basis choice of Section 2.1 was to remove the operator $\mathcal{O}^{f_i}_R$ corresponding to a light fermion. Performing an analogous analysis for $\mathcal{O}^{F_i}_{K3L}$ we reach the same conclusion: neither of the two operator's scaling affects the anomalous dimension of the set of bosonic operators in eq. (A.1). As in the case of $\mathcal{O}'_{WL,BL,BR}$, the same comment applies here: even-though the Wilson coefficient of the dipoles is shifted by the above manipulations, we do not conclude that they are renormalized by the bosonic operators.

Now, the remaining operators are redefined into our basis by performing field redefinitions as showed in eq. (2.3). Consider the 37 independent field redefinitions

$$\Lambda^2\delta G^A_\mu = \alpha_{2G}(D^\nu G^A_{\mu\nu}) + g_S\sum_i \alpha^i_{QG}\bar{Q}^i_L T^A\gamma_\mu Q^i_L + g_S\sum_{i,q}\alpha^i_{qG}\bar{q}^i_R T^A\gamma_\mu q^i_R,\,,$$

$$\Lambda^2\delta W^a_\mu = ig\alpha_W(H^\dagger\sigma^a\overset{\leftrightarrow}{D^\mu}H) + \alpha_{2W}(D^\nu W^a_{\mu\nu}) + g\sum_{i,F}\alpha^i_{FW}\bar{F}^i_L\sigma^a\gamma_\mu F^i_L,$$

$$\Lambda^2\delta B_\mu = ig'\alpha_B(H^\dagger\overset{\leftrightarrow}{D^\mu}H) + \alpha_{2B}(\partial^\nu B_{\mu\nu}) + g'\sum_{i,F}Y_F\alpha^i_{FB}\bar{F}^i_L\gamma_\mu F^i_L + g'\sum_{i,f}Y_f\alpha^i_{fB}\bar{f}^i_R\gamma_\mu f^i_R,$$

$$\Lambda^2\delta H = \alpha_1 H|H|^2 + \alpha_2\left((D^2 H) - y^{ij}_e\bar{e}^i_R L^j_L - y^{ij}_d\bar{d}^i_R Q^j_L - y^{ij}_u i\sigma^2(\bar{u}^i_R Q^j_L)^*\right),$$

$$\tag{A.11}$$

with $F = \{L, Q\}$, $f = \{e, d, u\}$, $q = \{d, u\}$ and $i = 1, 2, 3$. These generate the following shifts for the Wilson coefficients of the dimension 6 operators:

$$
\begin{aligned}
c_H &\to c_H + 2(\alpha_1 + 2\lambda\alpha_2) - \alpha_W g^2 & c_r &\to c_r + 2(\alpha_1 + 2\lambda\alpha_2) + \alpha_W g^2 \\
c_T &\to c_T - \alpha_B g'^2 & c_{K4} &\to c_{K4} - 2\alpha_2 \\
c_B &\to c_B + \alpha_{2B} - 2\alpha_B & c_{WL}^{F_i} &\to c_{WL}^{F_i} + \tfrac{1}{2}\alpha_{2W} - \alpha_{FW}^i \\
c_W &\to c_W + \alpha_{2W} - 2\alpha_W & c_{BL}^{F_i} &\to c_{BL}^{F_i} + Y_F(\alpha_{2B} - \alpha_{FB}^i) \\
c_{2B} &\to c_{2B} + 2\alpha_{2B} & c_{BR}^{f_i} &\to c_{BR}^{f_i} + Y_f(\alpha_{2B} - \alpha_{fB}^i) \\
c_{2W} &\to c_{2W} + 2\alpha_{2W} & c_{LL}^{(3)F_i} &\to c_{LL}^{(3)F_i} + \tfrac{g^2}{2}\alpha_{FW}^i \\
c_{2G} &\to c_{2G} + 2\alpha_{2G} & c_{LL}^{F_i} &\to c_{LL}^{F_i} + (Y_F g')^2\alpha_{FB}^i \\
c_6 &\to c_6 - 4\alpha_1 & c_{RR}^{f_i} &\to c_{RR}^{f_i} + (Y_f g')^2\alpha_{fB}^i \\
c_{y_f}^i &\to c_{y_f}^i - \alpha_1 + 2\lambda\alpha_2 & c_{LR}^{F_i f_j} &\to c_{LR}^{F_i f_j} + (Y_F Y_f g'^2)(\alpha_{fB}^i + \alpha_{FB}^i) \\
c_{y_f y_f}^{ij} &\to c_{y_f y_f}^{ij} + 2\alpha_2 & c_L^{(3)F_i} &\to c_L^{(3)F_i} + \tfrac{g^2}{2}(\alpha_W + \alpha_{FW}^i) \\
c_{RR}^{u^i d^j} &\to c_{RR}^{u^i d^j} + g'^2 Y_u Y_d(\alpha_{uB}^i + \alpha_{dB}^j) & c_L^{F_i} &\to c_L^{F_i} + Y_F g'^2(\alpha_B + \tfrac{1}{2}\alpha_{FB}^i) \\
& & c_R^{f_i} &\to c_R^{f_i} + Y_f g'^2(\alpha_B + \tfrac{1}{2}\alpha_{fB}^i) \\
& & c_{GL,R}^{q_i} &\to c_{GL,R}^{q_i} + \alpha_{2G} - \alpha_{qG}^i \quad \text{for } q = Q, u, d \\
& & c_{RR}^{(8)u^i d^j} &\to c_{RR}^{(8)u^i d^j} + g_s^2(\alpha_{uG}^i + \alpha_{dG}^j).
\end{aligned}
\tag{A.12}
$$

Notice that using Fierz identities we can always trade the operator $\mathcal{O}_{LL}^{F_i}$ for $\mathcal{O}_{LL}^{(3)F_i}$: $\mathcal{O}_{LL}^{F_i} = \mathcal{O}_{LL}^{(3)F_i}$. This means that the shift in $c_{LL}^{F_i}$ can be recast as a shift in $c_{LL}^{(3)F_i}$, which becomes:

$$
c_{LL}^{(3)F_i} \to c_{LL}^{(3)F_i} + \frac{g^2}{2}\alpha_{FW}^i + \left(c_{LL}^{F_i} + (Y_F g')^2\alpha_{FB}^i\right).
\tag{A.13}
$$

We use the freedom given by the field redefinitions to set to zero the following 37 coefficients: $c_r, c_{K4}, c_{LL}^{(3)L_1}, c_{RR}^{e_1}, c_L^{(3)L_1}, c_R^{e_1}, c_{WL}^{F_i}, c_{BL}^{F_i}, c_{BR}^{f_i}, c_{GL}^{Q_i}, c_{GR}^{u_i}, c_{GR}^{d_i}, c_{RR}^{(8)u^1 d^1}$. This fixes all the shift parameters α_i and gives shift invariant combinations, under eq. (A.12), of the Wilson coefficients

of the operators in our basis:

$$c_H \to c_H - c_r + 6(c_L^{(3)L_1} - \tilde{c}_{LL}^{(3)L_1}) \,,$$

$$c_T \to c_T + \frac{1}{Y_e}(c_R^{e_1} - \frac{1}{2Y_e}c_{RR}^{e_1}) \,,$$

$$c_W \to c_W - 2c_{WL}^{L_1} - 4c_{WL}^{\prime L_1} + \frac{4}{g^2}(c_L^{(3)L_1} - 2\tilde{c}_{LL}^{(3)L_1}) \,,$$

$$c_B \to c_B - \frac{1}{Y_e}c_{BR}^{e_1} - \frac{2}{Y_e}c_{BR}^{\prime e_1} + \frac{2}{Y_e g^{\prime 2}}(c_R^{e_1} - \frac{1}{Y_e}c_{RR}^{e_1}) \,,$$

$$c_{2W} \to c_{2W} - 4c_{WL}^{L_1} - 8c_{WL}^{\prime L_1} - \frac{8}{g^2}\tilde{c}_{LL}^{(3)L_1} \,,$$

$$c_{2B} \to c_{2B} - \frac{2}{Y_e}c_{BR}^{e_1} - \frac{4}{Y_e}c_{BR}^{\prime e_1} - \frac{2}{Y_e^2 g^{\prime 2}}c_{RR}^{e_1} \,,$$

$$c_6 \to c_6 + 2c_r + 4\lambda c_{K4} - 8(c_L^{(3)L_1} - \tilde{c}_{LL}^{(3)L_1}) \,,$$

$$c_{2G} \to c_{2G} - c_{GR}^{d_1} - 2c_{GR}^{\prime d_1} - c_{GR}^{u_1} - 2c_{GR}^{\prime u_1} - \frac{1}{g_s^2}c_{RR}^{(8)u^1 d^1} \,,$$

(A.14)

where

$$\tilde{c}_{LL}^{(3)L_1} = c_{LL}^{(3)L_1} + c_{LL}^{F_1} + g^{\prime 2}Y_L \left(c_{BL}^{L_1} + 2c_{BL}^{\prime L_1} - \frac{Y_L}{Y_e}(c_{BR}^{e_1} + 2c_{BR}^{\prime e_1} + \frac{1}{g^{\prime 2}Y_e}c_{RR}^{e_1}) \right)$$

(A.15)

and eq. (A.9) has already been taken into account. This completes the removal of the operators in eq. (A.2) in terms of the bosonic operators. After these shifts, the anomalous dimensions of the operators in eq. (A.1) are redefined as

$$\gamma_{c_H} \to \gamma_{c_H} - \gamma_{c_r} + 6(\gamma_{c_L^{(3)L_1}} - \tilde{\gamma}_{c_{LL}^{(3)L_1}}) \,,$$

$$\gamma_{c_T} \to \gamma_{c_T} + \frac{1}{Y_e}(\gamma_{c_R^{e_1}} - \frac{1}{2Y_e}\gamma_{c_{RR}^{e_1}}) \,,$$

$$\gamma_{c_W} \to \gamma_{c_W} - 2\gamma_{c_{WL}^{L_1}} - 4\gamma_{c_{WL}^{\prime L_1}} + \frac{4}{g^2}(\gamma_{c_L^{(3)L_1}} - 2\tilde{\gamma}_{c_{LL}^{(3)L_1}}) \,,$$

$$\gamma_{c_B} \to \gamma_{c_B} - \frac{1}{Y_e}\gamma_{c_{BR}^{e_1}} - \frac{2}{Y_e}\gamma_{c_{BR}^{\prime e_1}} + \frac{2}{Y_e g^{\prime 2}}(\gamma_R^{e_1} - \frac{1}{Y_e}\gamma_{c_{RR}^{e_1}}) \,,$$

$$\gamma_{c_{2W}} \to \gamma_{c_{2W}} - 4\gamma_{c_{WL}^{L_1}} - 8\gamma_{c_{WL}^{\prime L_1}} - \frac{8}{g^2}\tilde{\gamma}_{c_{LL}^{(3)L_1}} \,,$$

$$\gamma_{c_{2B}} \to \gamma_{c_{2B}} - \frac{2}{Y_e}\gamma_{c_{BR}^{e_1}} - \frac{4}{Y_e}\gamma_{c_{BR}^{\prime e_1}} - \frac{2}{Y_e^2 g^{\prime 2}}\gamma_{c_{RR}^{e_1}} \,,$$

$$\gamma_{c_6} \to \gamma_{c_6} + 2\gamma_{c_r} + 4\lambda\gamma_{c_{K4}} - 8(\gamma_{c_L^{(3)L_1}} - \tilde{\gamma}_{c_{LL}^{(3)L_1}}) \,,$$

$$\gamma_{c_{2G}} \to \gamma_{c_{2G}} - \gamma_{c_{GR}^{d_1}} - \gamma_{c_{GR}^{\prime d_1}} - \gamma_{c_{GR}^{u_1}} - \gamma_{c_{GR}^{\prime u_1}} - \frac{1}{g_s^2}\gamma_{c_{RR}^{(8)u^1 d^1}} \,,$$

(A.16)

where

$$\tilde{\gamma}_{c_{LL}^{(3)L_1}} = \gamma_{c_{LL}^{(3)L_1}} + \gamma_{c_{LL}^{F_1}} + g^{\prime 2}Y_L \left(\gamma_{c_{BL}^{L_1}} + 2\gamma_{c_{BL}^{\prime L_1}} - \frac{Y_L}{Y_e}(\gamma_{c_B R^{e_1}} + 2\gamma_{c_{BR}^{\prime e_1}} + \frac{1}{g^{\prime 2}Y_e}\gamma_{c_{RR}^{e_1}}) \right).$$

(A.17)

The remaining bosonic operators, not of the CC type, are not affected by these field redefinitions and therefore their anomalous dimension is not affected. In this way we can go back to our original

basis taking into account that some operators are generated radiatively even if we set their Wilson coefficient to zero at the matching scale. In the main body of the thesis, Tables 2.4 and 2.7, we give the physical anomalous dimensions obtained using the right hand side of eq. (A.16). As expected, the ξ-dependence cancels out in the physical combinations of γ_{c_i}'s, which can be easily checked using eq. (A.16).

APPENDIX B

Non-linear realizations of a global symmetry

In refs. [134, 135], Callan, Coleman, Wess and Zumino showed how to build effective chiral Lagrangians able to describe the low-energy dynamics of NGBs of a generic global symmetry breaking $\mathcal{G} \to \mathcal{H}$. Here we review some basic aspects of this approach following closely the presentation of ref. [228].

Let us assume that the theory is invariant under transformations of a global symmetry group $\mathcal{G}$, and that this symmetry is spontaneously broken to a subgroup $\mathcal{H}$. This means that $\mathcal{H}$ is the group of transformations h which leave the vacuum invariant,

$$h \langle \Phi \rangle = \langle \Phi \rangle \ , \tag{B.1}$$

where $\Phi = \{\phi_1, \phi_2 \ldots \phi_N\}$ includes all the fields in the theory which belong, in general, to some reducible representation of $\mathcal{G}$. For non-scalar fields of course $\langle \phi_n \rangle = 0$ by Lorentz invariance.

Let us now remove from $\Phi(x)$ the NGB degrees of freedom by defining

$$\Phi_n(x) = U_{nm}(x)\tilde{\Phi}_m(x) \ , \tag{B.2}$$

where $U(x) \in \mathcal{G}$. Eq. (B.2) ensures that the transformation $U(x)$ is universal for all fields in the theory. Since the NGBs are aligned along some linear combinations of the $T^{\hat{a}}_{nm}\langle \Phi_m \rangle$ vectors, the condition $\tilde{\Phi}$ needs to satisfy in order not to contain NGBs is

$$\tilde{\Phi}_n(x)T^{\hat{a}}_{nm}\langle \Phi_m \rangle = 0 \ . \tag{B.3}$$

These are N_{NGB} independent equations, where N_{NGB} is the number of broken generators $T^{\hat{a}}$, $N_{\mathrm{NGB}} = \dim(\mathcal{G})$ - dim $(\mathcal{H})$, i.e. the number of Nambu-Goldstone bosons. Since the theory is invariant under global $\mathcal{G}$ transformations, the matrix $U(x)$ will enter only via its derivatives.

Let us now show that it is always possible to choose $U(x)$ so that eq. (B.3) is satisfied. Given a field configuration Φ, let us consider the function of a group transformation $g \in \mathcal{G}$ defined as

$$V_\Phi(g) = \Phi_n g_{nm}\langle \Phi_m \rangle, \tag{B.4}$$

which is continuos and limited since $\mathcal{G}$ is compact. This implies that for any given x, $V_{\Phi(x)}(g)$ has a maximum corresponding to some group element $U(x) \in \mathcal{G}$, therefore V is stationary in that point. Given the group element U, a nearby element is given by

$$U' = U + \delta U = U(1 + i\epsilon^\alpha T^\alpha) = U + i\epsilon^\alpha U T^\alpha, \tag{B.5}$$

that is $\delta U = i\epsilon^\alpha U T^\alpha$. The variation of $V_{\Phi(x)}(U(x))$ is

$$\delta V_{\Phi(x)}(U(x)) = i\epsilon^\alpha \Phi_n(x) U_{nl}(x) T^\alpha_{lm} \langle \Phi_m \rangle = i\epsilon^\alpha U^T_{ln}(x) \Phi_n(x) T^\alpha_{lm} \langle \Phi_m \rangle \equiv 0. \tag{B.6}$$

Since this should hold $\forall \epsilon^\alpha$ and since $U^T = U^{-1}$, we get

$$U^{-1}_{ln}(x) \Phi_n(x) T^\alpha_{lm} \langle \Phi_m \rangle = 0, \tag{B.7}$$

that is, comparing with (B.2), we obtained $\tilde{\Phi}(x) = U^{-1}(x)\Phi(x)$.

Let us now find how to parametrize $U(x)$. First of all, the choice of the matrix U is not unique: since the vacuum expectation value of the fields is $\mathcal{H}$-invariant by hypothesis, the function (B.4) is invariant under a right-multiplication by $h \in \mathcal{H}$:

$$V_\Phi(g) = V_\Phi(gh). \tag{B.8}$$

Therefore, if $U(x)$ is a stationary value for V_Φ, then also $U(x)h$ is such $\forall h \in \mathcal{H}$. It follows that the elements of $\mathcal{G}$ can be divided in *equivalence classes*, where $U_1, U_2 \in \mathcal{G}$ are equivalent if $\exists\, h \in \mathcal{H}$ such that $U_1 = U_2 h$. It is possible to verify that this is indeed an equivalence relation, being reflective, symmetric and transitive. These classes are known as *laterals* of $\mathcal{G}$ with respect to $\mathcal{H}$, the space of these laterals is $\mathcal{G}/\mathcal{H}$. Parametrizing this space is the same as choosing a particular representative for all equivalent classes. In general, it is always possible to write any element of G as

$$g = e^{i\theta^{\hat{a}} T^{\hat{a}}} e^{i\theta^a T^a}. \tag{B.9}$$

Since $U(x)$ is defined up to a right-multiplication by h, it is possible to choose the representative for each lateral of $\mathcal{G}/\mathcal{H}$ as

$$U(x) = e^{i\xi^{\hat{a}}(x) T^{\hat{a}}}, \tag{B.10}$$

where the n $\xi^{\hat{a}}(x)$ are, up to some normalization factor, the NGBs.

Let us now study how the fields $\xi^{\hat{a}}(x)$ and $\tilde{\Phi}(x)$ transform under a $g \in \mathcal{G}$ transformation. Since Φ trasforms linearly according to its representation, we have:

$$\Phi'(x) = g\Phi(x) = gU(\xi(x))\tilde{\Phi}(x), \tag{B.11}$$

where, with an abuse of notation, we call by g both the element of the group and the matrix of the associated transformation in the representation of Φ. For any x, since $U(\xi(x)) \in \mathcal{G}$, from

the definition of group follows that $\forall g \in \mathcal{G}$ also $gU(\xi(x)) \in \mathcal{G}$, therefore $gU(\xi(x))$ will belong to some lateral of $\mathcal{G}/\mathcal{H}$. Thus, we can write

$$gU(\xi(x)) = U(\xi'(x))h(\xi(x), g) \quad \rightarrow \quad U(\xi'(x)) = g\, U(\xi(x))\, h(\xi(x), g)^{-1}, \tag{B.12}$$

where $h(\xi(x), g)$ is a local $\mathcal{H}$ transformation, depending on $\xi(x)$ and g. We see that the transformation under $\mathcal{G}$ of the NGB is non-linear, since the transformation matrix $h(\xi(x), g)^{-1}$ depends on the $\xi(x)$ in a non-linear way. Substituting this expression in (B.11) we get

$$\Phi'(x) = g\Phi(x) = U(\xi'(x))h(\xi(x), g)\tilde{\Phi}(x) \equiv U(\xi'(x))\tilde{\Phi}'(x), \tag{B.13}$$

where

$$\tilde{\Phi}'(x) = h(\xi(x), g)\tilde{\Phi}(x). \tag{B.14}$$

The last equation implies that also the matter fields $\tilde{\Phi}$ transform non-linearly under $\mathcal{G}$ according to some $h \in \mathcal{H}$ matrix: a global $g \in \mathcal{G}$ transformation acts non-linearly on the matter fields as a local transformation under the unbroken group, $h(\xi(x), g) \in \mathcal{H}$.

In the particular case where the global transformation belongs to the unbroken group $\mathcal{H}$, let us show that it is always possible to choose the NGBs such that they transform linearly, that is they belong to some linear representation of $\mathcal{H}$. In fact if $g = h \in \mathcal{H}$, in (B.12) we can always choose a representative of the lateral such that $h(\xi, g) = h$. Using the property $Ae^B A^{-1} = e^{ABA^{-1}}$ we get

$$h\, e^{i\xi(x)}h^{-1} = e^{ih\xi(x)h^{-1}} \equiv e^{i\xi'(x)}, \tag{B.15}$$

from which follows the transformation law of the NGBs under $h \in \mathcal{H}$:

$$\xi'(x) = h\, \xi(x)\, h^{-1}. \tag{B.16}$$

Let us now start defining the structures needed to build our Lagrangians. Performing the substitution (B.2), from the terms with derivatives of Φ one gets:

$$\partial_\mu \Phi(x) = \partial_\mu \left(U(x)\tilde{\Phi}(x)\right) = U(x)\left[\partial_\mu \tilde{\Phi}(x) + \left(U^{-1}(x)\partial_\mu U(x)\right)\tilde{\Phi}(x)\right], \tag{B.17}$$

where the NGB appear in the anti-Hermitian combination $U^\dagger(x)\partial_\mu U(x)$. In general, since this structure belongs to the algebra, it is possible to decompose it in linear combinations of broken and unbroken generators:

$$U^\dagger(x)\partial_\mu U(x) = id_\mu^{\hat{a}}T^{\hat{a}} + iE_\mu^a T^a. \tag{B.18}$$

From eq. (B.12) follows the transformation laws of the terms in eq. (B.18) under $g \in \mathcal{G}$:

$$U^{-1}(\xi')\partial_\mu U(\xi') = h(\xi, g)\left[U(\xi)^{-1}\partial_\mu U(\xi)\right]h(\xi, g)^{-1} - [\partial_\mu h(\xi, g)]\, h^{-1}(\xi, g). \tag{B.19}$$

In terms of the $d^{\hat{a}}_{\mu}$ and E^a_{μ} structures defined in (B.18), this transformation is equivalent to

$$
\begin{aligned}
d'_{\mu} &= h(\xi, g) d_{\mu} h^{-1}(\xi, g); &\text{(B.20)} \\
E'_{\mu} &= h(\xi, g) E_{\mu} h^{-1}(\xi, g) + i \left[\partial_{\mu} h(\xi, g) \right] h^{-1}(\xi, g),
\end{aligned}
$$

in particular E_{μ} transforms as a gauge field. From eq. (B.14) follows that the derivative of $\tilde{\Phi}$ transforms according to

$$
\partial_{\mu} \tilde{\Phi}' = (\partial_{\mu} h) \tilde{\Phi} + h \partial_{\mu} \tilde{\Phi} = h \left(\partial_{\mu} + h^{-1} \partial_{\mu} h \right) \tilde{\Phi}. \tag{B.21}
$$

This motivates the introduction of the covariant derivative

$$
\nabla_{\mu} \equiv \partial_{\mu} + i E_{\mu}(x), \tag{B.22}
$$

such that $\nabla'_{\mu} \tilde{\Phi}' = h(\xi, g)(\nabla_{\mu} \tilde{\Phi})$. Analogously to gauge fields, with $E_{\mu}(\xi(x))$ it is possible to define

$$
E_{\mu\nu} = \partial_{\nu} E_{\mu} - \partial_{\mu} E_{\nu} - i[E_{\mu}, E_{\nu}], \tag{B.23}
$$

which transforms non-linearly under $g \in \mathcal{G}$ according to

$$
E'_{\mu\nu} = h(\xi, g) \, E_{\mu\nu} \, h^{-1}(\xi, g). \tag{B.24}
$$

A Lagrangian written in terms of the $\tilde{\Phi}$, $\nabla_{\mu} \tilde{\Phi}$, $E_{\mu\nu}$ and d_{μ} structures, invariant under local $\mathcal{H}$ transformations, will also be invariant under global $\mathcal{G}$ transformations, which would be non-linearly realized.

B.1   Approximate symmetry

In many applications, such as those relevant for the QCD chiral Lagrangian and for composite Higgs models, the symmetry under $\mathcal{G}$ transformation is not exact, but only approximate. In other words, there exist a term in the Lagrangian, suppressed by some small parameter (for example quark mass terms m_q/f_{π}, gauge couplings or fermion mixing terms ϵ/f), which is not invariant under these transformations.

Let us consider the case in which the breaking term in the Lagrangian, $\Delta\mathcal{L}$, is not invariant under $\mathcal{G}$ but transforms as some linear representation of $\mathcal{G}$. This amounts to give some spurionic transformation properties under $\mathcal{G}$ to the symmetry breaking terms.

$$
\Delta\mathcal{L} = c_A \mathcal{O}_A, \tag{B.25}
$$

where $\mathcal{O}_A = \mathcal{O}_A(\Phi(x))$ are operators which transform under $g \in \mathcal{G}$ according to some representation $D[g]$:

$$
\mathcal{O}_A \xrightarrow{g} D[g]_{AB} \mathcal{O}_B. \tag{B.26}
$$

Substituting $\Phi(x)$ with $U(\xi(x))\tilde{\Phi}(x)$, this transformation becomes

$$\mathcal{O}_A[\xi, \tilde{\Phi}] \xrightarrow{g} \mathcal{O}_A[\xi', h(\xi, g)\tilde{\Phi}] = D[g]_{AB}\mathcal{O}_B[\xi, \tilde{\Phi}], \tag{B.27}$$

where $\xi' = \xi'(\xi, g)$ comes from $U(\xi'(\xi, g))h^{-1}(\xi, g) = gU(\xi)$ and eq. (B.10).

Let us now show how to build an operator which transform linearly according to eq. (B.26) from the fields $\tilde{\Phi}$ and ξ, which transform linearly under $\mathcal{H}$ but non-linearly under $\mathcal{G}$. In the $\xi = 0$ case let us take the transformation $g = U(\xi')$; since $U(\xi) = U(0) = 1$, from the transformation law for ξ we get that $gU(\xi) = g = U(\xi')$, that is $h(0, U(\xi')) = 1$ and $\xi'(0, U(\xi')) = \xi'$. Substituting these relations in eq. (B.27) one has

$$\mathcal{O}_A[\xi', \tilde{\Phi}] = D[U(\xi')]_{AB}\mathcal{O}_B[0, \tilde{\Phi}], \tag{B.28}$$

which shows how to include the ξ-dependence of the operator $\mathcal{O}_A$ starting from an operator defined only in terms of the $\tilde{\Phi}$ fields.

Considering now the case with $\xi = 0$ and $g = h \in \mathcal{H}$ we have that $gU(\xi) = g = h$, that is $h(0, h) = h$ and $U(\xi'(0, h)) = 1$, i.e. $\xi'(0, h) = \xi' = 0$. Substituting this result in eq. (B.27) we obtain

$$\mathcal{O}_A[0, h\tilde{\Phi}] = D[h]_{AB}\mathcal{O}_B[0, \tilde{\Phi}], \tag{B.29}$$

that is under a transformation $h \in \mathcal{H}$, if $\xi = 0$, then the operators $\mathcal{O}_A[0, \tilde{\Phi}]$ transform linearly according to the representation $D[h]_{AB}$.

Let us finally show that any operator satisfying eq. (B.29), can also satisfy eq. (B.26). Using eqs. (B.28) and (B.29) in eq. (B.27) we get

$$
\begin{aligned}
\mathcal{O}_A[\xi'(\xi, g), h(\xi, g)\tilde{\Phi}] &= D[U(\xi'(\xi, g))]_{AB}\mathcal{O}_B[0, h(\xi, g)\tilde{\Phi}] = \tag{B.30}\\
&= D[U(\xi'(\xi, g))]_{AB}D[h(\xi, g)]_{BC}\mathcal{O}_C[0, \tilde{\Phi}] = \\
&= D[U(\xi'(\xi, g))h(\xi, g)]_{AB}\mathcal{O}_B[0, \tilde{\Phi}] = D[gU(\xi)]_{AB}\mathcal{O}_B[0, \tilde{\Phi}] = \\
&= D[g]_{AB}D[U(\xi)]_{BC}\mathcal{O}_C[0, \tilde{\Phi}] = D[g]_{AB}\mathcal{O}_B[\xi, \tilde{\Phi}]
\end{aligned}
$$

q.e.d.

In summary, to obtain an operator $\mathcal{O}$ which transform linearly under $\mathcal{G}$ starting from an operator $\mathcal{O}[0, \tilde{\Phi}]$ defined in terms of the non-linearly transforming fields $\tilde{\Phi}$, which belong to $\mathcal{H}$ representation in eq. (B.29), it is enough to multiply it by the NGB matrix $U(\xi)$, written in the same representation $(D[U(\xi)])$, that is as in eq. (B.28).

This is exactly the construction we used to introduce the mixing terms between elementary and composite fermions Ψ in section 3.3.2. The latter belong to irreducible representations of $\mathcal{H}$ and we dressed those with the NGB matrix U in order to create an operator transforming linearly under $\mathcal{G}$: $\mathcal{O} = U\Psi$.

APPENDIX C

Non-analytic terms in the potential

For $s_h \ll 1$, the tree-level + one-loop potential $V = V^{(0)} + V^{(1)}$ admits an expansion of the form

$$V = -\gamma s_h^2 + \beta s_h^4 + \delta s_h^4 \log s_h + \mathcal{O}(s_h^6) \,. \tag{C.1}$$

The last non-analytic term cannot obviously be obtained by a Taylor expansion around $s_h = 0$. It arises at the one-loop level and is due to the contribution of particles whose mass vanishes for $s_h = 0$. In a naive expansion around $s_h = 0$, its presence would be detected by the appearance of a spurious IR divergence in the coefficient β. At first order in δ, the non trivial minimum of the potential is found at

$$\langle s_h^2 \rangle \equiv \xi = \xi_0 \Big(1 - \frac{\delta}{4\beta}(1 + 2 \log \xi_0) \Big) \,, \tag{C.2}$$

where

$$\xi_0 = \frac{\gamma}{2\beta} \tag{C.3}$$

is the leading order minimum for $\delta = 0$. The Higgs mass is given by

$$m_h^2 = \frac{8\beta}{f^2} \xi_0 (1 - \xi_0) + \frac{4\delta\xi_0}{f^2} \Big(1 - \frac{\xi_0}{2} + \xi_0 \log \xi_0 \Big). \tag{C.4}$$

For $\xi_0 \ll 1$ we get

$$m_h^2 \simeq (m_h^0)^2 \Big(1 + \frac{\delta}{2\beta} \Big), \tag{C.5}$$

where

$$(m_h^0)^2 \simeq \frac{8\beta}{f^2} \xi_0 \tag{C.6}$$

is the leading order mass for $\delta = 0$.

In the models we considered, the particles massless at $s_h = 0$ are always the top, in the matter sector, and the W and the Z gauge boson, in the gauge sector. Correspondingly, the explicit form of $\delta = \delta_{gauge} + \delta_{matter}$ is universal and given by

$$\delta_{matter} = -\frac{N_c}{8\pi^2} \lambda_{top}^4 f^4 \,,$$
$$\delta_{gauge} = \frac{3f^4(3g^4 + 2g^2 g'^2 + g'^4)}{512\pi^2} \,, \tag{C.7}$$

with $N_c = 3$ the QCD color factor and $M_{top} \equiv \lambda_{top} v$.

APPENDIX D

Results for Other Simple Models

In this appendix we briefly present the results for all the models studied in our analysis. They differ by the number of spin-1 and spin-1/2 resonances introduced. In all the models studied, and presented schematically below, EWSB is due to a tuning between the fermionic and gauge contributions to γ. In the parameter scans we performed, we have set $M_{top}(\text{TeV}) \simeq 150$ GeV and $\xi = 0.1$, solving these constraints for two of the input parameters. We have then imposed a cut for a light Higgs, $m_H \in [100, 150]$ GeV.

Minimal model: $N_Q = 1$, $N_S = 1$, $N_\rho = 1$, $N_a = 1$

For illustration, we consider here two versions of the minimal model, differing on how the Weinberg sum rules (3.97) are satisfied. We denote by "type 1" the model where $\epsilon_{tS} = \epsilon_{tQ} = \epsilon_{qS} = -\epsilon_{qQ} = \epsilon$, $m_S \neq m_Q$ (as in eq.(3.98)), and by "type 2" the model where $\epsilon_{tS} = \epsilon_{tQ} \equiv \epsilon_t$, $\epsilon_{qS} = -\epsilon_{qQ} \equiv \epsilon_Q$, $m_Q = m_S \equiv m$. In the first model the LFR is either t' or χ, while in the second one the LFR is necessarily χ. In both cases the vector resonance's mass is bounded from above by $m_\rho \lesssim 2$ TeV, which implies that the S parameter is too big ($\Delta S \gtrsim 0.3$) and both models don't pass the EWPT, see fig. D.1(b,d).

It is not difficult to see in more detail the tension present in this model. Let us for definiteness consider the type 1 model. The numerical scan show that EWSB mostly occurs in the region $\omega_L \ll 1$, $\omega_R \simeq 1$. Taking $\omega_R = 1$ and expanding at leading order in ω_L, one finds

$$\frac{m_\rho^2}{m_H^2} \simeq \frac{8\pi^2}{9\log 2}\frac{f(\omega_L)}{g^2\xi} \leq \frac{8\pi^2}{9\log 2}\frac{1}{g^2\xi} \tag{D.1}$$

where

$$f(\omega_L) = \frac{8(1 + \log \omega_L^2)}{1 + 8\log \omega_L^2 - \log 4/\xi} \tag{D.2}$$

is a smooth function $f(x) \leq 1$, for any x. Using eq.(D.1) for $m_H \simeq 125$ GeV, we immediately find an upper bound for m_ρ (for $\xi = 1/10$):

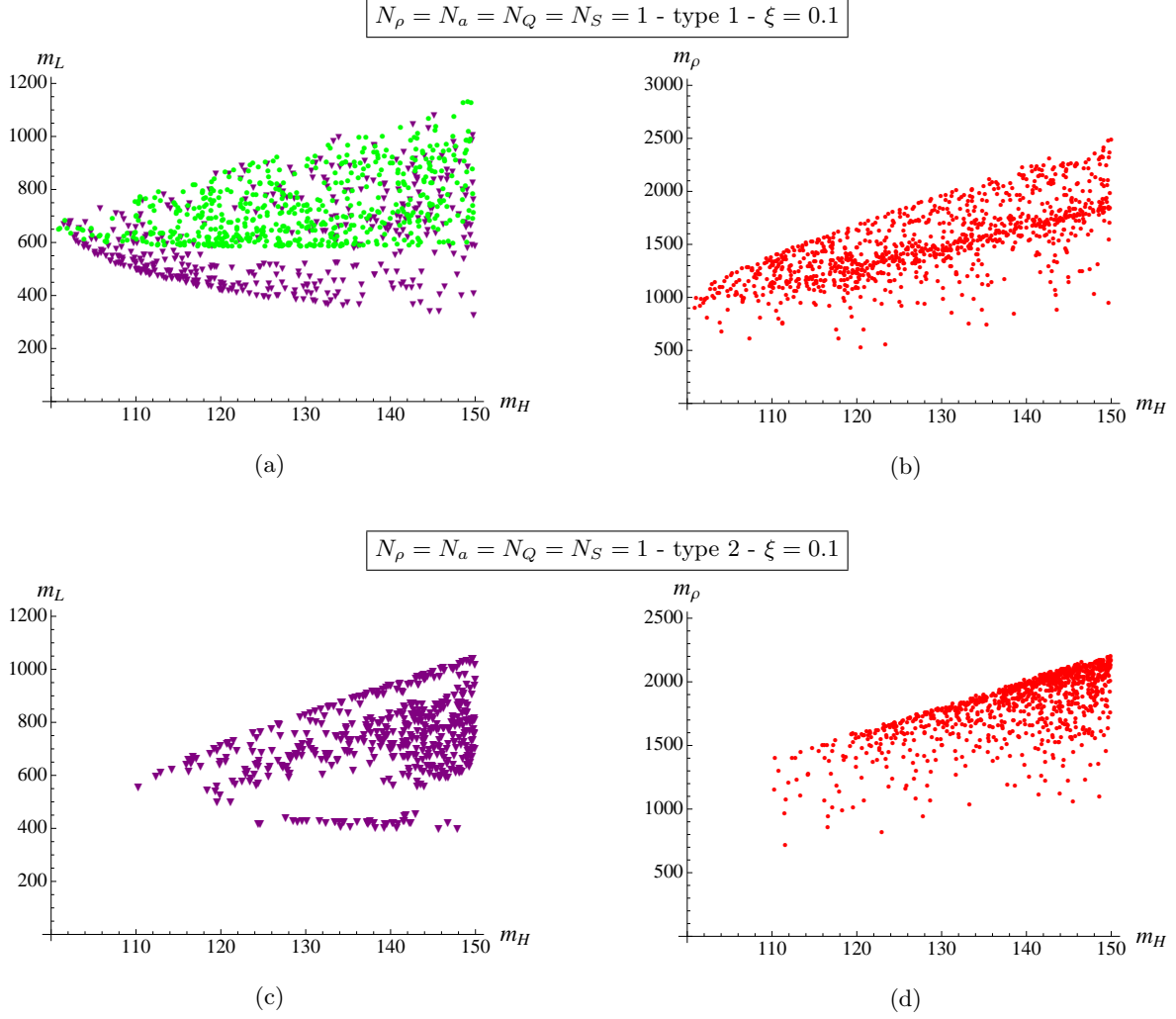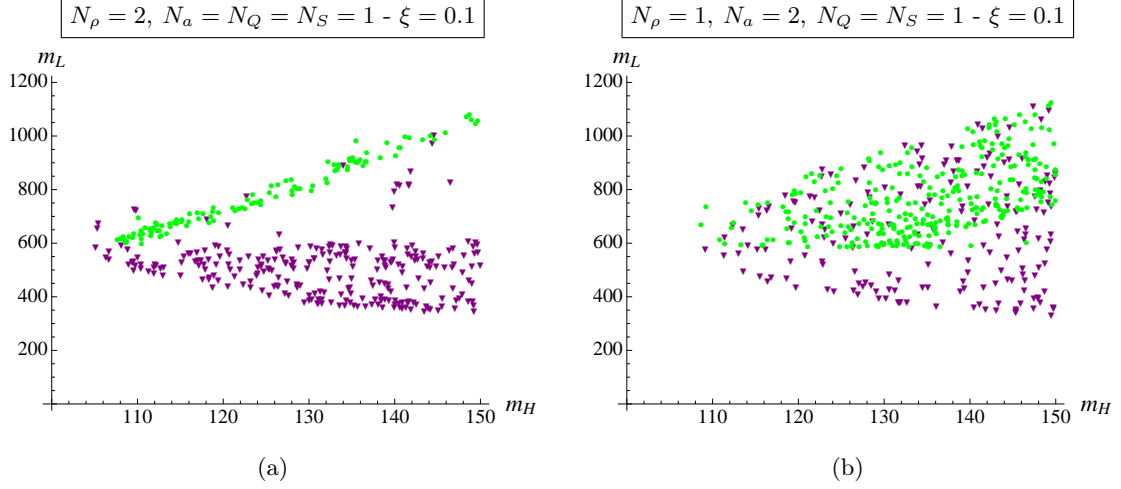$$m_\rho \lesssim 1.8 \,\text{TeV} \,. \tag{D.3}$$

Figure D.1: (a,c) Mass of the LFR, before EWSB, as a function of the Higgs mass. The green circles represent the (lightest) singlet while the purple triangles represent the (lightest) exotic doublet with $Y = 7/6$. (b,d) Mass of the ρ_μ vector as a function of the Higgs mass. One can see that for $m_H \lesssim 130$ GeV, $m_\rho \lesssim 1.8$ TeV, which is too low for the model to pass the EWPT. In (a,b) we took the masses $m_Q, m_S \in [0, 5f]$, $a_\rho \in [1/\sqrt{2}, 2]$ while ϵ and m_ρ have been obtained by fixing m_{top} and ξ. In (c,d) the same range has been taken for the parameters m, ϵ_q and a_ρ, while ϵ_t and m_ρ have been obtained by fixing M_{top} and ξ.

Demanding $\Delta\hat{S} \lesssim 2 \times 10^{-3}$ [83] in eq.(3.85), with $f_\rho = f/\sqrt{2}$, gives $m_\rho \gtrsim 1.8$ TeV, only marginally in agreement with the bound in of eq. (D.3).

Two vectors: $N_Q = 1$, $N_S = 1$, $N_\rho = 2$, $N_a = 1$

We choose the type 1 finiteness condition for the fermionic sector. The numerical scan shows that the vector mass eigenstates and the axial vector can be arbitrarily heavy and therefore

Figure D.2: Mass of the LFR, before EWSB, as a function of the Higgs mass. The green circles represent the (lightest) singlet while the purple triangles represent the (lightest) exotic doublet with $Y = 7/6$. In the model (a) the range in which we scanned the parameters is the same as in fig.3.7. For the model (b), instead, we took the fermionic masses in $[0, 5f]$, $a_\rho \in [1/\sqrt{2}, 2]$, $a_{1a} \in [0, \sqrt{a_\rho^2 - 1/2}]$ and m_{a1}/m_ρ in a region $[0.2, 2]$ times the value for which $\Delta\hat{S}$ vanishes. As usual, m_ρ and ϵ have been obtained by fixing ξ and M_{top}.

having a small $\Delta\hat{S}$ is no longer a problem. The LFR is either χ, with $m_{7/6} \sim 500$ GeV, or t', with $m_0 \sim 600 - 1000$ GeV, see fig.D.2(a). The bound (3.52) rules out almost the whole region with a light X fermion. The lightest vector can be as light as 1.5 TeV, while the axial is always heavier than ~ 2.2 TeV.

Two axials: $N_Q = 1$, $N_S = 1$, $N_\rho = 1$, $N_a = 2$

We choose the type 1 finiteness condition for the fermionic sector. The results in this sector are completely analogue to the minimal model with the same type of finiteness condition. In particular, the vector resonance is always light: $m_\rho \lesssim 2$ TeV, see fig.D.3(a). The tree level $\hat{S}$ parameter of this model can be written as

$$\Delta\hat{S}_{tree} = 2m_W^2 \frac{(m_{a1}^2 + m_{a2}^2)m_\rho^2 + 2f_\rho^2/f^2(m_{a1}^2 - m_\rho^2)(m_{a2}^2 - m_\rho^2)}{2m_{a1}^2 m_{a2}^2 m_\rho^2} \ , \tag{D.4}$$

after having solved the two Weinberg sum rules in terms of the two axial decay constants. We can see that $\Delta\hat{S}$ can be made small or even negative by choosing the two masses of the axial resonances such that $m_{a1} < m_\rho < m_{a2}$. The lightest axial resonance has a mass $m_{a1} \sim 300 - 900$ GeV, see fig.D.3(b). This model has therefore a potentially interesting phenomenology, but it is fair to say that a model with light axial resonances and negative $\hat{S}$ parameter looks quite "exotic" and might not admit a consistent UV completion.
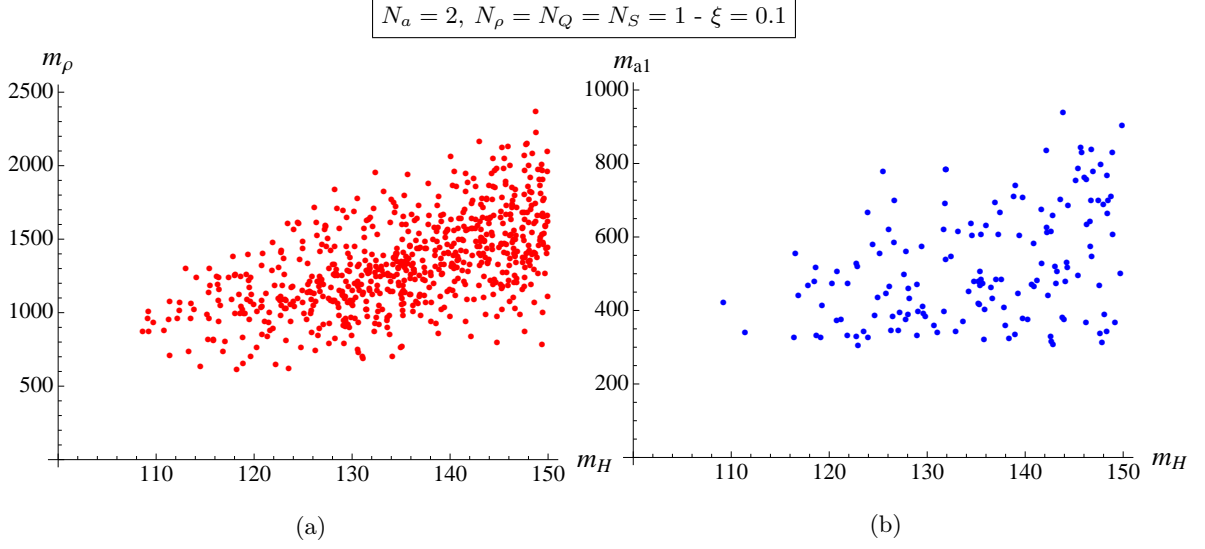
Figure D.3: (a) Mass of the vector resonance ρ_μ and (b) of the lightest axial vector, as a function of the Higgs mass. The range of the parameters is the same as in fig.D.2(b).

Two singlets: $N_Q = 1$, $N_S = 2$, $N_\rho = 1$, $N_a = 1$

See section 3.7.3 for a more complete description of this model. In this case, the LFR is the singlet S_1, with $m_0 \simeq 300 - 800$ GeV, see fig.D.4(a), the second singlet S_2 being always much heavier. The vector resonance can be as heavy as 5-6 TeV, due to the fact that now γ_f can be bigger than the minimal case.

Two bidoublets: $N_Q = 2$, $N_S = 1$, $N_\rho = 1$, $N_a = 1$

In this case the LFR can be either the singlet or the lightest $Y = 7/6$ doublet, their masses being always below ~ 1 TeV, see fig.D.4(b). Analogously to the previous case, the vector resonance can be heavy and thus $\Delta \hat{S}_{tree}$ small.

Two singlets and bidoublets: $N_Q = 2$, $N_S = 2$, $N_\rho = 1$, $N_a = 1$

The most general solution for eq.(3.96) is given in terms of four angles and two mixings:

$$
\begin{aligned}
\vec{\epsilon}_{qQ} &= (\epsilon_q \cos\theta_{qQ}, \ \epsilon_q \sin\theta_{qQ}), & \vec{\epsilon}_{qS} &= (\epsilon_q \cos\theta_{qS}, \ \epsilon_q \sin\theta_{qS}), \\
\vec{\epsilon}_{tQ} &= (\epsilon_t \cos\theta_{tQ}, \ \epsilon_t \sin\theta_{tQ}), & \vec{\epsilon}_{tS} &= (\epsilon_t \cos\theta_{tS}, \ \epsilon_t \sin\theta_{tS}).
\end{aligned}
\tag{D.5}
$$

Now one can solve eq.(3.97) for one of the remaining parameters, in the parameter scans we choose to solve it for ϵ_q, as this allows us to go in the light singlet region. The scan shows that the LFR tends to be the first singlet, see fig.D.4(c). As in the previous two cases, the points which pass the direct bound of eq. (3.52) have $m_\rho > 2$ TeV, T' as the LFR with $m_0 \simeq 700 - 1000$ GeV, the other resonances being generally heavier than 1 TeV.
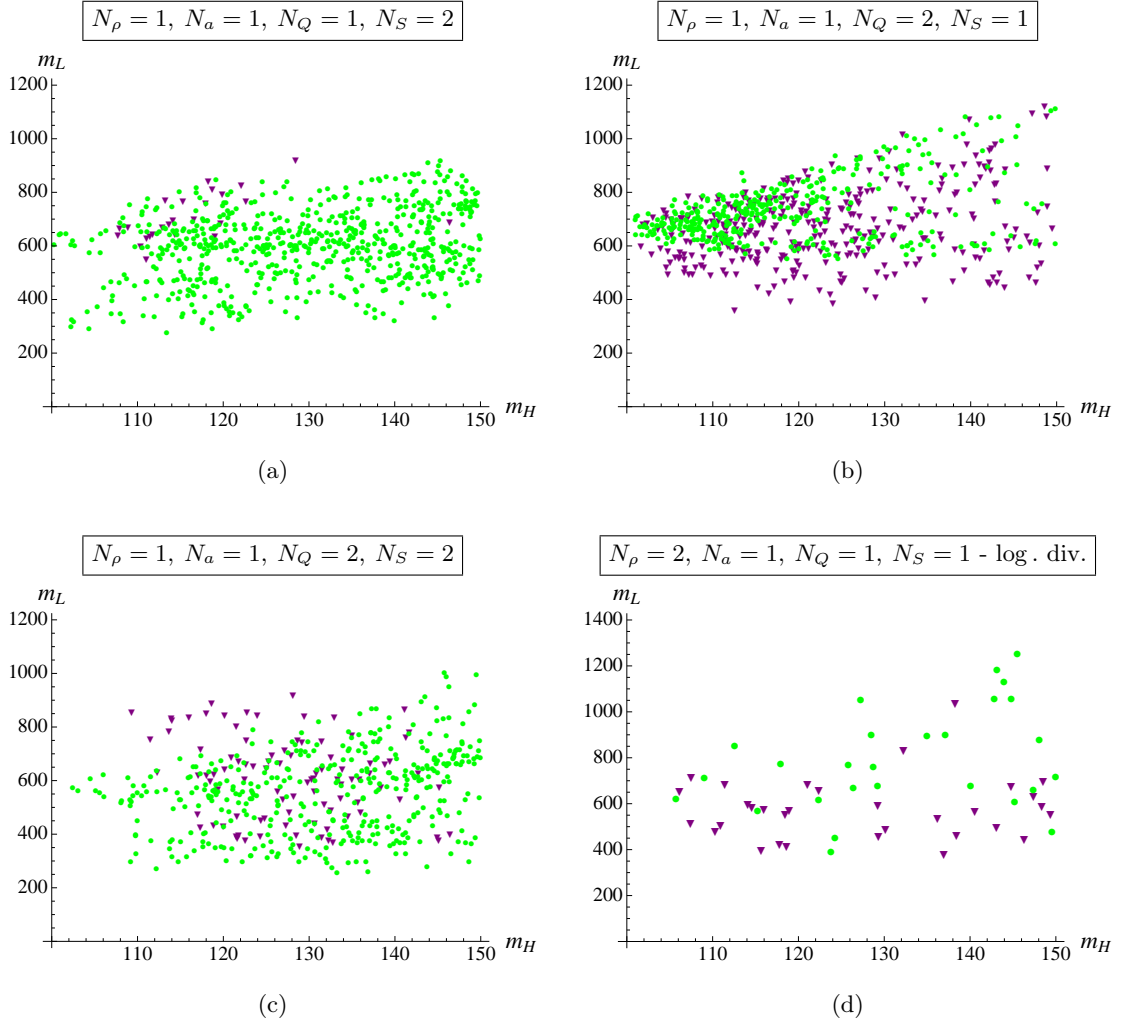
Figure D.4: Mass of the LFR, before EWSB, as a function of the Higgs mass. The green circles represent the (lightest) singlet while the purple triangles represent the (lightest) exotic doublet with $Y = 7/6$. The range of the parameters in the model (a) is the same as in fig.3.8. For the models (b,c) we took all the fermion masses $m_{iQ}, m_{iS} \in [0, 8f]$ and $a_\rho \in [1/\sqrt{2}, 2]$, while ϵ_t and m_ρ have been obtained by fixing respectively M_{top} and ξ. In the log. divergent case, (d), the range is $m_Q, m_S, \epsilon_t \in [0, 8f]$ while ϵ_q has been obtained by fixing M_{top}.

Minimal Model with Logarithmic Divergence

As we have seen above, the minimal model with $N_Q = N_S = N_\rho = N_a = 1$ is not viable because of a too light vector resonance, which implies a too big $\hat{S}$ parameter at tree-level. This problem can be circumvented by relaxing the second Weinberg sum rules, so that the Higgs potential keeps a logarithmic divergence. This obviously implies that the MHP hypothesis is no longer defendable, since local operators have to arise in order to renormalize the logarithmic divergence. In other words, the coefficients $\gamma_g^{(NDA)}$ and $\gamma_f^{(NDA)}$ introduced in eq.(3.67) run and

can be assumed to be vanishing only at a given energy scale. One could however hope that their impact is somehow small, so that it is still possible to make good estimates for the parameter ξ integrating the form factors only up to the cutoff $\Lambda \sim 4\pi f$. To satisfy the first Weinberg sum rule in the fermion sector we can assume that

$$\epsilon_{qS} = -\epsilon_{qQ} = \epsilon_q, \qquad \epsilon_{tS} = \epsilon_{tQ} = \epsilon_t. \tag{D.6}$$

The logarithmically divergent term in γ_f is proportional to the square of the mixing parameters, $\gamma_f \propto (\epsilon_t^2 - \epsilon_q^2) \log \Lambda/m$ where m is a generic fermion mass. This is the same effect seen when adding more fermions which would allow higher values of γ_f and, therefore, heavier vector masses. Doing a numerical scan of such model we indeed obtain these results but, on the other side, we notice that the physics (that is, the value of ξ and m_H) is too sensitive to the value of Λ: changing it by a factor of 2 has an $\mathcal{O}(1)$ effect on these observables, making the model unpredictable.

We can adopt another approach to deal with the logarithmic divergence, which is accepting that γ, and therefore ξ, is uncalculable. Assuming a given value of ξ and using eq.(3.102) we can still compute the Higgs mass, being β finite. The relation $\gamma_f \simeq -\gamma_g$, connecting the fermion and the gauge sector in a crucial way, is now lost. Given that $\beta_g \ll \beta_f$, as far as the Higgs potential is concerned, the gauge sector is completely negligible and thus unconstrained. This allows the model to pass the EWPT, although in a somewhat trivial way. Neglecting the gauge sector and performing a parameter scan for the minimal model presented above, we still obtain that a light Higgs implies light fermionic resonances, as can be seen from fig.D.4(d).

Similar considerations would of course apply to the non-minimal models. As far as the Higgs sector is concerned, the price to be paid is high since EWSB is no longer under control. Moreover, as we have seen, non-minimal models are viable without the need of relaxing the second Weinberg sum rules. For these reasons, we have decided to not explore any further models where a logarithmic divergence in the Higgs potential is kept.

APPENDIX E

A dictionary for deconstructed models

In chapter 3 we constructed a general framework for composite Higgs models, based only on the assumptions of SO(5)/SO(4) symmetry breaking pattern and the MHP hypothesis. In this appendix we explicitly show how this general setup is able to reproduce the physics of two deconstructed composite Higgs models and how in these cases the Weinberg sum rules are automatically satisfied due to the enhanced symmetry of the models.

E.1 Discrete Composite Higgs Model

Let us start with the two and three sites deconstructed models described in ref. [119]. The two sites model is based on the coset $SO(5)_L \otimes SO(5)_R / SO(5)_V$, where the SM group is embedded in $SO(5)_L$. From this coset one has 10 Goldstones π^A, transforming in the adjoint of $SO(5)_V$. The SO(4) subgroup of $SO(5)_R$ is gauged by introducing six gauge fields $\tilde{\rho}^a_\mu$, which become massive by eating the six Goldstone bosons π^a. The Lagrangian of this model is (in the notation of ref. [119])

$$\mathcal{L}^{g,2-sites}_{PW} = \frac{\tilde{f}^2}{4} \text{Tr} \left[(D_\mu U)^t D^\mu U \right] - \frac{1}{4} \text{Tr} \left[\tilde{\rho}_{\mu\nu} \tilde{\rho}^{\mu\nu} \right] + \mathcal{L}^{gauge}_{SM}, \tag{E.1}$$

where the Goldstone matrix is $U = \exp\left[i\sqrt{2}\pi^A T^A / f_\pi \right]$, the covariant derivative is $D_\mu U = \partial_\mu U - i(g_0 W^\alpha_\mu T^\alpha_L + g'_0 B_\mu T^3_R) U + i\tilde{g}_* U \tilde{\rho}^a_\mu T^a$ and $\mathcal{L}^{gauge}_{SM}$ is the usual gauge Lagrangian for the SM EW gauge bosons. Going in the gauge where the only non-zero Goldstones are the ones along the generators of the coset $SO(5)_V / SO(4)$ ("holographic gauge"), $\pi^{\hat{a}}$, this model is described by the Lagrangian of eq.(3.33), with one vector multiplet in the adjoint of SO(4), no axial resonances, and fixing the parameters as (imposing invariance under LR symmetry):

$$\text{2-sites:} \qquad f = f_\pi = \tilde{f}, \qquad g_\rho = \tilde{g}_*, \qquad m^2_\rho = \frac{1}{2}\tilde{g}^2_* \tilde{f}^2, \qquad f^2_\rho = \frac{\tilde{f}^2}{2}. \tag{E.2}$$

One can check that only the first Weinberg sum rule is satisfied and the gauge contribution to the Higgs potential remains logarithmically divergent.

In order to get a finite potential, the authors of [119] add to the model another site, doubling the coset to $(SO(5)_L^2 \otimes SO(5)_R^1)/SO(5)_V^1 \times (SO(5)_L^2 \otimes SO(5)_R^2)/SO(5)_V^2$. From this symmetry breaking pattern 20 Goldstone bosons arise and can be parametrized by two $SO(5)$ matrices $U_1 = U(\pi_1^A)$ and $U_2 = U(\pi_2^A)$. Sixteen NGB's are eaten by the gauging of $SO(4) \subset SO(5)_R^2$ by $\tilde{\rho}_\mu^a$ and of the diagonal combination of $SO(5)_R^1 \otimes SO(5)_L^2$ by the gauge field ρ_μ^A:

$$D_\mu U_1 = \partial_\mu U_1 - i(g_0 W_\mu^\alpha T_L^\alpha + g_0' B_\mu T_R^3)U_1 + ig_* U_1 \rho_\mu^A T^A,$$
$$D_\mu U_2 = \partial_\mu U_2 - ig_* \rho_\mu^A T^A U_2 + i\tilde{g}_* U_2 \tilde{\rho}_\mu^a T^a. \tag{E.3}$$

The Lagrangian of this model is

$$\mathcal{L}_{PW}^{g,3-sites} = \frac{\tilde{f}^2}{4} \text{Tr}\left[(D_\mu U_1)^t D^\mu U_1\right] + \frac{\tilde{f}^2}{4} \text{Tr}\left[(D_\mu U_2)^t D^\mu U_2\right] - \frac{1}{4} \text{Tr}\left[\tilde{\rho}_{\mu\nu}\tilde{\rho}^{\mu\nu}\right] - \frac{1}{4} \text{Tr}\left[\rho_{\mu\nu}\rho^{\mu\nu}\right] + \mathcal{L}_{SM}^{gauge}. \tag{E.4}$$

In the holographic gauge where $\pi_2^A = \pi_1^a = 0$, one obtains the Lagrangian of (3.33) for two vectors and one axial resonances, with LR symmetry and the following parameters:

$$\text{3-sites:} \begin{cases} f = f_\pi = \dfrac{\tilde{f}}{\sqrt{2}}, & f_a = \dfrac{\tilde{f}}{2}, & f_{\rho_1} = \dfrac{\tilde{f}}{\sqrt{2}}, & f_{\rho_2} = 0, \\[2mm] f_{mix} = \dfrac{\tilde{f}}{\sqrt{2}}, & g_a = g_{\rho_1} = g_*, & g_{\rho_2} = \tilde{g}_*, & \Delta = -\dfrac{1}{2}. \end{cases} \tag{E.5}$$

Both Weinberg sum rules (3.81) and (3.82) are now satisfied. Notice that the term proportional to f_{ρ_2} is absent in the deconstructed model because it would correspond to a non-local interaction in field space.

The fermionic sector of [119] can be studied directly in the holographic gauge. As we are interested only in the leading contribution to the 1-loop Higgs potential, we neglect in the following interactions between fermions and spin-1 fields (gauge bosons, vector and axial resonances) as well as composite fermions necessary to give mass to SM fermions other than the top. In the two sites model the authors introduce a complete multiplet in the fundamental of $SO(5)_R$, $\tilde{\psi} = \tilde{Q} + \tilde{S}$, with a mass term that is only $SO(4)_R$ invariant:

$$\mathcal{L}_{PW}^{f,2-sites} = \mathcal{L}^{elem} + \mathcal{L}^{comp} + \mathcal{L}^{mix}, \tag{E.6}$$

where $\mathcal{L}^{elem}$ is the kinetic term for the SM fermions,

$$\mathcal{L}^{comp} = i\bar{\tilde{Q}}\slashed{D}\tilde{Q} + \tilde{m}_Q \bar{\tilde{Q}}\tilde{Q} + i\bar{\tilde{S}}\slashed{D}\tilde{S} + \tilde{m}_T \bar{\tilde{S}}\tilde{S}, \tag{E.7}$$

$$\mathcal{L}^{mix} = y_L \tilde{f}\bar{\xi}_L U\left(\tilde{Q} + \tilde{S}\right) + y_R \tilde{f}\bar{\xi}_R U\left(\tilde{Q} + \tilde{S}\right) + h.c. \tag{E.8}$$

Comparing this Lagrangian to the general one of eq.(3.39), it is immediate to recognize that the models are the same once we fix $N_Q = N_S = 1$ and

$$\text{2 sites:} \qquad \epsilon_{qQ} = \epsilon_{qS} = y_L f, \qquad \epsilon_{tQ} = \epsilon_{tS} = \sqrt{2} y_R f, \qquad m_Q = -\tilde{m}_Q, \qquad m_S = -\tilde{m}_T. \tag{E.9}$$

One can check that the sum rules of (3.96) are satisfied while the one in eq.(3.97) is generically not, so that the potential is logarithmically divergent. One could however impose the finiteness of the one loop potential setting $y_L = \sqrt{2}y_R$.

In the three sites model there are two composite fermionic multiplets, one in the fundamental of $SO(5)_R^1$, $\psi = Q + S$, and another one in the fundamental of $SO(5)_R^2$, $\tilde{\psi} = \tilde{Q} + \tilde{S}$. In the holographic gauge, the Lagrangian is

$$\mathcal{L}^{comp} = i\bar{\tilde{Q}}\slashed{D}\tilde{Q} + i\bar{\tilde{S}}\slashed{D}\tilde{S} + i\bar{Q}\slashed{D}Q + i\bar{S}\slashed{D}S +$$
$$\tilde{m}_Q\bar{\tilde{Q}}\tilde{Q} + \tilde{m}_T\bar{\tilde{S}}\tilde{S} + m(\bar{Q}Q + \bar{S}S) + \Delta(\bar{Q}\tilde{Q} + \bar{S}\tilde{S}) + h.c. , \tag{E.10}$$
$$\mathcal{L}^{mix} = y_L\tilde{f}\bar{\xi}_L U \left(Q + S\right) + y_R\tilde{f}\bar{\xi}_R U \left(Q + S\right) + h.c.$$

Note that Δ, as well as the gauging by ρ_μ^A, explicitly breaks $SO(5)_R^1 \otimes SO(5)_L^2$ to the diagonal subgroup $SO(5)_D$. As the composite mass terms are not diagonal, one needs to diagonalize them before comparing this model with our setup:

$$\begin{cases} Q_1 = c_{\theta_Q}\tilde{Q} + s_{\theta_Q}Q, \\ Q_2 = -s_{\theta_Q}\tilde{Q} + c_{\theta_Q}Q, \end{cases} \quad \begin{cases} S_1 = c_{\theta_S}\tilde{S} + s_{\theta_S}S, \\ S_2 = -s_{\theta_S}\tilde{S} + c_{\theta_S}S. \end{cases} \tag{E.11}$$

After doing that, we obtain that this three sites model can be described by the Lagrangian (3.39) for $N_Q = N_S = 2$ and

$$3\text{-sites:} \begin{cases} m_{1,2\,Q} = \dfrac{1}{2}\left(m + \tilde{m}_Q \mp \sqrt{(m - \tilde{m}_Q)^2 + 4\Delta^2}\right), \\[2mm] m_{1,2\,S} = \dfrac{1}{2}\left(m + \tilde{m}_S \mp \sqrt{(m - \tilde{m}_S)^2 + 4\Delta^2}\right), \\[2mm] \tan\theta_Q = \dfrac{\Delta}{\sqrt{\Delta^2 + (m - \tilde{m}_Q)\left(m - \tilde{m}_Q + \sqrt{(m - \tilde{m}_Q)^2 + 4\Delta^2}\right)}}, \\[4mm] \tan\theta_S = \dfrac{\Delta}{\sqrt{\Delta^2 + (m - \tilde{m}_S)\left(m - \tilde{m}_S + \sqrt{(m - \tilde{m}_S)^2 + 4\Delta^2}\right)}}, \\[4mm] \epsilon_{qQ}^1 = y_L\tilde{f}s_{\theta_Q}, \quad \epsilon_{qQ}^2 = y_L\tilde{f}c_{\theta_Q}, \\[1mm] \epsilon_{qS}^1 = y_L\tilde{f}s_{\theta_S}, \quad \epsilon_{qS}^2 = y_L\tilde{f}c_{\theta_S}, \\[1mm] \epsilon_{tQ}^1 = \sqrt{2}y_R\tilde{f}s_{\theta_Q}, \quad \epsilon_{tQ}^2 = \sqrt{2}y_R\tilde{f}c_{\theta_Q}, \\[1mm] \epsilon_{tS}^1 = \sqrt{2}y_R\tilde{f}s_{\theta_S}, \quad \epsilon_{tS}^2 = \sqrt{2}y_R\tilde{f}c_{\theta_S}. \end{cases} \tag{E.12}$$

One can check that the sum rules (3.96) and (3.97) are satisfied. One can also check that the fermion contribution to the potential has a leading mass term proportional to the square of the mixings, which can be tuned away for $y_L \simeq \sqrt{2}y_R$, allowing for a successful EWSB, confirming what stated in [119].

E.2   Minimal 4D Composite Higgs

Let us now write a similar dictionary for the deconstructed model described in ref. [120]. This model is based on a two-coset Lagragian: $\mathrm{SO}(5)_L \otimes \mathrm{SO}(5)_R / \mathrm{SO}(5)_D$, described by the NGB matrix $\Omega_1 = \exp(i\sqrt{2}\tilde{\pi}^A T^a / f_1)$, and another coset $\mathrm{SO}(5)/\mathrm{SO}(4)$, described by the matrix $\Omega_2 = \exp(i\sqrt{2}\bar{\pi}^{\hat{a}} T^{\hat{a}} / f_2)$. The SM gauging is embedded in $\mathrm{SO}(5)_L$ and to absorb the 10 exceeding NGB's, the diagonal subgroup of $\mathrm{SO}(5)_R \otimes \mathrm{SO}(5)$ is gauged by the field ρ_μ^A. In the notation of ref. [120], the Lagrangian is

$$\mathcal{L} = \frac{f_1^2}{4}\mathrm{Tr}\,|D_\mu\Omega_1|^2 + \frac{f_2^2}{2}(D_\mu\Phi_2)^t D^\mu\Phi_2 - \frac{1}{4g_\rho^2}\rho_{\mu\nu}^A\rho^{A\mu\nu}, \tag{E.13}$$

where $\Phi_2 = \Omega_2\phi_0$ $(\phi_0 = (0,0,0,0,1)^t)$ and

$$D_\mu\Omega_1 = \partial_\mu\Omega_1 - iA_\mu\Omega_1 + i\Omega_1\rho_\mu, \qquad D_\mu\Omega_2 = \partial_\mu\Omega_2 - i\rho_\mu\Omega_1. \tag{E.14}$$

Going again to the holographic gauge, where $\Omega_2 = 1$ and $\Omega_1 \equiv U = \exp(i\sqrt{2}\tilde{\pi}^{\hat{a}} T^{\hat{a}} / f_1)$, and redefining the NGB fields as $\tilde{\pi}^{\hat{a}} = f_1/f\pi^{\hat{a}}$, one can write the Lagrangian as in eq.(3.33):

$$\mathcal{L} = \frac{f_1^2 f_2^2}{4(f_1^2 + f_2^2)}\mathrm{Tr}\,[d_\mu d^\mu] + \frac{f_1^2}{4}\mathrm{Tr}\,\left[(g_\rho\rho_\mu - E_\mu)^2\right] + \frac{f_1^1 + f_2^2}{4}\mathrm{Tr}\,\left[(g_\rho a_\mu - \frac{f_1^2}{f_1^2 + f_2^2}d_\mu)^2\right] - \frac{1}{4}\rho_{\mu\nu}^2 - \frac{1}{4}a_{\mu\nu}^2, \tag{E.15}$$

from which we obtain the dictionary for $N_\rho = N_a = 1$:

$$\left\{ \begin{array}{ll} f^2 = \dfrac{f_1^2 f_2^2}{f_1^2 + f_2^2}, \qquad f_\rho^2 = \dfrac{f_1^2}{2}, \qquad g_a = g_\rho, \\[3mm] \Delta = \dfrac{f_1^2}{f_1^2 + f_2^2}, \qquad \dfrac{f_a^2}{\Delta^2} = \dfrac{f_1^2 + f_2^2}{2}. \end{array} \right. \tag{E.16}$$

It is straightforward to check that both Weinberg sum rules are satisfied with these parameters.

The fermion sector of [120], as far as the top is concerned, consists of the elementary SM fields and two complete multiplets in the fundamental of $\mathrm{SO}(5)$: $\tilde{\psi} = (\tilde{Q}, \tilde{S})$, $\psi = (Q, S)$, where we have decomposed them in the irreducible representations of $\mathrm{SO}(4)$. In the holographic gauge, the fermion Lagrangian is[1]

$$\begin{aligned} \mathcal{L}^{ferm} &= \mathcal{L}^{elem} + i\bar{\tilde{Q}}\slashed{D}\tilde{Q} + i\bar{\tilde{S}}\slashed{D}\tilde{S} + i\bar{Q}\slashed{D}Q + i\bar{S}\slashed{D}S + \\ &- m_T(\bar{Q}Q + \bar{S}S) - m_{\tilde{T}}(\bar{\tilde{Q}}\tilde{Q} + \bar{\tilde{S}}\tilde{S}) + \\ &- (m_{Y_T} + Y_T)\bar{S}_L\tilde{S}_R - m_{Y_T}\bar{Q}_L\tilde{Q}_R + h.c. + \\ &+ \Delta_{t_L}\bar{\xi}_L U(Q_R + S_R) + \Delta_{t_R}\bar{\xi}_R U(\tilde{Q}_L + \tilde{S}_L) + h.c. \,. \end{aligned} \tag{E.17}$$

---

[1]We thank Michele Redi and Andrea Tesi for having pointed out that in their model $\Delta_{t_L} \neq \Delta_{t_R}$ in general.

To compare this Lagrangian with our framework, we need to diagonalize the composite mass terms via biunitary transformations:

$$
M_Q = \begin{pmatrix} m_T & m_{Y_T} \\ 0 & m_{\tilde{T}} \end{pmatrix} = V_{Q_L}(\theta_{Q_L}) M_Q^d V_{Q_R}(\theta_{Q_R})^\dagger,
$$
$$
M_S = \begin{pmatrix} m_T & m_{Y_T} + Y_T \\ 0 & m_{\tilde{T}} \end{pmatrix} = V_{S_L}(\theta_{S_L}) M_S^d V_{S_R}(\theta_{S_R})^\dagger,
$$

(E.18)

where $M_Q^d = \mathrm{diag}(m_{1Q}, m_{2Q})$, $M_S^d = \mathrm{diag}(m_{1S}, m_{2S})$,

$$
m_{1,2\,Q} = \frac{1}{\sqrt{2}} \sqrt{ m_T^2 + m_{\tilde{T}}^2 + m_{Y_T}^2 \mp \sqrt{(m_T^2 + m_{\tilde{T}}^2 + m_{Y_T}^2)^2 - 4 m_T^2 m_{\tilde{T}}^2} },
$$
$$
\tan\theta_{Q_L} = \frac{ m_{\tilde{T}}^2 - m_T^2 - m_{Y_T}^2 - \sqrt{(m_{\tilde{T}}^2 - m_T^2)^2 + m_{Y_T}^2 (m_{Y_T}^2 + 2 m_{\tilde{T}} + 2 m_T^2)} }{ 2 m_{\tilde{T}} m_{Y_T} },
$$
$$
\tan\theta_{Q_R} = \frac{ m_{\tilde{T}}^2 - m_T^2 + m_{Y_T}^2 - \sqrt{(m_{\tilde{T}}^2 - m_T^2)^2 + m_{Y_T}^2 (m_{Y_T}^2 + 2 m_{\tilde{T}} + 2 m_T^2)} }{ 2 m_T m_{Y_T} },
$$

(E.19)

and $m_{1,2\,S}$, $\tan\theta_{S_L}$ and $\tan\theta_{S_R}$ are the same as above with the substitution $m_{Y_T} \to Y_T + m_{Y_T}$. Writing the Lagrangian in terms of the mass eigenstates (before EWSB),

$$
\begin{cases} Q_L = \cos\theta_{Q_L} Q_{1L} - \sin\theta_{Q_L} Q_{2L} \\ \tilde{Q}_L = \sin\theta_{Q_L} Q_{1L} + \cos\theta_{Q_L} Q_{2L} \end{cases},
$$

(E.20)

and analogously for the other cases, we obtain the Lagrangian (3.39) for $N_Q = N_S = 2$ and

$$
\begin{cases}
\epsilon_{qQ}^1 = \Delta_{t_L} c_{\theta_{Q_R}}, & \epsilon_{qQ}^2 = -\Delta_{t_L} s_{\theta_{Q_R}}, \\
\epsilon_{qS}^1 = \Delta_{t_L} c_{\theta_{S_R}}, & \epsilon_{qS}^2 = -\Delta_{t_L} s_{\theta_{S_R}}, \\
\epsilon_{tQ}^1 = \sqrt{2} \Delta_{t_R} s_{\theta_{Q_L}}, & \epsilon_{tQ}^2 = \sqrt{2} \Delta_{t_R} c_{\theta_{Q_L}}, \\
\epsilon_{tS}^1 = \sqrt{2} \Delta_{t_R} s_{\theta_{S_L}}, & \epsilon_{tS}^2 = \sqrt{2} \Delta_{t_R} c_{\theta_{S_L}}.
\end{cases}
$$

(E.21)

One can check that all the sum rules are satisfied by this model and therefore the Higgs potential is finite at 1-loop level. One can also check that the leading term in γ_f, quadratic in the mixing $\Delta_{t_{L,R}}$, is proportional to $Y_T(\Delta_{t_L}^2 m_T^2 - 2\Delta_{t_R}^2 m_{\tilde{T}}^2)(2 m_{Y_T} + Y_T)$.

APPENDIX F

Parametrizing the $\mathrm{SO}(6)/\mathrm{SO}(5)$ coset and physical couplings

In this appendix, after providing some definitions useful for our work, we present three different parametrizations of the physical h and η fields, used in previous literature, and the relations among them. In particular, we show how the couplings among the physical fields differ between the parametrizations: only physical observables are parametrization-independent.

Let us first define the broken and unbroken generators of $\mathrm{SO}(6)/\mathrm{SO}(5)$ in the fundamental representation of $\mathrm{SO}(6)$. We classify them in the five broken ones of $\mathrm{SO}(6)/\mathrm{SO}(5)$ and the ten unbroken generators of the $\mathrm{SO}(5)$ subgroup, which can be further divided into the six of the $\mathrm{SU}(2)_L \otimes \mathrm{SU}(2)_R \sim \mathrm{SO}(4) \subset \mathrm{SO}(5)$ subgroup and the four of the $\mathrm{SO}(5)/\mathrm{SO}(4)$ coset

$$
\begin{aligned}
T_{ij}^{\hat{a}} &= -\frac{i}{\sqrt{2}}\left(\delta^{\hat{a}i}\delta^{6j} - \delta^{\hat{a}j}\delta^{6i}\right) , \\
T_{ij}^{a_{L,R}} &= -\frac{i}{2}\left[\frac{1}{2}\epsilon^{abc}(\delta^{bi}\delta^{cj} - \delta^{bj}\delta^{ci}) \pm (\delta^{ai}\delta^{4j} - \delta^{aj}\delta^{4i})\right] , \\
T_{ij}^{\alpha} &= -\frac{i}{\sqrt{2}}\left(\delta^{\alpha i}\delta^{5j} - \delta^{\alpha j}\delta^{5i}\right) ,
\end{aligned}
\tag{F.1}
$$

where $\hat{a} = 1, \ldots, 5$, $a_{L,R} = 1, 2, 3$ and $\alpha = 1, \ldots, 4$.

The five NGBs can be parametrized by a 6×6 unitary matrix obtained exponentiating a linear combination of the broken generators,

$$
U(x) = \exp\left[i\sqrt{2}\frac{\theta^{\hat{a}}(x)}{f}T^{\hat{a}}\right] ,
\tag{F.2}
$$

which transforms under a global $\mathrm{SO}(6)$ transformation g as $U(x) \to g\, U(x)\, k^{\dagger}(g, \theta^{\hat{a}}(x))$, where k is a local transformation of the unbroken group $\mathrm{SO}(5)$, which depends on g and on the position via the NGB dependence. From the NGB matrix U one can define the standard CCWZ structures d_μ and E_μ as

$$
d_\mu^{\hat{a}}T^{\hat{a}} + E_\mu^{a}T^{a} = -i(U^{\dagger}D_\mu U) .
\tag{F.3}
$$

Defining $\Sigma(x) \equiv U(x)\Sigma_0$, with $\Sigma_0 = (0,0,0,0,0,1)^t$, one gets

$$\Sigma = \sin\frac{\theta}{f}\left(\frac{\theta^{\hat{1}}}{\theta}, \frac{\theta^{\hat{2}}}{\theta}, \frac{\theta^{\hat{3}}}{\theta}, \frac{\theta^{\hat{4}}}{\theta}, \frac{\theta^{\hat{5}}}{\theta}, \cot\frac{\theta}{f}\right)$$

$$= \frac{1}{f}\left(h_1, h_2, h_3, h_4, \eta, \sqrt{f^2 - h^2 - \eta^2}\right) , \tag{F.4}$$

where $\theta^2 \equiv \sum_{\hat{a}=1}^{5}(\theta^{\hat{a}})^2$ and $h^2 \equiv \sum_{i=1}^{4} h_i^2$. The usual Higgs doublet can can be constructed as $H = \frac{1}{\sqrt{2}}(h_1 + ih_2, h_3 + ih_4)^t$. The fields $h_i(x)$ and $\eta(x)$ live in the region $\sqrt{h^2 + \eta^2} \leq f$. In the unitary gauge $h_1(x) = h_2(x) = h_4(x) = 0$ and $h(x) \equiv h_3(x)$

$$\Sigma_{unitary} = \sin\frac{\theta}{f}\left(0, 0, \frac{\theta^{\hat{3}}}{\theta}, 0, \frac{\theta^{\hat{5}}}{\theta}, \cot\frac{\theta}{f}\right)$$

$$= \frac{1}{f}\left(0, 0, h, 0, \eta, \sqrt{f^2 - h^2 - \eta^2}\right) \tag{F.5}$$

$$= \left(0, 0, \sin\frac{\phi}{f}\cos\frac{\psi}{f}, 0, \sin\frac{\phi}{f}\sin\frac{\psi}{f}, \cos\frac{\phi}{f}\right) ,$$

where in the third line we introduced another parametrization [45], in terms of two angles, which is related to the previous two as

$$\phi = \sqrt{(\theta^{\hat{3}})^2 + (\theta^{\hat{5}})^2} , \qquad \tan\frac{\psi}{f} = \frac{\theta^{\hat{5}}}{\theta^{\hat{3}}} ,$$

$$\sin\frac{\phi}{f} = \frac{1}{f}\sqrt{h^2 + \eta^2} , \qquad \tan\frac{\psi}{f} = \frac{\eta}{h} . \tag{F.6}$$

Let us call the first parametrization, in terms of the $\theta^{\hat{a}}$ variables, *Cartesian*, the one we use throughout the paper, in terms of h and η, *constrained* and the third one, in terms of the angles ϕ and ψ, *polar*. In the rest of this appendix we will show how the physical fields in the three parametrization have qualitatively different couplings, both from the chiral Lagrangian and from the effective potential. In the computation of physical quantities such as cross-sections or decay widths, these differences conspire and give the exact same result, as expected.

The leading-order chiral Lagrangian, eq. (4.8), can be written in a compact form in both the constrained and in the polar parametrization, it reads

$$\mathcal{L}_{chiral} = \frac{f^2}{4}\text{Tr}\left[d_\mu d^\mu\right] = \frac{f^2}{2}(D_\mu\Sigma)^t D^\mu\Sigma =$$

$$= \frac{1}{2}\left[\sin^2\frac{\phi}{f}(\partial_\mu\psi)^2 + (\partial_\mu\phi)^2\right] + \frac{f^2}{8}\sin^2\frac{\phi}{f}\cos^2\frac{\psi}{f}\,(\tilde{g}^2 A_\mu A^\mu) \tag{F.7}$$

$$= \frac{1}{2}\left[(\partial_\mu h)^2 + (\partial_\mu\eta)^2 + \frac{(h\partial_\mu h + \eta\partial_\mu\eta)^2}{f^2 - h^2 - \eta^2}\right] + \frac{h^2}{8}(\tilde{g}^2 A_\mu A^\mu) ,$$

where, for convenience, we defined $\tilde{g}^2 A_\mu A^\mu \equiv g_0^2[(W_\mu^1)^2 + (W_\mu^2)^2] + (g_0' B_\mu - g_0 W_\mu^3)^2$. In the three parametrizations, the EWSB vacuum can be identified as $(\langle\theta^{\hat{3}}\rangle = f\sin^{-1}\sqrt{\xi}, \langle\theta^{\hat{5}}\rangle = 0)$,

$(\sin\langle\phi\rangle = \sqrt{\xi}, \langle\psi\rangle = 0)$ or $(\langle h\rangle = v = f\sqrt{\xi}, \langle\eta\rangle = 0)$, where $\xi = v^2/f^2$. It is then straightforward to identify the physical Higgs and DM fields in the three parametrizations

$$\theta^{\hat{3}} = f\sin^{-1}\sqrt{\xi} + h_{Cart} , \qquad \theta^{\hat{5}} = f\frac{\sin^{-1}\sqrt{\xi}}{\sqrt{\xi}} + \eta_{Cart} ;$$

$$\phi = f\sin^{-1}\sqrt{\xi} + h_{pol} , \qquad \psi = \frac{1}{\sqrt{\xi}}\,\eta_{pol} ; \qquad\qquad\text{(F.8)}$$

$$h = v + \sqrt{1-\xi}\,h_{con} , \qquad \eta = \eta_{con} .$$

Let us now look at the effective potential. With a simple spurionic analysis it is possible to obtain the possible functional dependence of the potential on the pNGBs. The gauge contribution to the potential depends only on $h^2 = f^2\sin^2\frac{\phi}{f}\cos^2\frac{\psi}{f}$, instead the functional dependence of the fermion contribution depend on the particular embedding of the SM fermions in $SO(6)$ representations. In our models, that is embedding the third generation quarks in fundamentals as in eq. (4.15), the functional dependences are $h^2 = f^2\sin^2\frac{\phi}{f}\cos^2\frac{\psi}{f}$ and $(h^2 + \eta^2) = f^2\sin^2\frac{\phi}{f}$. Expanding for small values of h^2, η^2 and keeping terms up to quartic order, the effective potential can thus be parametrized as

$$\begin{aligned}
V_{\text{eff}} &= \frac{\mu_h^2}{2}h^2 + \frac{\lambda_h}{4}h^4 + \frac{\mu_\eta^2}{2}\eta^2 + \frac{\lambda}{2}h^2\eta^2 + \frac{\lambda_\eta}{4}\eta^4 + \dots && \text{(F.9)} \\
&= -\gamma\sin^2\frac{\phi}{f}\cos^2\frac{\psi}{f} + \beta\sin^4\frac{\phi}{f}\cos^4\frac{\psi}{f} + \delta\sin^2\frac{\phi}{f} + \sigma\sin^4\frac{\phi}{f}\cos^2\frac{\psi}{f} + \chi\sin^4\frac{\phi}{f} + \dots.
\end{aligned}$$

The relation between the coefficients in the two formalisms, at this order, is

$$\mu_h^2 f^2 = -2(\gamma - \delta) , \qquad \mu_\eta^2 f^2 = 2\delta ,$$
$$\lambda_h f^4 = 4(\beta + \sigma + \chi) , \qquad \lambda f^4 = 2(\sigma + 2\chi) , \qquad \lambda_\eta f^4 = 4\chi . \qquad\text{(F.10)}$$

The EWSB minimum is given by

$$\xi = \frac{v^2}{f^2} = -\frac{\mu_h^2}{\lambda_h f^2} = \frac{\gamma - \delta}{2(\beta + \sigma + \chi)} . \qquad\qquad\text{(F.11)}$$

The mass matrix for physical fields defined in eq. (F.8), in all three parametrizations, is the same

$$m_h^2 = \left.\frac{\partial^2 V(h_{phys}, \eta_{phys})}{\partial h_{phys}^2}\right|_{min} = 2\lambda_h v^2(1-\xi) = \frac{8(\beta + \sigma + \chi)}{f^2}\xi(1-\xi) , \qquad\text{(F.12)}$$

$$m_\eta^2 = \left.\frac{\partial^2 V(h_{phys}, \eta_{phys})}{\partial \eta_{phys}^2}\right|_{min} = \mu_\eta^2 + \lambda v^2 = \frac{2\delta}{f^2} + \frac{2(\sigma + 2\chi)}{f^2}\xi , \qquad\text{(F.13)}$$

$$m_{h\eta}^2 = \left.\frac{\partial^2 V(h_{phys}, \eta_{phys})}{\partial h_{phys}\partial\eta_{phys}}\right|_{min} = 0 . \qquad\qquad\text{(F.14)}$$

Which confirms that the physical fields defined above are indeed mass eigenstates.

Let us now move to study the couplings of the physical fields in the three parametrizations arising from the Lagrangian of eq. (F.7) and the potential in eq. (F.10). We parametrize the

generic couplings of the physical fields following, and adapting, the formalism of ref. [104]. Up to four-particle interaction terms and assuming custodial invariance and parity under $\eta \to -\eta$, (from now on we neglect the subscript "*phys*"), we write the phenomenological Lagrangian

$$
\begin{aligned}
\mathcal{L}_{\text{pheno}} = {} & \frac{1}{2}(\partial_\mu h)^2 \left(1 + 2a_{hh}\frac{h}{v} + b_{hh}\frac{h^2}{v^2} + b_{h\eta}\frac{\eta^2}{v^2} + \dots \right) \\
& + \frac{1}{2}(\partial_\mu \eta)^2 \left(1 + 2a_{\eta h}\frac{h}{v} + b_{\eta h}\frac{h^2}{v^2} + b_{\eta\eta}\frac{\eta^2}{v^2} + \dots \right) \\
& + (\partial_\mu \eta \partial^\mu h)\left(c_\eta \frac{\eta}{v} + d_{\eta h}\frac{\eta h}{v^2} + \dots \right) - V_{\text{eff}}(h,\eta) \\
& + \left[M_W^2 W_\mu^+ W^{-\mu} + \frac{M_Z^2}{2}Z_\mu Z^\mu \right]\left(1 + 2a_{Vh}\frac{h}{v} + b_{Vh}\frac{h^2}{v^2} + b_{V\eta}\frac{\eta^2}{v^2} + \dots \right) \\
& - m_f \bar{\psi}_f \psi \left(1 + c_{fh}\frac{h}{v} + b_{fh}\frac{h^2}{v^2} + b_{f\eta}\frac{\eta^2}{v^2} + \dots \right) \;,
\end{aligned}
\tag{F.15}
$$

where $f = u^i, d^i, e^i$ represents any SM fermion and

$$
V_{\text{eff}}(h,\eta) = \frac{m_h^2}{2}h^2 + \frac{m_\eta^2}{2}\eta^2 + \frac{\lambda_{h^3}}{2}h^3 v + \frac{\lambda_{h^4}}{4}h^4 + \frac{\lambda_{\eta^2 h}}{2}\eta^2 h + \frac{\lambda_{\eta^2 h^2}}{4}\eta^2 h^2 + \frac{\lambda_{\eta^4}}{4}\eta^4 \;.
\tag{F.16}
$$

We report the expression of the couplings in the three parametrizations, as functions of ξ, in table F.1. It can be noticed that the constrained parametrization offers the cleanest expressions for the physical couplings. For this reason, and for its intuitive relation with the physical Higgs and DM fields, we decided to use this parametrization throughout the work.

In table F.1 it can be noted that the couplings of the physical fields differ also qualitatively among the three parametrizations. It can be checked that, however, when computing physical observables (for example cross-sections) they all give the same result. As an example it can be easily checked that the NGB scattering amplitudes for high energies, $E^2 \gg m_h^2, m_\eta^2, M_{W,Z}^2$, go like $|\mathcal{A}|^2 \sim E^4/f^4$ in all three parametrizations. In order to check that also the couplings from the potential provide the same physical results (which can not be tested from the previous check), we explicitly computed the unpolarized cross-section $\sum_{pol} \sigma(\eta\eta \to W^+W^-)$ in all parametrizations and for all energies above threshold and confirmed that the result is indeed the same in all three cases.

Coupling	Constrained	Polar	Cartesian
a_{Vh}	$\sqrt{1-\xi}$	$\sqrt{1-\xi}$	$\sqrt{1-\xi}$
b_{Vh}	$1-\xi$	$1-2\xi$	$1-2\xi$
$b_{V\eta}$	0	-1	$-1+\frac{\sqrt{1-\xi}}{\sqrt{\xi}}\sin^{-1}\sqrt{\xi}$
a_{hh}	$\frac{\xi}{\sqrt{1-\xi}}$	0	0
b_{hh}	$\frac{\xi(1+3\xi)}{1-\xi}$	0	0
$b_{h\eta}$	$\frac{\xi^2}{1-\xi}$	0	$-1+\frac{\xi}{(\sin^{-1}\sqrt{\xi})^2}$
$a_{\eta h}$	0	$\sqrt{1-\xi}$	$\sqrt{1-\xi}-\frac{\sqrt{\xi}}{\sin^{-1}\sqrt{\xi}}$
$b_{\eta h}$	0	$1-2\xi$	$1-2\xi+\frac{3\xi}{(\sin^{-1}\sqrt{\xi})^2}-\frac{4\sqrt{\xi}\sqrt{1-\xi}}{\sin^{-1}\sqrt{\xi}}$
$b_{\eta\eta}$	$\frac{\xi}{1-\xi}$	0	$-2+\sqrt{1-\xi}\frac{\sin^{-1}\sqrt{\xi}}{\sqrt{\xi}}+\frac{(\sin^{-1}\sqrt{\xi})^2}{\xi}$
c_η	$\frac{\xi}{1-\xi}$	0	$\frac{\sin^{-1}\sqrt{\xi}}{\sqrt{\xi}}-\frac{\sqrt{\xi}}{\sin^{-1}\sqrt{\xi}}$
$d_{\eta h}$	$\frac{\xi(1+\xi)}{1-\xi}$	0	$-1+\frac{3\xi}{(\sin^{-1}\sqrt{\xi})^2}-\frac{2\sqrt{\xi}\sqrt{1-\xi}}{\sin^{-1}\sqrt{\xi}}$
c_{fh}	$\frac{1-2\xi}{\sqrt{1-\xi}}$	$\frac{1-2\xi}{\sqrt{1-\xi}}$	$\frac{1-2\xi}{\sqrt{1-\xi}}$
b_{fh}	$-\frac{(3-2\xi)\xi}{2(1-\xi)}$	-2ξ	-2ξ
$b_{f\eta}$	$-\frac{\xi}{2(1-\xi)}$	$-\frac{1}{2}$	$-\frac{1}{2}\left(1-\frac{1-2\xi}{\sqrt{1-\xi}}\frac{\sin^{-1}\sqrt{\xi}}{\sqrt{\xi}}\right)$
λ_{h^3}	$2\lambda_h(1-\xi)^{3/2}$	$2\lambda_h\sqrt{1-\xi}(1-2\xi)$	$2\lambda_h\sqrt{1-\xi}(1-2\xi)$
λ_{h^4}	$\lambda_h(1-\xi)^2$	$\lambda_h(1-\frac{28}{3}\xi(1-\xi))$	$\lambda_h(1-\frac{28}{3}\xi(1-\xi))$
$\lambda_{\eta^2 h}$	$2\lambda\sqrt{1-\xi}$	$2\frac{\mu_\eta^2}{v^2}+2(2\lambda-\lambda_h)\sqrt{1-\xi}$	$2\lambda-\frac{2}{3}\frac{\mu_\eta^2}{f^2}+\mathcal{O}(\xi)$
$\lambda_{\eta^2 h^2}$	$2\lambda(1-\xi)$	$2\frac{\mu_\eta^2}{v^2}(1-2\xi)+6\lambda(1-\frac{4}{3}\xi)-\lambda_h(5-6\xi)$	$\lambda-\frac{1}{3}\frac{\mu_\eta^2}{f^2}+\mathcal{O}(\xi)$
λ_{η^4}	λ_η	$-\frac{2}{3}\frac{\mu_\eta^2}{v^2}+\lambda_\eta+\lambda_h-\frac{8}{3}\lambda$	$\lambda_\eta-\frac{2}{3}\frac{\mu_\eta^2}{f^2}+\mathcal{O}(\xi)$

Table F.1: Expression of the couplings in eqs. (F.15) and (F.16) in the three parametrizations considered. For the couplings to fermions we assumed the embedding of eq. (4.15). In the last three rows of the Cartesian parametrization we show the leading term for small ξ, since the whole expressions do not fit in the table.

APPENDIX G

Parametrization of the PMNS matrix

In the present Appendix we show how the parametrisation of eq. (5.30) follows from the ones in eqs. (5.27) and (5.28). We start by writing explicitly the PMNS matrix as

$$U = \Phi_e^* R_{12}(\theta_{12}^e) R_{23}(\theta_{23}^e) \Psi R_{23}(\theta_{23}^\nu) R_{12}(\theta_{12}^\nu) \Phi_\nu, \tag{G.1}$$

where $\Psi = \mathrm{diag}(1, e^{i\psi}, e^{i\omega})$, without loss of generality. Any 2×2 unitary matrix V can be recast in the form $V = PR(\theta)Q$, where $P = \mathrm{diag}(e^{i\phi_1}, e^{i\phi_2})$, $Q = \mathrm{diag}(1, e^{i\omega_2})$ and $R(\theta)$ is a 2×2 rotation. We use this to write

$$R_{23}(\theta_{23}^e) \Psi R_{23}(\theta_{23}^\nu) = \Phi' R_{23}(\hat{\theta}_{23})\Omega, \tag{G.2}$$

where $R_{23}(\hat{\theta}_{23})$ is an orthogonal rotation in the 23 block with

$$\sin\hat{\theta}_{23} = \left| \cos\theta_{23}^e \sin\theta_{23}^\nu + e^{i(\omega-\psi)} \sin\theta_{23}^e \cos\theta_{23}^\nu \right|, \tag{G.3}$$

$\Phi' = \mathrm{diag}(e^{i\phi_1}, e^{i\phi_2}, e^{i\phi_3})$, and $\Omega = \mathrm{diag}(1, e^{i\omega_2}, e^{i\omega_3})$. An explicit solution for the angles in terms of the original parameters is

$$\phi_1 = 0, \qquad \phi_2 = \delta_c + \delta_s + \psi - \omega, \qquad \phi_3 = 0,$$
$$\omega_2 = -\delta_s + \omega, \qquad \omega_3 = -\delta_c + \omega, \tag{G.4}$$

where

$$\delta_s = \mathrm{Arg}\left(\cos\theta_{23}^e \sin\theta_{23}^\nu + e^{i(\omega-\psi)} \sin\theta_{23}^e \cos\theta_{23}^\nu \right),$$
$$\delta_c = \mathrm{Arg}\left(\cos\theta_{23}^e \cos\theta_{23}^\nu - e^{i(\omega-\psi)} \sin\theta_{23}^e \sin\theta_{23}^\nu \right). \tag{G.5}$$

Considering now also the $R_{12}(\theta_{12}^\nu)$ rotation, we obtain

$$R_{23}(\hat{\theta}_{23})\Omega R_{12}(\theta_{12}^\nu) = \Phi'' R_{23}(\hat{\theta}_{23}) R_{12}(\theta_{12}^\nu) \, Q'', \tag{G.6}$$

with $\Phi'' = \mathrm{diag}(1, e^{i\omega_2}, e^{i\omega_2})$ and $Q'' = \mathrm{diag}(1, 1, e^{i(\omega_3-\omega_2)})$. The phases in Q'' add to the ones in Q' and are Majorana phases. The ones in Φ'', instead, add to the ones in Φ':

$$\Phi'\Phi'' = e^{i\phi_1} \, \mathrm{diag}(1, e^{i(\phi_2-\phi_1+\omega_2)}, e^{i(\phi_3-\phi_1+\omega_2)}). \tag{G.7}$$

The phase in the 33 position commutes with $R_{12}(\theta_{12}^e)$. Together with the overall phase ϕ_1, it will describe the unphysical phase matrix P in eq. (5.30):

$$P = e^{i\phi_1} \operatorname{diag}(1, 1, e^{i(\phi_3 - \phi_1 + \omega_2)}). \tag{G.8}$$

We see that the only physical Dirac CP violating phase in this parametrisation is contained in the matrix $\Phi = \operatorname{diag}(1, e^{i\phi}, 1)$, with

$$\phi = \phi_2 - \phi_1 + \omega_2 = \psi + \delta_c. \tag{G.9}$$

APPENDIX H

Statistical analysis

In this appendix we describe the simplified statistical analysis performed to obtain the results. Our aim is to use the results of the global fit performed in ref. [196] to assess how well each of the models introduced in the previous section can fit the data. In particular, we use the constraints on the PMNS angles $\theta_{13}, \theta_{12}, \theta_{23}$ and on the phase δ for the normal hierarchy (NH) and inverted hierarchy (IH) cases, as derived in ref. [196]. There, the results are reported by plotting the value of $N_\sigma \equiv \sqrt{\Delta\chi^2}$ (with $\Delta\chi^2 = \chi^2 - \chi^2_{min}$) as a function of each observable, with the remaining ones marginalized away. We construct an approximate global likelihood from these functions as

$$L_j(\alpha_j) = \exp\left(-\frac{\Delta\chi^2_j(\alpha_j)}{2}\right), \qquad L(\vec{\alpha}) = \prod_j^n L_j(\alpha_j), \qquad (H.1)$$

where $\vec{\alpha} = \{\sin^2\theta_{13}, \sin^2\theta_{23}, \sin^2\theta_{12}, \delta\}$ are the observables relevant for our analysis, and we define

$$\chi^2(\vec{\alpha}) \equiv -2\log L(\vec{\alpha})/L_{max} \qquad (H.2)$$

and $N_\sigma(\vec{\alpha}) = \sqrt{\chi^2(\vec{\alpha})}$. In using this procedure we loose any information about possible correlations between different observables. The effect of this loss of information is however negligible, as one can check comparing our 1σ, 2σ and 3σ contours in the $(\sin^2\theta_{23}, \sin^2\theta_{13})$ and $(\sin^2\theta_{13}, \delta)$ planes shown in figure H.1 with the ones in Fig. 5, Fig. 6 and Fig. 7 of ref. [196]. Only in the $\sin^2\theta_{23}$ vs. δ plane there is a visible deformation of the distribution at the 3σ level.

Each model introduced in the previous section (which we dub with an index m) depends on a set of parameters $\mathbf{x}^m = \{x_i^m\}$, which are related to the observables via expressions $\alpha_j = \alpha_j^m(\mathbf{x}^m)$, obtained from eqs. (5.31), (5.55). We then construct the likelihood function in the space of the parameters $\mathbf{x}^m$ as

$$L^m(\mathbf{x}^m) = L(\vec{\alpha}^m(\mathbf{x}^m)). \qquad (H.3)$$

We define $\chi^2(\mathbf{x}^m) = -2\log L^m(\mathbf{x}^m)$ and $N_\sigma(\mathbf{x}^m) = \sqrt{\chi^2(\mathbf{x}^m)}$. The last one is the function we use to produce the plots shown in figures 5.2-5.6, once we marginalize over the variables which are not shown in each plot. Finally, to obtain the best-fit point we use the maximum likelihood method.
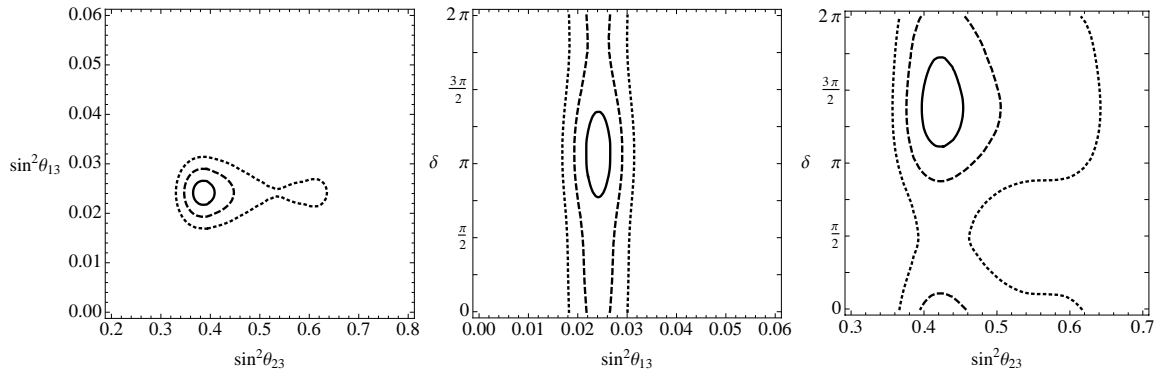
Figure H.1: $1\sigma, 2\sigma, 3\sigma$ contours (respectively solid, dashed and dotted lines) of our global likelihood function in the $(\sin^2\theta_{23}, \sin^2\theta_{13})$ plane (left), $(\sin^2\theta_{13}, \delta)$ plane (center) and $(\sin^2\theta_{23}, \delta)$ plane (right), using the data for NH. These plots can be compared with Fig. 5, Fig. 6 and Fig. 7 of ref. [196] for NH. Undisplayed variables have been marginalized.

Bibliography

[1] D. Marzocca, M. Serone, and J. Shu *JHEP* **1208** (2012) 013, [arXiv:1205.0770].

[2] D. Marzocca and A. Urbano *JHEP* **1407** (2014) 107, [arXiv:1404.7419].

[3] D. Marzocca, A. Parolini, and M. Serone *JHEP* **1403** (2014) 099, [arXiv:1312.5664].

[4] J. Elias-Miró, C. Grojean, R. S. Gupta, and D. Marzocca *JHEP* **1405** (2014) 019, [arXiv:1312.2928].

[5] D. Marzocca *Proc. of the 49th Rencontres de Moriond* (2014) [arXiv:1405.3841].

[6] D. Marzocca, S. T. Petcov, A. Romanino, and M. Spinrath *JHEP* **1111** (2011) 009, [arXiv:1108.0614].

[7] D. Marzocca, S. Petcov, A. Romanino, and M. Sevilla *JHEP* **1305** (2013) 073, [arXiv:1302.0423].

[8] S. Weinberg *Phys.Rev.Lett.* **19** (1967) 1264–1266.

[9] [ATLAS Collaboration], G. Aad et al. *Phys.Lett.* **B716** (2012) 1–29, [arXiv:1207.7214].

[10] [CMS Collaboration], S. Chatrchyan et al. *Phys.Lett.* **B716** (2012) 30–61, [arXiv:1207.7235].

[11] P. W. Higgs *Phys.Lett.* **12** (1964) 132–133.

[12] F. Englert and R. Brout *Phys.Rev.Lett.* **13** (1964) 321–323.

[13] G. Guralnik, C. Hagen, and T. Kibble *Phys.Rev.Lett.* **13** (1964) 585–587.

[14] S. Glashow *Nucl.Phys.* **22** (1961) 579–588.

[15] A. Salam *Conf.Proc.* **C680519** (1968) 367–377.

[16] G. 't Hooft *Nucl.Phys.* **B35** (1971) 167–188.

[17] S. R. Coleman and E. J. Weinberg *Phys.Rev.* **D7** (1973) 1888–1910.

[18] [ATLAS Collaboration], G. Aad et al. `arXiv:1406.3827`.

[19] [CMS Collaboration], V. Khachatryan et al. `arXiv:1407.0558`.

[20] D. Ross and M. Veltman *Nucl.Phys.* **B95** (1975) 135.

[21] M. Veltman *Acta Phys.Polon.* **B8** (1977) 475.

[22] M. Veltman *Nucl.Phys.* **B123** (1977) 89.

[23] [ALEPH, DELPHI, L3, OPAL, LEP Electroweak], S. Schael et al. *Phys.Rept.* **532** (2013) 119–244, [`arXiv:1302.3415`].

[24] G. F. Giudice `arXiv:0801.2562`.

[25] P. A. Dirac *Nature* **139** (1937) 323.

[26] P. A. Dirac *Proc.Roy.Soc.Lond.* **A165** (1938) 199–208.

[27] D. Buttazzo, G. Degrassi, P. P. Giardino, G. F. Giudice, F. Sala, et al. *JHEP* **1312** (2013) 089, [`arXiv:1307.3536`].

[28] E. Gildener *Phys.Rev.* **D14** (1976) 1667.

[29] S. Weinberg *Phys.Lett.* **B82** (1979) 387.

[30] L. Susskind *Phys.Rev.* **D20** (1979) 2619–2625.

[31] K. G. Wilson *Phys.Rev.* **D3** (1971) 1818.

[32] G. 't Hooft *Proc of 1979 Cargèse Institute, Plenum Press, New York* (1980) 135.

[33] P. Fayet *Proc. Europhysics Study Conference in Erice, Plenum Press, New York* (1980) 587.

[34] L. Maiani *Proc. École d'été de physique des particules, Gif-sur-Yvette* (1979).

[35] M. Veltman *Acta Phys.Polon.* **B12** (1981) 437.

[36] E. Witten *Nucl.Phys.* **B188** (1981) 513.

[37] D. B. Kaplan and H. Georgi *Phys.Lett.* **B136** (1984) 183.

[38] D. B. Kaplan, H. Georgi, and S. Dimopoulos *Phys.Lett.* **B136** (1984) 187.

[39] L. Randall and R. Sundrum *Phys.Rev.Lett.* **83** (1999) 3370–3373, [`hep-ph/9905221`].

[40] J. M. Maldacena *Adv.Theor.Math.Phys.* **2** (1998) 231–252, [`hep-th/9711200`].

[41] R. Contino, Y. Nomura, and A. Pomarol *Nucl.Phys.* **B671** (2003) 148–174, [hep-ph/0306259].

[42] R. Contino and A. Pomarol *JHEP* **0411** (2004) 058, [hep-th/0406257].

[43] K. Agashe, R. Contino, and A. Pomarol *Nucl.Phys.* **B719** (2005) 165–187, [hep-ph/0412089].

[44] O. Matsedonskyi, G. Panico, and A. Wulzer *JHEP* **1301** (2013) 164, [arXiv:1204.6333].

[45] M. Redi and A. Tesi *JHEP* **1210** (2012) 166, [arXiv:1205.0232].

[46] A. Pomarol and F. Riva *JHEP* **1208** (2012) 135, [arXiv:1205.6434].

[47] D. Pappadopulo, A. Thamm, and R. Torre *JHEP* **1307** (2013) 058, [arXiv:1303.3062].

[48] [Supernova Search Team], A. G. Riess et al. *Astron.J.* **116** (1998) 1009–1038, [astro-ph/9805201].

[49] [Supernova Cosmology Project], S. Perlmutter et al. *Astrophys.J.* **517** (1999) 565–586, [astro-ph/9812133].

[50] S. Weinberg *Phys.Rev.Lett.* **59** (1987) 2607.

[51] V. Agrawal, S. M. Barr, J. F. Donoghue, and D. Seckel *Phys.Rev.* **D57** (1998) 5480–5492, [hep-ph/9707380].

[52] K. G. Wilson *Phys.Rev.* **179** (1969) 1499–1512.

[53] I. Brivio, T. Corbett, O. Éboli, M. Gavela, J. Gonzalez-Fraile, et al. *JHEP* **1403** (2014) 024, [arXiv:1311.1823].

[54] I. Brivio, O. Éboli, M. Gavela, M. Gonzalez-Garcia, L. Merlo, et al. arXiv:1405.5412.

[55] W. Buchmuller and D. Wyler *Nucl.Phys.* **B268** (1986) 621–653.

[56] S. Weinberg *Phys.Rev.Lett.* **43** (1979) 1566–1570.

[57] B. Grzadkowski, M. Iskrzynski, M. Misiak, and J. Rosiek *JHEP* **1010** (2010) 085, [arXiv:1008.4884].

[58] G. Giudice, C. Grojean, A. Pomarol, and R. Rattazzi *JHEP* **0706** (2007) 045, [hep-ph/0703164].

[59] M. E. Peskin and T. Takeuchi *Phys.Rev.Lett.* **65** (1990) 964–967.

[60] R. Barbieri, A. Pomarol, R. Rattazzi, and A. Strumia *Nucl.Phys.* **B703** (2004) 127–146, [hep-ph/0405040].

[61] Z. Han and W. Skiba *Phys.Rev.* **D71** (2005) 075009, [hep-ph/0412166].

[62] G. Cacciapaglia, C. Csaki, G. Marandella, and A. Strumia *Phys.Rev.* **D74** (2006) 033011, [hep-ph/0604111].

[63] C. Grojean, E. Salvioni, M. Schlaffer, and A. Weiler *JHEP* **1405** (2014) 022, [arXiv:1312.3317].

[64] A. Pomarol and F. Riva *JHEP* **1401** (2014) 151, [arXiv:1308.2803].

[65] J. Elias-Miro, J. Espinosa, E. Masso, and A. Pomarol *JHEP* **1311** (2013) 066, [arXiv:1308.1879].

[66] K. Hagiwara, R. Szalapski, and D. Zeppenfeld *Phys.Lett.* **B318** (1993) 155–162, [hep-ph/9308347].

[67] K. Hagiwara, S. Ishihara, R. Szalapski, and D. Zeppenfeld *Phys.Rev.* **D48** (1993) 2182–2203.

[68] J. Elias-Miró, J. Espinosa, E. Masso, and A. Pomarol *JHEP* **1308** (2013) 033, [arXiv:1302.5661].

[69] S. Narison and R. Tarrach *Phys.Lett.* **B125** (1983) 217.

[70] A. Y. Morozov *Sov.J.Nucl.Phys.* **40** (1984) 505.

[71] K. Hagiwara, S. Matsumoto, D. Haidt, and C. Kim *Z.Phys.* **C64** (1994) 559–620, [hep-ph/9409380].

[72] S. Alam, S. Dawson, and R. Szalapski *Phys.Rev.* **D57** (1998) 1577–1590, [hep-ph/9706542].

[73] R. Barbieri, B. Bellazzini, V. S. Rychkov, and A. Varagnolo *Phys.Rev.* **D76** (2007) 115008, [arXiv:0706.0432].

[74] C. Grojean, E. E. Jenkins, A. V. Manohar, and M. Trott *JHEP* **1304** (2013) 016, [arXiv:1301.2588].

[75] E. E. Jenkins, A. V. Manohar, and M. Trott *JHEP* **1310** (2013) 087, [arXiv:1308.2627].

[76] E. E. Jenkins, A. V. Manohar, and M. Trott *JHEP* **1401** (2014) 035, [arXiv:1310.4838].

[77] R. S. Gupta, A. Pomarol, and F. Riva `arXiv:1405.0181`.

[78] K. Gaemers and G. Gounaris *Z.Phys.* **C1** (1979) 259.

[79] K. Hagiwara, R. Peccei, D. Zeppenfeld, and K. Hikasa *Nucl.Phys.* **B282** (1987) 253.

[80] G. Gounaris, J. Kneur, D. Zeppenfeld, Z. Ajaltouni, A. Arhrib, et al. `hep-ph/9601233`.

[81] O. Domenech, A. Pomarol, and J. Serra *Phys.Rev.* **D85** (2012) 074030, [`arXiv:1201.6510`].

[82] E. H. Simmons and P. L. Cho `hep-ph/9504401`.

[83] M. Baak, M. Goebel, J. Haller, A. Hoecker, D. Kennedy, et al. *Eur.Phys.J.* **C72** (2012) 2205, [`arXiv:1209.2716`].

[84] R. Barbieri and G. Giudice *Nucl.Phys.* **B306** (1988) 63.

[85] M. Ciuchini, E. Franco, S. Mishima, and L. Silvestrini *JHEP* **1308** (2013) 106, [`arXiv:1306.4644`].

[86] C. Grojean, O. Matsedonskyi, and G. Panico *JHEP* **1310** (2013) 160, [`arXiv:1306.4655`].

[87] R. Contino, C. Grojean, D. Pappadopulo, R. Rattazzi, and A. Thamm *JHEP* **1402** (2014) 006, [`arXiv:1309.7038`].

[88] S. Dawson, A. Gritsan, H. Logan, J. Qian, C. Tully, et al. `arXiv:1310.8361`.

[89] H. Baer, T. Barklow, K. Fujii, Y. Gao, A. Hoang, et al. `arXiv:1306.6352`.

[90] F. Gianotti, M. Mangano, T. Virdee, S. Abdullin, G. Azuelos, et al. *Eur.Phys.J.* **C39** (2005) 293–333, [`hep-ph/0204087`].

[91] [TLEP Design Study Working Group], M. Bicer et al. *JHEP* **1401** (2014) 164, [`arXiv:1308.6176`].

[92] M. Baak, A. Blondel, A. Bodek, R. Caputo, T. Corbett, et al. `arXiv:1310.6708`.

[93] S. Mishima *Talk at the Sixth TLEP Workshop* (2013).

[94] R. Contino `arXiv:1005.4269`.

[95] B. Bellazzini, C. Csáki, and J. Serra `arXiv:1401.2457`.

[96] J. M. Cornwall, D. N. Levin, and G. Tiktopoulos *Phys.Rev.* **D10** (1974) 1145.

[97] B. W. Lee, C. Quigg, and H. Thacker *Phys.Rev.* **D16** (1977) 1519.

[98] H. G. Veltman *Phys.Rev.* **D41** (1990) 2294.

[99] A. Wulzer `arXiv:1309.6055`.

[100] T. Banks *Nucl.Phys.* **B243** (1984) 125.

[101] H. Georgi, D. B. Kaplan, and P. Galison *Phys.Lett.* **B143** (1984) 152.

[102] H. Georgi and D. B. Kaplan *Phys.Lett.* **B145** (1984) 216.

[103] M. J. Dugan, H. Georgi, and D. B. Kaplan *Nucl.Phys.* **B254** (1985) 299.

[104] R. Contino, C. Grojean, M. Moretti, F. Piccinini, and R. Rattazzi *JHEP* **1005** (2010) 089, [`arXiv:1002.1011`].

[105] R. Contino, D. Marzocca, D. Pappadopulo, and R. Rattazzi *JHEP* **1110** (2011) 081, [`arXiv:1109.1570`].

[106] K. Agashe, A. Delgado, M. J. May, and R. Sundrum *JHEP* **0308** (2003) 050, [`hep-ph/0308036`].

[107] H. Davoudiasl, J. Hewett, and T. Rizzo *Phys.Lett.* **B473** (2000) 43–49, [`hep-ph/9911262`].

[108] A. Pomarol *Phys.Lett.* **B486** (2000) 153–157, [`hep-ph/9911294`].

[109] N. Arkani-Hamed, A. G. Cohen, and H. Georgi *Phys.Rev.Lett.* **86** (2001) 4757–4761, [`hep-th/0104005`].

[110] N. Arkani-Hamed, A. G. Cohen, and H. Georgi *Phys.Lett.* **B513** (2001) 232–240, [`hep-ph/0105239`].

[111] N. Arkani-Hamed, A. Cohen, E. Katz, A. Nelson, T. Gregoire, et al. *JHEP* **0208** (2002) 021, [`hep-ph/0206020`].

[112] N. Arkani-Hamed, A. Cohen, E. Katz, and A. Nelson *JHEP* **0207** (2002) 034, [`hep-ph/0206021`].

[113] Y. Hosotani *Phys.Lett.* **B126** (1983) 309.

[114] I. Antoniadis, K. Benakli, and M. Quiros *New J.Phys.* **3** (2001) 20, [`hep-th/0108005`].

[115] L. J. Hall, Y. Nomura, and D. Tucker-Smith *Nucl.Phys.* **B639** (2002) 307–330, [`hep-ph/0107331`].

[116] C. A. Scrucca, M. Serone, and L. Silvestrini *Nucl.Phys.* **B669** (2003) 128–158, [`hep-ph/0304220`].

[117] C. Scrucca, M. Serone, L. Silvestrini, and A. Wulzer *JHEP* **0402** (2004) 049, [`hep-th/0312267`].

[118] R. Contino, T. Kramer, M. Son, and R. Sundrum *JHEP* **0705** (2007) 074, [`hep-ph/0612180`].

[119] G. Panico and A. Wulzer *JHEP* **1109** (2011) 135, [`arXiv:1106.2719`].

[120] S. De Curtis, M. Redi, and A. Tesi *JHEP* **1204** (2012) 042, [`arXiv:1110.1613`].

[121] F. Caracciolo, A. Parolini, and M. Serone *JHEP* **1302** (2013) 066, [`arXiv:1211.7290`].

[122] A. Parolini `arXiv:1405.4875`.

[123] A. Birkedal, Z. Chacko, and M. K. Gaillard *JHEP* **0410** (2004) 036, [`hep-ph/0404197`].

[124] P. H. Chankowski, A. Falkowski, S. Pokorski, and J. Wagner *Phys.Lett.* **B598** (2004) 252–262, [`hep-ph/0407242`].

[125] Z. Berezhiani, P. H. Chankowski, A. Falkowski, and S. Pokorski *Phys.Rev.Lett.* **96** (2006) 031801, [`hep-ph/0509311`].

[126] N. Seiberg *Nucl.Phys.* **B435** (1995) 129–146, [`hep-th/9411149`].

[127] D. B. Kaplan *Nucl.Phys.* **B365** (1991) 259–278.

[128] Y. Grossman and M. Neubert *Phys.Lett.* **B474** (2000) 361–371, [`hep-ph/9912408`].

[129] T. Gherghetta and A. Pomarol *Nucl.Phys.* **B586** (2000) 141–162, [`hep-ph/0003129`].

[130] K. Agashe, A. Delgado, and R. Sundrum *Annals Phys.* **304** (2003) 145–164, [`hep-ph/0212028`].

[131] R. Barbieri, D. Buttazzo, F. Sala, D. M. Straub, and A. Tesi *JHEP* **1305** (2013) 069, [`arXiv:1211.5085`].

[132] B. Gripaios, A. Pomarol, F. Riva, and J. Serra *JHEP* **0904** (2009) 070, [`arXiv:0902.1483`].

[133] J. Mrazek, A. Pomarol, R. Rattazzi, M. Redi, J. Serra, et al. *Nucl.Phys.* **B853** (2011) 1–48, [`arXiv:1105.5403`].

[134] S. R. Coleman, J. Wess, and B. Zumino *Phys.Rev.* **177** (1969) 2239–2247.

[135] J. Callan, Curtis G., S. R. Coleman, J. Wess, and B. Zumino *Phys.Rev.* **177** (1969) 2247–2250.

[136] K. Agashe, R. Contino, L. Da Rold, and A. Pomarol *Phys.Lett.* **B641** (2006) 62–66, [`hep-ph/0605341`].

[137] G. Ecker, J. Gasser, H. Leutwyler, A. Pich, and E. de Rafael *Phys.Lett.* **B223** (1989) 425.

[138] A. De Simone, O. Matsedonskyi, R. Rattazzi, and A. Wulzer *JHEP* **1304** (2013) 004, [`arXiv:1211.5663`].

[139] A. Azatov, M. Salvarezza, M. Son, and M. Spannowsky *Phys.Rev.* **D89** (2014) 075001, [`arXiv:1308.6601`].

[140] A. Urbano `arXiv:1310.5733`.

[141] A. Falkowski, F. Riva, and A. Urbano *JHEP* **1311** (2013) 111, [`arXiv:1303.1812`].

[142] [ATLAS Collaboration] `ATLAS-CONF-2014-009`, CERN, (2014).

[143] [CMS Collaboration] `CMS-PAS-HIG-13-005`, CERN, (2013).

[144] [ATLAS Collaboration], G. Aad et al. *Phys.Rev.Lett.* **112** (2014) 201802, [`arXiv:1402.3244`].

[145] [CMS Collaboration] `CMS-PAS-HIG-13-028`, CERN, (2013).

[146] P. P. Giardino, K. Kannike, I. Masina, M. Raidal, and A. Strumia *JHEP* **1405** (2014) 046, [`arXiv:1303.3570`].

[147] D. Carmi, A. Falkowski, E. Kuflik, T. Volansky, and J. Zupan *JHEP* **1210** (2012) 196, [`arXiv:1207.1718`].

[148] A. Azatov, R. Contino, and J. Galloway *JHEP* **1204** (2012) 127, [`arXiv:1202.3415`].

[149] M. Montull and F. Riva *JHEP* **1211** (2012) 018, [`arXiv:1207.1716`].

[150] J. Espinosa, C. Grojean, M. Muhlleitner, and M. Trott *JHEP* **1212** (2012) 045, [`arXiv:1207.1717`].

[151] J. Ellis and T. You *JHEP* **1306** (2013) 103, [`arXiv:1303.3879`].

[152] D. Pappadopulo, A. Thamm, R. Torre, and A. Wulzer `arXiv:1402.4431`.

[153] N. Vignaroli *Phys.Rev.* **D89** (2014) 095027, [`arXiv:1404.5558`].

[154] [CMS Collaboration], S. Chatrchyan et al. *Phys.Rev.Lett.* **112** (2014) 171801, [`arXiv:1312.2391`].

[155] [ATLAS Collaboration] `ATLAS-CONF-2012-130`, CERN, (2012).

[156] [CMS Collaboration], S. Chatrchyan et al. *Phys.Lett.* **B729** (2014) 149–171, [`arXiv:1311.7667`].

[157] [ATLAS Collaboration] `ATLAS-CONF-2013-060`, CERN, (2013).

[158] [ATLAS Collaboration] `ATLAS-CONF-2013-018`, CERN, (2013).

[159] G. Panico, M. Safari, and M. Serone *JHEP* **1102** (2011) 103, [`arXiv:1012.2875`].

[160] S. Weinberg *Phys.Rev.Lett.* **18** (1967) 507–509.

[161] A. Orgogozo and S. Rychkov *JHEP* **1203** (2012) 046, [`arXiv:1111.3534`].

[162] M. E. Peskin and T. Takeuchi *Phys.Rev.* **D46** (1992) 381–409.

[163] E. Witten *Phys.Rev.Lett.* **51** (1983) 2351.

[164] M. Serone *New J.Phys.* **12** (2010) 075013, [`arXiv:0909.5619`].

[165] [CMS Collaboration], S. Chatrchyan et al. *JHEP* **1205** (2012) 123, [`arXiv:1204.1088`].

[166] M. Frigerio, A. Pomarol, F. Riva, and A. Urbano *JHEP* **1207** (2012) 015, [`arXiv:1204.2808`].

[167] V. Silveira and A. Zee *Phys.Lett.* **B161** (1985) 136.

[168] J. McDonald *Phys.Rev.* **D50** (1994) 3637–3649, [`hep-ph/0702143`].

[169] C. Burgess, M. Pospelov, and T. ter Veldhuis *Nucl.Phys.* **B619** (2001) 709–728, [`hep-ph/0011335`].

[170] B. Patt and F. Wilczek `hep-ph/0605188`.

[171] W.-C. Huang, A. Urbano, and W. Xue *JCAP* **1404** (2014) 020, [`arXiv:1310.7609`].

[172] [Planck Collaboration], P. Ade et al. `arXiv:1303.5076`.

[173] J. M. Cline and K. Kainulainen *JCAP* **1301** (2013) 012, [`arXiv:1210.4196`].

[174] P. Ciafaloni, D. Comelli, A. De Simone, E. Morgante, A. Riotto, et al. *JCAP* **1310** (2013) 031, [`arXiv:1305.6391`].

[175] F. Boudjema, G. D. La Rochelle, and A. Mariano `arXiv:1403.7459`.

[176] [LUX Collaboration], D. Akerib et al. *Phys.Rev.Lett.* **112** (2014) 091303, [`arXiv:1310.8214`].

[177] A. Berlin, D. Hooper, and S. D. McDermott `arXiv:1404.0022`.

[178] P. Junnarkar and A. Walker-Loud *Phys.Rev.* **D87** (2013), no. 11 114510, [`arXiv:1301.1114`].

[179] G. Bertone, J. Silk, B. Moore, J. Diemand, J. Bullock, et al. *Cambridge, UK: Univ. Pr.* (2010) 738.

[180] M. Cirelli, G. Corcella, A. Hektor, G. Hutsi, M. Kadastik, et al. *JCAP* **1103** (2011) 051, [`arXiv:1012.4515`].

[181] [BESS Collaboration], T. Maeno et al. *Astropart.Phys.* **16** (2001) 121–128, [`astro-ph/0010381`].

[182] [PAMELA Collaboration], O. Adriani et al. *Phys.Rev.Lett.* **105** (2010) 121101, [`arXiv:1007.0821`].

[183] A. W. Graham, D. Merritt, B. Moore, J. Diemand, and B. Terzic *Astron.J.* **132** (2006) 2685–2700, [`astro-ph/0509417`].

[184] J. F. Navarro, C. S. Frenk, and S. D. White *Astrophys.J.* **462** (1996) 563–575, [`astro-ph/9508025`].

[185] A. Burkert *IAU Symp.* **171** (1996) 175, [`astro-ph/9504041`].

[186] C. Evoli, I. Cholis, D. Grasso, L. Maccione, and P. Ullio *Phys.Rev.* **D85** (2012) 123511, [`arXiv:1108.0664`].

[187] [Daya-Bat Collaboration], F. An et al. *Phys.Rev.Lett.* **108** (2012) 171803, [`arXiv:1203.1669`].

[188] [Daya Bay Collaboration], F. An et al. *Chin.Phys.* **C37** (2013) 011001, [`arXiv:1210.6327`].

[189] S. M. Bilenky and S. Petcov *Rev.Mod.Phys.* **59** (1987) 671.

[190] [Particle Data Group], J. Beringer et al. *Phys. Rev.* **D86** (2012) 010001.

[191] S. M. Bilenky, J. Hosek, and S. Petcov *Phys.Lett.* **B94** (1980) 495.

[192] S. M. Bilenky, N. Nedelcheva, and S. Petcov *Nucl.Phys.* **B247** (1984) 61.

[193] C. Jarlskog *Z.Phys.* **C29** (1985) 491–497.

[194] C. Jarlskog *Phys.Rev.Lett.* **55** (1985) 1039.

[195] P. Krastev and S. Petcov *Phys.Lett.* **B205** (1988) 84–92.

[196] F. Capozzi, G. Fogli, E. Lisi, A. Marrone, D. Montanino, et al. *Phys.Rev.* **D89** (2014) 093018, [arXiv:1312.2878].

[197] [T2K Collaboration], K. Abe et al. *Phys.Rev.Lett.* **107** (2011) 041801, [arXiv:1106.2822].

[198] [RENO collaboration], J. Ahn et al. *Phys.Rev.Lett.* **108** (2012) 191802, [arXiv:1204.0626].

[199] [Double Chooz Collaboration], Y. Abe et al. *Phys.Rev.* **D86** (2012) 052008, [arXiv:1207.6632].

[200] [Daya Bay Collaboration] talk at Neutrino 2014, (2014).

[201] G. Fogli, E. Lisi, A. Marrone, D. Montanino, A. Palazzo, et al. *Phys.Rev.* **D86** (2012) 013012, [arXiv:1205.5254].

[202] M. Gonzalez-Garcia, M. Maltoni, J. Salvado, and T. Schwetz *JHEP* **1212** (2012) 123, [arXiv:1209.3023].

[203] Z.-z. Xing *Phys.Rev.* **D64** (2001) 093013, [hep-ph/0107005].

[204] C. Giunti and M. Tanimoto *Phys.Rev.* **D66** (2002) 053013, [hep-ph/0207096].

[205] P. Frampton, S. Petcov, and W. Rodejohann *Nucl.Phys.* **B687** (2004) 31–54, [hep-ph/0401206].

[206] S. Petcov and W. Rodejohann *Phys.Rev.* **D71** (2005) 073002, [hep-ph/0409135].

[207] A. Romanino *Phys.Rev.* **D70** (2004) 013003, [hep-ph/0402258].

[208] G. Altarelli, F. Feruglio, and I. Masina *Nucl.Phys.* **B689** (2004) 157–171, [hep-ph/0402155].

[209] S. King *JHEP* **0508** (2005) 105, [hep-ph/0506297].

[210] I. Masina *Phys.Lett.* **B633** (2006) 134–140, [hep-ph/0508031].

[211] S. Antusch and S. F. King *Phys.Lett.* **B631** (2005) 42–47, [hep-ph/0508044].

[212] K. Hochmuth, S. Petcov, and W. Rodejohann *Phys.Lett.* **B654** (2007) 177–188, [arXiv:0706.2975].

[213] S. Antusch and V. Maurer *Phys.Rev.* **D84** (2011) 117301, [arXiv:1107.3728].

[214] A. Meroni, S. Petcov, and M. Spinrath *Phys.Rev.* **D86** (2012) 113003, [arXiv:1205.5241].

[215] C. H. Albright, A. Dueck, and W. Rodejohann *Eur.Phys.J.* **C70** (2010) 1099–1110, [arXiv:1004.2798].

[216] P. Harrison, D. Perkins, and W. Scott *Phys.Lett.* **B530** (2002) 167, [hep-ph/0202074].

[217] F. Vissani hep-ph/9708483.

[218] V. D. Barger, S. Pakvasa, T. J. Weiler, and K. Whisnant *Phys.Lett.* **B437** (1998) 107–116, [hep-ph/9806387].

[219] S. Petcov *Phys.Lett.* **B110** (1982) 245–249.

[220] S. Petcov arXiv:1405.6006.

[221] I. Girardi, A. Meroni, S. Petcov, and M. Spinrath *JHEP* **1402** (2014) 050, [arXiv:1312.1966].

[222] S. Antusch and M. Spinrath *Phys.Rev.* **D79** (2009) 095004, [arXiv:0902.4644].

[223] Z.-z. Xing, H. Zhang, and S. Zhou *Phys.Rev.* **D77** (2008) 113016, [arXiv:0712.1419].

[224] H. Leutwyler *Nucl.Phys.Proc.Suppl.* **94** (2001) 108–115, [hep-ph/0011049].

[225] L. J. Hall, R. Rattazzi, and U. Sarid *Phys.Rev.* **D50** (1994) 7048–7065, [hep-ph/9306309].

[226] H. Georgi and C. Jarlskog *Phys.Lett.* **B86** (1979) 297–300.

[227] A. Pineda *Phys.Rev.* **D65** (2002) 074007, [hep-ph/0109117].

[228] S. Weinberg, *The Quantum Theory of Fields, Volume 2: Modern Applications.* Cambridge University Press, 1996.

Acknowledgements

The results obtained during this four years of PhD would not have been possible to achieve without the guidance of my supervisors and the collaboration with a number of professors, postdocs and PhD students, each of whom helped in some way or another to make me grow as a theoretical physicist.

First of all I would like to thank my supervisors, Andrea Romanino and Marco Serone, for guiding me throughout the different projects with countless and invaluable discussions, for supporting me during all the PhD and for giving me many chances to interact with the international physics community.

I am also very thankful to Serguey T. Petcov for guidance during the projects on neutrino physics and to Christophe Grojean for welcoming and supporting me during my stay at CERN in 2013, and for giving me a chance to collaborate in a very challenging and stimulating project on the SM effective theory. I want also to thank again my Master supervisor, Roberto Contino, for stimulating my interest in this field with his example.

The discussions with each collaborator in the different projects always offered some invaluable lesson to be learned, so many thanks also to Alberto, Jing, Joan, Martin and Sandeepan.

A PhD is a long and sometimes difficult road, so having some friends which are in the same boat is fundamental in order to reach the end with a (somewhat) sane state of mind. I would like then to thank Alberto, Bethan, Carlo, Claudia, Flavio, Gabriele, Lorenzo, Marco, Marko and Piermarco for the countless shared lunches, breaks, beers and evenings in Trieste. Thanks also to Daniele and Valerio for the constant connection, regardless of where we might end up.

I want also to thank my family for supporting me in my choices and for being always there when I need them. Last, but absolutely not least, I thank Weronika for making me happier every day and for putting up with me during this years.